Dynamics in bacterial flagellar systems

Dissertation

zur Erlangung des akademischen

Grades Doktor der Naturwissenschaft (Dr. rer. nat.)

dem Fachbereich Biologie der

Philipps-Universität Marburg (HKZ: 1180)

am 2.5.2016

vorgelegt von

Susanne Brenzinger

geboren in Dormagen

Erstgutachter: Prof. Dr. Kai Thormann

Zweitgutachter: Prof. Dr. Victor Sourjik

Tag der Disputation:

Marburg an der Lahn, 2016

Die Untersuchungen zur vorliegenden Arbeit wurden von November 2011 bis April 2016 unter der Leitung von Prof. Dr. Kai Thormann am Max-Planck-Institut für terrestrische Mikrobiologie in Marburg an der Lahn und am Institut für Molekularbiologie und Mikrobiologie an der Justus-Liebig-Universität Gießen durchgeführt.

Vom Fachbereich Biologie der Philipps-Universität Marburg (HKZ: 1180)

als Dissertation angenommen am:

Erstgutachter: Prof. Dr. Kai Thormann

Zweitgutachter: Prof. Dr. Victor Sourjik

Tag der Disputation:

Die in dieser Dissertation beschriebenen Ergebnisse sind in folgenden Publikationen veröffentlicht bzw. zur Veröffentlichung vorgesehen:

Chapter 2

Paulick A., Delalez N.J., **Brenzinger S.**, Steel B.C., Berry R.M., Armitage J.P., Thormann K.M. (2015) Dual stator dynamics in the *Shewanella oneidensis* MR-1 flagellar motor. Mol Microbiol. 96(5):993-1001.

Chapter 3

Brenzinger S., Dewenter L., Delalez N.J., Leicht O., Berndt V., Berry R.M., Thanbichler M., Armitage J.P., Maier B., Thormann K.M. Mechanistic consequences of functional stator mutations in the bacterial flagellar motor. Mol Microbiol. *Submitted*

Chapter 4

Brenzinger S., Rossmann F., Knauer C., Dörrich A.K., Bubendorfer S., Ruppert U., Bange G., Thormann K.M. (2015) The role of FlhF and HubP as polar landmark proteins in *Shewanella putrefaciens* CN-32. Mol Microbiol. 98(4):727-42.

Ergebnisse aus Projekten, die in dieser Dissertation nicht erwähnt wurden, sind in folgender Originalpublikation veröffentlicht:

Dwarakanath S., **Brenzinger S**., Gleditzsch D., Plagens A., Klingl A., Thormann K., Randau L. (2015) Interference activity of a minimal Type I CRISPR-Cas system from *Shewanella putrefaciens*. Nucleic Acids Res. 43(18):8913-23.

Erklärung

Ich versichere, dass ich meine Dissertation

„Dynamics in bacterial flagellar systems“

selbständig und ohne unerlaubte Hilfe angefertigt habe und mich keiner als der von mir ausdrücklich bezeichneten Quellen und Hilfen bedient habe. Diese Dissertation wurde in der jetzigen oder ähnlichen Form noch bei keiner anderen Hochschule eingereicht und hat noch keinen sonstigen Prüfungszwecken gedient.

Marburg an der Lahn, 29.4.2014

_____

Susanne Brenzinger

Seht ihr den Mond dort stehen?
Er ist nur halb zu sehen,
Und ist doch rund und schön!
So sind wohl manche Sachen,
Die wir getrost belachen,
Weil unsre Augen sie nicht sehn.

Matthias Claudius

Content

Summary

Bacterial cells are highly organized with respect to their shape, structure or function. In particular flagellar motility and chemotaxis of many bacteria require a precise spatiotemporal regulation of the corresponding components to avoid wasting energy. Despite the tight regulation, flagellar motility and chemotaxis are also targets of adaptation in response to extra- and intracellular cues. The balance between tight regulation and flexible adaptation allows bacteria to efficiently thrive in changing and potentially nutrient limiting environments.

This thesis focuses on the adaptation of the flagella-mediated motility of the γ-proteobacterium *Shewanella oneidensis* MR-1 by dynamically exchanging one of its motor components and a system in *Shewanella putrefaciens* CN-32 that ensures proper polar localization of several proteins, among them the chemotaxis system.

S. oneidensis MR-1 possesses a single polar flagellar system but harbors two types of ion-channels, the so-called stators, that power flagellar rotation. The second chapter demonstrates that both stators, the native Na^+-dependent PomAB and putatively acquired H^+-dependent MotAB complex, are solely sufficient to drive motility in liquid environments and may interact with the flagellar rotor in varying configurations depending on sodium-ion concentrations, likely forming a hybrid motor. The principal environmental cue that can be integrated and reacted to by PomAB/MotAB stator swapping is the external Na^+ concentration. Functionality of MotAB on the other hand seems to be tied to the membrane potential and load on the flagellum. Some limitations of MotAB can be overcome by small point mutations in the plug domain of MotB, likely by changing the MotAB channel properties and/or its mechanosensing capability.

The second system studied was a landmark protein that serves as an organizational platform involved in different cellular processes including chemotaxis. This transmembrane protein was identified as the functional orthologue of *Vibrio cholerae* HubP. In *S. putrefaciens* CN-32 it is required for polar localization and possibly the correct function of the chemotaxis components, but not for placement of the flagellum which depends on the GTPase FlhF. Localization of HubP itself may be dependent on its LysM peptidoglycan-binding domain. Since the swimming speed was decreased when *hubP* was deleted, a so far unidentified modulator of flagellar motility might require HubP for proper function. In addition, deletion of *hubP* caused an impairment in twitching motility and affected proper localization of the chromosome partitioning system. Due to its structural similarity to *Pseudomonas aeruginosa* FimV and partially matching phenotypes upon deletion, the group of HubP/FimV homologs, characterized by a rather conserved N-terminal periplasmic section and a highly variable acidic cytoplasmic part, may serve as polar markers in various bacterial species with respect to different cellular functions. Thus, two separate systems target the flagellum and chemotaxis system to the cell pole.

Zusammenfassung

Bakterienzellen sind hinsichtlich ihrer Form, Struktur und Funktionalität hoch organisiert. Insbesondere Komponenten, die an der von Flagellen angetriebenen Motilität und Chemotaxis beteiligt sind, bedürfen einer präzisen räumlichen und zeitlichen Regulierung um eine Energieverschwendung zu vermeiden. Trotz der stringenten Regulierung sind die flagellare Motilität sowie die Chemotaxis temporären Anpassungen an extra- und intrazellulärer Signale unterworfen. Die Balance zwischen Regulierung und flexibler Anpassung ermöglicht es Bakterienpopulationen in wechselnden und potenziell nährstoffarmen Umgebungen effizient zu wachsen.

Die hier vorgelegte Dissertation fokussiert sich auf die im γ-Proteobacterium *Shewanella oneidensis* MR-1 gefundene Anpassung der Flagellen-vermittelten Motilität durch den dynamischen Austausch von Motorkomponenten und ein System in *Shewanella putrefaciens* CN-32, das die polare Lokalisation mehrerer Proteine, unter anderem die des Chemotaxis-Systems, gewährleistet.

S. oneidensis MR-1 verfügt über ein einzelnes polares Flagellensystem sowie zwei Ionenkanal-Typen, die so genannten Statoren, die die Flagellenrotation antreiben können. Das zweite Kapitel zeigt, dass beide Statoren, der native Na^+-abhängige PomAB und mutmaßlich erworbene H^+-abhängige MotAB Komplex, allein ausreichen um die bakterielle Beweglichkeit in planktonischer Umgebung zu gewährleisten. Abhängig von der Salzkonzentration des jeweiligen Habitats können die Statoren in variierenden Zusammensetzungen mit dem Rotor interagieren. *S. oneidensis* MR-1 verfügt somit möglicherweise über einen Hybridmotor. Der wichtigste Umweltfaktor, der den Statoraustausch beeinflusst, ist die externe Na^+-Konzentration. Die Funktionalität von MotAB scheint darüber hinaus an das Membranpotential und die Belastung des Flagellums gebunden zu sein. Die limitierte Funktionalität von MotAB kann durch Punktmutationen in der „Plug“-Domäne von MotB überwunden werden. Diese Mutationen führen möglicherweise zu Änderungen der Kanaleigenschaften und/ oder seiner Fähigkeit, die Belastung der Flagelle zu detektieren.

Bei dem zweiten untersuchten System handelt es sich um ein Markierungsprotein, das verschiedenen zellulären Prozessen einschließlich Chemotaxis als Organisationsplattform dient. Dieses Transmembranprotein wurde als funktionelles Ortholog von *Vibrio cholerae* HubP identifiziert. In *S. putrefaciens* CN-32 ist es für die polare Lokalisierung und möglicherweise auch für die korrekte Funktion der Chemotaxis-Komponenten erforderlich, jedoch nicht für die Platzierung des Flagellums, deren Lokalisierung wiederum von der GTPase FlhF abhängt. Die polare Lokalisierung von HubP selbst wird möglicherweise durch dessen LysM Peptidoglykan-Bindungsdomäne bedingt. Da die Schwimmgeschwindigkeit nach einer Deletion von *hubP* geringer ausfiel, könnte eine bisher nicht identifizierte Komponente der flagellaren Motilität HubP für ihre ordnungsgemäße Funktion benötigen. Darüber hinaus ist die „twitching“ Motilität und die Lokalisation des chromosomalen Teilungsapparates beeinträchtig. Aufgrund seiner strukturellen Ähnlichkeit zu FimV von *Pseudomonas*

aeruginosa und den teilweise übereinstimmenden Phänotypen bei deren Deletion, scheinen HubP und FimV Homologe, die sich durch ihren konservierten N-terminalen periplasmatischen Abschnitt und eine stark variable sauren zytoplasmatischen Teil kennzeichnen, gemeinsam eine Gruppe polare Markerproteine zu bilden. Diese Markerproteine können in verschiedenen bakteriellen Spezies für unterschiedliche Zellfunktionen wichtig sein.

Chapter I

Introduction

Initial remarks

Bacterial species benefit significantly from the ability to actively move towards attractants or away from repellents. To this end, several sophisticated molecular machineries of locomotion have evolved (see reviews Bardy, Ng, and Jarrell 2003; Jarrell and McBride 2008). Motility mediated by one or several rotating filaments, the so-called flagella, conveys the fastest directed movement of bacteria with speeds of several cell body lengths per second in liquid environments (Macnab 1984). Most flagellated cells also generate enough torque to move through viscous environments like mucus (Martinez et al. 2014). Additionally, flagella enable bacteria to navigate in structured habitats such as sediments towards the most favorable condition. Flagella rotate counterclockwise (CCW) or clockwise (CW) and switching between the two orientations frequently leads to a reorientation of the swimming direction. By modulating the frequency of these reorientation events in dependence of extracellular stimuli, cells achieve a biased random walk towards or away from attractants or repellents. This behavior is called chemotaxis (see reviews by Wadhams and Armitage 2004; Sourjik and Wingreen 2012).

Aspects of flagellar motility that have been subject of intensive research for decades are I) its intricate self-assembling structure composed out of multiple different proteins of varying stoichiometry combined with a II) tight regulation pattern of production and placement. III) Furthermore, polar flagella are excellent marker to study cell polarity. IV) Flagellar motility is adaptable on various levels to suit the prevailing environmental conditions. V) In addition, the flagellum is widespread among the kingdom of bacteria and, thus, of interest regarding its evolution.

Members of the genus *Shewanella* have been selected to serve as a model organism of flagellar motility for several reasons: A few of its members, among them *Shewanella putrefaciens* CN-32, possess a polar and a lateral flagellar gene set (Paulick et al. 2009). About half the cells of *S. putrefaciens* CN-32 produce a polar flagellum and up to 12% were found to possess 1-3 additional lateral flagella in planktonic culture. This allows the study of placement of the two flagella types, the regulatory interplay between two flagella gene clusters, the impact of heterogeneity of flagellation at population level and the specificity of single flagellar components (Bubendorfer et al. 2012; 2014). *Shewanella oneidensis* MR-1 on the other hand possesses a single flagellum but two types of static motor components (stators), one of which has most likely been acquired via lateral gene transfer (Paulick et al. 2009). This strain is therefore suitable to study the interplay of acquired components to a native flagellum and the consequences on its behavior.

The presented dissertation focuses on the adaptation of the flagellar motor by the additional stator complex in *S. oneidensis* MR-1 and the achievement of polarity of several components important for flagellar motility of *S. putrefaciens* CN-32. Therefore, the following introduction will initially focus on the general structure, assembly and function of the flagellum. Furthermore, the current knowledge of

control of flagella number and placement is explained. Finally, mechanisms of flagellar motility adaptation to environmental cues are highlighted.

The flagellar architecture and organization

Flagella are large proteinaceous structures that span the whole bacterial cell envelope. Their overall architecture can be divided into three major parts: The long helical filament, a flexible hook and the basal body (Figure 1). Despite this conserved general appearance, flagella show a high variance across the different species in terms of their structural composition, position and number, operon structure and underlying gene expression control. A common feature is, however, the existence of several core structures, a tiered-controlled expression and hierarchical self-assembly (Macnab and Aizawa 1984; Dasgupta et al. 2003; Bilchik et al. 2006; Minamino and Imada 2015). The tight regulation of expression, number and placement may be necessary to control the high amount of energy required for production and function of the flagellum which may use up to 10% of the total cell carbon in nutrient-limited small cells (Mitchell 2002).

The flagellum is assembled from the in- to the outside of the cell, and the required components are expressed in that order. In the γ-proteobacteria *Vibrio* and *Pseudomonas*, the first component produced is the σ^{54}-dependent master regulator FlrA (also termed FleQ or FlaK) (Prouty, Correa, and Klose 2001; Syed et al. 2009). FlrA activates the transcription of the first set of structural proteins that build up the MS-ring embedded in the cytoplasmic membrane (FliF), the transport system (FlhAB FliOPQR) with its ATPase ring complex (FliHIJ) and the C-ring (FliGMN) which is attached to the cytoplasmic side of the MS-ring. Whether the MS-ring or the transport system is the first component inserted into the membrane and, thus, starting flagellar assembly is controversially discussed (see review by Altegoer and Bange, 2015). FliL, which is also expressed in this tier, was recently described to be a membrane embedded protein important in motor function (Partridge, Nieto, and Harshey 2015). Furthermore, a set of regulatory proteins is produced: The two component system FlrBC (or FleRS in *Pseudomonas*), which is required for σ^{54}-dependent activation of the next class of genes as well as the alternative sigma factor FliA (Ritchings et al. 1995; Starnbach and Lory 1992; Klose and Mekalanos 1998; Prouty, Correa, and Klose 2001). Under the control of FlrBC, the basal body is further compiled. The central rod (FlgBCFG) connects the MS-ring with the flexible hook (FlgE) (Zuberi et al. 1991; Muller et al. 1992; Minamino, Yamaguchi, and Macnab 2000; Saijo-Hamano et al. 2004). The rod is enclosed by ring structures embedded in the peptidoglycan (FlgI) and outer membrane (FlgH) that act as a bushing (Jones, Homma, and Macnab 1989). In *Vibrio,* the major flagellin FlaA, the building

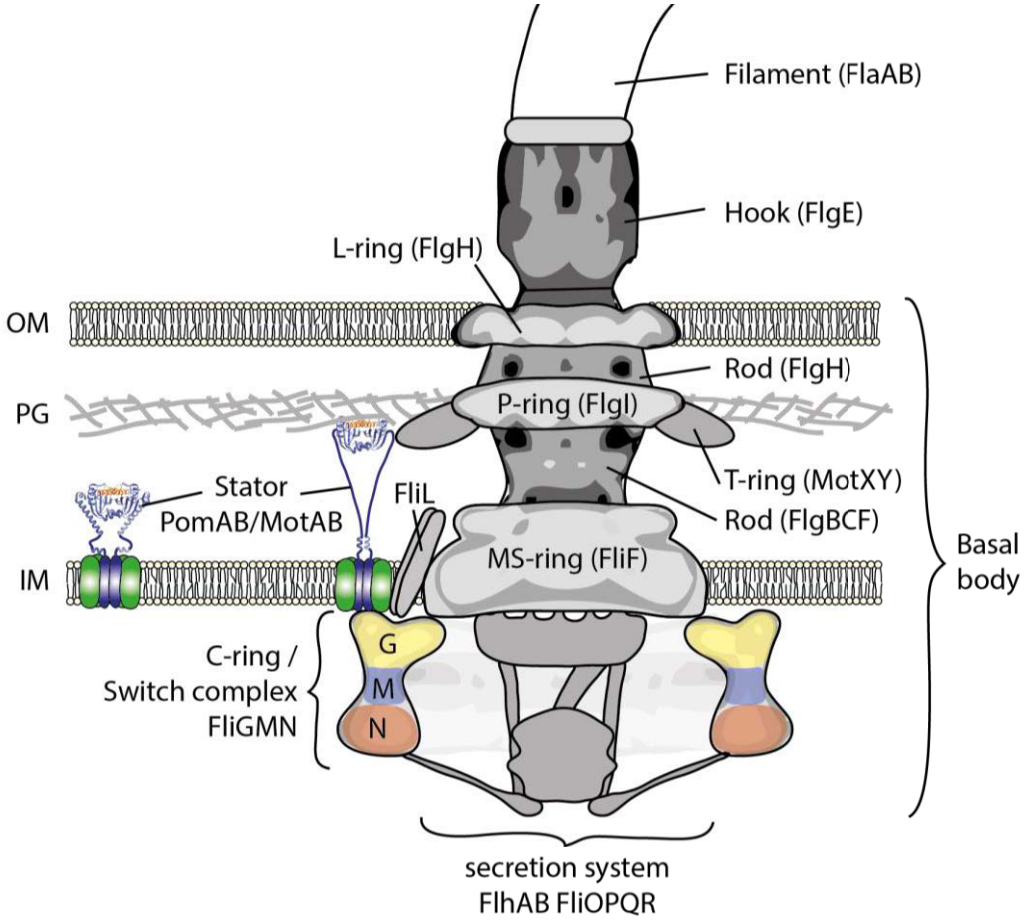

Figure 1: Simplified model of the core components of the flagellum. The flagellum consists of three main structures: The filament, the flexible hook and the basal body. The latter is composed of several ring structures, a central rod and also includes the motor that powers flagellar rotation. Torque is likely generated by the interaction of stators and the C-ring. OM = outer membrane; PG = peptidoglycan; CM = cytoplasmic membrane. Crystal structure modified from (Kojima et al. 2009).

block of the filament, its chaperone FliS and the cap structures for hook and filament are also produced in this class of flagellar genes. The last tier of flagellar genes are transcribed in a FliA-dependent manner. It also comprises the anti-sigma factor FlgM which represses FliA activity until the basal body and hook are assembled (Frisk et al. 2002; Kutsukake and Iino 1994). At that point FlgM is secreted and depleted from the cytoplasm. Furthermore, in the last tier alternative flagellins and the so-called stators are expressed. These latter components are either proton- or sodium ion-dependent channels composed of MotAB and PomAB, respectively. They are part of the rotary motor which converts ion flux across the cytoplasmic membrane into torque and thus powers rotation of the filament (Berg 2003; Minamino, Imada, and Namba 2008).

In addition to the mentioned proteins, the flagellar gene clusters of some bacteria encode additional structural components that are not part of the flagellum in all bacteria. In marine species such as *Vibrio* and *Shewanella,* MotXY forms the additional T-ring structure beneath the peptidoglycan layer and was shown to interact with PomAB (Okabe et al. 2002; Koerdt et al. 2009). *Vibrio* also possesses an additional ring structure flanking the L-ring termed H-ring (FlgO and FlgT), which is associated with the

T-ring, and a disk structure beneath the outer membrane composed of FlgP. These periplasmic structures are not found in most proton-dependent flagella such as the *Salmonella* strains. It has been speculated that these additional periplasmic components may be required for the basal body to withstand the high speed of the Na^+-driven motor and may allow generation of higher torque (Martinez et al. 2010; Terashima et al. 2013; Beeby et al. 2016).

The flagellar motor

Structure of the stator complexes

As previously mentioned, flagellar motility depends on the continuous rotation of the filament and thus on the function of its rotary motor. Like all other rotary motors, the flagellar motor consists of a static and a rotating part. The latter is composed of the MS- and C-ring whereas the former comprises complexes of two proteins: MotA and MotB in H^+-driven flagellar motors such as those of *Salmonella typhimurium*, *Escherichia coli* and the lateral flagellum of *S. putrefaciens* CN-32 or PomA and PomB in Na^+-driven motors such as the polar motors of *Vibrio cholerae* or *S. putrefaciens* CN-32 (see reviews by Thormann and Paulick 2010; Kojima 2015). The stator complexes surround the central rotor in a ring-like fashion. Since the structure of the complete stator complex has never been solved, current knowledge of the nature of the channel, conformational changes and torque generation is mostly based on mutational analysis, speed-torque calculations and mathematical models. Both stator types are similar in their structure and composition: each stator is a hetero-hexameric complex consisting of four A- and two B-subunits (Figure 2) (Sato and Homma 2000; Kojima and Blair 2004). MotA and PomA are composed of four membrane-embedded α-helices connected by two short periplasmic and a large cytoplasmic loop between

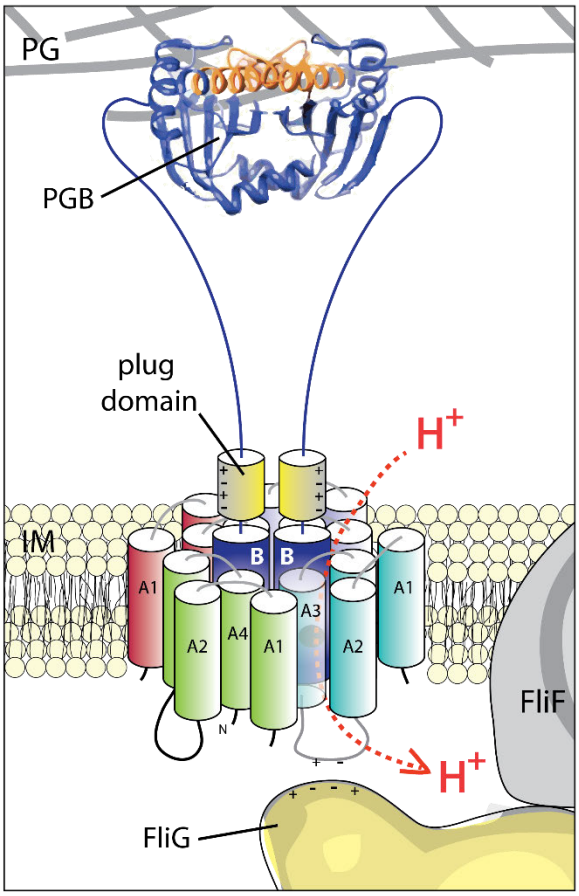

Figure 2: Model of the proposed stator composition and rotor-stator interaction. Each stator complex is formed by four A-subunits surrounding two B-subunits. MotA or PomA consist of four TMs (A1-4) while MotB or PomB consists of a single TM (dark blue) followed by the plug domain helix (yellow) and a large C-terminal part that includes OmpA C-like peptidoglycan binding domain (PGB). The ion-channel is assumed to be formed by the TM of the B-subunit and TM3 and TM4 of the A-subunit. The stators likely interact with FliG of the switch complex via electrostatic interactions. Crystal structure modified from (Kojima et al. 2009). PG = peptidoglycan; CM = cytoplasmic membrane.

transmembrane domain (TM) two and three. MotB and PomB contain a short cytoplasmic part, a single TM followed by the so-called plug domain and a C-terminal OmpA-like peptidoglycan-binding motif that anchors the stator to the cell wall (Dean et al. 1984; Chun and Parkinson 1988; De Mot and Vanderleyden 1994; Zhou, Fazzio, and Blair 1995; Sharp, Zhou, and Blair 1995b; Asai et al. 1997). Each stator forms two ion channels between the single TM of the B-subunit and TM3 and TM4 of the neighboring A-subunit (Stolz and Berg 1991; Braun et al. 2004). Stators that are not incorporated into the motor are thought to remain in a closed conformation. In these inactive precomplexes the plug domain, a short amphipathic alpha helix, was shown to be important for preventing premature ion flow through the stator. Only upon incorporation into the motor the stator channel is opened by a rearrangement of the stator that involves a drastic conformational change in the periplasmic part of the B-subunit (Hosking et al. 2006; Kojima et al. 2009; Li, Kojima, and Homma 2011; Zhu et al. 2014). In the channel, Asp32 of MotB was found to be essential for stator function and is proposed to be the ion-binding site of the stator (Kojima and Blair 2001). Tryptophan-scanning mutagenesis revealed a relatively hydrophobic channel surface with only few polar amino acid side chains (Sharp, Zhou, and Blair 1995a; Sharp, Zhou, and Blair 1995b).

Torque generation

A recent model developed by Nishihara and Kitao suggests that the channel formed by *E. coli* MotAB is usually in a closed conformation with a few water molecules entering from the cytoplasmic and periplasmic side. These water molecules are not forming a continuous water wire and are thus not able to transfer protons due to the gating function of Leu46 in MotB at the narrowest part of the channel. Protons can enter the channel and pass this gate by diffusion of H_3O^+. After entry of the channel, the H_3O^+ molecules reorients upon H-bonding with Ala39. This reorientation leads to the formation of a temporary water wire and the protonation of the conserved Asp32 residue of MotB likely via proton-hopping along the wire. The protonation of this aspartate causes H-bonding with the neighboring Asp170 of MotA which induces a straightening of TM3 of MotA. This segment is thought to exist in a kinked position starting from Pro173 as long as Asp32 is not protonated. The water wire collapses upon Asp32 deprotonation and further diffusion of the H_3O^+ molecule. As a consequence, TM3 returns into its kinked conformation and the chemomechanical cycle of the stator is completed (Nishihara and Kitao 2015). Contrary to this model, other studies propose a mechanism that depends on interaction of protonated Asp32 with the carbonyl group of Gly169. This interaction is thought to induce the kink, therefore, the TM3 is proposed to be in a straight conformation in the non-protonated state (Kim et al. 2008; Mandadapu et al. 2015). Both scenarios are predicted to result in a displacement of the cytoplasmic loop between TM2 and TM3. While Nishihara et al. propose this motion induces a

ratchet-like propulsion of the flagellum, most other recent studies suggest that rotation is generated by a powerstroke. This is experimentally supported by torque-speed measurements that result in concave-down shaped curves with two distinct regimes which match the powerstroke-model, but not the ratchet-model (Berry and Berg 1999; Chen and Berg 2000). At the first regime with low speed and high load, the speed seems to be determined by the number of stators and the overall ion-motive force rather than the rate of ion transfer. In the high speed (and low load) regime the flagellum can be rotated at maximum speed by a single stator. Here, the crossing of the ion through the channel, and consequently the dissociation of the proton, is rate limiting (see reviews by Morimoto and Minamino, 2014). The powerstroke model is further supported by studies that predict an electrostatic interaction between the cytoplasmic loop of MotA and the C-terminal part of FliG. In *E. coli*, these amino acids are Arg90 and Glu98 of MotA and Arg281, Asp288 and Asp289 of the C-terminal domain of FliG (Zhou and Blair 1997; Zhou, Lloyd, and Blair 1998). The replacement of single charged residues at this FliG-MotA interface with the opposite charge led to a strong suppression of motility. The same was observed for the exchange of charged residues with neutral ones in certain combinations. This led to the conclusion that several residues of the MotA loop and FliG interact electrostatically. None of the interactions is alone essential for motor function but together they likely provide the necessary attraction to transfer the displacement of the MotA loop onto the rotor ring. Similar constellations in the cytoplasmic loop and FliG can be found in Na^+-dependent motors, thus, both stator types presumably function based on the same mechanism (Yakushi et al. 2006; Takekawa et al. 2012).

Motor energetics

Motors powered by PomAB are recorded to reach high speeds with up to 1700 Hz while proton-driven motor rotate as fast as ~300 Hz (Magariyama et al. 1994; Yuan et al. 2008). The reason for this higher speed has, to my knowledge, not been addressed specifically. However, for both stators speed at a fixed load is proportional to the ion motive force. The sodium motive force (smf) was shown to reach -185 mV at pH 7 where the pmf is typically around -150 mV, thus, a higher speed in sodium-driven motors may partially be reached because of the higher smf (Gabel and Berg 2003; Lo et al. 2007). Several attempts have been made to calculate the amount of ions required for a single revolution of the rotor and to determine whether ion flow through the channel is tightly coupled or not. In the tight ion-coupling scenario each ion passing the channel would induce a chemomechanical cycle and cause the rotor to move one step. This would result in a high efficiency of the motor wasting almost no energy. A recent study calculated 37 ions per revolution which is in conflict with the observation that one revolution takes 26 steps (Berry and Berg 1999; Sowa et al. 2005; Lo et al. 2013). The 26 steps are consistent with the notion that the FliG ring is composed of 26 copies of FliG molecules (Francis et al.

1992; Oosawa, Ueno, and Aizawa 1994). A newer study revealed that the FliG ring of *Aquifex aeolicus* has a 34-fold symmetric ring of FliG molecules which would be closer to the calculated 37 ions in a tightly coupled motor (Lee et al. 2010). Another possible scenario that unites the 37 measured ions with the 26 molecule FliG ring is based on the assumption that both channels of a stator complex can but must not contribute to each powerstroke. In this flexible model two bound protons can induce a more forceful powerstroke than a single proton binding event but both contribute to motility under most conditions (Boschert, Adler, and Blair 2015).

As stated above, most of these models and predictions are based on biochemical and physiological measurements combined with computational modeling, and more structural data is needed to verify these statements.

Dynamic adaptation of flagellar function

Dynamical exchange of the flagellar motor

As mentioned previously, under low nutrient availability flagellar motility cuts a significant share out of the total energy budget of the cell, thus, the function has to be adjustable to the environmental circumstances to be of an overall benefit. One factor that was shown to be variable is the stator number and type (see reviews by Thormann and Paulick 2010; Kojima 2015). The adaptation of the motor is only possible if the stator ring composition is dynamic rather than fixed. Indeed, the stators were found to be surprisingly dynamic in terms of their dwell time at the flagellar motor. Up to 12 stator complexes surround the central rotor in a ring-like fashion (Khan, Khan, and Reese 1991; Reid et al. 2006). Fluorescence recovery after photobleaching (FRAP) analysis demonstrated that each stator complex remains in a fully assembled and rotating motor for ~30 seconds (Leake et al. 2006). The structural basis of incorporation of the stator into the motor, activation and deactivation are not well understood. This transient incorporation, however, allows a relatively quick modulation of flagella rotation by engaging and disengaging individual stator units. The number of stator clusters of *E. coli* and *Vibrio alginolyticus* was drastically reduced when the coupling ion was depleted or the channel blocked chemically, indicating that stator association with the motor is imf-dependent (Fukuoka et al. 2009; Tipping et al. 2013). At least in *E. coli* this disengagement was not induced by lack of rotation but by the inability to produce torque. Furthermore, this force was predicted to be sensed by the stator itself and responsible for recruitment of stators: At high loads the highest number of stators are found at the motor while rotation at low loads was supported by a single stator element (Tipping et al. 2013).

Besides the adjustment of stator number, some bacteria were found to possess and use alternative stator elements. Many species encode more stator sets than flagellar systems and may therefore drive rotation with more than one stator type (Thormann and Paulick 2010). *Bacillus subtilis* encodes a single peritrichous flagella system and two different stators: the H^+-dependent MotAB and Na^+-coupled MotPS. Under elevated viscosity, pH and Na^+-concentrations, MotPS contributes noticeable to motility, however, due to its slower speed its benefit is not obvious under the laboratory conditions tested (Ito et al. 2005). Interestingly, MotPS of the alkaliphilic bacterium *Bacillus alcalophilus* Vedder 1934 is thought to conduct Na^+, K^+ or Rb^+-ions. A single mutation in the TM of MotS abolishes the ability to use K^+ and Rb^+-ions. Sequence alignments of B-subunits indicated that MotS has a methionine (Met33) at the position where proton-driven MotAB possess a valine and sodium-dependent stators a leucine (Terahara, Sano, and Ito 2012). This position aligns to the predicted narrowest part of the stator channel (A-subunit: Val184 (TM3) and Thr209 (TM4); B-subunit: Leu42 and Leu46) of *E. coli*, and may contribute to gating. A further example of stator swapping is found in *S. oneidensis* MR-1, which encodes a polar flagellum along with a proton- (MotAB) and a sodium ion-dependent (PomAB) stator set. The latter is thought to be the native stator whereas the GC-content and homology of *motAB* suggest it to be acquired via lateral gene transfer. Under most conditions PomAB is found to be dominant, but at low sodium concentrations proton-powered MotAB is beneficial (Paulick et al. 2009).

Surprisingly, components of the switch ring were also found to be dynamic. In *E. coli,* a subpopulation of FliM from the C-ring was exchanged in a phosphorylated CheY-dependent manner (Delalez et al. 2010). Likewise, FliN, which binds to and stabilizes FliM, showed a similar turnover and is discussed to be exchanged together with FliM. Interestingly, the stoichiometry of FliN differs in motors locked in CCW or CW orientation (Delalez, Berry, and Armitage 2014). Whether the turnover of these components is important for motor switching is not known.

Chemo- and energy taxis

The most prominent adaptation of flagellar motility is the chemotactic response to repellents and attractants. The chemotaxis system of *E. coli* is one of the most comprehensively studied signaling system and will be introduced exemplarily. As bacterial cells are too small to sense a spatial gradient of a given substance along its cell body, navigation towards a favorable environment is conferred via a biased random walk in response to a temporal change in substance concentration. Switching between counterclockwise and clockwise rotation of the flagellum causes the cell to change direction of swimming and the intervals between switching events are controlled by the signaling network of the chemotaxis system (Wadhams and Armitage 2004; Sourjik and Wingreen 2012). Changes in an environmental signal are sensed by the methyl-accepting chemotaxis proteins (MCPs) which are

membrane-spanning chemoreceptors organized in large arrays of hexagonal units made of six trimers of dimers (Briegel et al. 2009; Sourjik and Armitage 2010). MCPs are connected to the histidine autokinase CheA via the coupling protein CheW. CheA autophosphorylation activity is dependent on the binding status of stimulants to the receptor domain of the MCPs. In the presence of an attractant, CheA activity is low and moderate in the absence of a stimulus. Upon binding of a repellent to the MCP, CheA activity is high. Autophopsphorylation enables CheA to transfer its phosphoryl group onto the response regulator CheY (Borkovich et al. 1989; Gegner et al. 1992; Parkinson 1993). In this state, CheY can bind to the N-terminal part of FliM of the switch complex and increase the probability of change of rotational direction (Welch et al. 1993; Bren and Eisenbach 1998). The phosphatase CheZ constantly dephosphorylates CheY and terminates its signal transmission (Hess et al. 1988). The response to an increasing concentration of attractants thus induces longer straight swimming periods due to the low CheA activity while repellents induce a higher switching frequency. To avoid a loss of sensitivity in an environment with a homogenous background stimulus, receptor sensitivity is modulated by the methyltesterase CheB and the methyltransferase CheR (Sherris and Parkinson 1981). Addition of methyl groups by CheR to the MCPs ultimately results in an increased activity of CheA. CheR methylates active MCPs while CheB on the other hand removes the methyl groups preferably from inactive MCPs. Since CheA activates CheB by phosphorylation, the demethylation can be regarded as a feedback loop. Thus, CheB and CheR are essential to ensure an exact adaptation to allow a restoration of the initial baseline tumbling frequency when a stimulus is present but unchanged over time (Sourjik and Berg 2002).

Although the signal transduction by the two-component phosphorelay found in *E. coli* is highly conserved in its core in most chemotactic bacteria, the MCPs and the chemotaxis adaptation system of many other species exhibit considerable variations or higher complexity. These differences may be based on the presence of redundant proteins, multiple copies of components or even entire systems or the replacement of single components by proteins that exert the same function (Szurmant and Ordal 2004; Wadhams and Armitage 2004). For example, as many other chemotactic bacteria, *B. subtilis* does not possess a copy of CheZ, its function is executed by FliY and CheC. *Heliobacter pylori*, on the other hand, encodes no CheB or CheR orthologue but three copies of CheV, a protein that can couple CheA to the MCPs (as CheW does) and is also involved in signal adaptation in *B. subtilis*. How CheV acts in *H. pylori* is, however, still unclear (Lertsethtakarn, Ottemann, and Hendrixson 2011). *Rhodobacter sphaeroides* encodes multiple copies of CheA, CheB, CheR, CheW and CheY as well as 13 putative MCPs in three different loci on the chromosome. Not all of them are required for normal chemotaxis but the signaling pathways formed by the appropriate components seem to be interconnected (Porter et al. 2002). The phosphorylation pattern of *B. subtilis* was found to be inverse to the one in *E. coli*: Addition of high concentrations of attractant stimulated CheA autophosphorylation activity, thus, a high

amount of CheY-P leads to CCW rotation of the flagellum and smooth swimming (Szurmant and Ordal 2004). The study of chemotaxis systems of further species will likely disclose additional variations.

A different approach on finding the optimal location is termed “energy taxis”. Cells monitor the internal energy level and adapt the tumbling frequency accordingly. Therefore, all metabolites that alter the metabolic rate and affect the electron transport system are indirectly integrated into this tactic response. Cues that can be sensed are related to the rate of the electron transport system, such as its redox state or the proton motif force itself (Alexandre, Greer-Phillips, and Zhulin 2004). Several studies have demonstrated how the redox status is sensed by Aer receptors (Gauden and Armitage 1995; Rebbapragada et al. 1997; Alexandre, Greer, and Zhulin 2000; Repik et al. 2000). The sensor that monitors the pmf remains to be identified. Although one sensing system is generally dominant in each species, all sensors of the chemotaxis and energy taxis systems ultimately contribute to the same CheY-P pool. Therefore, their activity may complement or antagonize each other but nevertheless result in one output (the reversal frequency) (Alexandre, Greer, and Zhulin 2000; Falke and Hazelbauer 2001).

Despite the mentioned differences in sensing and signal transduction, all bacteria have to ensure a correct localization and distribution of the chemotaxis components during cell division. Most of the MCPs organize into large and rather stable arrays at the pole of the cell. Other organisms like *R. sphaerioides* and *V. cholerae* express additional cytoplasmic receptors that form distinct cluster in the cytoplasm. Clustering of the membrane embedded receptors depends on CheA and CheW while the cytoplasmic arrays only seem to depend on CheW. Correct localization and assembly was shown to be important for correct chemotactic behavior (Maddock and Shapiro 1993; Harrison et al. 1999; Sourjik and Berg 2000; Bardy and Maddock 2005; Wadhams et al. 2005; Briegel et al. 2008; Schulmeister et al. 2008; Briegel et al. 2014). In *E. coli*, *n*ewly produced MCPs are inserted along the whole cell body and either nucleate into new cluster or join existing ones in a stochastic fashion (Thiem and Sourjik 2008). The intrinsic curvature of the dimer-timers of MCPs alone was suggested to be sufficient for favoring polar clustering and discouraging formation of lateral arrays (Endres 2009). Recent studies on *V. cholerae* and *Pseudomonas aeruginosa* demonstrate, however, that the number of cells with polar clusters of chemotaxis proteins decrease if the polar landmark proteins HubP and FlhF, respectively, are missing (Yamaichi et al. 2012; Kulasekara et al. 2013). Notably, *V. cholerae* and *P. aeruginosa* are polar-flagellated species, thus, the requirement of targeting systems for proper placement of the chemotaxis system may be connected to the flagellation pattern.

Landmark proteins in flagellar motility

Many processes in the bacterial cell require a spatiotemporal regulation of the respective components, including the regulation of expression, degradation and localization of proteins. This is particularly true for formation, maintenance and function of the flagellum. In nutrient-rich environments, the production of the flagellum as well as the perpetuation of rotation may be negligible in the total energy budget of the cell. However, under nutrient-limited conditions, the assembly of the flagellum itself may use up to more than 10% of the overall cellular carbon and the fraction of energy required for torque generation increases significantly compared to the total available energy (Mitchell 2002). Not only does this create pressure to select energy-efficient motors but may also favor a strict control of polar placement of the flagellum in rod-shaped cells which decreases the drag coefficient. Single-polarly flagellated organisms have developed specialized systems relying on so-called landmark proteins to target the flagellum to its position. The diversity of these polar positioning systems, together with other mechanisms of flagellar placement has been reviewed recently (Schuhmacher, Thormann, and Bange 2015). The following section will only address the systems relevant to motility of *Shewanella* and other γ-proteobacteria.

FlhF and FlhG

Most knowledge on the physiological role of FlhF and FlhG is based on studies on polar-flagellated monotrichious bacteria although both proteins are essential to establish the correct number and positioning of flagella in amphi-, peri- and lophoptrichious species as well (see review Schuhmacher, Thormann, and Bange 2015). In polar-flagellated monotrichious bacteria such as *Vibrio, Pseudomonas* and *Shewanella,* deletion of *flhF* frequently results in aflagellated cells and/or delocalization of flagella while its overexpression leads to a lophotrichous phenotype. Additionally, CheA of *Pseudomonas* is also found to be delocalized when *flhF* is deleted (Kulasekara et al. 2013). A lophotrichous flagellation pattern is also observed in the absence of *flhG* (Correa, Peng, and Klose 2005; Kusumoto et al. 2006; Kusumoto et al. 2008; Green et al. 2009; Gao et al. 2015; Ono et al. 2015; Schuhmacher et al. 2015). An early hypothesis outlined a scenario in which FlhF recruits components to the cell pole and is inhibited by capture through FlhG in the cytoplasm. Accordingly, a deletion of FlhG would result in an increase of FlhF at the pole and hence to an increase in flagella (Kusumoto et al. 2006). However, experimental evidence illustrating under which condition and at which cellular location FlhG and FlhF interact are currently lacking.

Several studies increased the body of knowledge during recent years with respect to structural information. FlhF is a signal recognition particle type GTPase while FlhG is a member of the MinD/ParA

ATPase flamily. Both belong to the signal recognition particle, MinD and BioD (SIMIBI)-type nucleoside triphosphate-binding proteins. For both proteins the crystal structure has been solved (Gert Bange et al. 2007; Schuhmacher et al. 2015). SIMIBI proteins require the presence of triggers, activators and effectors for correct function. The triggering mechanism for cell division regulator MinD for example was determined to be its interaction with phospholipids and only their presence as well as the bound nucleotide allow stable homodimer formation. The effector (e.g. MinC for MinD) has a rather passive role compared to the activator (e.g. MinE for MinD), which stimulates hydrolysis activity and thus induces the partition of the dimer (Bange and Sinning 2013). In case of FlhF and FlhG the nature of many of these factors is not clear. Similar to MinD, FlhG also possesses an amphipathic helix that can interact with the membrane. FlhF was observed to localize to the cell pole in several organisms by an unknown mechanism. In the GTP-bound dimeric form the N-terminus of FlhG stimulates GTP hydrolysis of FlhF, FlhG can thus be regarded as the activator of FlhF (Bange et al. 2011). Effector and activator of FlhG are currently not identified. FlhG has been shown to bind to the N-terminal EIDAL motif of FliM, but this interaction was shown to be independent of nucleotide-binding. In vitro, FlhG enhances binding of FliM/FliY (FliN) complexes to FliG of *B. subtilis*. As FlhG can also interact with FlhF in the presence of lipids and ATP, it is speculated that the formation of the switch ring may be coordinated by FlhG in a lipid- and ATP-dependent manner. Interestingly, the deletion of FliM or the deletion of its EIDAL motif phenocopies the deletion of *flhG*, thus, the localization and/or function of FlhG may depend on its interaction with FliM (Schuhmacher et al. 2015).

HubP and FimV

While flagella placement and number are regulated by FlhFG in many species, the recruitment of other components required in motility to the pole, e.g. the chemotaxis system, by this system was only described for *Pseudomonas*. In *Vibrio*, another protein termed HubP, was found to be required for polar localization (Yamaichi et al. 2012). HubP is a protein of >150 kDa with a potential LysM peptidoglycane binding domain at its N-terminus, a transmembrane domain and a large cytoplasmic part that harbors multiple highly acidic repeats. These traits are also found in the homolog FimV of *P. aeruginosa,* TspA of *Neisseria* and putative homologs of FimV of *Legionella pneumophila* and *S. putrefaciens* CN-32 (Semmler et al. 2000). HubP, TspA and FimV proteins may therefore be homologs that convey a different set of functions in each species. All mentioned proteins were implied to participate in type-IV pili mediated twitching motility (Wehbi et al. 2011; Semmler et al. 2000). In addition, *fimV* deletions altered the morphology of *P. aeruginosa* and *L. pneumphila*, pigmentation in *L. pneumphila* and type-II-secretion system dependent protein secretion in *P. aeruginosa* (Semmler et al. 2000; Coil and Anné 2010; Michel et al. 2011). HubP does not only coordinate the localization of

chemotaxis components but seems to be required for multiple other processes. For example, it also coordinates the correct placement of the ParA-like ATPase ParC and ParP. The latter one was found to promote localization and stability of the arrays through its interaction with CheA (Ringgaard et al. 2014). HubP is furthermore involved in polar positioning of the ATPase ParA1 to the pole (Yamaichi et al. 2012). ParA1 is a homolog of the bacterial plasmid partitioning protein and targets chromosome I of *V. cholerae* to the old pole of the cell after cell division. ParA1 interacts with ParB1, which in turn can bind to a distinct site on the chromosome called *parS*1. ParA1 forms a filament that pulls ParB1 and the chromosome to the pole through its depolymerisation (Fogel and Waldor 2006). In addition to the chromosome segregation process, HubP is also involved in modulating the localization of FlhF and FlhG at the pole. How and whether that affects the function of and interaction between FlhF and FlhG is currently under investigation.

Aims

Flagellar motility has been studied for decades as it has important implications for bacterial spreading and proliferation. However, several aspects are still not well understood.

The function of the stator and its interaction with the motor under different condition is one of these aspects. This is especially true for bacterial species with an uneven ratio of stator sets to flagellar systems, which are, although widespread within the kingdom of bacteria, addressed by only a small number of studies limited to a few species. The first part of this thesis (chapter 2 and 3) aims to:

I. Analyze the benefits provided by the potentially acquired stator MotAB.

This aspect is addressed in the second chapter by determining the speeds of *S. oneidensis* MR-1 cells encoding both or one stator set under high and low Na^+ concentrations.

Furthermore, the third chapter focuses on:

II. The potentially acquired stator MotAB of *S. oneidensis* MR-1 is functionally characterized under increased viscosity or decreased oxygen concentration in the environment.
III. Mutated versions of MotAB that exhibit distinct characteristics under these conditions are identified and one of them is compared in detail with the wild type stator.

The fourth chapter is dedicated to the analysis of how polarity is established in *S. putrefaciens* CN-32, with an emphasis on flagellar and chemotaxis components. As described in the introduction, localization of the chemotaxis system in *Pseudomonas*, but not in *Vibrio*, relies on FlhF. In *V. cholerae*

the landmark protein HubP was shown be required for correct placement of the chemotaxis components. In *Shewanella*, a close relative to *Vibrio* and *Pseudomonas*, the chemotaxis components reside at the same pole as the polar flagellum but the mechanisms that recruit both to that site have not been elucidated yet. Therefore, the fourth chapter aims to determine:

IV. How are the polar flagellum and the chemotaxis system recruited to the cell pole in *S. putrefaciens* CN-32?

V. Which further components are recruited to the cell pole by HubP?

As my contribution to this study was the analysis of the swimming and twitching motility of *S. putrefaciens* CN-32 as well as the localization of the chemotaxis components and the chromosome partitioning system in dependence of HubP, the final discussion in this dissertation will only focus on these aspects.

Sources

Alexandre, G., S. E. Greer, and I. B. Zhulin. 2000. “Energy Taxis Is the Dominant Behavior in Azospirillum Brasilense.” *Journal of Bacteriology* 182 (21): 6042–48. doi:10.1128/JB.182.21.6042-6048.2000.

Alexandre, G., S. Greer-Phillips, and I. B. Zhulin. 2004. “Ecological Role of Energy Taxis in Microorganisms.” *FEMS Microbiology Reviews*. doi:10.1016/j.femsre.2003.10.003.

Altegoer, F., and G. Bange. 2015. “Undiscovered Regions on the Molecular Landscape of Flagellar Assembly.” *Curr Opin Microbiol* 28: 98–105. doi:10.1016/j.mib.2015.08.011.

Asai, Y., S. Kojima, H. Kato, N. Nishioka, I. Kawagishi, and M. Homma. 1997. “Putative Channel Components for the Fast-Rotating Sodium-Driven Flagellar Motor of a Marine Bacterium.” *J Bacteriol* 179 (16): 5104–10.

Bange, G., N. Kummerer, P. Grudnik, R. Lindner, G. Petzold, D. Kressler, E. Hurt, K. Wild, and I. Sinning. 2011. “Structural Basis for the Molecular Evolution of SRP-GTPase Activation by Protein.” *Nat Struct Mol Biol* 18 (12): 1376–80. doi:10.1038/nsmb.2141.

Bange, G., G. Petzold, K. Wild, and I. Sinning. 2007. “Expression, Purification and Preliminary Crystallographic Characterization of FlhF from Bacillus Subtilis.” *Acta Crystallographica Section F Structural Biology And Crystallization Communications* 64: 449–51. doi:10.1107/S1744309108000924.

Bange, G., and I. Sinning. 2013. “SIMIBI Twins in Protein Targeting and Localization.” *Nature Structural & Molecular Biology* 20 (7): 776–80. doi:10.1038/nsmb.2605.

Bardy, S. L., and J. R. Maddock. 2005. “Polar Localization of a Soluble Methyl-Accepting Protein of Pseudomonas Aeruginosa.” *Journal of Bacteriology* 187 (22): 7840–44. doi:10.1128/JB.187.22.7840-7844.2005.

Bardy, S. L., S. Y. Ng, and K. F. Jarrell. 2003. “Prokaryotic Motility Structures.” *Microbiology*. doi:10.1099/mic.0.25948-0.

Beeby, M., D. A. Ribardo, C. A. Brennan, E. G. Ruby, and G. J. Jensen. 2016. “Diverse High-Torque Bacterial Flagellar Motors Assemble Wider Stator Rings Using a Conserved Protein Scaffold,” *Proceedings of the National Academy of Sciences of the United States of America* 113 doi:10.1073/pnas.1518952113.

Berg, H. C. 2003. “The Rotary Motor of Bacterial Flagella.” *Annual Review of Biochemistry* 72: 19–54. doi:10.1146/annurev.biochem.72.121801.161737.

Berry, R. M., and H. C. Berg. 1999. “Torque Generated by the Flagellar Motor of Escherichia Coli While Driven Backward.” *Biophysical Journal* 76 (1 Pt 1): 580–87. doi:10.1016/S0006-3495(99)77226-7.

Bilchik, A. J., M. DiNome, S. S., R. R. Turner, D. Wiese, M. McCarter, D. S. Hoon, and D. L. Morton. 2006. “Prospective Multicenter Trial of Staging Adequacy in Colon Cancer: Preliminary Results.” *Arch Surg* 141 (6): 524–27. doi:10.1001/archsurg.141.6.527.

Borkovich, K., N. Kaplan, J. F. Hess, and M. I. Simon. 1989. “Transmembrane Signal Transduction in Bacterial Chemotaxis Involves Ligand-Dependent Activation of Phosphate Group Transfer.” *Proceedings of the National Academy of Sciences of the United States of America* 86 (4): 1208–12. doi:10.1073/pnas.86.4.1208.

Boschert, R., F. R. Adler, and D. F. Blair. 2015. “Loose Coupling in the Bacterial Flagellar Motor.” *Proceedings of the National Academy of Sciences of the United States of America* 112 (15): 4755–60. doi:10.1073/pnas.1419955112.

Braun, T. F., L. Q. Al-Mawsawi, S. Kojima, and D. F. Blair. 2004. “Arrangement of Core Membrane

Segments in the MotA/MotB Proton-Channel Complex of Escherichia Coli." *Biochemistry* 43 (1): 35–45. doi:10.1021/bi035406d.

Bren, A., and M. Eisenbach. 1998. "The N Terminus of the Flagellar Switch Protein, FliM, Is the Binding Domain for the Chemotactic Response Regulator, CheY." *Journal of Molecular Biology* 278 (3): 507–14. doi:10.1006/jmbi.1998.1730.

Briegel, A., M. S. Ladinsky, C. Oikonomou, C. W. Jones, M. J. Harris, D. J. Fowler, Y. W. Chang, L. K. Thompson, J. P. Armitage, and G. J. Jensen. 2014. "Structure of Bacterial Cytoplasmic Chemoreceptor Arrays and Implications for Chemotactic Signaling." *eLife* 2014 (3): 1–16. doi:10.7554/eLife.02151.

Briegel, A., Z. Li, J. Werner, Z. Gitai, R. B. Jensen, and G. J. Jensen. 2008. "Location and Architecture of the Caulobacter Crescentus Chemoreceptor Array." *Molecular Microbiology* 69 (1): 30–41. doi:10.1111/j.1365-2958.2008.06219.x.

Briegel, A., D. R. Ortega, E. I. Tocheva, K. Wuichet, Z. Li, S. Chen, A. Müller, et al. 2009. "Universal Architecture of Bacterial Chemoreceptor Arrays." *Proceedings of the National Academy of Sciences of the United States of America* 106 (40): 17181–86. doi:10.1073/pnas.0905181106.

Bubendorfer, S., S. Held, N. Windel, A. Paulick, A. Klingl, and K. M. Thormann. 2012. "Specificity of Motor Components in the Dual Flagellar System of Shewanella Putrefaciens CN-32." *Mol Microbiol* 83 (2): 335–50. doi:10.1111/j.1365-2958.2011.07934.x.

Bubendorfer, S., M. Koltai, F. Rossmann, V. Sourjik, and K. M. Thormann. 2014. "Secondary Bacterial Flagellar System Improves Bacterial Spreading by Increasing the Directional Persistence of Swimming." *Proceedings of the National Academy of Sciences of the United States of America* 111 (31): 11485–90. doi:10.1073/pnas.1405820111.

Chen, X., and H. C. Berg. 2000. "Torque-Speed Relationship of the Flagellar Rotary Motor of Escherichia Coli." *Biophysical Journal* 78 (2): 1036–41. doi:10.1016/S0006-3495(00)76662-8.

Chun, S. Y., and J. S. Parkinson. 1988. "Bacterial Motility: Membrane Topology of the Escherichia Coli MotB Protein." *Science* 239 (4837): 276–78. doi:10.1126/science.2447650.

Coil, D. A., and J. Anné. 2010. "The Role of fimV and the Importance of Its Tandem Repeat Copy Number in Twitching Motility, Pigment Production, and Morphology in Legionella Pneumophila." *Archives of Microbiology* 192: 625–31. doi:10.1007/s00203-010-0590-8.

Correa, N. E., F. Peng, and K. E. Klose. 2005. "Roles of the Regulatory Proteins FlhF and FlhG in the Vibrio Cholerae Flagellar Transcription Hierarchy" *Journal of Bacteriology* 187 (18): 6324–32. doi:10.1128/JB.187.18.6324.

Dasgupta, N., M. C. Wolfgang, A. L. Goodman, S. K. Arora, J. Jyot, S. Lory, and R. Ramphal. 2003. "A Four-Tiered Transcriptional Regulatory Circuit Controls Flagellar Biogenesis in Pseudomonas Aeruginosa." *Molecular Microbiology* 50 (3): 809–24. doi:10.1046/j.1365-2958.2003.03740.x.

De Mot, R., and J. Vanderleyden. 1994. "The C-Terminal Sequence Conservation between OmpA-Related Outer Membrane Proteins and MotB Suggests a Common Function in Both Gram-Positive and Gram- Negative Bacteria, Possibly in the Interaction of These Domains with Peptidoglycan." *Molecular Microbiology* 12 (2): 333–34. doi:10.1111/j.1365-2958.1994.tb01021.x.

Dean, G. E., R. M. Macnab, J. Stader, P. Matsumura, and C. Burks. 1984. "Gene Sequence and Predicted Amino Acid Sequence of the motA Protein, a Membrane-Associated Protein Required for Flagellar Rotation in Escherichia Coli." *Journal of Bacteriology* 159 (3): 991–99.

Delalez, N. J., G. H. Wadhams, G. Rosser, Q. Xue, M. T. Brown, I. M. Dobbie, R. M. Berry, M. C. Leake, and J. P. Armitage. 2010. "Signal-Dependent Turnover of the Bacterial Flagellar Switch Protein

FliM." *Proceedings of the National Academy of Sciences of the United States of America* 107 (25): 11347–51. doi:10.1073/pnas.1000284107.

Delalez, N. J., R. M. Berry, and J. P. Armitage. 2014. "Stoichiometry and Turnover of the Bacterial Flagellar Switch Protein FliN." *mBio* 5 (4). doi:10.1128/mBio.01216-14.

Endres, R. G. 2009. "Polar Chemoreceptor Clustering by Coupled Trimers of Dimers." *Biophysical Journal* 96 (2): 453–63. doi:10.1016/j.bpj.2008.10.021.

Falke, J. J., and G. L. Hazelbauer. 2001. "Transmembrane Signaling in Bacterial Chemoreceptors." *Trends in Biochemical Sciences*. doi:10.1016/S0968-0004(00)01770-9.

Fogel, M. A., and M. K. Waldor. 2006. "A Dynamic, Mitotic-like Mechanism for Bacterial Chromosome Segregation." *Genes and Development* 20 (23): 3269–82. doi:10.1101/gad.1496506.

Francis, N. R., V. M. Irikura, S. Yamaguchi, D. J. DeRosier, and R. M. Macnab. 1992. "Localization of the Salmonella Typhimurium Flagellar Switch Protein FliG to the Cytoplasmic M-Ring Face of the Basal Body." *Proceedings of the National Academy of Sciences of the United States of America* 89 (14): 6304–8. doi:10.1073/pnas.89.14.6304.

Frisk, A., J. Jyot, S. K. Arora, and R. Ramphal. 2002. "Identification and Functional Characterization of flgM, a Gene Encoding the Anti-Sigma 28 Factor in Pseudomonas Aeruginosa." *J Bacteriol* 184 (6): 1514–21. doi:10.1128/JB.184.6.1514-1521.2002.

Fukuoka, H., T. Wada, S. Kojima, A. Ishijima, and M. Homma. 2009. "Sodium-Dependent Dynamic Assembly of Membrane Complexes in Sodium-Driven Flagellar Motors." *Molecular Microbiology* 71 (4): 825–35. doi:10.1111/j.1365-2958.2008.06569.x.

Gabel, C. V., and H. C. Berg. 2003. "The Speed of the Flagellar Rotary Motor of Escherichia Coli Varies Linearly with Protonmotive Force." *Proceedings of the National Academy of Sciences of the United States of America* 100: 8748–51. doi:10.1073/pnas.1533395100.

Gao, T., M. Shi, L. Ju, and H. Gao. 2015. "Investigation into FlhFG Reveals Distinct Features of FlhF in Regulating Flagellum Polarity in Shewanella Oneidensis." *Molecular Microbiology* 98 (3): 571–85. doi:10.1111/mmi.13141.

Gauden, D. E., and J. P. Armitage. 1995. "Electron Transport-Dependent Taxis in Rhodobacter Sphaeroides." *Journal of Bacteriology* 177 (20): 5853–59.

Gegner, J. A., D. R. Graham, A. F. Roth, and F. W. Dahlquist. 1992. "Assembly of an MCP Receptor, CheW, and Kinase CheA Complex in the Bacterial Chemotaxis Signal Transduction Pathway." *Cell* 70 (6): 975–82. doi:10.1016/0092-8674(92)90247-A.

Green, J. C. D., C. Kahramanoglou, A. Rahman, A. M.C. Pender, N. Charbonnel, and G. M. Fraser. 2009. "Recruitment of the Earliest Component of the Bacterial Flagellum to the Old Cell Division Pole by a Membrane-Associated Signal Recognition Particle Family GTP-Binding Protein." *Journal of Molecular Biology* 391 (4). Elsevier Ltd: 679–90. doi:10.1016/j.jmb.2009.05.075.

Harrison, D. M., J. Skidmore, J. P. Armitage, and J. R. Maddock. 1999. "Localization and Environmental Regulation of MCP-like Proteins in Rhodobacter Sphaeroides." *Molecular Microbiology* 31 (3): 885–92. doi:10.1046/j.1365-2958.1999.01226.x/full/.

Hess, J. F., K. Oosawa, N. Kaplan, and M. I. Simon. 1988. "Phosphorylation of Three Proteins in the Signaling Pathway of Bacterial Chemotaxis." *Cell* 53: 79–87. doi:10.1016/0092-8674(88)90489-8.

Hosking, E. R., C. Vogt, E. P. Bakker, and M. D. Manson. 2006. "The Escherichia Coli MotAB Proton Channel Unplugged." *J Mol Biol* 364 (5): 921–37. doi:DOI 10.1016/j.jmb.2006.09.035.

Ito, M., N. Terahara, S. Fujinami, and T. A. Krulwich. 2005. "Properties of Motility in Bacillus Subtilis

Powered by the H+-Coupled MotAB Flagellar Stator, Na+-Coupled MotPS or Hybrid Stators MotAS or MotPB." *J Mol Biol* 352 (2): 396–408. doi:10.1016/j.jmb.2005.07.030.

Jarrell, K. F., and M. J. McBride. 2008. "The Surprisingly Diverse Ways That Prokaryotes Move." *Nature Reviews. Microbiology* 6 (6): 466–76. doi:10.1038/nrmicro1900.

Jones, C. J., M. Homma, and R. M. Macnab. 1989. "L-, P-, and M-Ring Proteins of the Flagellar Basal Body of Salmonella Typhimurium: Gene Sequences and Deduced Protein Sequences." *Journal of Bacteriology* 171 (7): 3890–3900.

Khan, S., I. H. Khan, and T. S. Reese. 1991. "New Structural Features of the Flagellar Base in Salmonella Typhimurium Revealed by Rapid-Freeze Electron Microscopy." *Journal of Bacteriology* 173 (9): 2888–96.

Kim, E. A., M. Price-Carter, W. C. Carlquist, and D. F. Blair. 2008. "Membrane Segment Organization in the Stator Complex of the Flagellar Motor: Implications for Proton Flow and Proton-Induced Conformational Change." *Biochemistry* 47 (43): 11332–39. doi:10.1021/bi801347a.

Klose, K. E., and J. J. Mekalanos. 1998. "Distinct Roles of an Alternative Sigma Factor during Both Free-Swimming and Colonizing Phases of the Vibrio Cholerae Pathogenic Cycle." *Molecular Microbiology* 28 (3): 501–20. doi:10.1046/j.1365-2958.1998.00809.x.

Koerdt, A., A. Paulick, M. Mock, K. Jost, and K. M. Thormann. 2009. "MotX and MotY Are Required for Flagellar Rotation in Shewanella Oneidensis MR-1." *Journal of Bacteriology* 191 (16): 5085–93. doi:10.1128/JB.00206-09.

Kojima, S., and D. F. Blair. 2004. "Solubilization and Purification of the MotA/MotB Complex of Escherichia Coli." *Biochemistry* 43 (1): 26–34. doi:10.1021/bi035405l.

Kojima, S., K. Imada, M. Sakuma, Y. Sudo, C. Kojima, T. Minamino, M. Homma, and K. Namba. 2009. "Stator Assembly and Activation Mechanism of the Flagellar Motor by the Periplasmic Region of MotB." *Mol Microbiol* 73 (4): 710–18. doi:10.1111/j.1365-2958.2009.06802.x.

Kojima, S.. 2015. "Dynamism and Regulation of the Stator, the Energy Conversion Complex of the Bacterial Flagellar Motor." *Current Opinion in Microbiology*. doi:10.1016/j.mib.2015.07.015.

Kojima, S., and D. F. Blair. 2001. "Conformational Change in the Stator of the Bacterial Flagellar Motor." *Biochemistry* 40 (43): 13041–50. doi:10.1021/bi011263o.

Kojima, S., K. Imada, M. Sakuma, Y. Sudo, C. Kojima, T. Minamino, M. Homma, and K. Namba. 2009. "Stator Assembly and Activation Mechanism of the Flagellar Motor by the Periplasms Region of MotB." *Molecular Microbiology* 73 (4): 710–18. doi:10.1111/j.1365-2958.2009.06802.x.

Kulasekara, B. R., C. Kamischke, H. D. Kulasekara, M. Christen, P. A. Wiggins, and S. I. Miller. 2013. "C-Di-GMP Heterogeneity Is Generated by the Chemotaxis Machinery to Regulate Flagellar Motility." *eLife* 2: e01402. doi:10.7554/eLife.01402.

Kusumoto, A., K. Kamisaka, T. Yakushi, H. Terashima, A. Shinohara, and M. Homma. 2006. "Regulation of Polar Flagellar Number by the flhF and flhG Genes in Vibrio Alginolyticus." *Journal of Biochemistry* 139 (1): 113–21. doi:10.1093/jb/mvj010.

Kusumoto, A., A. Shinohara, H. Terashima, S. Kojima, T. Yakushi, and M. Homma. 2008. "Collaboration of FlhF and FlhG to Regulate Polarflagella Number and Localization in Vibrio Alginolyticus." *Microbiology* 154 (5): 1390–99. doi:10.1099/mic.0.2007/012641-0.

Kutsukake, K., and T. Iino. 1994. "Role of the FliA-FlgM Regulatory System on the Transcriptional Control of the Flagellar Regulon and Flagellar Formation in Salmonella Typhimurium." *Journal of Bacteriology* 176 (12): 3598–3605.

Leake, M. C., J. H. Chandler, G. H. Wadhams, F. Bai, R. M. Berry, and J. P. Armitage. 2006. “Stoichiometry and Turnover in Single, Functioning Membrane Protein Complexes.” *Nature* 443 (7109): 355–58. doi:10.1038/nature05135.

Lee, L. K., M. A. Ginsburg, C. Crovace, M. Donohoe, and D. Stock. 2010. “Structure of the Torque Ring of the Flagellar Motor and the Molecular Basis for Rotational Switching.” *Nature* 466 (7309): 996–1000. doi:10.1038/nature09300.

Lertsethtakarn, P., K. M. Ottemann, and D. R. Hendrixson. 2011. “Motility and Chemotaxis in Campylobacter and Helicobacter.” *Annual Review of Microbiology* 65 (1): 389–410. doi:10.1146/annurev-micro-090110-102908.

Li, N., S. Kojima, and M. Homma. 2011. “Characterization of the Periplasmic Region of PomB, a Na+-Driven Flagellar Stator Protein in Vibrio Alginolyticus.” *J Bacteriol* 193 (15): 3773–84. doi:Doi 10.1128/Jb.00113-11.

Lo, C.-J., M. C. Leake, T. Pilizota, and R. M. Berry. 2007. “Nonequivalence of Membrane Voltage and Ion-Gradient as Driving Forces for the Bacterial Flagellar Motor at Low Load.” *Biophysical Journal* 93 (1): 294–302. doi:10.1529/biophysj.106.095265.

Lo, C.-J., Y. Sowa, T. Pilizota, and R. M. Berry. 2013. “Mechanism and Kinetics of a Sodium-Driven Bacterial Flagellar Motor.” *Proceedings of the National Academy of Sciences of the United States of America* 110: E2544–51. doi:10.1073/pnas.1301664110.

Macnab, R. M. and S. Aizawa. 1984. “Bacterial Motility and the Bacterial Flagellar Motor.” *Annu Rev Biophys Bioeng* 13: 51–83.

Macnab, R. M. and S. Aizawa. 1984. “Bacterial Motility and the Bacterial Flagellar Motor.” *Annu Rev Biophys Bioeng* 13: 51–83. doi:10.1146/annurev.bb.13.060184.000411.

Maddock, J. R. and L. Shapiro. 1993. “Polar Location of the Chemoreceptor Complex in the Escherichia Coli Cell.” *Science (New York, N.Y.)* 259 (5102): 1717–23. doi:10.1126/science.8456299.

Magariyama, Y., S. Sugiyama, K. Muramoto, Y. Maekawa, I. Kawagishi, Y. Imae, and S. Kudo. 1994. “Very Fast Flagellar Rotation.” *Nature* 371 (6500): 752.

Mandadapu, K. K., J. A. Nirody, R. M. Berry, and G. Oster. 2015. “Mechanics of Torque Generation in the Bacterial Flagellar Motor.” *Proceedings of the National Academy of Sciences* 112 (32): E4381–89. doi:10.1073/pnas.1501734112.

Martinez, R. M., B. A. Jude, T. J. Kirn, K. Skorupski, and R. K. Taylor. 2010. “Role of FlgT in Anchoring the Flagellum of Vibrio Cholerae.” *Journal of Bacteriology* 192 (8): 2085–92. doi:10.1128/JB.01562-09.

Martinez, V. A., J. Schwarz-Linek, M. Reufer, L. G. Wilson, A. N. Morozov, and W.C. K. Poon. 2014. “Flagellated Bacterial Motility in Polymer Solutions.” *Proceedings of the National Academy of Sciences of the United States of America* 111 (50): 17771–76. doi:10.1073/pnas.1415460111.

Michel, G. P. F., A. Aguzzi, G. Ball, C. Soscia, S. Bleves, and R. Voulhoux. 2011. “Role of fimV in Type II Secretion System-Dependent Protein Secretion of Pseudomonas Aeruginosa on Solid Medium.” *Microbiology (Reading, England)* 157 (Pt 7): 1945–54. doi:10.1099/mic.0.045849-0.

Minamino, T., and K. Imada. 2015. “The Bacterial Flagellar Motor and Its Structural Diversity.” *Trends Microbiol* 23 (5): 267–74. doi:10.1016/j.tim.2014.12.011.

Minamino, T., S. Yamaguchi, and R. M. Macnab. 2000. “Interaction between FliE and FlgB, a Proximal Rod Component of the Flagellar Basal Body of Salmonella.” *Journal of Bacteriology* 182 (11): 3029–36.

Minamino, T., K. Imada, and K. Namba. 2008. “Molecular Motors of the Bacterial Flagella.” *Current Opinion in Structural Biology* 18 (Figure 3): 693–701. doi:10.1016/j.sbi.2008.09.006.

Mitchell, J. G. 2002. “The Energetics and Scaling of Search Strategies in Bacteria.” *The American Naturalist* 160 (6): 727–40. doi:10.1086/343874.

Morimoto, Y., and T. Minamino. 2014. “Structure and Function of the Bi-Directional Bacterial Flagellar Motor.” *Biomolecules* 4 (1): 217–34. doi:10.3390/biom4010217.

Muller, V., C. J. Jones, I. Kawagishi, S. Aizawa, and R. M. Macnab. 1992. “Characterization of the fliE Genes of Escherichia Coli and Salmonella Typhimurium and Identification of the FliE Protein as a Component of the Flagellar Hook-Basal Body Complex.” *J Bacteriol* 174 (7): 2298–2304.

Nishihara, Y., and A. Kitao. 2015. “Gate-Controlled Proton Diffusion and Protonation-Induced Ratchet Motion in the Stator of the Bacterial Flagellar Motor.” *Proceedings of the National Academy of Sciences*, 201502991. doi:10.1073/pnas.1502991112.

Okabe, M., T. Yakushi, M. Kojima, and M. Homma. 2002. “MotX and MotY, Specific Components of the Sodium-Driven Flagellar Motor, Colocalize to the Outer Membrane in Vibrio Alginolyticus.” *Molecular Microbiology* 46 (1): 125–34. doi:10.1046/j.1365-2958.2002.03142.x.

Ono, H., A. Takashima, H. Hirata, M. Homma, and S. Kojima. 2015. “The MinD Homolog FlhG Regulates the Synthesis of the Single Polar Flagellum of Vibrio Alginolyticus.” *Molecular Microbiology* 98 (1): 130–41. doi:10.1111/mmi.13109.

Oosawa, K., T. Ueno, and S. Aizawa. 1994. “Overproduction of the Bacterial Flagellar Switch Proteins and Their Interactions with the MS Ring Complex in Vitro.” *Journal of Bacteriology* 176 (12): 3683–91.

Parkinson, J. S. 1993. “Signal Transduction Schemes of Bacteria.” *Cell* 73 (5): 857–71. doi:10.1016/0092-8674(93)90267-T.

Partridge, J. D., V. Nieto, and R. M. Harshey. 2015. “A New Player at the Flagellar Motor: FliL Controls Both Motor Output and Bias.” *mBio* 6 (2). doi:10.1128/mBio.02367-14.

Paulick, A., A. Koerdt, J. Lassak, S. Huntley, I. Wilms, F. Narberhaus, and K. M. Thormann. 2009. “Two Different Stator Systems Drive a Single Polar Flagellum in Shewanella Oneidensis MR-1.” *Mol Microbiol* 71 (4): 836–50. doi:10.1111/j.1365-2958.2008.06570.x.

Paulick, A., A. Koerdt, J. Lassak, S. Huntley, I. Wilms, F. Narberhaus, and K. M. Thormann. 2009. “Two Different Stator Systems Drive a Single Polar Flagellum in Shewanella Oneidensis MR-1.” *Molecular Microbiology* 71 (4): 836–50. doi:10.1111/j.1365-2958.2008.06570.x.

Porter, S. L., A. V. Warren, A. C. Martin, and J. P. Armitage. 2002. “The Third Chemotaxis Locus of Rhodobacter Sphaeroides Is Essential for Chemotaxis.” *Molecular Microbiology* 46 (4): 1081–94. doi:10.1046/j.1365-2958.2002.03218.x.

Prouty, M. G., N. E. Correa, and K. E. Klose. 2001. “The Novel sigma54- and sigma28-Dependent Flagellar Gene Transcription Hierarchy of Vibrio Cholerae.” *Mol Microbiol* 39 (6): 1595–1609.

Rebbapragada, A., M. S. Johnson, G. P. Harding, A. J. Zuccarelli, H. M. Fletcher, I. B. Zhulin, and B. L. Taylor. 1997. “The Aer Protein and the Serine Chemoreceptor Tsr Independently Sense Intracellular Energy Levels and Transduce Oxygen, Redox, and Energy Signals for Escherichia Coli Behavior.” *Proceedings of the National Academy of Sciences of the United States of America* 94 (20): 10541–46. doi:10.1073/pnas.94.20.10541.

Reid, S. W., M. C. Leake, J. H. Chandler, C.-J. Lo, J. P. Armitage, and R. M. Berry. 2006. “The Maximum Number of Torque-Generating Units in the Flagellar Motor of Escherichia Coli Is at Least 11.” *Proceedings of the National Academy of Sciences of the United States of America* 103 (21): 8066–

71. doi:10.1073/pnas.0509932103.

Repik, A., A. Rebbapragada, M. S. Johnson, J. Ö. Haznedar, I. B. Zhulin, and B. L. Taylor. 2000. “PAS Domain Residues Involved in Signal Transduction by the Aer Redox Sensor of Escherichia Coli.” *Molecular Microbiology* 36 (4): 806–16. doi:10.1046/j.1365-2958.2000.01910.x.

Ringgaard, S., M. Zepeda-Rivera, X. Wu, K. Schirner, B. M. Davis, and M. K. Waldor. 2014. “ParP Prevents Dissociation of CheA from Chemotactic Signaling Arrays and Tethers Them to a Polar Anchor.” *Proceedings of the National Academy of Sciences of the United States of America* 111 (2): E255–64. doi:10.1073/pnas.1315722111.

Ritchings, B. W., E. C. Almira, S. Lory, and R. Ramphal. 1995. “Cloning and Phenotypic Characterization of fleS and fleR, New Response Regulators of Pseudomonas Aeruginosa Which Regulate Motility and Adhesion to Mucin.” *Infection and Immunity* 63: 4868–76.

Saijo-Hamano, Y., N. Uchida, K. Namba, and K. Oosawa. 2004. “In Vitro Characterization of FlgB, FlgC, FlgF, FlgG, and FliE, Flagellar Basal Body Proteins of Salmonella.” *Journal of Molecular Biology* 339 (2): 423–35. doi:10.1016/j.jmb.2004.03.070.

Sato, K., and M. Homma. 2000. “Functional Reconstitution of the Na+-Driven Polar Flagellar Motor Component of Vibrio Alginolyticus.” *Journal of Biological Chemistry* 275 (8): 5718–22. doi:10.1074/jbc.275.8.5718.

Schuhmacher, J. S., F. Rossmann, F. Dempwolff, C. Knauer, F. Altegoer, W. Steinchen, A. K. Dörrich, et al. 2015. “MinD-like ATPase FlhG Effects Location and Number of Bacterial Flagella during C-Ring Assembly.” *Proceedings of the National Academy of Sciences* 112 (10): 201419388. doi:10.1073/pnas.1419388112.

Schuhmacher, J. S., K.M. Thormann, and G. Bange. 2015. “How Bacteria Maintain Location and Number of Flagella?” *FEMS Microbiology Reviews*, no. May: fuv034. doi:10.1093/femsre/fuv034.

Schulmeister, S., M. Ruttorf, S. Thiem, D. Kentner, D. Lebiedz, and V. Sourjik. 2008. “Protein Exchange Dynamics at Chemoreceptor Clusters in Escherichia Coli.” *Proceedings of the National Academy of Sciences of the United States of America* 105 (17): 6403–8. doi:10.1073/pnas.0710611105.

Semmler, A. B. T., C. B. Whitchurch, A. J. Leech, and J. S. Mattick. 2000. “Identification of a Novel Gene, fimV, Involved in Twitching Motility in Pseudomonas Aeruginosa.” *Microbiology* 146 (6): 1321–32.

Sharp, L. L., J. Zhou, and D. F. Blair. 1995a. “Features of MotA Proton Channel Structure Revealed by Tryptophan-Scanning Mutagenesis.” *Proceedings of the National Academy of Sciences of the United States of America* 92 (17): 7946–50. doi:10.1073/pnas.92.17.7946.

Sharp, L. L., J. Zhou, and D. F. Blair. 1995b. “Tryptophan-Scanning Mutagenesis of MotB, an Integral Membrane Protein Essential for Flagellar Rotation in Escherichia Coli.” *Biochemistry* 34 (28): 9166–71. doi:7619816.

Sherris, D., and J. S. Parkinson. 1981. “Posttranslational Processing of Methyl-Accepting Chemotaxis Proteins in Escherichia Coli.” *Proceedings of the National Academy of Sciences of the United States of America* 78 (10): 6051–55. doi:10.1073/pnas.78.10.6051.

Sourjik, V., and N. S. Wingreen. 2012. “Responding to Chemical Gradients: Bacterial Chemotaxis.” *Current Opinion in Cell Biology* 24 (2): 262–68. doi:DOI 10.1016/j.ceb.2011.11.008.

Sourjik, V., and J. P. Armitage. 2010. “Spatial Organization in Bacterial Chemotaxis.” *The EMBO Journal* 29 (16): 2724–33. doi:10.1038/emboj.2010.178.

Sourjik, V., and H. C. Berg. 2002. “Receptor Sensitivity in Bacterial Chemotaxis.” *Proceedings of the National Academy of Sciences of the United States of America* 99 (1): 123–27.

doi:10.1073/pnas.011589998.

Sourjik, V., and H. C. Berg. 2000. “Localization of Components of the Chemotaxis Machinery of Escherichia Coli Using Fluorescent Protein Fusions.” *Molecular Microbiology* 37 (4): 740–51. doi:10.1046/j.1365-2958.2000.02044.x.

Sowa, Y., A. D. Rowe, M. C. Leake, T. Yakushi, M. Homma, A. Ishijima, and R. M. Berry. 2005. “Direct Observation of Steps in Rotation of the Bacterial Flagellar Motor.” *Nature* 437 (7060): 916–19. doi:10.1038/nature04003.

Starnbach, M. N., and S. Lory. 1992. “The fliA (rpoF) Gene of Pseudomonas Aeruginosa Encodes an Alternative Sigma Factor Required for Flagellin Synthesis.” *Molecular Microbiology* 6 (4): 459–69.

Stolz, B., and H. C. Berg. 1991. “Evidence for Interactions between MotA and MotB, Torque-Generating Elements of the Flagellar Motor of Escherichia Coli.” *Journal of Bacteriology* 173 (21): 7033–37.

Syed, K. A., S. Beyhan, N. Correa, J. Queen, J. Liu, F. Peng, K. J. Satchell, F. Yildiz, and K. E. Klose. 2009. “The Vibrio Cholerae Flagellar Regulatory Hierarchy Controls Expression of Virulence Factors.” *J Bacteriol* 191 (21): 6555–70. doi:10.1128/JB.00949-09.

Szurmant, H., and G. W. Ordal. 2004. “Diversity in Chemotaxis Mechanisms among the Bacteria and Archaea.” *Microbiology and Molecular Biology Reviews : MMBR* 68 (2): 301–19. doi:10.1128/MMBR.68.2.301-319.2004.

Takekawa, N., N. Li, S. Kojima, and M. Homma. 2012. “Characterization of PomA Mutants Defective in the Functional Assembly of the Na+-Driven Flagellar Motor in Vibrio Alginolyticus.” *Journal of Bacteriology* 194: 1934–39. doi:10.1128/JB.06552-11.

Terahara, N., M. Sano, and M. Ito. 2012. “A Bacillus Flagellar Motor That Can Use Both Na+ and K+ as a Coupling Ion Is Converted by a Single Mutation to Use Only Na+.” *PLoS ONE* 7 (9). doi:10.1371/journal.pone.0046248.

Terashima, H., N. Li, M. Sakuma, M. Koike, S. Kojima, M. Homma, and K. Imada. 2013. “Insight into the Assembly Mechanism in the Supramolecular Rings of the Sodium-Driven Vibrio Flagellar Motor from the Structure of FlgT.” *Proceedings of the National Academy of Sciences of the United States of America* 110 (15): 6133–38. doi:10.1073/pnas.1222655110.

Thiem, S., and V. Sourjik. 2008. “Stochastic Assembly of Chemoreceptor Clusters in Escherichia Coli.” *Molecular Microbiology* 68 (5): 1228–36. doi:10.1111/j.1365-2958.2008.06227.x.

Thormann, K. M., and A. Paulick. 2010. “Tuning the Flagellar Motor.” *Microbiology*. doi:10.1099/mic.0.029595-0.

Tipping, M. J., B. C. Steel, N. J. Delalez, R. M. Berry, and J. P. Armitage. 2013. “Quantification of Flagellar Motor Stator Dynamics through in Vivo Proton-Motive Force Control.” *Molecular Microbiology* 87 (2): 338–47. doi:10.1111/mmi.12098.

Wadhams, G. H., and J. P. Armitage. 2004. “Making Sense of It All: Bacterial Chemotaxis.” *Nature Reviews. Molecular Cell Biology* 5 (12): 1024–37. doi:10.1038/nrm1524.

Wadhams, G. H., A. C. Martin, A. V. Warren, and J. P. Armitage. 2005. “Requirements for Chemotaxis Protein Localization in Rhodobacter Sphaeroides.” *Molecular Microbiology* 58 (3): 895–902. doi:10.1111/j.1365-2958.2005.04880.x.

Wehbi, H., E. Portillo, H. Harvey, A. E. Shimkoff, E. M. Scheurwater, P. L. Howell, and L. L. Burrows. 2011. “The Peptidoglycan-Binding Protein FimV Promotes Assembly of the Pseudomonas Aeruginosa Type IV Pilus Secretin.” *Journal of Bacteriology* 193 (2): 540–50. doi:10.1128/JB.01048-10.

Welch, M., K. Oosawa, S. Aizawa, and M. Eisenbach. 1993. “Phosphorylation-Dependent Binding of a Signal Molecule to the Flagellar Switch of Bacteria.” *Proceedings of the National Academy of Sciences of the United States of America* 90 (October): 8787–91. doi:10.1073/pnas.90.19.8787.

Yakushi, T., J. Yang, H. Fukuoka, M. Homma, and D. F. Blair. 2006. “Roles of Charged Residues of Rotor and Stator in Flagellar Rotation: Comparative Study Using H+-Driven and Na+-Driven Motors in Escherichia Coli.” *Journal of Bacteriology* 188 (4): 1466–72. doi:10.1128/JB.188.4.1466-1472.2006.

Yamaichi, Y., R. Bruckner, S. Ringgaard, A. Möll, D. E. Cameron, A. Briegel, G. J. Jensen, B. M. Davis, and M. K. Waldor. 2012. “A Multidomain Hub Anchors the Chromosome Segregation and Chemotactic Machinery to the Bacterial Pole.” *Genes and Development* 26 (20): 2348–60. doi:10.1101/gad.199869.112.

Yuan, J., J. Yuan, and Howard C Berg. 2008. “Resurrection of the Flagellar Rotary Motor near Zero Load.” *Proceedings of the National Academy of Sciences of the United States of America* 105 (4): 1182–85. doi:10.1073/pnas.0711539105.

Zhou, J., and D. F. Blair. 1997. “Residues of the Cytoplasmic Domain of MotA Essential for Torque Generation in the Bacterial Flagellar Motor.” *Journal of Molecular Biology* 273: 428–39. doi:10.1006/jmbi.1997.1316.

Zhou, J., S. A. Lloyd, and D. F. Blair. 1998. “Electrostatic Interactions between Rotor and Stator in the Bacterial Flagellar Motor.” *Proc Natl Acad Sci U S A* 95 (11): 6436–41. doi:DOI 10.1073/pnas.95.11.6436.

Zhou, J., R. T. Fazzio, and D. F. Blair. 1995. “Membrane Topology of the MotA Protein of *Escherichia Coil*.” *Journal of Molecular Biology* 251 (2): 237–42.

Zhu, S., M. Takao, N. Li, M. Sakuma, Y. Nishino, M. Homma, S. Kojima, and K. Imada. 2014. “Conformational Change in the Periplamic Region of the Flagellar Stator Coupled with the Assembly around the Rotor.” *Proceedings of the National Academy of Sciences of the United States of America* 111 (37): 13523–28. doi:10.1073/pnas.1324201111.

Zuberi, A. R., C. Ying, D. S. Bischoff, and G. W. Ordal. 1991. “Gene-Protein Relationships in the Flagellar Hook-Basal Body Complex of Bacillus Subtilis: Sequences of the flgB, flgC, flgG, fliE and fliF Genes.” *Gene* 101: 23–31. doi:10.1016/0378-1119(91)90220-6.

Chapter 2

Research article (published in *Molecular Microbiology)*

Dual stator dynamics in the Shewanella oneidensis MR-1 flagellar motor.

Anja Paulick[a,#,*], Nicolas J. Delalez[c,e,#], Susanne Brenzinger[a,b], Bradley C. Steel[d], Richard M. Berry[d], Judith P. Armitage[c] and Kai M. Thormann[a,b,*]

Mol Microbiol. 2015 Jun; 96(5):993-1001. [PMID:25727785]

a) Max-Planck-Institut für terrestrische Mikrobiologie, Department of Ecophysiology, 35043 Marburg, Germany
b) Justus-Liebig-Universität Gießen, Department of Microbiology and Molecular Biology at the IFZ, 35392 Gießen, Germany
c) University of Oxford, Biochemistry Department, Oxford OX1 3QU, United Kingdom
d) University of Oxford, Physics Department, Oxford OX1 3QU, United Kingdom
e) current address: School of Life Sciences, University of Warwick, Gibbet Hill Campus, Coventry CV4 7AL, UK
[#] these authors contributed equally to this study

Contributions:

A.P. designed the study, performed laboratory experiments (strain constructions, stoichiometry, stator dynamics and immunofluorescence analysis), evaluated the data and wrote the manuscript.

N.J.D. designed the study, performed laboratory experiments (stoichiometry and stator dynamics), evaluated the data and wrote the manuscript.

S.B. designed the study, performed laboratory experiments (determination of swimming speed), evaluated the data and wrote the manuscript.

B.C.S. evaluated the data.

R.M.B. designed the study and wrote the manuscript.

J.P.A. designed the study and wrote the manuscript.

K.M.T. designed the study and wrote the manuscript.

Molecular Microbiology (2015) 96(5), 993–1001 ■
doi:10.1111/mmi.12984
First published online 31 March 2015

Dual stator dynamics in the *Shewanella oneidensis* MR-1 flagellar motor

Anja Paulick,[1,*,#,‡] Nicolas J. Delalez,[2,†,‡] Susanne Brenzinger,[1,3] Bradley C. Steel,[4] Richard M. Berry,[4] Judith P. Armitage[2] and Kai M. Thormann[1,3*]

[1]*Max-Planck-Institute für terrestrische Mikrobiologie, Department of Ecophysiology, 35043 Marburg, Germany.*

[2]*Biochemistry Department, University of Oxford, Oxford OX1 3QU, UK.*

[3]*Justus-Liebig-Universität Gießen, Department of Microbiology and Molecular Biology at the IFZ, Gießen 35392, Germany.*

[4]*Physics Department, University of Oxford, Oxford OX1 3QU, UK.*

Summary

The bacterial flagellar motor is an intricate nanomachine which converts ion gradients into rotational movement. Torque is created by ion-dependent stator complexes which surround the rotor in a ring. *Shewanella oneidensis* MR-1 expresses two distinct types of stator units: the Na^+-dependent $PomA_4B_2$ and the H^+-dependent $MotA_4B_2$. Here, we have explored the stator unit dynamics in the MR-1 flagellar system by using mCherry-labeled PomAB and MotAB units. We observed a total of between 7 and 11 stator units in each flagellar motor. Both types of stator units exchanged between motors and a pool of stator complexes in the membrane, and the exchange rate of MotAB, but not of PomAB, units was dependent on the environmental Na^+-levels. In 200 mM Na^+, the numbers of PomAB and MotAB units in wild-type motors was determined to be about 7:2 (PomAB:MotAB), shifting to about 6:5 without Na^+. Significantly, the average swimming speed of MR-1 cells at low Na^+ conditions was increased in the presence of MotAB. These data strongly indicate that the *S. oneidensis* flagellar motors simultaneously use H^+ and Na^+ driven stators in a configuration governed by MotAB incorporation efficiency in response to environmental Na^+ levels.

Accepted 26 February, 2015. *For correspondence. E-mail kai.thormann@mikro.bio.uni-giessen.de; Tel. (+49) 064 1993 5545; Fax (+49) 064 1993 5549 and E-mail Anja.Paulick@synmikro.mpi-marburg.mpg.de; Tel. (+49) 0642 1282 1482; Fax (+49) 064212821485. Present address: #Max-Planck-Intitut für terrestrische Mikrobiologie & LOEWE Research Center for Synthetic Microbiology, Department of Systems and Synthetic Microbiology, 35043 Marburg, Germany. †School of Life Sciences, University of Warwick, Gibbet Hill Campus, Coventry CV4 7AL, UK. ‡These authors contributed equally to this study.

Introduction

Many bacterial species are motile by means of flagella, long rotating helical filaments extending from the cell body which allow highly efficient movement through liquid environments or across surfaces. The bacterial flagellar motor which drives flagellar rotation is an intricate nanomachine which is embedded in the cell envelope and consists of at least 13 different proteins at various stoichiometries (Berg, 2003). This rotary machine is fueled by ion flux across the membrane. Most flagellar motors, such as the paradigm systems of *Escherichia coli* or *Salmonella* sp., are powered by H^+ gradients (Manson *et al*., 1977; Blair, 2003). However, the flagellar motors of several other species use Na^+ as the coupling ion, particularly those of alkaliphilic or marine bacteria, such as *Vibrio* and some *Bacillus* sp. (Hirota *et al*., 1981; Yorimitsu and Homma, 2001). Two major components of the flagellar motor, the rotor and the stator, are required to convert ion flux into rotational movement (reviewed in (Minamino *et al*., 2008; Sowa and Berry, 2008; Stock *et al*., 2012)). The C ring, or 'switch complex', is the cytoplasmic part of the rotor and consists of multiple copies of the proteins FliG, FliM, and FliN arranged in a ring-like structure of about 50 nm in diameter. FliM can interact with the phosphorylated response regulator CheY and thereby links the flagellar motors to the chemotaxis system (reviewed in (Porter *et al*., 2011; Sourjik and Wingreen, 2012)). The second major part of the motor, the stator, consists of individual stator units surrounding the rotor in a ring. The stator units are bound to the peptidoglycan to allow generation of torque to effectively rotate the flagellar filament. An individual stator unit is a complex composed of two different subunits, typically named MotA and MotB in H^+-dependent motors and PomA and PomB in Na^+-powered motors, in a 4A-2B stoichiometry forming two ion-specific channels (Sato and Homma, 2000; Braun *et al*., 2004; Kojima and Blair, 2004). Ion flux is thought to result in conformational changes of the stator unit which are translated into rotational movement by electrostatic

interactions of MotA/PomA with FliG in the rotor complex (Minamino *et al*., 2008; Sowa and Berry, 2008).

Several studies have provided evidence that the composition of the stator ring is highly dynamic. Controlled ectopic production of stator units in tethered *E. coli* cells whose motors operate at high load resulted in a characteristic stepwise increase in flagellar rotation speed, strongly indicating successive incorporation of stator units into the flagellar motor in a process referred to as 'resurrection' (Block and Berg, 1984; Blair and Berg, 1988). The number of discrete increments and direct quantification by fluorescence microscopy determined the maximal number of torque-generating stator units within a single *E. coli* flagellar motor to be at least 11 (Leake *et al*., 2006; Reid *et al*., 2006). In addition, the stator units within the motor constantly exchange with a pool of stator complexes at a turnover time of about 30 s while the flagellum continues to rotate (Leake *et al*., 2006). This pool of pre-stators is localized in the cytoplasmic membrane, and a so-called 'plug domain' prevents premature ion leakage prior to incorporation into the flagellar motor (Hosking *et al*., 2006; Li *et al*., 2011). The rate of stator incorporation into the flagellar motor is governed by at least two different factors. For both the H^+-driven *E. coli* MotAB stator and its Na^+-dependent counterpart PomAB in *Vibrio alginolyticus*, functional incorporation into the motor depends on the corresponding ion motive force, pmf and smf, respectively (Fung and Berg, 1995; Sowa *et al*., 2005; Fukuoka *et al*., 2009; Tipping *et al*., 2013b). In addition, recent studies showed that the number of units within the *E. coli* flagellar stator ring increases with the amount of load acting on the flagellar motor (Lele *et al*., 2013; Tipping *et al*., 2013a). Thus, the composition of the stator ring and motor performance can be adjusted appropriately according to the environmental conditions.

While most bacterial species use a single type of stator units (either MotAB or PomAB) to operate a corresponding flagellar system, a number of bacteria harbor two or more types of stator units to drive rotation of a single flagellar motor system (reviewed in (Thormann and Paulick, 2010)). Among those are species, such as *Bacillus subtilis* and *Shewanella oneidensis* MR-1, which possess functional Na^+- and H^+-dependent stator complexes (Ito *et al*., 2004; 2005; Paulick *et al*., 2009). In *S. oneidensis* MR-1, Na^+-dependent PomAB, present in all members of the genus *Shewanella*, is the main stator, whereas H^+-driven MotAB was likely acquired by horizontal gene transfer (Paulick *et al*., 2009). Fluorescently tagged PomAB localized to the flagellated cell pole at high and low environmental Na^+ concentrations, whereas localization of H^+-dependent MotAB-mCherry stator units at the flagellated cell pole was observed only under conditions of low Na^+. The pattern of stator localization strongly suggested co-occurrence of both stators in the flagellar motor in a subpopulation of cells at low Na^+ levels (Paulick *et al*., 2009). This implicated that the flagellar motors of *S. oneidensis* MR-1 may be concurrently powered by Na^+- and H^+-gradients similar to what has recently been demonstrated for a genetically engineered flagellar system in *E. coli* (Sowa *et al*., 2014). In this study, we used fluorescence microscopy on functional, fluorescently labeled PomAB or MotAB stator units to determine the composition of and the protein exchange in the stator ring of the *S. oneidensis* MR-1 flagellar system. We found that both PomAB and MotAB are dynamically exchanged in the flagellar motor. In the wild type, the stator ring consists of both PomAB and MotAB units in a configuration which depends on the environmental Na^+ levels. The results indicate the presence of a hybrid-fueled flagellar motor in *S. oneidensis* MR-1 and demonstrate how a newly acquired component can mechanistically upgrade a molecular machine.

Results

Stator abundance and turnover in a PomAB-driven flagellar motor

A number of studies suggest that stator-rotor configurations in bacterial flagellar systems are highly dynamic. Based on our earlier observations, we hypothesized that this would similarly apply to the dual stator system of *S. oneidensis* MR-1 and might be exploited by this species to adjust flagellar functions according to environmental Na^+ levels. To determine stator number and turnover in the stator ring of the flagellar motor, we constructed C-terminal fluorophor fusions of MotB or PomB. Due to the periplasmic localization of both PomB and MotB C-termini, mCherry was used as fluorophor which is folded and fluorescent after export from the cytoplasm. Both fusions were chromosomally integrated into *S. oneidensis* MR-1 to replace the corresponding native genes. Immunofluorescence analysis revealed that the fusions were stably produced and only minor degradation occurred with MotB-mCherry (Fig. S1). Both fusion proteins mediated robust swimming as demonstrated by motility assays (Fig. S2).

The Na^+-dependent stator PomAB is present in all species of *Shewanella* and represents the dominant unit for driving rotation of the polar flagellar filament in MR-1. Therefore, we first determined the number and turnover of stator units in a flagellar motor driven by PomAB only (*ΔmotAB pomB-mCherry*) at high (200 mM NaCl) and low Na^+ concentration (0 mM NaCl). Under both conditions, polar foci were observed in about 75% of the cells. Immunoblotting analysis showed a significantly lower total concentration of PomB in cells grown at low Na^+ levels (Fig. S1). To analyze the stoichiometry of PomB-mCherry proteins, we performed stepwise photobleaching experiments on stationary polar fluorescent foci which were

considered to be part of the stator ring system (Leake *et al*., 2006) (Fig. S3A). As each stator unit contains two B-subunits, the number of PomAB stator units within the flagellar motor was determined to be 7 ± 2 in the presence of 200 mM Na^+ (Fig. 1A; Table S1). Under conditions of low Na^+ levels, 8 ± 3 PomAB stator units were observed to be present in the motor. In addition, we observed high lateral mobility of stator complexes all over the cell surface, consistent with a diffusing pool of stators in the membrane.

To explore the dynamics of PomAB stator complexes within the flagellar motor, we performed **F**lourescence **R**ecovery **A**fter **P**hotobleaching (FRAP) experiments on the PomB-mCherry cluster at the cell pole (Fig. 1A, right panel, Table S2; Fig S3B). Fluorescence recovery under conditions of high Na^+ occurred at an estimated rate of 0.023 s^{-1} (half-time of about 31 s) and was not significantly different from that at low Na^+ levels (0.029 s^{-1}; half time about 33 s). Notably, while the rate of fluorescence recovery was consistent, the maximal level of fluorescence recovery varied between cells and rarely reached more then about 60 % of the prebleaching signal intensity at both high and low Na^+ levels. This finding strongly suggested that, while a major fraction of the PomAB stators is undergoing dynamic exchange, some units are not turned over or turned over only at a very slow rate.

Thus, in the absence of MotAB, about 8 PomAB stator units are present in the *S. oneidensis* MR-1 flagellar motor. At least a fraction of the PomAB units is constantly exchanged with units from outside the motor structure, while a separate fraction appears to remain more stably in the motor. The environmental Na^+ levels and the overall PomAB abundance had no significant effect on the number of units within the motor or their average exchange rate.

Stator abundance and turnover in a MotAB-driven flagellar motor

We then used the same system to determine stator number and turnover within the flagellar motor with Mot-stator units only. To this end, we constructed a *S. oneidensis* MR-1 strain in which *pomAB* was deleted and *motB* was fused to *mCherry* (*ΔpomAB motB-mCherry*). As observed for PomB-mCherry, the overall amount of MotB-mCherry was lower under conditions of low Na^+ (Fig. S1). Irrespective of the Na^+ levels, MotB-mCherry localized to the cell pole in about 80 % of the cells. Quantification of the stator units by stepwise photobleaching revealed that, under conditions of high Na^+, 8 ± 3 MotAB stator units reside in the stator ring of the flagellar motor (Fig. 1B, left panel; Table S1). At low Na^+ levels, the number of MotAB units increased to 11 ± 3. This higher number of MotAB stator units in the flagellar motor compared to that of PomAB units (about 8) might indicate that, under the conditions tested, not all potential vacant positions in the stator ring are occupied by PomAB or that the MotAB stators do not diffuse far from the motor. FRAP experiments strongly indicated that the MotAB units are also constantly exchanged (Fig. 1B, right panel). In contrast to PomAB-driven motors, fluorescence recovered to higher levels, suggesting that a greater number, or even the whole population, of MotAB units within the motor is exchanged. Under conditions of low Na^+ concentrations fluorescence recovered at a rate of 0.030 s^{-1} (half-time 36 s), at high Na^+ levels recovery occurred about two times faster (0.055 s^{-1}; half time 16 s). Taken together, the results indicate that the stator ring of the *S. oneidensis* MR-1 flagellar motor might contain up to 11 units. The MotAB stator units in the motor are turned over at a rate comparable to that of the dynamic fraction of PomAB units. As opposed to the PomAB units, the exchange rate of MotAB increases at high levels of Na^+.

The presence of both PomAB and MotAB enhances stator exchange

Having defined the number and turnover of stator units for flagellar motors with either PomAB or MotAB, we determined these parameters in motors with both stators present. Immunodetection revealed that amount and stability of neither PomB-mCherry nor MotB-mCherry was affected by the presence of the other stator in cells of the appropriate strains (*pomB-mCherry* and *motB-mCherry*; Fig. S1). In the presence of MotAB at high Na^+ concentrations, the number of PomAB stator units in the motor was determined to be 7 ± 2 (Fig. 1C; Table S1). At low Na^+ levels, the number of PomAB stators was slightly lower at 6 ± 2. Notably, compared to motors in which MotAB was absent, the turnover of PomAB stator units within the motor was only slightly increased under high (recovery rate 0.041 s^{-1}; half time 25 s) but was significantly faster at low Na^+ levels (0.09 s^{-1}; half time 9 s). FRAP analysis indicated that, as found in *ΔmotAB pomB-mCherry* cells, in the presence of both PomAB and MotAB stators only a subpopulation of PomAB units appears to be dynamically exchanged. Turnover was also drastically increased for the MotAB complexes in the presence of PomAB. Under both conditions of high and low Na^+ concentrations, fluorescence recovery occurred too quickly to obtain reliable measurements. The estimated number of MotAB stator units in the motor was 2 ± 1 at high Na^+ levels and increased to 5 ± 2 when Na^+ levels were low.

These findings suggest that the presence of both MotAB and PomAB units results in a competition for recruitment into the flagellar motor and significantly increases the rate of stator unit exchange. The estimation of the stator unit numbers within the motor strongly indicates that PomAB and MotAB units are simultaneously present in the flagellar

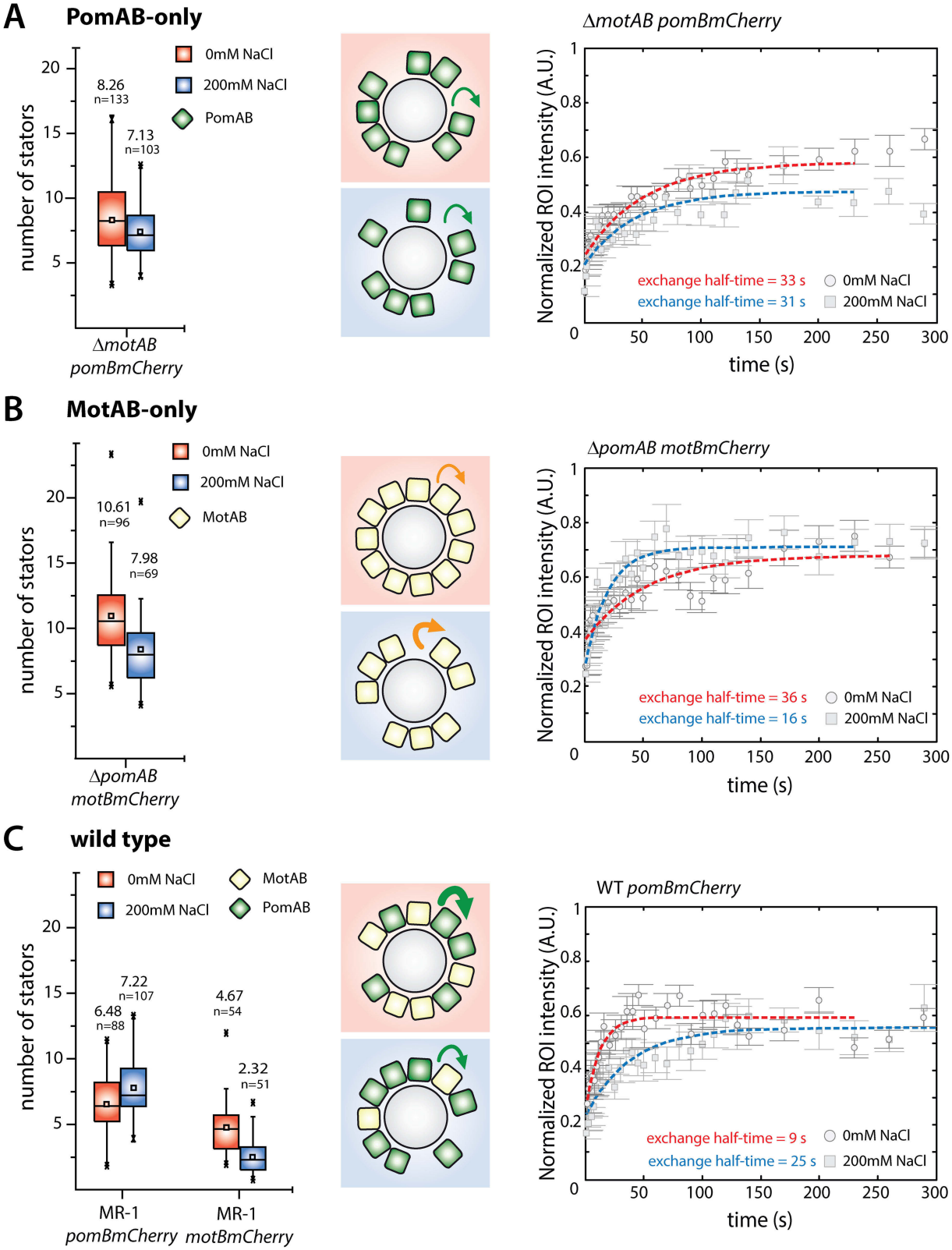

Fig. 1. Quantity and exchange half-time of stators in *S. oneidensis* MR-1 flagellar motors driven by PomAB only (A), MotAB only (B) and in the presence of both PomAB and MotAB (wild type, C). Left panel: quantification of single PomB- and MotBmCherry molecules at 0 mM (red) and 200 mM NaCl (blue) in *ΔmotABpomBmCherry*, *ΔpomABmotBmCherry*, and the wild type (from top to bottom). The number of single mCherry molecules was calculated by the number of distinct steps in intensity loss during photobleaching. The estimated number of stators is presented in a box-whisker-plot, with the box representing the middle 50 % of the data. The average and the median number of stators are shown as '□' and '—', respectively. The whiskers denote the data range of the 5th and 95th percentile. Middle panel: Cartoon displaying the estimated rotor-stator configuration at low (red background) and high (blue background) Na^+ concentrations. The stators are indicated as colored rectangles (dark green, PomAB; yellow, MotAB) surrounding the rotor (grey circle). The thickness of the arrow indicates the rate of stator exchange under the corresponding conditions. Right panel: Rate of stator exchange as determined by FRAP. The normalized averaged fluorescence intensity is displayed as a function of time for PomB- and MotBmCherry in *ΔmotAB pomBmCherry* (D) and *ΔpomAB motBmCherry* (F), respectively, at 0 mM ('o') and 200 mM NaCl ('□'). The exchange half-times were obtained by fitting an exponential decay to the averaged normalized fluorescence intensity of clusters of three cells with a similar recovery intensity for at least 5 independent clusters (Table S2). Error bars indicate the standard error of the mean. Note that the exchange half-time of MotB-mCherry in wild-type cells was not determined because the exchange occurred too quickly to obtain reliable measurements.

motor of *S. oneidensis* MR-1. Both exchange rate and stoichiometry depend on the environmental Na^+ concentration. Since in PomAB-only motors the stator exchange occurred independently of the smf, we conclude that the observed differences between the single and dual stator regimes are mainly due to the more efficient incorporation of MotAB under conditions of low Na^+.

The presence of both PomAB and MotAB increases swimming speed under conditions of low Na^+

To further determine whether MotAB contributes to the flagellar motor performance, we applied swimming assays. Previous studies have indicated that MotAB might not be fully functional because *S. oneidensis* mutants lacking PomAB show little motility on soft agar plates or when visualized microscopically (Paulick *et al.*, 2009). We hypothesized that this might be due to a rapid loss of the pmf upon oxygen starvation. Therefore, we measured swimming of aerated planktonic cultures immediately after sampling (Fig. 2; Table S3). Under these conditions, all three strains (wt, *ΔpomAB*, *ΔmotAB*) showed vigorous swimming. At high Na^+ levels, wild-type and *ΔmotAB* cells had similar swimming speeds (53.2 and 52.4 μm s^{-1}, respectively), while *ΔpomAB* mutants were significantly slower (34.8 μm·s^{-1}). However, at low Na^+ concentrations, wild-type and *ΔpomAB* cells were significantly faster (30.6 / 40.5 μm s^{-1}) than *ΔmotAB* mutants, which still displayed robust motility (16.6 μm s^{-1}). We therefore conclude that MotAB significantly contributes to flagellar rotation under appropriate conditions of low Na^+ concentrations.

Discussion

Numerous bacterial species possess more than one distinct set of stators to drive rotation of a single rotor system, raising the question of how appropriate rotor-stator configurations can be achieved in these species and how this affects motor functions. By using fluorescence microscopy, we have explored the composition and dynamics in PomAB-, MotAB-, and dual stator-driven motors of *S. oneidensis* MR-1. In the absence of PomAB, the stator ring consisted of about 11 MotAB stator units, a number similar to the one which has previously been determined for *E. coli* motors (Khan *et al.*, 1988; Reid *et al.*, 2006) and has also been estimated for PomAB-driven *Vibrio* motors (Yorimitsu and Homma, 2001). In *S. oneidensis* MR-1, MotAB units exchange with a pool of stators outside the motor. The occurrence of fluorescent foci within the cell envelope strongly indicate that MotAB precomplexes freely diffuse in the membrane and are not exclusively confined within

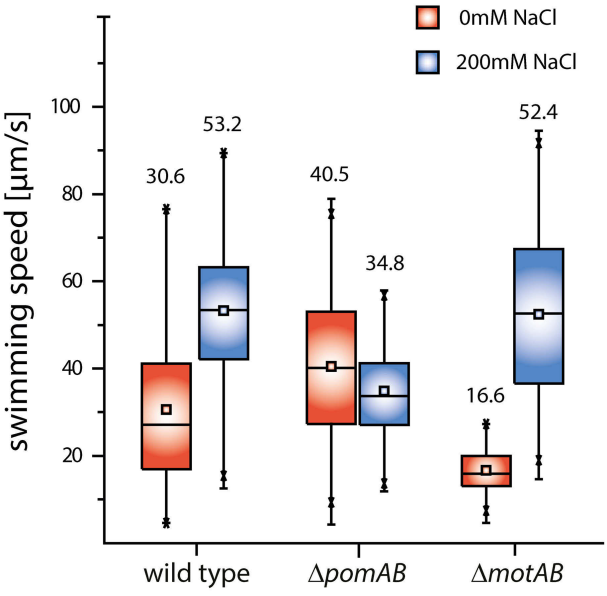

Fig. 2. Swimming speed of the wild type and *ΔmotAB* and *ΔpomAB* mutants under conditions of high and low Na^+ concentrations. The swimming speeds obtained for wild type (MR-1), *ΔpomAB* and *ΔmotAB* are summarized in a box-whisker-plot displayed in red (0 mM Na^+) or blue (200 mM Na^+). The box represents the middle 50% of the data. The average and the median are shown as '□' and '—', and the whiskers denote the data range of the 5th and 95th percentile. Maxima and minima are represented by 'x'. Swimming speed was determined for 120 cells for each strain under both conditions. Performance of the wild-type flagellar motor at 0 mM NaCl is significantly different from the exclusively PomAB-driven motor (ANOVA, p-Value 0.05). For detailed statistics, see Table S3.

close proximity of the flagellar motor. Notably, the exchange rate of MotAB stator units in the motor was dependent on the environmental Na^+ concentrations, and the exchange half time significantly increased from 16 s at high concentration of Na^+ to about 36 s at low Na^+ levels. These data are consistent with those obtained for MotAB in the *E. coli* flagellar system (Leake *et al*., 2006) and additionally show that efficient incorporation of MotAB into the *S. oneidensis* MotAB motor depends on the smf/pmf.

A major effect of the imf on functional stator incorporation into the flagellar motor has previously been demonstrated for both H^+- and Na^+-dependent flagellar systems (Armitage and Evans, 1985; Fung and Berg, 1995; Sowa *et al*., 2005; Tipping *et al*., 2013b). Loss of the pmf results in uncoupling of MotAB from the *E. coli* motor (Tipping *et al*., 2013b), and, in the *V. alginolyticus* polar flagellar motor requires both Na^+-binding and ion flux for PomAB stator incorporation. In the absence of Na^+, the PomAB stator units completely disassemble from the *V. alginolyticus* flagellar motor (Fukuoka *et al*., 2009). Compared to *Vibrio*, our data demonstrated a more stable rotor-stator interaction of *S. oneidensis* PomAB. Even at low concentrations of Na^+ PomAB stators did not disengage from the motor, and the turnover rate of stator units remained constant under conditions of both high and low Na^+ concentrations. This finding is consistent with the observation that PomAB-driven motors are still capable of supporting motility when no additional Na^+ is supplemented to the medium (Paulick *et al*., 2009). In addition, our FRAP experiments on mCherry-labeled PomAB stators strongly suggest that a subpopulation of the PomAB units in the motor exchanges at a much slower rate. PomAB is the exclusive stator unit for the polar flagellar motors of most *Shewanella* species (Paulick *et al*., 2009), and members of this genus have been found to thrive within a wide range of environmental Na^+ concentrations (Nealson and Scott, 2003; Hau and Gralnick, 2007). Thus, the rather robust PomAB-rotor interaction at low smf may have evolved to support efficient motility even when cells encounter conditions of low Na^+.

S. oneidensis MR-1 is the only *Shewanella* species identified so far which possesses two different sets of stators to drive rotation of the polar flagellum. Our study demonstrates how the acquisition of H^+-dependent MotAB by *S. oneidensis* MR-1, probably through lateral gene transfer, had significantly affected the dynamics of the rotor-stator composition. In the presence of both PomAB and MotAB in *S. oneidensis* MR-1 cells, the exchange rate of both units in the flagellar motor was significantly increased at low Na^+ concentrations, which may be due to competition of the different stator units for incorporation into the stator ring. At high Na^+-levels, MotAB is recruited less efficiently into the flagellar motor, thus resulting in a 7 PomAB: 2 MotAB configuration. At low Na^+-levels, incorporation of PomAB into the motor still dominates, however, the increased competition for rotor-stator interactions in concert with the changes in MotAB incorporation efficiencies leads to a shift towards PomAB:MotAB numbers of 6:5 (Fig. 2). As the presence of MotAB significantly benefits flagellar rotation and swimming speed of *S. oneidensis* MR-1 under conditions of low Na^+, this configuration strongly implies the presence of a hybrid motor which is simultaneously powered by H^+ and Na^+ gradients. The proof of concept for this hypothesis was recently provided by demonstrating that in genetically engineered *E. coli* motors Na^+- and H^+-dependent stators can contribute simultaneously to flagellar rotation (Sowa *et al*., 2014). Based on measurements of increments in rotation speed due to the incorporation of single stator units, the study clearly demonstrated that the configuration of both stator types in the flagellar motor depends on the Na^+ concentration as well as the overall abundance of the stator units. The resultant rotation speed was the sum of speeds conferred by the number and type of stator units, demonstrating the functionality of hybrid-fueled flagellar motors which are simultaneously powered by H^+ and Na^+. Based on our study, we now extend this concept to a naturally occurring bacterial motor driven by a dual stator system.

Under the conditions used in this study, the PomB(mCherry) and MotB(mCherry) protein levels were lower at low Na^+ levels, suggesting downregulation or decreased protein stability under these conditions. Earlier studies indicated that both *pomAB* and *motAB* expression does not significantly change in response to environmental Na^+ (Paulick *et al*., 2009), but how stator protein stability is affected remains to be shown. However, the ratio of PomB(mCherry) and MotB(mCherry) protein levels were similar at high and low Na^+ concentrations. This implies that, in our set of experiments, the shift in the stator-rotor configuration was predominantly governed by the incorporation efficiency of MotAB into the flagellar motor dependent on the environmental Na^+ concentration. Thus, effective adjustment of motor functions by stator exchange may occur by a rather simple mechanism that allows the use of stator units which have been acquired by lateral gene transfer and are not fully adjusted to the novel host system with respect to both function and regulation. In *S. oneidensis*, the FliG motor protein has evolved to interact with PomAB, and MotAB is probably still evolving towards an efficient interaction.

Several studies have provided evidence that regulation of stator-motor configurations can be far more complex. Differences in expression and production, as implicated *in B. subtilis* (Terahara *et al*., 2006), and/or load acting on the motor for stator recruitment, as has recently been demonstrated for the MotAB-driven motors of *E. coli* (Lele *et al*., 2013; Tipping *et al*., 2013a), may play additional roles under appropriate conditions in *S. oneidensis* MR-1.

An even more elaborate means of controlling motor-stator configuration has recently been described for *Pseudomonas aeruginosa* (Kuchma *et al*., 2014), a species which harbors two H^+-dependent stator complexes MotAB and MotCD (Doyle *et al*., 2004; Toutain *et al*., 2005). In *P. aeruginosa*, localization of MotCD to the flagellar motor is affected by levels of the secondary messenger c-di-GMP. Thus, in this species stator selection is not exclusively depending on factors such as stator abundance and ion-dependent exchange, a circumstance that adds another potential layer of regulation to motor-stator dynamics of bacterial flagella. Future studies will show which combination of adaptations in motor function is accomplished in the various bacterial species with multiple stator systems.

Experimental procedures

Strains, growth conditions and media

Strains used in this study are summarized in Table S4. *E. coli* strains were cultivated in LB medium at 37°C. Medium for the 2,6-diamino-pimelic acid (DAP)-auxotroph *E. coli* WM3064 was supplemented with DAP at final concentration of 300 μM. *S. oneidensis* MR-1 strains were routinely cultivated in LB medium or LM (10 mM HEPES, pH 7.3; 100 mM NaCl; 100 mM KCl; 0.02% yeast extract; 0.01% peptone; 15 mM lactate) at 30°C. For solidification, 1.5% (w/v) agar was added. When necessary, media were supplemented with 50 μg ml^{-1} kanamycin and/or 10% (w/v) sucrose.

Strain constructions

DNA manipulations were carried out according standard protocols (Sambrook *et al*., 1989) using appropriate kits (VWR International GmbH, Darmstadt, Germany) and enzymes (New England Biolabs, Frankfurt, Germany; Fermentas, St Leon-Rot, Germany). Markerless in-frame deletions and fusions were introduced by sequential homologous crossover using vector pNTPS-138-R6K essentially as previously reported (Lassak *et al*., 2010; Bubendorfer *et al*., 2012). Vectors were constructed using appropriate primer pairs (Table S4). *pomB* and *motB* were C-terminally fused to codon-optimized *mCherry* adding a GGS-GGS-GGS linker region. Immunofluorescence analysis revealed that PomB-mCherry is stably produced and that only minor MotB-mCherry degradation occurred (Fig. S1). Swimming speed and soft agar assays revealed that tagged stator proteins still mediated robust performance (Fig. S3).

Epi-fluorescence microscopy

Stoichiometry. Prior to microscopy, cultures of *motB-mCherry*, *pomB-mCherry* and *ΔmotAB pomB-mCherry* were pregrown overnight and subsequently subcultured in LM media with the appropriate NaCl concentration (200 mM KCl for low Na^+; 200 mM NaCl for high Na^+). Cells grown to mid-exponential phase were washed two times at 3000 g in mineral medium (4M) buffer (50 mM HEPES, 15 mM Lactate pH 7.0) with the appropriate amount of NaCl or KCl, and 5 μl were spotted on an agar pad made with the same buffer. Fluorescent movies were recorded using a custom-made inverted microscope with a Plan Fluor 100 ×/1.45 Oil objective (Nikon, UK) and an excitation wavelength of 550 nm as described previously (Leake *et al*., 2006; Tipping *et al*., 2013a) with modifications. Movies were recorded at 24 Hz using a 128 × 128-pixel, cooled, back-thinned electron-multiplying charge-coupled device camera (iXon DV860-BI; Andor Technology) for 500 frames or until the fluorescent foci were completely bleached. Each individual frame was exposed for 0.05 s by applying a laser power of 70 mW.

The number of single mCherry molecules was calculated using an algorithm to identify the number of distinct steps in intensity loss during photobleaching as previously described (Leake *et al*., 2006). Briefly, intensity trajectories over time were filtered (Chung Kennedy, median filter) and the initial intensity was calculated (Smith, 1998). The dominant peak in the power spectrum of the pairwise difference distribution function was used to extract the brightness of a single mCherry molecule and hence the number of mCherry molecules originally present in the polar spot. Data analysis was carried out using custom-written scripts in MATLAB (Mathworks) and statistics of the stator distribution were done in Origin 6.1. The resulting data were tested for normal distribution and significance by using the Kolmogorov-Smirnov test of goodness and the Mann Whitney test ($p = 0.05$), respectively in R (see Table S1).

Stator dynamics. To determine the stator dynamics by Fluorescence Recovery After Photobleaching (FRAP) analysis, cells were grown and immobilized for microscopy as described above. Image series were recorded before and after photobleaching with an exposure time of 40 ms, a laser-power of 70 mW at an excitation wavelength of 550 nm. Fluorescent polar motor spots were photobleached by exposure of 420 ms to a centered focused laser spot (~ 3 mW*μm^{-2}). ImageJ was used to determine the average fluorescence intensity of the motor spot (**R**egion **O**f **I**nterest), the total cell intensity (T) and the background intensity (BG) over time. Fluorescence intensity was corrected for photobleach and acquisition bleaching using:

$$I_{normalised} = [(ROI(t) - BG(t))/(ROI(0) - BG(0))] \times [(T(0) - BG(0))/(T(t) - BG(t))]$$

where *ROI(0)* is the average of the spot intensity of ten frames before bleaching. Average curves were generated for FRAP and fitted using: $S(t) = A\text{-}B\ e^{-kt}$. Recovery rate *k* related to the recovery half-time *t1/2* by $t1/2 = ln(2)/k$ and R-square for the goodness of the fitting curve were calculated using MatLab (Mathworks). In this formula *A* corresponds to the normalized recovery level and *(A-B)* to the postbleach relative fluorescence intensity.

We also attempted to fit curves from individual experiments separately. Due to experimental noises this was not always possible. Therefore, cells with the same recovery level were clustered and individual clusters were fitted accordingly (see Table S2). The average results for at least 5 clusters were similar to the average profile shown.

Immunofluorescence analysis

Production and stability of the fusions were determined by immunoblot analyses. Protein lysates were prepared from exponentially growing cultures. Cell suspensions were uniformly adjusted to an OD600 of 10. Protein separation and immunoblot detection were essentially carried out as described earlier (Paulick *et al*., 2009) using polyclonal antibodies raised against PomB or mCherry (Eurogentec Deutschland GmbH, Köln, Germany). Signals were detected using the SuperSignal® West Pico Chemiluminescent Substrate (Thermo Scientific, Schwerte, Germany) and documented using the CCD System LAS 4000 (Fujifilm, Düsseldorf, Germany).

Determination of swimming speed

Cells of the appropriate strains from overnight cultures were used to inoculate LM medium supplemented with 200 mM or no NaCl to an OD600 of 0.05. Medium without NaCl contained 200 mM KCl to yield a comparable overall salt concentration. At an OD600 of 0.4–0.5 cells were harvested by gentle centrifugation at 4500 g for two minutes and washed twice in 4M buffer (25 mM HEPES, 40 mM lactate (85% (v/v), pH 7.0) containing either 200 mM NaCl or KCl. Cells were finally resuspended in an adequate volume of 4M buffer and 200 μl of the suspension directly placed on a microscope slide. The coverslip was fixed by four droplets of silicone to create a space of 1–2 mm width. Movies of 11.4 s (150 frames) were taken with a Leica DMI 6000 B inverse microscope (Leica, Wetzlar, Germany) equipped with a SCMOS camera (Visitron Systems, Puchheim, Germany) and a HCX PL APO 100 × /1.4 objective. Speeds of at least 120 cells per strain and condition were determined using the MTrackJ plugin of ImageJ. The resulting data were tested for significance by using ANOVA ($p = 0.05$), respectively in R version 3.0.1 (see supplementary Table S3). Motility was further assessed by placing 3 μl of a planktonic culture of the corresponding strains on soft agar plates containing LB medium with an agar concentration of 0.2% (w/v). Plates were incubated for 24h at 30°C. Strains to be directly compared were always placed on the same plate.

Acknowledgements

The work was supported by the Deutsche Forschungsgemeinschaft (DFG TH831/4-1), the Max Planck Society and the International Max Planck Research School (A.P., S.B, K.M.T). A.P. was further supported by a SYNMIKRO Fellowship and an EMBO-STF grant. We would also like to acknowledge funding by the Biotechnology and Biological Sciences Research Coucil (BBSRC) to N. J. D. and J. P. A. We thank Sean Murray for fruitful discussions and help with Matlab-coding and statistics and Benjamin Kendzia for help with statistics.

Conflict of interests

The authors declare no conflict of interests.

References

Armitage, J.P., and Evans, M.C.W. (1985) Control of the protonmotive force in *Rhodopseudomonas sphaeroides* in the light and dark and its effect on the initiation of flagellar rotation. *Biochim Biophys Acta* **806:** 42–55.

Berg, H.C. (2003) The rotary motor of bacterial flagella. *Annu Rev Biochem* **72:** 19–54.

Blair, D.F. (2003) Flagellar movement driven by proton translocation. *FEBS Lett* **545:** 86–95.

Blair, D.F., and Berg, H.C. (1988) Restoration of torque in defective flagellar motors. *Science* **242:** 1678–1681.

Block, S.M., and Berg, H.C. (1984) Successive incorporation of force-generating units in the bacterial rotary motor. *Nature* **309:** 470–472.

Braun, T.F., Al-Mawsawi, L.Q., Kojima, S., and Blair, D.F. (2004) Arrangement of core membrane segments in the MotA/MotB proton-channel complex of *Escherichia coli*. *Biochemistry* **43:** 35–45.

Bubendorfer, S., Held, S., Windel, N., Paulick, A., Klingl, A., and Thormann, K.M. (2012) Specificity of motor components in the dual flagellar system of *Shewanella putrefaciens* CN-32. *Mol Microbiol* **83:** 335–350.

Doyle, T.B., Hawkins, A.C., and McCarter, L.L. (2004) The complex flagellar torque generator of *Pseudomonas aeruginosa*. *J Bacteriol* **186:** 6341–6350.

Fukuoka, H., Wada, T., Kojima, S., Ishijima, A., and Homma, M. (2009) Sodium-dependent dynamic assembly of membrane complexes in sodium-driven flagellar motors. *Mol Microbiol* **71:** 825–835.

Fung, D.C., and Berg, H.C. (1995) Powering the flagellar motor of *Escherichia coli* with an external voltage source. *Nature* **375:** 809–812.

Hau, H.H., and Gralnick, J.A. (2007) Ecology and biotechnology of the genus *Shewanella*. *Annu Rev Microbiol* **61:** 237–258.

Hirota, N., Kitada, M., and Imae, Y. (1981) Flagellar motors of alkalophilic *Bacillus* are powered by an electrochemical potential gradient of Na. *FEBS Lett* **132:** 278–280.

Hosking, E.R., Vogt, C., Bakker, E.P., and Manson, M. (2006) The *Escherichia coli* MotAB proton channel unplugged. *J Mol Biol* **364:** 921–937.

Ito, M., Hicks, D.B., Henkin, T.M., Guffanti, A.A., Powers, B.D., Zvi, L., *et al*. (2004) MotPS is the stator-force generator for motility of alkaliphilic *Bacillus*, and its homologue is a second functional Mot in *Bacillus subtilis*. *Mol Microbiol* **53:** 1035–1049.

Ito, M., Terahara, N., Fujinami, S., and Krulwich, T.A. (2005) Properties of motility in *Bacillus subtilis* powered by the H+-coupled MotAB flagellar stator, Na+-coupled MotPS or hybrid stators MotAS or MotPB. *J Mol Biol* **352:** 396–408.

Khan, S., Dapice, M., and Reese, T.S. (1988) Effects of mot gene expression on the structure of the flagellar motor. *J Mol Biol* **202:** 575–584.

Kojima, S., and Blair, D.F. (2004) Solubilization and purification of the MotA/MotB complex of *Escherichia coli*. *Biochemistry* **43:** 26–34.

Kuchma, S.L., Delalez, N.J., Filkins, L.M., Snavely, E.A., Armitage, J.P., and O;Toole, G.A. (2014) c-di-GMP-mediated repression of swarming motility by *Pseudomonas aeruginosa* PA14 requires the MotAB stator. *J Bacteriol* **197:** 420–430.

Lassak, J., Henche, A.L., Binnenkade, L., and Thormann, K.M. (2010) ArcS, the cognate sensor kinase in an atypical Arc system of *Shewanella oneidensis* MR-1. *Appl Environ Microbiol* **76:** 3263–3274.

Leake, M.C., Chandler, J.H., Wadhams, G.H., Bai, F., Berry, R.M., and Armitage, J.P. (2006) Stoichiometry and turnover in single, functioning membrane protein complexes. *Nature* **443:** 355–358.

Lele, P.P., Hosu, B.G., and Berg, H.C. (2013) Dynamics of mechanosensing in the bacterial flagellar motor. *Proc Natl Acad Sci USA* **110:** 11839–11844.

Li, N., Kojima, S., and Homma, M. (2011) Characterization of the periplasmic region of PomB, a Na^+-driven flagellar stator protein in *Vibrio alginolyticus*. *J Bacteriol* **193:** 3773–3784.

Manson, M.D., Tedesco, P., Berg, H.C., Harold, F.M., and Van der Drift, C. (1977) A protonmotive force drives bacterial flagella. *Proc Natl Acad Sci USA* **74:** 3060–3064.

Minamino, T., Imada, K., and Namba, K. (2008) Molecular motors of the bacterial flagella. *Curr Opin Struct Biol* **18:** 693–701.

Nealson, K.H., and Scott, J. (2003) Ecophysiology of the genus *Shewanella*. In *The Prokaryotes: An Evolving Electronic Resource for the Microbial Community*. Dworkin, M. (ed.). New York, USA: Springer-NY, LLC, pp. 1133–1151.

Paulick, A., Koerdt, A., Lassak, J., Huntley, S., Wilms, I., Narberhaus, F., and Thormann, K.M. (2009) Two different stator systems drive a single polar flagellum in *Shewanella oneidensis* MR-1. *Mol Microbiol* **71:** 836–850.

Porter, S.L., Wadhams, G.H., and Armitage, J.P. (2011) Signal processing in complex chemotaxis pathways. *Nat Rev Microbiol* **9:** 153–165.

Reid, S.W., Leake, M.C., Chandler, J.H., Lo, C.J., Armitage, J.P., and Berry, R.M. (2006) The maximum number of torque-generating units in the flagellar motor of *Escherichia coli* is at least 11. *Proc Natl Acad Sci USA* **103:** 8066–8071.

Sambrook, K., Fritsch, E.F., and Maniatis, T. (1989) *Molecular Cloning: A laboratory manual*. Cold Spring Harbor, NY: Cold Spring Harbor Press.

Sato, K., and Homma, M. (2000) Functional reconstitution of the Na(+)-driven polar flagellar motor component of *Vibrio alginolyticus*. *J Biol Chem* **275:** 5718–5722.

Smith, D.A. (1998) A quantitative method for the detection of edges in noisy time-series. *Philos Trans R Soc Lond B Biol Sci* **353:** 1969–1981.

Sourjik, V., and Wingreen, N.S. (2012) Responding to chemical gradients: bacterial chemotaxis. *Curr Opin Cell Biol* **24:** 262–268.

Sowa, Y., and Berry, R.M. (2008) Bacterial flagellar motor. *Q Rev Biophys* **41:** 103–132.

Sowa, Y., Rowe, A.D., Leake, M.C., Yakushi, T., Homma, M., Ishijima, A., and Berry, R.M. (2005) Direct observation of steps in rotation of the bacterial flagellar motor. *Nature* **437:** 916–919.

Sowa, Y., Homma, M., Ishijima, A., and Berry, R.M. (2014) Hybrid-fuel bacterial flagellar motors in *Escherichia coli*. *Proc Natl Acad Sci USA* **111:** 3436–3441.

Stock, D., Namba, K., and Lee, L.K. (2012) Nanorotors and self-assembling macromolecular machines: the torque ring of the bacterial flagellar motor. *Curr Opin Biotechnol* **23:** 545–554.

Terahara, N., Fujisawa, M., Powers, B., Henkin, T.M., Krulwich, T.A., and Ito, M. (2006) An intergenic stem-loop mutation in the *Bacillus subtilis ccpA-motPS* operon increases *motPS* transcription and the MotPS contribution to motility. *J Bacteriol* **188:** 2701–2705.

Thormann, K.M., and Paulick, A. (2010) Tuning the flagellar motor. *Microbiology* **156:** 1275–1283.

Tipping, M.J., Delalez, N.J., Lim, R., Berry, R.M., and Armitage, J.P. (2013a) Load-dependent assembly of the bacterial flagellar motor. *MBio* **4**. doi: 10.1128/mBio.00551-13; pii: e00551-13.

Tipping, M.J., Steel, B.C., Delalez, N.J., Berry, R.M., and Armitage, J.P. (2013b) Quantification of flagellar motor stator dynamics through in vivo proton-motive force control. *Mol Microbiol* **87:** 338–347.

Toutain, C.M., Zegans, M.E., and O;Toole, G.A. (2005) Evidence for two flagellar stators and their role in the motility of *Pseudomonas aeruginosa*. *J Bacteriol* **187:** 771–777.

Yorimitsu, T., and Homma, M. (2001) Na(+)-driven flagellar motor of *Vibrio*. *Biochim Biophys Acta* **1505:** 82–93.

Supporting information

Additional supporting information may be found in the online version of this article at the publisher's web-site.

Dual stator dynamics in the *Shewanella oneidensis* MR-1 flagellar motor

Anja Paulick[a,#,*], Nicolas J. Delalez[c,e,#], Susanne Brenzinger[a,b], Bradley C. Steel[d], Richard M. Berry[d], Judith P. Armitage[c] and Kai M. Thormann[a,b,*]

a) Max-Planck-Institut für terrestrische Mikrobiologie, Department of Ecophysiology, 35043 Marburg, Germany
b) Justus-Liebig-Universität Gießen, Department of Microbiology and Molecular Biology at the IFZ, 35392 Gießen, Germany
c) University of Oxford, Biochemistry Department, Oxford OX1 3QU, United Kingdom
d) University of Oxford, Physics Department, Oxford OX1 3QU, United Kingdom
e) current address: School of Life Sciences, University of Warwick, Gibbet Hill Campus, Coventry CV4 7AL, UK

- supplemental material –

Figure S1: Detection of MotB-mCherry and PomB-mCherry fusion proteins by immunoblot analysis

Figure S2: Spreading efficiency of cells with labeled stators in soft agar

Figure S3: Analysis of stator stoichiometry and turnover by fluorescence microscopy

Table S1: Statistics for the determination of stator stoichiometry by fluorescence microscopy

Table S2: Statistical analysis of FRAP data for stator exchange

Table S3: Statistics of the swimming speed analysis

Table S4: Strains, plasmids and oligonucleotides used in this study

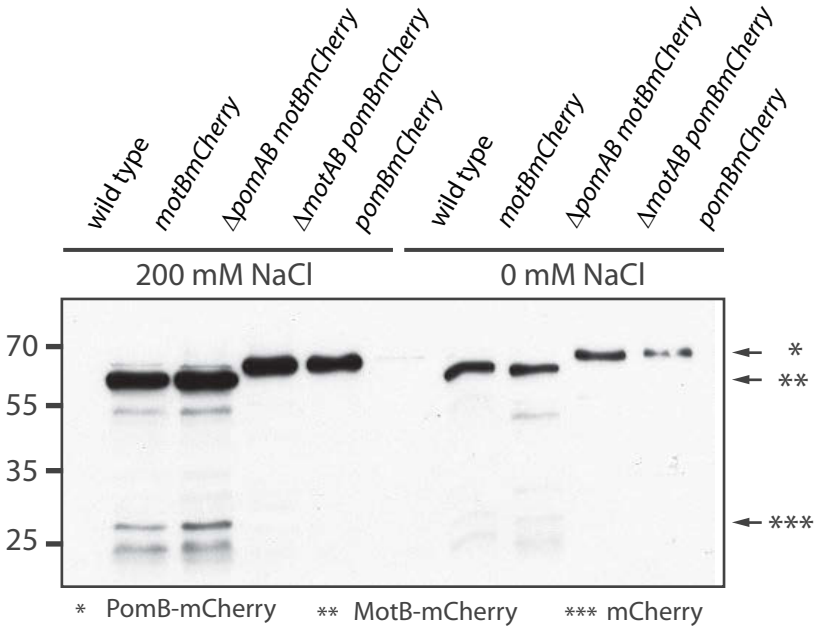

Figure S1: Detection of MotB-mCherry and PomB-mCherry fusion proteins by immunoblot analysis. Cell lysates of the indicated strains grown under appropriate conditions were subjected to SDS-PAGE followed by immunoblot analysis using an antibody raised against mCherry. Arrows with asterisks mark the positions corresponding to the estimated molecular masses of PomB-mCherry (61 kDa), MotB-mCherry (57 kDa) and mCherry (29 kDa), respectively. Wild-type cells not labeled with mCherry were used as negative control.

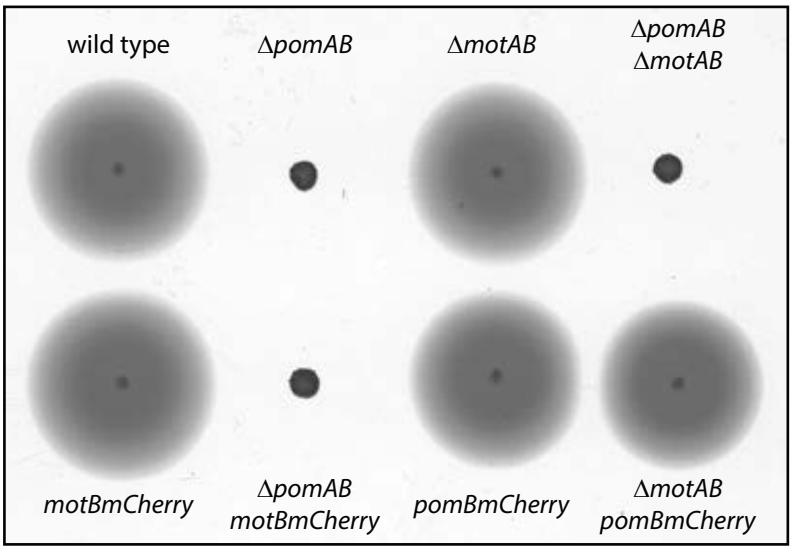

Supplemental Figure 2: Spreading efficiency of cells with labeled stators in soft agar.
3 µl of exponentially growing cultures of the indicated strains were placed on 0.3 % soft agar and allowed to spread for 18 h. *ΔpomAB* strains were non-motile under these conditions but exhibited robust movement when observed by light microscopy.

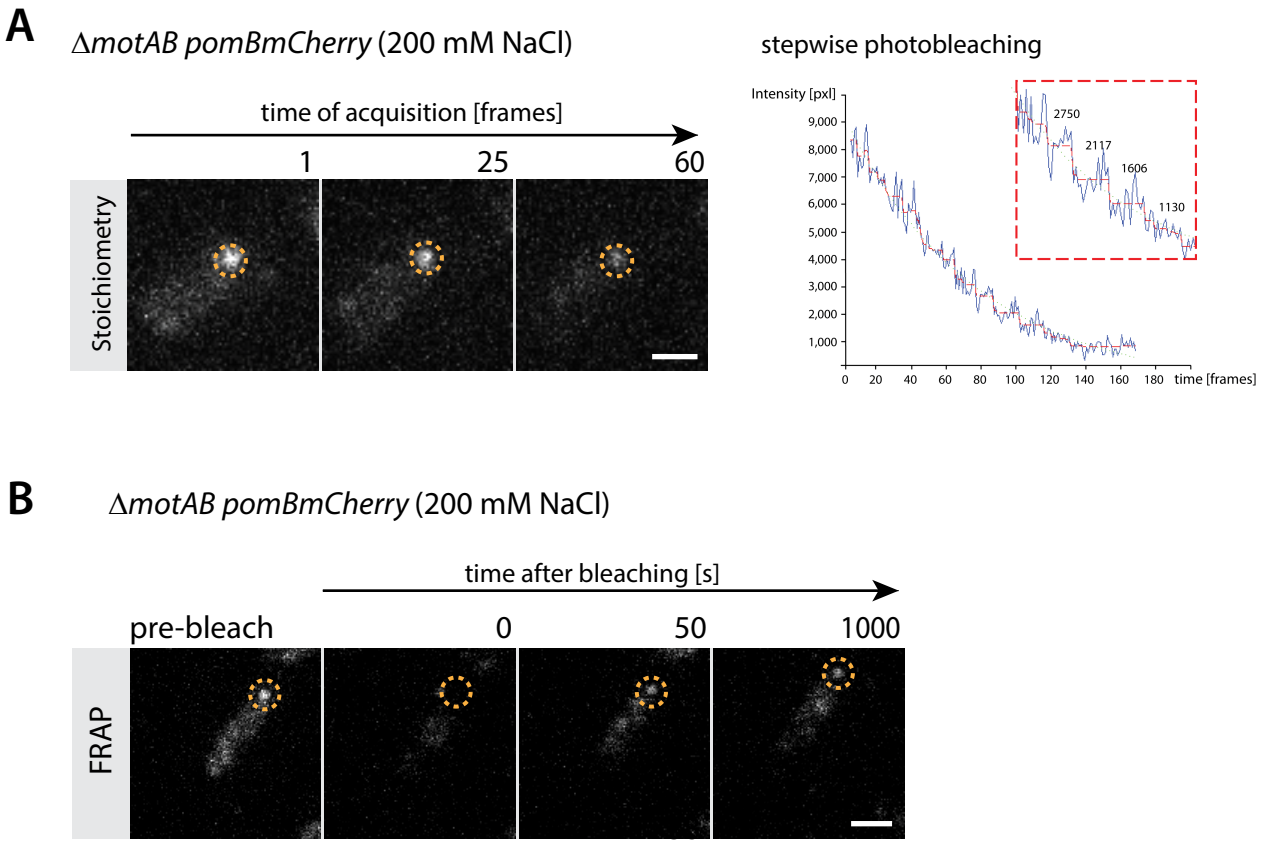

Supplemental Figure 3: Analysis of stator stoichiometry and turnover by fluorescence microscopy
A) Determination of stator molecules. Displayed are representative examples of fluorescence micrographs during photobleaching at the indicated timepoints (frames) of *ΔmotAB pomBmCherry* in 4M buffer supplemented with 200 mM NaCl (left) and an example for the stepwise photobleaching of fluorescence intensity using Matlab (right). **B) FRAP analysis:** Fluorescence micrographs for FRAP analysis of *ΔmotAB pomBmCherry* at 200 mM NaCl at the indicated timepoints (s); left panel pre-bleach, right panels micrographs after bleaching. Micrographs in (A) and (B) were modified in ImageJ, using the same contrast settings. Polar localization of stator complexes is highlighted by yellow circles. Scale bar, 2 µm.

Table S1: Statistics for the determination of stator stoichiometry by fluorescence microscopy

a) Stator numbers in dependence of Na^+ concentrations

strain	mM	N	Mean	SD	Median	P25	P75	P-Value[1]	P-Value[2]
WT-PomBmCherry	200	107	7.79	2.16	7.22	6.39	9.27	<0.01	0.0002
	0	88	6.53	2.17	6.48	5.25	8.20	>0.15	
Δmot-PomBmCherry	200	103	7.41	2.22	7.13	5.98	8.67	0.033	0.0043
	0	133	8.32	2.87	8.26	6.29	10.54	0.060	
WT-MotBmCherry	200	51	2.49	1.27	2.32	1.54	3.27	0.086	<0.0001
	0	54	4.77	2.00	4.67	3.11	5.71	>0.15	
Δpom-MotBmCherry	200	69	8.39	3.07	7.98	6.11	9.64	0.032	<0.0001
	0	96	10.94	3.05	10.61	8.71	12.57	>0.15	

Abbreviations: SD=Standard deviation; P25= 25th percentile; P75=75th percentile

[1]P-value of Kolmogorov-Smirnov test of goodness of fit. If p-value below 0.05 mean variable is **not normally distributed**.

[2]P-Value of Mann Whitney test. If p-value below 0.05 means medians of variables are **significantly different**.

b) Differences of stator numbers in the wild type compared to mutants with only a single stator

strain	mM	N	Mean	SD	Median	P25	P75	P-Value[1]	P-Value[2]
WT-PomBmCherry	200	107	7.79	2.16	7.22	6.39	9.27	<0.01	0.0660
Δmot-PomBmCherry	200	103	7.41	2.22	7.13	5.98	8.67	0.033	
Δmot-PomBmCherry	0	133	8.32	2.87	8.26	6.29	10.54	0.060	<0.0001
WT-PomBmCherry	0	88	6.53	2.17	6.48	5.25	8.20	>0.15	
WT-motBmCherry	200	51	2.49	1.27	2.32	1.54	3.27	0.086	<0.0001
*Δpom*MotBmCherry	200	69	8.39	3.07	7.98	6.11	9.64	0.032	
Δpom-MotBmCherry	0	96	10.94	3.05	10.61	8.71	12.57	>0.15	<0.0001
WT-*motBmCherry*	0	54	4.77	2.00	4.67	3.11	5.71	>0.15	

Abbreviations: SD=Standard deviation; P25= 25th percentile; P75=75th percentile

[1]P-value of Kolmogorov-Smirnov test of goodness of fit. If p-value below 0.05 mean variable is **not normally distributed**.

[2]P-Value of Mann Whitney test. If p-value below 0.05 means medians of variables are **significantly different**.

Table S2: Statistical analysis of FRAP data for stator exchange

strain	mM	N	Number of Clusters[1]	Exchange half-time[2]	SE	Exchange recovery rates[2]	SE	Exchange half-time[3]	R-square[4]
WT-PomBmCherry	200	15	5	24.52	2.81	0.041	0.0061	26.52	0.84
PomAB and MotAB	0	17	6	8.95	0.67	0.090	0.0055	8.18	0.82
Δmot-PomBmCherry	200	15	5	30.80	2.57	0.023	0.014	29.88	0.78
(PomAB only)	0	27	9	32.59	1.5	0.029	0.00312	34.73	0.94
Δpom-MotBmCherry	200	18	6	16.36	1.5	0.055	0.005	13.45	0.92
(MotAB only)	0	18	6	36.10	3.16	0.030	0.0059	36.01	0.81

Abbreviations: SE=Standard error

[1] cells were clustered according to their plateau of recovery of fluorescence intensity

[2] exchange half-time was derived by averaging the fit to clusters of three cells with a similar range of plateau for fluorescence recovery

[3]exchange half-time derived from the average fit of all analysed cells

[4] R-square was derived for the fit to the average of the normalised fluorescence intensity data for FRAP as shown in figure 1

Table S 3: Statistics of the swimming speed analysis

a) Swimming speed [µm/s] of different strains in dependence of Na^+ concentrations

strain	NaCl [mM]	N	Mean	SD
S. oneidensis MR-1	200	120	53.2	16.0
	0	120	30.6	17.4
ΔmotAB	200	120	52.4	19.1
	0	120	16.6	5.1
ΔpomAB	200	120	34.8	10.0
	0	120	40.5	15.6

Abbreviations: SD=Standard deviation

b) Comparison of the swimming speed [µm/s] of different strains at high and low Na^+ concentrations.

strain	NaCl [mM]	P-Value[1]	NaCl [mM]	P-Value[1]
S. oneidensis MR-1 *ΔmotAB*	200	0.981556	0 0	<0.0001
S. oneidensis MR-1 *ΔpomAB*	200	<0.0001	0 0	<0.0001
ΔmotAB *ΔpomAB*	200	<0.0001	0 0	<0.0001
S. oneidensis MR-1	200 0	<0.0001		
ΔmotAB	200 0	<0.0001		
ΔpomAB	200 0	0.372937		

[1]P-value of ANOVA test. If p-value below 0.05 mean variables are **significantly different.**

Table S4: Strains, plasmids and oligonucleotides used in this study

strain	relevant genotype or phenotype	source or reference
E. coli		
DH5αλpir	*recA1 gyrA* (*lacIZYA-argF*) (80d *lac* [*lacZ*] M15) *pir* RK6	(1)
WM3064	*thrB1004 pro thi rpsL hsdS lacZ* ΔM15 RP4-1360 Δ(*araBAD*) 567Δ*dapA* 1341::[*erm pir*(wt)]	W. Metcalf, University of Illinois,Urbana-Champaign
***In frame* deletions**		
***S. oneidensis* MR-1**	**wild type**	**(2)**
Δ*pomAB*	ΔSO_1529-30	(3)
Δ*motAB*	ΔSO_4287-86	(3)
Δ*pomAB*/Δ*motAB*	ΔSO_1529-30*;* ΔSO_4287-86	(3)
***In frame* insertion of fluorescence protein fusions**		
motB-mCherry	*motB::mCherry*; Km^r; C-terminal fusion *mCherry* to *motB*	This work
pomB-mCherry	*pomB::mCherry*; Km^r; C-terminal fusion *mCherry* to pom*B*	This work
Δ*pomAB* *motB-mCherry*	ΔSO_1529-30*;* *motB::mCherry*; Km^r; C-terminal fusion *mCherry* to *motB*	This work
Δ*motAB* *pomB-mCherry*	ΔSO_4287-86*;* *pomB::mCherry*; Km^r; C-terminal fusion *mCherry* to *pomB*	This work
fliN-Gfp	*fliN::gfp*	This work

plasmid	relevant genotype or phenotype	Source or reference
pCR2.1-mCherry-SO	synthesized *mCherry* (monomeric), codon usage *S. oneidensis* MR-1 in pCR2.1 blunt end inserted	GenScript (USA)
pET21-sfGfp	fast maturating *gfp*	(4)
pNPTS138-R6KT	pUC origin pNPTS138 exchanged with γ-origin from pUC18R6KT-mini-Tn7T	(3)
Fluorescent protein fusion constructs		
pNPTS-C-*pomB*(GGS)-*mCherry*	C-terminal fusion of *mCherry to pomB*; linker (GGS) inserted upstream	This work
pNPTS-C-*motB*(GGS)-*mCherry*	C-terminal fusion of *mCherry to motB*; linker (GGS) inserted upstream	This work
pNPTSR6KT-*fliN-gfp*	C-terminal fusion of *gfp* to *fliN*	This work
***In frame* deletion constructs**		
pGPSac28Km-Δ*pomAB*	*in frame pomAB* deletion fragment in pGPSac28Km; Km^r	(3)
pGPSac28Km-Δ*motAB*	*in frame motAB* deletion fragment in pGPSac28Km; Km^r	(3)

Km^r, kanamycin resistance

oligonucleotide	Sequence 5'-3'*	Restriction endonuclease
Fluorescent protein fusions		
PspOMI-pomB-C-mCherry-up-fw	CTC ATA GGG CCC TTG GCT ACA TTT GCC GAT TTG ATG	*PspOMI*
pomB-C-mCherry-up-rev	TGG AAA CGC TGC CGC CAT TTG GTT TAT CCA CTT GAA TCT CTT CC	-
pomB-C-mCherry-OL-fw	AAT GGC GGC AGC GTT TCC AAA GGG GAA GAG GAC AAT ATG	-
pomB-C-mCherry-OL-rev	TGA GGA CGT GTT ATT TGT ATA ACT CAT CCA TAC CAC CAG	-
pomB-C-mCherry-dwn-fw	T AAC ACG TCC TCA TAT TCA GCC GTG	-
NheI-pomB-C-mCherry-dwn-rev	TGC TAG CAA GCC ACC TAA ACC TTC GAT ACG	*NheI*
PspOMI-motB-C-mCherry-up-fw	CTC ATA GGG CCC ACC AGA AAA TCA TGA GCG TTG G	*PspOMI*
motB-C-mCherry-up-rev	CTT TGG AAA CGC TGC CGC CCT CAG GAA TGG GAA TAT GGC TTT C	-
motB-C-mCherry-OL-fw	TGA GGG CGG CAG CGT TTC CAA AGG GGA AGA GGA CAA TAT G	-
motB-C-mCherry-OL-rev	AGG AGT ATT CTT TAT TTG TAT AAC TCA TCC ATA CCA CCA G	-
motB-C-mCherry-dwn-fw	TAA AGA ATA CTC CTT CTT AGA TGT GTT TTA ATT TGA C	-
NheI-motB-C-mCherry-dwn-rev	TGC TAG CTA ACT GGC TTA TCT ATT ATG TTC TTA ATC	*NheI*
FliN-I-fw-SphI	CAA TGC ATG CGC CAC CAT TGT CAG CCC AAC CGA AG	*SphI*
FliN-I-rv-Eco	CAT CGA ATT CCA TCT CAC TTC ACC TTT ATA ATT CTG	*EcoRI*
FliN-II-fw-Bam	AAG TGG ATC CAG TAC AGA TGA CGA TTG GGC AGC	*BamHI*
FliN-II-rv-Pst	GTT ACT GCA GCC GTT GCC GCA CTA CCT TCA TTG	*PstI*
Gfp138-fw-Eco-NL	CTT GAA TTC CGT AAA GGA GAA GAA CTT TTC AC	*EcoRI*
Gfp138-rv-G-Bam	GAA GGA TCC TCC TCC GCC TCC TTT GTA TAG	*BamHI*
"check" Primer		
pomB-C-fluo-chk-fw	ATG GCT AAG TGC AAC TGT CCA CC	
pomB-C-fluo-chk-rev	ATA CGC CCG AGT CGA AAC CAC	
motB-C-fluo-chk-fw	TAA CTG GTA TCG CTG ACG GTG AG	
motB-C-fluo-chk-rev	AAC CTG ACA CAG AAT TAT GAA CAG CC	
chk-pomAB-SO-rv	GCA CGC CAA TCG CAT CGG TAA	-
chk-pomAB-SO-fw	TGC ATT GAC TAA CAC GCT GAT TCG	-
chk-motAB-SO-fw	ACG TTA ATG GAG CGT CAC TTT AGT TC	-
chk-motAB-SO-rv	CTG ACA CAG AAT TAT GAA CAG CCT CT	-

Additional References

(1) **Miller VL, Mekalanos JJ**. 1988. A novel suicide vector and its use in construction of insertion mutations: osmoregulation of outer membrane proteins and virulence determinants in *Vibrio cholerae* requires *toxR*. J Bacteriol **170**:2575-2583.

(2) **Venkateswaran K, Moser DP, Dollhopf ME, Lies DP, Saffarini DA, MacGregor BJ, Ringelberg DB, White DC, Nishijima M, Sano H, et al.** 1999. Polyphasic taxonomy of the genus *Shewanella* and description of *Shewanella oneidensis* sp. nov. Int J Syst Bacteriol **49**:705-724.

(3) **Paulick A, Koerdt A, Lassak J, Huntley S, Wilms I, Narberhaus F, Thormann KM.** 2009. Two different stator systems drive a single polar flagellum in *Shewanella oneidensis* MR-1. *Mol Microbiol* **71**:836-850.

(4) **Pedelacq JD, Cabantous S, Tran T, Terwilliger TC, Waldo GS.** 2006. Engineering and characterization of a superfolder green fluorescent protein. *Nat Biotechnol* **24**:79-88

Chapter 3

Research article (submitted to *Molecular Microbiology)*

Mechanistic consequences of functional stator mutations in the bacterial flagellar motor

Susanne Brenzinger[1,2], Lena Dewenter[3], Nicolas J Delalez[4], Oliver Leicht[5], Volker Berndt[2], Richard M. Berry[6], Martin Thanbichler[5,7], Judith P Armitage[4], Berenike Maier[3], Kai M Thormann[1,*]

1) Justus-Liebig-Universität Gießen, Department of Microbiology and Molecular Biology at the IFZ, 35392 Gießen, Germany
2) Max-Planck-Institut für terrestrische Mikrobiologie, Department of Ecophysiology, 35043 Marburg, Germany
3) University of Cologne, Department of Physics, 50674 Cologne, Germany
4) University of Oxford, Biochemistry Department, Oxford OX1 3QU, United Kingdom
5) Philipps-Universität Marburg, Faculty of Biology, Karl-von-Frisch-Str. 8, 35043 Marburg, Germany
LOEWE Center for Synthetic Microbiology, 35043 Marburg, Germany
6) University of Oxford, Physics Department, Oxford OX1 3QU, United Kingdom
7) Max Planck Institute for Terrestrial Microbiology & LOEWE Center for Synthetic Microbiology, 35043 Marburg, Germany

Contributions:

S.B. designed the study, performed laboratory experiments (strain and vector constructions, determination of transcriptional levels via lux fusions stoichiometry, fluorescence microscopy, motility assays, fluorescence recovery after photobleaching, stoichiometry, oxygen-speed dependency and immunofluorescence analysis), evaluated the data and wrote the manuscript.

L.D. designed the study, performed laboratory experiments (oxygen-speed dependency), and wrote the manuscript.

N.J.D. designed the study (stoichiometry and stator dynamics) and wrote the manuscript.

O.L. performed laboratory experiments (fluorescence recovery after photobleaching), evaluated the data and wrote the manuscript.

V.B. performed laboratory experiments (strain and vector constructions and motility assays).

R.M.B. designed the study and wrote the manuscript.

M.T. designed the study and wrote the manuscript.

J.P.A. designed the study and wrote the manuscript.

B.M. designed the study and wrote the manuscript.

K.M.T. designed the study and wrote the manuscript.

Mechanistic consequences of functional stator mutations in the bacterial flagellar motor

Susanne Brenzinger[1,2], Lena Dewenter[3], Nicolas J Delalez[4], Oliver Leicht[5], Volker Berndt[2], Richard M. Berry[6], Martin Thanbichler[5,7], Judith P Armitage[4], Berenike Maier[3], Kai M Thormann[1,*]

1) Justus-Liebig-Universität Gießen, Department of Microbiology and Molecular Biology at the IFZ, 35392 Gießen, Germany
2) Max-Planck-Institut für terrestrische Mikrobiologie, Department of Ecophysiology, 35043 Marburg, Germany
3) University of Cologne, Department of Physics, 50674 Cologne, Germany
4) University of Oxford, Biochemistry Department, Oxford OX1 3QU, United Kingdom
5) Philipps-Universität Marburg, Faculty of Biology, Karl-von-Frisch-Str. 8, 35043 Marburg, Germany
LOEWE Center for Synthetic Microbiology, 35043 Marburg, Germany
6) University of Oxford, Physics Department, Oxford OX1 3QU, United Kingdom
7) Max Planck Institute for Terrestrial Microbiology & LOEWE Center for Synthetic Microbiology, 35043 Marburg, Germany

Running title: MotB plug-domain mutants

Key words: flagellum, swimming, stator, torque, pmf

*corresponding author
Kai Thormann, Justus-Liebig-Universität Gießen, Department for Microbiology and Molecular Biology at the IFZ, Heinrich-Buff-Ring 26-32, 35392 Gießen, Germany, email: kai.thormann@mikro.bio.uni-giessen.de, ++49 (0) 641 9935545, fax: ++49 (0)641 9935549

Summary

Stators are crucial components of the flagellar motor and determine motor properties such as the coupling ion or the torque and speed that can be provided. *Shewanella oneidensis* MR-1 possesses two different stator units to drive flagellar rotation, the Na^+-dependent PomAB stator and the H^+-driven MotAB stator which was probably acquired by lateral gene transfer. In the absence of PomAB, MotAB-driven flagellar motors cannot support efficient cellular movement through structured environments such as soft agar. Here, we show that single point mutations which alter the amphipathic character of the so-called plug domain in MotB significantly affect motor functions, allowing cells to swim through media with increased viscosity, and to swim under anaerobic conditions. However, the swimming speed of MotAB*-driven planktonic cells was reduced, and the overexpression of these stators caused reduced growth rates. The number and exchange rate of mutated stator units around the rotor was not significantly affected. MotAB* requires MotX/Y, but not FliL for proper function. The results suggest that the MotB plug region is involved in regulating the rate of ion flow and the load-sensing sensing mechanism of the flagellar motor and may play a key role in functional adaptation and diversification of flagellar motors.

Abbreviated summary

The stators of the flagellar motor are key elements with respect to motor function and properties. Here, we found that mutations affecting the so-called plug domain in MotB allows higher torque and swimming under anaerobic conditions. We hypothesize that this region might be important in functional adaptation of flagellar motors.

Introduction

Numerous bacteria are able to actively move by rotating flagella, long helical filaments extending from the cell body. Rotation of the filament is conferred by a membrane-embedded motor, an intricate multiprotein complex which is powered by H^+ or Na^+ gradients. (reviewed in (Berg, 2003, Minamino *et al.*, 2008, Sowa and Berry, 2008, Stock *et al.*, 2012)). Two major components are required to convert ion fluxes into rotational movement, the cytoplasmic rotor and the stator. The rotor, referred to as the C-ring but also called switch complex is formed by multiple copies of the proteins FliG, FliM and FliN. The stator, locates in the cytoplasmic membrane, consists of several distinct stator units. These units are arranged in a ring-like fashion the surrounds the membrane-spanning part of the flagellar basal body, the MS-ring. Each stator unit is composed of two protein subunits, A and B, which assemble in a 4A:2B stoichiometry. They are commonly referred to as MotA and MotB in H^+-dependent motors and PomA and PomB in Na^+-conducting motors, MotA/PomA has four transmembrane helices and is thought to interact with the C-ring component FliG via a cytoplasmic loop. MotB/PomB has a single transmembrane domain and a periplasmic region containing a peptidoglycan-binding domain which enables binding of the unit to the rigid cell wall. Two A subunits and one B subunit form a single ion-specific channel, hence each stator unit harbors two ion channels (Sato and Homma, 2000a, Braun *et al.*, 2004, Kojima and Blair, 2004, Mandadapu *et al.*, 2015).

The composition of the stator ring has been shown to be highly dynamic in both MotAB (H^+)- and PomAB (Na^+)-driven flagellar systems. Stator units within the motor are constantly exchanged with a pool of membrane-located precomplexes. In species such as *Escherichia coli* or *Shewanella oneidensis* MR-1, about 11 stator units can be synchronously active within the flagellar motor to collectively contribute to torque generation (Paulick *et al.*, 2015, Leake *et al.*, 2006, Reid *et al.*, 2006). However, recent studies have provided evidence that the number of stator units engaged with the rotor varies the ion motive force (imf) and/or the load acting on the flagellar filament (Tipping *et al.*, 2013a, Tipping *et al.*, 2013b, Lele *et al.*, 2013, Fung and Berg, 1995, Sowa *et al.*, 2005, Fukuoka *et al.*, 2009). The dynamic composition of the stator ring enables the cells to appropriately adjust flagellar functions according to the environmental conditions or cellular requirements.

It is unclear how the stator units are recruited to the flagellar motor in an appropriate fashion. Each stator unit is produced as a non-active precomplex which diffuses within the cytoplasmic membrane prior to engagement with the flagellar motor. Premature ion flow through the precomplex is prevented by a periplasmic amphipathic region within the MotB protein which is referred to as ‘plug domain’ (Hosking *et al.*, 2006, Kojima *et al.*, 2009, Li *et al.*, 2011). Only after recruitment into the flagellar motor and binding to the peptidoglycan of the cell wall does the stator become active and competent for ion

channeling. The cytoplasmic loop within MotA as well as the C-terminal part of MotB appear to be important for functional motor-stator interactions (Kojima *et al.*, 2009, Kojima *et al.*, 2008b, Kojima *et al.*, 2008a, Hizukuri *et al.*, 2010, Morimoto *et al.*, 2010b, Sato and Homma, 2000b). Furthermore, several flagellar motors have been demonstrated to require additional components for efficient stator acquisition, such as FlgT, MotX, and MotY, which were shown to form additional ring structures at the flagellar basal body in *Vibrio* sp. (Terashima *et al.*, 2006, Terashima *et al.*, 2010). Recently, another flagellar component, FliL, has been proposed to directly interact with MotAB stators in *E. coli* and *Salmonella* as well as with PomAB stators in *Vibrio*, promoting retention of the stators within the flagellar motor (Partridge *et al.*, 2015, Zhu *et al.*, 2015). Efficient stator acquisition is further complicated by the fact that numerous bacterial species possess two or more distinct types of stator units to drive rotation of a single flagellar system (reviewed in (Thormann and Paulick, 2010)).

The gammaproteobacterium *Shewanella oneidensis* MR-1 is motile by means of a single polar flagellum which is, in contrast to other species of this genus, driven by two distinct stator units (Paulick *et al.*, 2009). Na^+-dependent PomAB is present in all *Shewanella* species whereas the second stator unit, MotAB, is H^+-dependent and was probably acquired through lateral gene transfer, as strongly suggested by phylogenetic analysis of the stator sequence and its corresponding genetic context. We have recently shown that the presence of MotAB leads to an increase of the stator exchange rate in the flagellar motor and the formation of a stator ring synchronously consisting of PomAB and MotAB units (Paulick *et al.*, 2015). Thus, the *S. oneidensis* MR-1 flagellum is probably driven by a 'hybrid' motor whose composition is adjusted according to the environmental Na^+ concentrations. We also showed that functional rotor/stator interaction of both MotAB and PomAB depends on the presence of the T-ring proteins MotX and MotY (Koerdt *et al.*, 2009). Notably, while MotAB is functional on its own and able to drive flagellar rotation, cells propelled by MotAB quickly cease active swimming in planktonic cultures and show no cellular spreading on soft agar plates (Paulick *et al.*, 2009, Paulick *et al.*, 2015). When cells lacking PomAB were incubated on soft agar plates for extended periods of time, we frequently observed mutants which displayed robust lateral extension and vigorous swimming in planktonic cultures (Paulick *et al.*, 2009). Here, we isolated several gain-of-function mutants and show that an increase in MotAB-mediated swimming was predominantly caused by single point mutations within the 'plug' domain of MotB, and we further explored the mechanistic consequences for stator-motor interactions and general motor functions.

Results

Identification of MotB gain-of-function mutants

To isolate spontaneous mutants that display active swimming through soft agar using only the MotAB stator system, *ΔpomAB* cells were inoculated on soft-agar plates for 72 h. At that time, several colonies displayed zones of increased extension into the soft agar. Chromosomal DNA was isolated from 8 individual mutants that retained the ability to swim through soft agar after several rounds of inoculation and incubation in planktonic cultures (. 1A), and the *motAB* region was sequenced. For all 8 isolates, mutations were identified in *motB*. 7 out of the 8 mutants revealed a T to C transition in three different loci resulting in amino acid substitutions (3 x Ser54Pro; 2x Ser56Pro; 2 x Leu60Ser). The remaining mutant had a deletion of 9 nucleotides resulting in the loss of three codons (residues 47-49, MetValGlu; ΔMVE) from the *motB* coding sequence. Western blotting and subsequent immunodetection of MotB revealed that all MotB variants were stably produced; however, the protein level varied between some of the mutants (Fig. 1B). An increase of MotB levels did not necessarily correlate with an increase of lateral extension in soft agar (Fig. 1A).

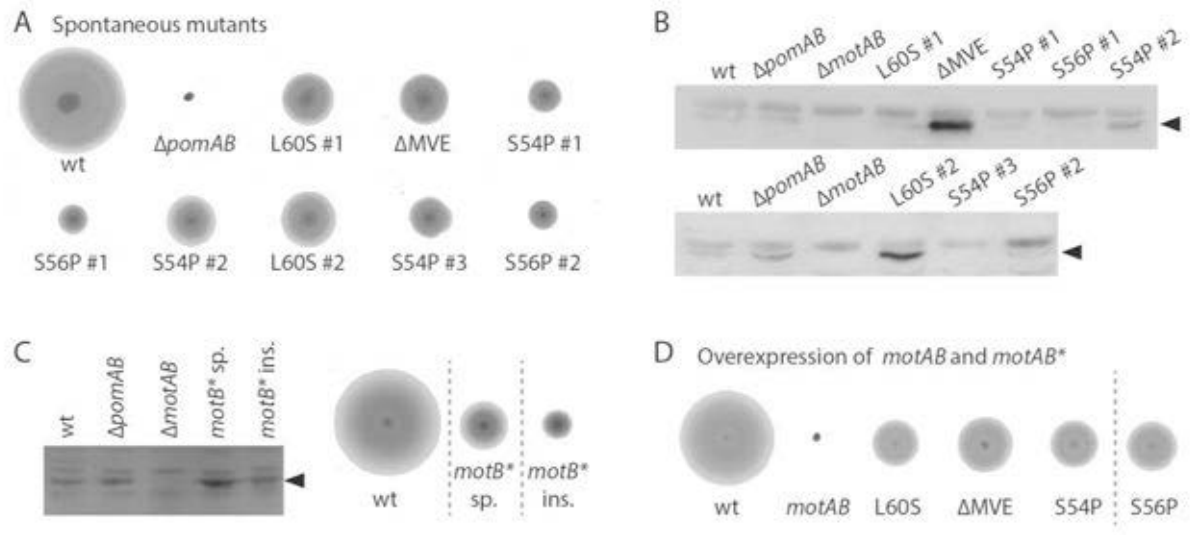

Figure 1: Characterization of point mutations in the plug domain of MotB. A) Soft agar swimming assays of the wild type (wt) and spontaneous mutants harboring an amino acid substitution in MotB as indicated. B) Immunoblot analysis of MotB production by the wild type, control strains (Δ*motAB* and Δ*pomAB*) and the spontaneous mutants as indicated, using an antibody raised against MotB. The arrows point to the position corresponding to the estimated molecular mass of MotB. See Fig. S1 for the corresponding loading control. C) Comparison of MotB production levels. Left panel: Shown is an immunoblot analysis of MotB production by the wild type, control strains (Δ*motAB* and Δ*pomAB*), the spontaneous ΔMVE mutant (sp.) and the mutant with an introduced ΔMVE deletion (ins.). The arrow points to the position corresponding to the estimated molecular mass of MotB. See Fig. S1 for the corresponding loading control. Right panel: Soft agar swimming assay of the wild type and the mutants harboring the spontaneous (sp.) or the introduced (ins.) ΔMVE deletion. D) Soft agar assay of wild-type and Δ*pomAB*Δ*motAB* mutant cells overproducing either wild-type MotAB or mutated versions from a plasmid under the control of an arabinose-inducible promoter. Note that each experiment is depicted at an individual scale. Therefore, every experiment has its own wild-type control. All soft agar assays were performed by placing small amounts of cells from plates on 0.25% soft-agar plates and followed by incubation at 30 °C for 24 h prior documentation of the lateral extension zones. Dashed lines indicate rearrangement of the original positions on the same soft-agar plate to allow a better comparison in the figure.

Next, we determined whether the observed gain of function of the MotAB stator was due to the substitutions/deletions identified in *motB* and not to other secondary mutations which might have occurred elsewhere in the genome. To this end, the mutated versions of *motAB* were individually expressed from a plasmid in the *ΔpomABΔmotAB* strain. Ectopic expression of all *motB* variants resulted in cells which displayed robust motility in soft-agar plates or when visualized microscopically (Fig. 1C). Overproduction of wild-type MotAB did not result in elevated swimming under both conditions (Fig. 1D). We therefore concluded that the identified mutations in *motB* are sufficient and predominantly responsible for the observed effect on swimming in the absence of PomAB.

To further determine whether the higher MotB levels observed in some of the mutants was due to elevated *motAB* expression or an increase in protein stability, we analyzed the *motB* transcript levels of the mutant bearing the ΔMVE deletion in MotB using a transcriptional *luxCDABE* reporter fusion (Fig. S2). Compared to the *ΔpomAB* strain, the *motB*ΔMVE allele showed an increased expression by a factor of about 4x, corresponding to the increase in the MotBΔMVE protein level. In contrast, an MVE deletion in *ΔpomAB* strains resulted in MotBΔMVE production to similar levels as non-mutated MotB cells, as confirmed by western immunoblotting (Fig. 1C). The strain retained the up-motile phenotype. Sequencing of the predicted promoter regions upstream of *motAB* did not reveal any further mutations, thus, the reason for an increase of *motB* expression in some of the strains is currently unknown.

Mutations in the 'plug domain' of MotB result in increased swimming ability conferred by MotAB

Interestingly, all mutations mapped to, or close to, the periplasmic region shortly upstream of the MotB transmembrane domain. This region is thought to form an amphipathic helix referred to as 'plug domain', which is required to prevent premature ion flow through the stator unit (Fig. 2A) (Hosking *et al.*, 2006, Kojima *et al.*, 2009, Li *et al.*, 2011). Accordingly, sequence analysis of MotB using HELIQUEST (Gautier *et al.*, 2008) predicted the occurrence of an amphipathic helix of 17 residues (MotB, aa 41-57). This stretch of amino acids also encompasses the residues found to be substituted or deleted in the MotB gain-of-function mutants, with the exception of Leu60Ser, which is located three residues downstream. All mutations that were isolated from gain-of-function mutants in MotB were found to break the amphipathic character of the 'plug domain'. To further confirm that mutations within this region of MotB might lead to increased swimming of MotAB-only driven cells, we introduced a series of mutations into MotB (Leu51Asp; Leu51Lys; Leu51Pro) which were predicted to affect the amphipathic nature of the domain. As expected, these MotB variants allowed motility in soft agar. In contrast, an amino acid substitution which does not interfere with the amphipathic character of the region (Phe46Lys) did not result in a MotB variant supporting motility in soft agar (Fig. 2B).

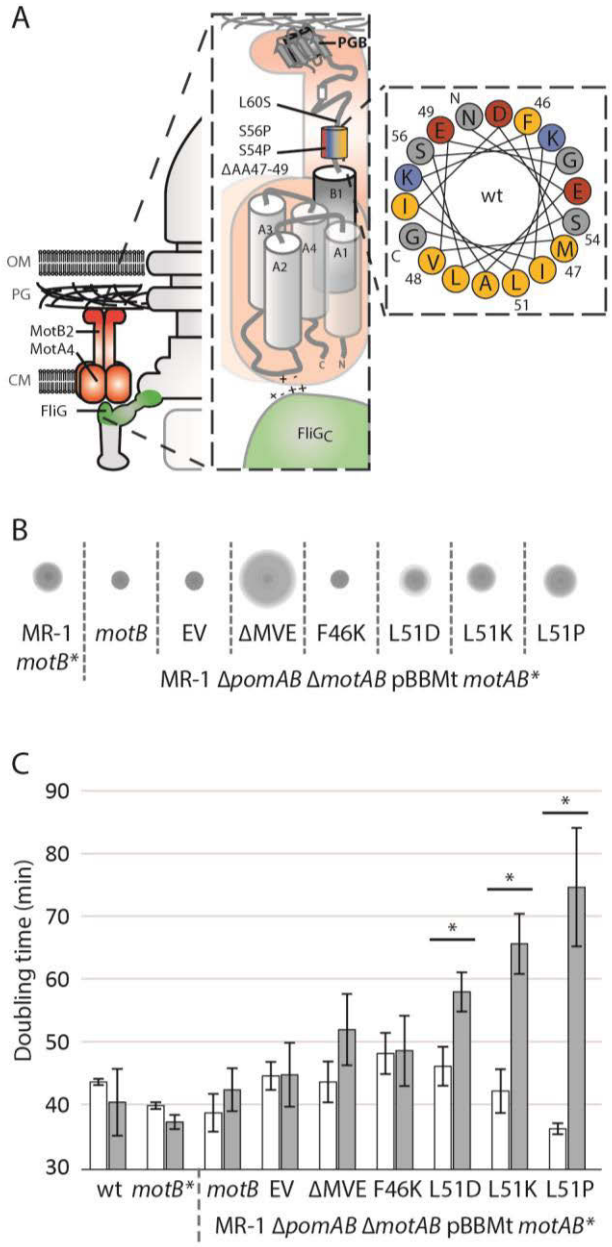

Figure 2: Analysis of the "plug domain" mutants. A) Schematic illustration of the MotAB stator and its plug domain (colored barrel). Right magnification shows a helix wheel projection of the plug domain from below. All amino acids mutated in this study are indicated by their number. B) Soft-agar assay of a ΔpomAB strain producing the inserted ΔMVE mutation (MR-1 motB*) and Δ*pomAB* Δ*motAB* mutants overproducing either wild-type MotAB or mutated versions from a plasmid under the control of an arabinose-inducible promoter. EV = empty vector control. Dashed lines indicate rearranged lateral extension zones from the same soft-agar plate. C) Doubling time [min] of wild-type (wt), MR-1 *motB** and the same Δ*pomAB* Δ*motAB* strains as in B overexpressing the indicated *motAB* variants from a plasmid under the control of an arabinose-inducible promoter. White bars show the doubling time without the addition of arabinose and grey bars the doubling time after addition of 0.2% arabinose (w/v). Error bar indicate the standard deviation. Asterisks indicate doubling times that are significantly different ($p < 0.05$).

Mutations in the 'plug domain' have previously been shown to result in ion leakage prior to incorporation into the flagellar motor (Hosking *et al.*, 2006) which may lead to reduced bacterial growth in the presence of elevated amounts of stator units upon overproduction (Li *et al.*, 2011). We therefore performed growth experiments on cells overproducing the mutated MotAB stator units to determine whether this similarly applies to *S. oneidensis* MR-1. To this end, the genes encoding the mutant variants of MotAB were ectopically expressed from a plasmid and growth of the cells was monitored. Cells overproducing MotAB variants in which the amphipathic nature of the periplasmic helix was disturbed exhibited a significantly lower growth rate, the extent varying between the different mutations (Fig. 1C). In contrast, production of the mutated stators at native levels had little or no effect on growth under the conditions tested (data not shown).

These results suggest that spontaneous mutations affecting the amphipathic character of the 'plug domain' in MotB may alter the properties of MotAB with respect to flagellar motor functions, allowing increased movement through viscous environments, but this comes at the expense of increased ion leakage through stators not engaged with the rotor. In addition, some mutants exhibit an increase in MotB levels. To further understand the effect of these mutations on motor functions we concentrated on the mutant

with a deletion of residues 47-49 (MetValGlu; MVE) in MotB, which was produced at similar amounts as the wild-type MotB (Fig. 1C) and has a pronounced gain-of-function phenotype with respect to motility while overexpression had little effect on growth. This mutant will henceforth be referred to as MotB* and, accordingly, the stator unit to as MotAB*.

MotAB* affects swimming speed and torque under planktonic conditions

To explore the properties of flagellar motors driven by MotAB*, we monitored the cellular swimming behavior under planktonic conditions at high and low levels of Na^+, as Na^+ levels have been demonstrated to affect MotAB recruitment into the flagellar motor (Paulick *et al*., 2015). At high Na^+ concentrations, cells driven by non-mutated MotAB were determined to swim at an average speed of 21.5 ± 10.9 µm · s^{-1}. In contrast, cells producing MotAB* were found to swim significantly slower at 13.4 ± 7.1 µm · s^{-1}. Also under conditions of low Na^+, MotAB*-driven cells were still swimming at a significantly lower speed (10.5 ± 5.5 µm · s^{-1}) compared to cells equipped with non-mutated MotAB (19 ± 13.4 µm · s^{-1}). In a previous study we have shown that, in *S. oneidensis* MR-1 wild-type cells, MotAB likely forms a hybrid stator ring together with Na^+-dependent PomAB stator units (Paulick *et al.*, 2015). We therefore looked at the effect of replacing MotAB with MotAB* in wild type motor. We found that MotAB* had no positive effect on swimming speeds compared to non-mutated MotAB in the presence of PomAB
at high or low levels of Na^+ (data not shown). In addition, we did not observe a significant difference between the average directional switching rate of MotAB- and MotAB*-driven cells (0.17 and 0.13 turns per second, respectively).

To further determine whether MotAB* had an effect on flagella-mediated movement under more viscous conditions, we compared the swimming speed of MotAB- and MotAB*-driven cells in medium in which the viscosity was increased by the addition of Ficoll. While at a concentration of 5% Ficoll the subpopulation of motile cells was not significantly different for MotAB and MotAB* (44 ± 12 % and 41 ± 8 %, respectively), the subpopulation of motile MotAB cells dropped sharply (10 ± 5 %) but remained almost constant for MotAB* (40 ± 7 %) in solutions containing 10% Ficoll. At a concentration of 12.5 % Ficoll, swimming of MotAB*-driven cells was almost completely inhibited, whereas a significant population (29 ± 8 %) of MotAB*-propelled cells still displayed robust swimming (Fig. 3).

Thus, while MotAB*-driven flagellar motors mediate lower swimming speed of the cells, they allow motility under conditions of elevated viscosity while not affecting the directional switching rates. We hypothesize that this property significantly benefits the movement of cells through environments structured by polysaccharides, such as soft-agar plates.

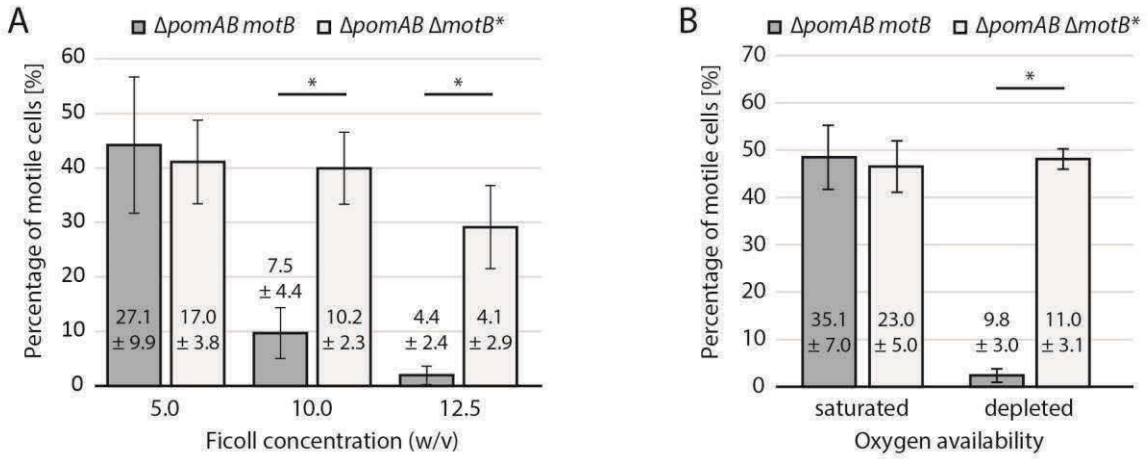

Figure 3: Motile fraction and swimming speeds at elevated viscosity. Motility of cells expressing either MotAB (grey bars) or MotAB* (white bars) was tested in LB broth containing 5, 10 or 12.5% (w/v) Ficoll (A) or in LM100 medium with saturated (left) and depleted (right) oxygen levels. The average swimming speed of each strain under each condition is indicated as numbers together with the corresponding bar. The error bars represent the standard deviation. The asterisks indicate the subpopulations [%] that were significantly different from each other ($p<0.05$).

MotAB* mediates motility under anaerobic conditions

When quantifying the swimming speed of the cells, we constantly observed that motility of MotAB-driven cells rapidly ceased, while cells of a MotAB* population at a comparable density continued vigorous swimming. However, swimming of MotAB-driven cells continued at higher dilutions, suggesting either nutrient levels or molecular oxygen might be limiting. Using a set-up previously established to monitor and quantify type IV pilus retraction and twitching motility while simultaneously determine the oxygen concentration, we measured the dependency of motility on oxygen levels (Kurre and Maier, 2012, Dewenter *et al.*, 2015). *ΔpomAB* cells harboring wild-type MotAB or mutated MotAB* were introduced into this system at an optical density of 0.05 and the percentage of actively swimming cells and the corresponding average speed were quantified in dependence of the oxygen concentration in the medium (Fig. 3B). At oxygen saturation levels, wild-type MotAB mediated robust motility at an average speed of about 35 µm ± 7 · s^{-1} in about 50 % of the population. The swimming speed remained relatively constant until the oxygen concentration reached about 5 µmol · l^{-1}. Between 5 and 0 µmol · l^{-1} oxygen concentration, the swimming speed of almost the whole population rapidly dropped to below threshold levels. When cells driven by the mutated MotAB* stators were monitored, the subpopulation of actively moving cells was determined to be similar (about 57 %) to that of wild-type MotAB-powered cells at a lower swimming speed (about 23 ± 5 µm · s^{-1}). Also for MotAB*-driven cells, the swimming speed started to drop sharply when the oxygen concentration reached 5 µmol · l^{-1}. However, the population of actively swimming cells remained constant at the same level at a speed of about 11 ± 3 µm · s^{-1} even when the molecular oxygen was consumed.

These results clearly demonstrate that activity of the MotAB stator is directly correlated with the amount of available molecular oxygen. While the normal MotAB stator stops functioning immediately when the measured oxygen is consumed, the MotAB* stator continues to support motility under anaerobic conditions, suggesting that these mutant stators can continue functioning at low proton gradients.

Similar exchange rate and stoichiometry of MotAB* in the flagellar motor

We have previously shown that 7-8 MotAB stator units are present in the *S. oneidensis* MR-1 flagellar motor at high Na^+ concentrations, which are constantly exchanged with membrane-located spares (Paulick *et al.*, 2015). To determine whether or not MotAB* engage in the motor at similar numbers and exchange at a similar rate, we used similar fluorescence microscopy approaches. To this end, we constructed fluorescent fusions to the periplasmic C-termini of MotB and MotB* using mCherry as a fluorophore, which is also fluorescent after export into the periplasm. Both *motB-mCherry* and *motB*-mCherry* fusions were integrated into the chromosome of *S. oneidensis* MR-1 *ΔpomAB*, where they replaced native *motB*. The fluorescently tagged MotB/MotB* proteins were stably produced and mediated robust motility (Fig. S3).

To determine the number of stator units within the motor, we performed stepwise photobleaching experiments on stationary fluorescent foci at the cell pole considered to be part of the flagellar motor.

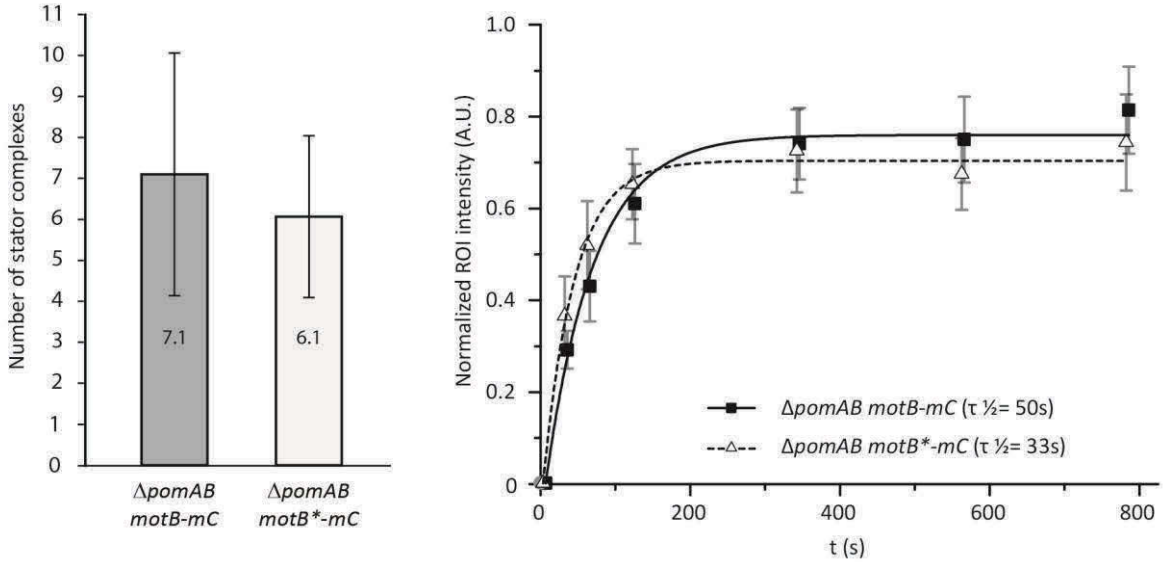

Figure 4: Quantity and exchange halt time of MotAB and MotAB*. Left panel: Quantification of single MotB (grey bar) and MotB* (white bar) units fused to mCherry. The number of single MotBmCherry molecules was calculated by the number of distinct steps in intensity loss during continuous photobleaching. The number of MotB*mCherry in the motor was subsequently calculated by comparison of the initial fluorescence intensities of whole stator cluster formed by MotBmCherry and MotB*mCherry. Error bars represent the standard deviation. Right panel: Normalized averaged fluorescence intensity as a function of time obtained from a FRAP analysis of MotBmCherry (solid black square and line) and MotB*mCherry (open triangle and dashed line). The half-times of recovery (τ ½) were calculated by fitting an exponential decay to the averaged normalized fluorescence intensity of clusters of 29 cells for each strain. Error bars indicate the standard error of the mean. mC = mCherry.

About 7 ± 4 MotAB stator units were found to be present in the flagellar motor (Fig. 4), which was consistent with our previous observations. Under similar conditions, the number of mutated MotAB* stator units (6 ± 2) was determined to not significantly differ from the number of the native MotAB stator units. To further quantify the extent of stator unit exchange in the flagellar motors, we performed Fluorescence Recovery After Photobleaching (FRAP) experiments on the MotB-mCherry or MotB*-mCherry clusters at the cell pole. Both wild-type and mutated stator complexes were found to undergo exchange within the motor, and fluorescence recovered to similar levels which indicated an exchange of the complete stator population. The exchange of MotAB*-mCherry and MotAB*-mCherry stator units occurred at a similar rate (half-time of recovery MotAB-mCherry, 50 ± 5 s; MotAB*-mCherry, 33 ± 5 s). This may suggest a less stable assembly of MotAB* in the flagellar motor, although these differences were not statistically different. Taken together, these results suggest that, under our experimental conditions, both MotAB and MotAB* stator units are similarly well recruited and retained by the rotor.

MotXY, but not FliL, are required for MotAB* activity

Correct stator recruitment and activity has been shown to depend on several components within the flagellar motor. One of these components is the T-ring, which is formed by the MotX and MotY proteins in many Na^+-dependent motors, such as those of *Vibrio*, *Shewanella*, or *Aeromonas* (Terashima *et al.*, 2006, Koerdt *et al.*, 2009, Molero *et al.*, 2011). To determine whether the activity of MotAB* also relies on the presence of MotX and MotY, *motX* and *motY* were deleted in *ΔpomAB* and *ΔpomAB motB** background strains. We then determined flagella-mediated movement of the resultant mutants. In the absence of MotX and/or MotY, neither MotAB nor the mutated MotAB* stator conferred motility on soft-agar plates or when observed microscopically (Fig. 5A). Thus, a mutation in the stator's plug domain does not alter the requirement of the T-ring for recruitment to and/or activation of MotAB the *S. oneidensis* MR-1 flagellar motor.

A second motor component involved in mediating proper rotor-stator interaction is FliL (Partridge *et al.*, 2015, Zhu *et al.*, 2015). To determine whether FliL has a similar role in *S. oneidensis* MR-1, we introduced an in-frame deletion in the corresponding gene and quantified the swimming speed of the resulting mutants. As previously observed in *Salmonella* and *Vibrio*, loss of FliL resulted in a significant reduction of swimming speed in *S. oneidensis* MR-1. Furthermore, fluorescently labeled FliL-mCherry displayed a similar localization pattern in the cell envelope and at the cell pole (Fig. 5D), strongly indicating that *So*FliL has a function similar to that previously reported for *Salmonella* and *Vibrio*. When *fliL* was deleted in a *ΔpomAB* mutant, the swimming speed significantly decreased from about 35 ± 12 $\mu m \cdot s^{-1}$ to 25 ± 11 $\mu m \cdot s^{-1}$. In contrast, cells whose flagella were driven by MotAB* do not show a significant drop in velocity in the absence of FliL (*motAB**, 26 ± 9 $\mu m \cdot s^{-1}$; *motAB*ΔfliL,* 22 ± 7 $\mu m \cdot s^{-1}$).

The data strongly suggests that, as reported for *Salmonella* (Partridge *et al.*, 2015), the mutation in the plug domain results in a stator unit whose function is less dependent on FliL.

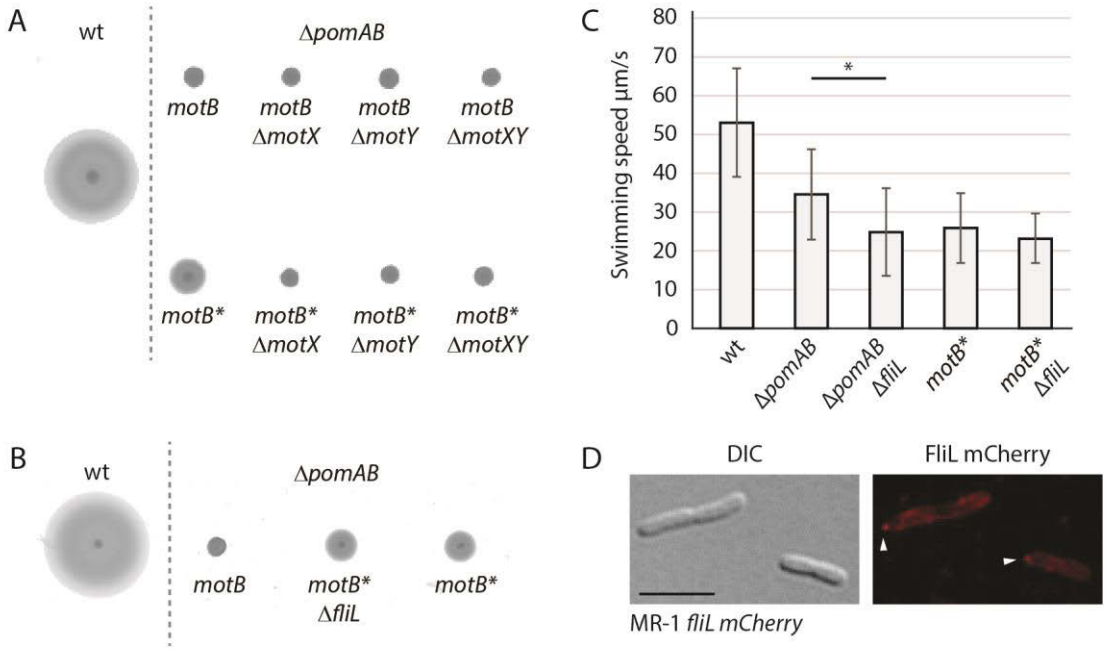

Figure 5: Role of FliL and MotXY in motility powered by MotAB and MotAB*. A, B) Soft-agar assay of wild-type (wt), MR-1 *motB* and MR-1 *motB** combined with deletions of *motX* and *motY* (A) or *fliL* (B). Cells of liquid cultures were inoculated on soft agar plates containing 0.25% (w/v) agar and incubated for 24h at 30°C prior to analysis of radial extensions. All strains right from the dashed line carried a deletion of *pomAB*. C) Swimming speeds of wild-type, MR-1 *motB* and MR-1 *motB** with and without deletions of *fliL*. Speed of MR-1 *motB* and MR-1 *motB* Δ*fliL* differed significantly as indicated by the asterisk. Error bars represent the mean standard deviation. C) Localization of FliL fused to mCherry. Displayed are DIC and fluorescent micrographs. Arrows point to polar fluorescent clusters and the scale bar represents 5µm.

Discussion

We previously showed that *S. oneidensis* MR-1 possesses two different distinct stator units, Na^+-dependent PomAB and H^+-driven MotAB, which are each solely capable of driving flagellar rotation. The MotAB stator increases flagella-mediated swimming under conditions of low environmental Na^+ concentrations (Paulick *et al.*, 2015, Paulick *et al.*, 2009). However, in the absence of PomAB, MotAB-driven flagellar motors do not allow cells to move efficiently through complex environments, such as soft agar, and, in addition, swimming under planktonic conditions is rapidly lost. Here we have isolated four independent MotB mutants that confer an up-motile phenotype on soft-agar plates, and each of the mutation was mapped to or close to the 'plug domain' of MotB. This domain, a short amphipathic helix located closely upstream of the N-terminal transmembrane region, is a common feature of B-subunits of stators. The 'plug domain' itself is not essential for general stator functions, as both MotB and PomB variants still form active stator complexes with the corresponding A-subunit when large regions including the amphipathic helix have been deleted (Li *et al.*, 2011, Muramoto and Macnab,

1998, Morimoto *et al.*, 2010a). A number of studies provided evidence that the 'plug domain' prevents ion leakage into the cytoplasm from stators diffusing in the membrane until conformational changes of the B-subunits induced upon stator binding to the rotor enable binding to the peptidoglycan and activation of ion flow (Hosking *et al.*, 2006, Kojima *et al.*, 2009, Zhu *et al.*, 2014, Kojima, 2015). As MotAB/PomAB crystal structures including this stator region are lacking, the exact orientation of this domain remains unclear. The amphipathic nature of the domain has led to the suggestion that interaction of the helix with the hydrophobic core of the membrane keeps the ion channels closed (Hosking *et al.*, 2006)). However, a recent model on the MotAB stator suggests that the expected length of the domain is too short to fulfill this function (Nishihara and Kitao, 2015). Overproduction of all isolated MotB variants in *S. oneidensis* MR-1 results in a significant growth phenotype, strongly indicating that the functional MotB variants become leaky upon breaking the amphipathic character of the 'plug domain'. The extent of the growth defect caused by the mutations in MotB differed considerably and did not correlate with the increase in cellular spreading through soft agar, suggesting that when engaged they function well and only when disengaged from the rotor do the plug domain mutations allow leakage.

It should be noted that, in a previous study on *S. oneidensis* MR-1 stators, we were unable to attribute an observed up-motile phenotype of *ΔpomAB* mutant cells to mutations within *motAB* (Paulick *et al.*, 2009). We therefore speculate that, in addition to those directly affecting the stator-encoding genes, other mutations may also improve the function of MotAB. Such mutations may occur in structures involved in stator recruitment and activation, such as MotX/Y and FliL, or rotor-stator interactions, such as FliG, or they might lead to an increase of the *motAB* expression levels. Here we showed that, in *S. oneidensis* MR-1, overexpression of wild-type *motAB* is not sufficient to induce an up-motile phenotype on soft-agar plates, unlike the *B. subtilis* MotPS stator (Terahara *et al.*, 2006). However, we found that MotB levels were not always consistent across *motB* mutants affected in the same amino acid residue but were isolated from independent cultures (Fig. 1A). In some instances, higher MotAB levels were found to correlate with a further increase in motility of the corresponding mutants on soft-agar plates (Fig. 1B). However, since overproduction of stator units with defects in the plug domain commonly entails a significant growth phenotype, we hypothesize that such mutations are rather rapidly lost when competing in planktonic cultures without selection for MotAB-driven motility, as we have observed previously (Paulick *et al.*, 2009).

The mutations in the 'plug region' of MotB allowed a number of changes in motor behavior. One major difference in motor properties conferred by MotAB* was that the mutated stator allows the cells to move through more viscous environments than wild-type MotAB. This could be explained by the loose

coupling model for flagellar motors (Boschert *et al.*, 2015). If the mutation induces a slight conformational change in the channel that increases the pK_a of the coupling ion-binding site (Asp21 in *S. oneidensis* MR-1 MotB), the resulting stator could provide more torque near stall than wild-type MotAB. Following this model, a higher pK_a would, on the other hand, result in a lower stepping rate and hence, slower speed. This is also in line with our observation that MotAB*-driven cells were significantly slower during normal planktonic swimming. Similar torque-speed relationships were recently reported for an *E. coli* MotB stator variant lacking a stretch of 28 amino acids located in the periplasmic domain of MotB almost immediately upstream of the plug region (Castillo *et al.*, 2013). Based on estimations of active stator components within the motor at medium load, the authors suggested that the deletion affects the normal load-sensing mechanism, which leads to an increase of active stator units upon elevated load on the filament (Lele *et al.*, 2013, Tipping *et al.*, 2013a). This may similarly apply to MotAB* in *S. oneidensis* MR-1. Under our experimental conditions, neither the number of MotAB* stator units nor the exchange rate within the motor at stall was significantly different from those of wild-type MotAB, suggesting that the ΔMVE deletion within the plug domain affects stator activity rather than stator recruitment. Accordingly, our results indicate that the activity of the mutated MotAB* stator is independent of the flagellar protein FliL. Recent studies on several bacterial species strongly indicate that this protein interacts with both the stator and the flagellar basal body to increase the ability of the stator/rotor system to create sufficient torque required under conditions such as swarming or moving through structured or viscous environments (Suaste-Olmos *et al.*, 2010, Partridge *et al.*, 2015, Zhu *et al.*, 2015). Our results are consistent with the studies on *Rhodobacter* and *Salmonella* MotB which both previously demonstrated that mutations affecting the 'plug region' effectively suppress motility phenotypes of mutants lacking *fliL*. We therefore concur with the corresponding models that FliL might favor the unplugged state of the stators to increase stator engangement with the motor and benefits stator activation and/or efficiency of ion flow (Partridge *et al.*, 2015, Suaste-Olmos *et al.*, 2010). In contrast, in *S. oneidensis* MR-1, the T-ring structure formed by MotX and MotY, which is commonly present in Na^+-driven motors, remains essential for MotB activity also when the plug domain is mutated. It remains to be shown whether the T-ring is also required for stator activation or whether it is rather required for retention and stability of the stator within the flagellar motor.

In addition to allowing spreading in soft-agar plates, the mutated MotAB* stators allowed the flagellar rotation under anaerobic conditions. By synchronous measurements of swimming speed and the concentration of molecular oxygen we show that swimming using the wild-type MotAB stator stops when the oxygen is used up, while MotAB*- (and also PomAB-)driven cells continued swimming. Lack of oxygen results in pronounced decrease in the *pmf* in *E. coli* and *Salmonella* (Setty *et al.*, 1983,

Kashket, 1981), and a reduction in aerobic respiration will be expected to have the same effect on *S. oneidensis* MR-1. Accordingly, previous studies on H^+- and Na^+-fueled motors provided evidence that functional rotor-stator interactions directly depend on the corresponding ion motive force (*imf*) (Tipping *et al.*, 2013b, Fukuoka *et al.*, 2009, Fung and Berg, 1995). Collapse of the *imf* may, but not necessarily has to, result in physical detachment of the stators from the motor (Morimoto *et al.*, 2010b, Tipping *et al.*, 2013b, Fukuoka *et al.*, 2009). Species of the genus *Shewanella* are able to use a wide array of alternative electron acceptors in the absence of oxygen, thus, it will be expected that the cells maintain a low *pmf* even after oxygen has been exhausted. We assume it rather unlikely that the different mutant strains used in this study maintain different levels of *pmf* under the same conditions. This is suggesting that at low *pmf*s the mutated MotAB stators remain engaged and functional while the native MotAB stators are closed and non-active, supporting the hypothesis that the mutations may alter the pK_a of ion-binding within the stator. Further studies will have to show whether or not MotAB (re-)activation and function requires a certain *pmf* level and whether the plug domain is involved in *imf*-dependent stator activation.

The stator units determine various flagellar motor properties with respect to the coupling ion that is used for rotation, and torque and speed that can be provided (reviewed in (Morimoto and Minamino, 2014, Kojima, 2015)). The general features of stator units, such as the domain organization of the A- and B-subunits and the position of critical residues are highly conserved across species and flagellar motors, irrespective of the coupling ion used. Therefore, stator units, or chimeras derived from different stators, are often functional when transferred into a different species and may even convert the coupling ion from Na^+ to H^+ and *vice versa* (Gosink and Häse, 2000, Asai *et al.*, 2003).
It easy to conceive that the addition of a second stator set, either by acquisition by horizontal gene transfer or formation of a paralogous system through duplication events, may be a useful asset to an existing flagellar machinery. Numerous bacterial species do possess two or more distinct stator systems to drive rotation of the flagellum (reviewed in (Thormann and Paulick, 2010)). Several lines of evidence suggest that *S. oneidensis* MR-1 has only recently acquired *motAB* by horizontal gene transfer and that the encoded set of stators is not yet fully adjusted to the originally PomAB-driven flagellar motor. We and others have shown that single nucleotide transitions within the stator genes are sufficient to significantly alter the flagellar motor properties and, thus, are potentially important drivers of the functional diversification of bacterial flagellar motors.

Experimental Procedures

Bacterial strains, growth conditions, media

All strains used in this study are listed in Table S1. *Shewanella oneidensis* MR-1 (MR-1) strains were cultivated at 32°C in LB, LM 100 (10 mM HEPES, pH 7.5; 100 mM NaCl; 0.02% yeast extract; 0.01% peptone; 15 mM lactate), or LM 0 (LM 100 without NaCl). *Escherichia coli* strains were cultured at 37°C in LB. *E. coli* WM3064 cultures were supplemented with 2,6-diamino-pimelic acid (DAP) to a final concentration of 300µM. When necessary, 50 µg ml^{-1} kanamycin or 10% (w/v) sucrose or 1.5% (w/v) agar was added to the media. Soft agar plates were prepared with LB and 0.2% (w/v) agar.

Strain constructions

Genetic manipulations of *S. oneidensis* MR-1 were always introduced into the genome to replace the native gene locus, unless stated otherwise. The in-frame deletions or chromosomal integration of gene variants or fusions were obtained by sequential double homologous recombination using vector pNTPS-138-R6K carried out essentially as previously described (Lassak *et al.*, 2010). Vectors were transferred into MR-1 cells by conjugation with *E. coli* WM3064.

Vector constructions

All vectors and oligonucleotides used in this study are listed in Tables S2 and S3. Construction of the vectors was carried out using either appropriate standard restriction/ligation or Gibson assembly (Gibson *et al.*, 2009). All kits for preparation and purification of nucleic acids (VWR International GmbH, Darmstadt, Germany) and enzymes (Fermentas, St. Leon-Rot, Germany) were used according to standard manufacturers' protocols. To generate markerless in-frame deletions, 500-750 bp fragments of the up- and downstream region of a gene were combined to create a deletion leaving only eight codons of the 5'- and 3'-termini of the corresponding genes. Compared to our previous study using mCherry-fused stators (Paulick *et al.*, 2015, Paulick *et al.*, 2009), the linker region connecting MotB and mCherry was modified to improve activity of the fluorescently tagged protein. To this end MotB was fused to mCherry via a 22 amino acids long linker by amplifying *mCherry* with flanking BglII and EcoRI sites following insertion into pVENC-2 and a release of the mCherry-linked fragment by HindIII and EcoRI. The resulting fragment was subsequently joined with amplicons of the regions flanking the C-terminus of *motB* via overlap PCR. FliL was N-terminally fused to mCherry connected by a 3 x GGS linker. To this end, ~750 bp long fragments encompassing the up- and downstream region of the *fliL* 5'-end were fused to the 5'- and 3'-end of *mCherry*. For the transcriptional *lux* reporter fusion a ~700 bp fragment upstream of *motB* including its start codon was amplified using either chromosomal DNA from wild-type or a strain carrying the ΔMVE deletion as a template and transcriptionally fused to the *luxCDABE* operon amplified from mini-Tn*7*T-Gm-*lux* (Choi *et al.*, 2005). The fusion product was ligated

into pNPTS-138-R6KT. The resulting vector pNPTS-138-R6KT *PmotB luxCDABE* was transferred into the appropriate strain by conjugation and integrated into the chromosome via a single homologous recombination.

For overexpression of the *motB* variants the pBBMt vector was constructed using the pBBR1-MCS2 backbone, the promoter and multiple cloning site region were amplified from pBAD/HisA (Thermo Fisher Scientific, Waltham, USA) and the terminator region from pUC18-mini-Tn*7*T-Gm-*lux* (Choi *et al.*, 2005). Promoter/MCS and terminator fragments were amplified using primer sets B207/SH144 and B205/B206, respectively. The promoter/MCS fragment as well as pBBR1-MCS2 backbone were cut using SacI and XbaI and ligated. The resulting plasmid and the terminator fragment were subsequently digested with KpnI and PspOMI and ligated to yield pBBMt.

Determination of transcriptional levels via lux *fusions*

To determine transcriptional activity of *motB*, appropriate strains bearing the transcriptional *lux* fusion were cultivated in LM100 overnight. The following day, 1/100 dilutions of the cultures were grown to an OD_{600} of ~0.25. Then, 180 µl aliquots were transferred to white polystyrene plates (Greiner Bio One, Frickenhausen, Germany), and luminescence was quantified using a Tecan Infinite M200 plate reader. Values of 6 measurements were averaged and luminescence normalized to the corresponding culture density (OD_{600}).

Fluorescence microscopy

Prior to microscopy, strains were cultivated overnight in LM media and subcultured in LM to exponential growth phase (OD_{600} = 0.2 - 0.3). 4µl of culture were spotted on a PBS agarose pad (137 mM NaCl, 2.7 mM KCl, 10 mM Na_2HPO_4 and 1.8 mM KH_2PO_4, adjusted to pH 7.4 and solidified by 1% (w/v) agarose). Fluorescence images were recorded using a Leica DMI 6000 B inverted microscope (Leica, Wetzlar, Germany) equipped with an sCMOS camera (Visitron Systems, Puchheim, Germany) and an HCX PL APO 100×/1.4 objective. Image processing and analysis was carried out using the ImageJ-based Fiji tool (Schindelin *et al.*, 2012).

Motility assays

Cells of MR-1 strains from overnight cultures were used to inoculate 10ml of LM medium to an OD_{600} of 0.01. After reaching an OD_{600} of 0.2-0.3 a 50 µl aliquot was placed under a coverslip fixed by four droplets of silicone (baysilone, VWR International GmbH, Darmstadt, Germany) to generate a space of 1-2mm hight. Movies of 100 frames were taken with a Leica DMI 6000 B inverse microscope (Leica, Wetzlar, Germany) equipped with an sCMOS camera (Visitron Systems, Puchheim, Germany) and an HCX PL APO 100×/1.4 objective. The speed of at least 150 cells per strain was quantified using the

MTrackJ plugin of Fiji (Meijering *et al.*, 2012). Significance was tested using ANOVA (p = 0.05) in R version 3.0.1. Motility in semi-solid environments was analyzed by placing 3µl of a planktonic culture or cell material from solid plates on soft agar plates followed by an incubation of 24h at 30°C. Strains to be directly compared were always placed on the same plate.

Fluorescence recovery after photobleaching (FRAP)

To determine the exchange rate of stators within the flagellar motor, we used the same FRAP setup as previously described (Rossmann *et al.*, 2015). Cells were cultured and immobilized on agarose pads as described above. After acquisition of a pre-bleach image a single laser pulse of 100 ms was used to bleach individual MotB-mCherry clusters. Fluorescence recovery was subsequently monitored at 30, 60, 120, 340, 560, 780, 1000 and 1220 sec post bleaching. The integrated fluorescence intensities of the whole cell, the bleached region and a background area were measured for each time point using Fiji. After background correction, the fluorescence intensities of the bleached regions were divided by the whole cell intensity to correct for general photobleaching during the imaging process. Average values of 29 cells for each strain were plotted using OriginPro 9.1. Recovery rates were determined by fitting the data obtained for the bleached region to the single exponential function $F(t) = \Delta F*(1-\exp(-x/t_1))+F_0$, where F(t) is the fluorescence at time t, ΔF the maximum change in fluorescence during recovery, x the time in min, $1/t_1$ the rate constant in min^{-1}, and F_0 the fluorescence intensity immediately after the bleaching step (t=0 min). In all cases, fits with $R2 \geq 0.99$ were obtained. Recovery half-times were calculated according to the equation $\tau_{1/2} = \ln(2)*t_1$.

Stoichiometry

Cells from overnight cultures were used to inoculate 10ml of LM supplemented with 100 mM KCl and adjusted to a pH of 7.3 to an OD_{600} of 0.05. At mid-exponential growth phase (OD_{600} of 0.2 – 0.3), 1 ml of cells was harvested by centrifugation and washed twice in 4M buffer (50 mM HEPES; 200 mM NaCl; 15 mM lactate, pH 7). 5µl of the suspension was spotted on an agarose pad prepared with 4M buffer. Stoichiometry of MotB stator complexes was determined essentially as described previously (Leake *et al.*, 2006, Paulick *et al.*, 2015) with the following modification: Movies of 300 frames were recorded with each frame being exposed for 0.1 s by applying a laser power of 0.1 mW with an excitation wavelength of 550 nm. Stoichiometry of MotB ΔMVE-mCherry stator was calculated by measuring initial fluorescence intensities of 450 stator cluster using ImageJ and relating them to MotB-mCherry. Statistical analyses were done using R version 3.0.1. Prior to analysis, data was log-transformed to satisfy the assumptions of homoscedasticity and normally distributed residuals. Significant differences were calculated using ANOVA ($p < 0.05$).

Oxygen-speed dependency

Measurement of oxygen concentration has been described in detail in (Kurre and Maier, 2012). In short, an oxygen sensor based on the oxygen sensitive dye Pt(II) meso-tetra(pentafluorophenyl)porphine PtTFPP (Frontier Scientific, Logan, Utah, USA) was fabricated to monitor oxygen consumption and bacterial motility simultaneously (Thomas *et al.*, 2009). The stock solution of PtTFPP (20mM in toluene) was stored at RT. PtTFPP is embedded in a Sylgard 184 polydimethylsiloxane network (PDMS, Dow Corning, Midland, Michigan, USA). Therefore, PDMS was mixed with Sylgard 184 curing agent (Ratio 10:1) and 1mM PtTFPP and directly spin-coated on cover slides to result in ~30 µm thin layers. In the end, oxygen sensors were cured at 60°C for at least 3 hours. Calibration and oxygen measurements are described in (Kurre and Maier, 2012). Images for oxygen measurements were taken every 60 s at a distance of 60 µm away from the site where the swimming speed was imaged to avoid photodamage. The swimming speed experiments were performed in a sealed chamber with a volume of 100µl in LM-medium. The density of bacteria was adjusted to OD_{600} of 0.1. This density supported swimming motility while enabling undisturbed swimming and tracking. Glass slides were sealed with VALAP. The chamber was mounted into an inverted microscope (Nikon TI). A built-in thermobox in the microscope maintained the temperature at 30°C. Swimming speed was measured as described above.

Immunofluorescence analysis

Production and stability of MotB and its fusions were determined by immunoblot analyses. Protein lysates were prepared from exponentially growing cultures. Cell suspensions were uniformly adjusted to an OD_{600} of 10. Protein separation and immunoblot detection were essentially carried out as described earlier (Bubendorfer *et al.*, 2012, Binnenkade *et al.*, 2014) using polyclonal antibodies raised against mCherry (Eurogentec Deutschland GmbH, Köln, Germany) or the periplasmic part of MotB. Signals were detected using the SuperSignal® West Pico Chemiluminescent Substrate (Thermo Scientific, Schwerte, Germany) and documented using a FUSION-SL chemiluminescence imager (Peqlab, Erlangen, Germany).

To determine the exchange rate of stators within the flagellar motor, we used the same FRAP setup as previously described (Rossmann *et al.*, 2015). Cells were cultured and immobilized on agarose pads as described above. After acquisition of a pre-bleach image a single laser pulse of 100 ms was used to bleach individual MotB-mCherry clusters. Fluorescence recovery was subsequently monitored at 30, 60, 120, 340, 560, 780, 1000 and 1220 sec post bleaching. The integrated fluorescence intensities of the whole cell, the bleached region and a background area were measured for each time point using Fiji. After background correction, the fluorescence intensities of the bleached regions were divided by

the whole cell intensity to correct for general photobleaching during the imaging process. Average values of 29 cells for each strain were plotted using OriginPro 9.1. Recovery rates were determined by fitting the data obtained for the bleached region to the single exponential function $F(t) = \Delta F*(1-\exp(-x/t_1))+F_0$, where F(t) is the fluorescence at time t, ΔF the maximum change in fluorescence during recovery, x the time in min, $1/t_1$ the rate constant in min^{-1}, and F_0 the fluorescence intensity immediately after the bleaching step (t=0 min). In all cases, fits with $R2 \geq 0.99$ were obtained. Recovery half-times were calculated according to the equation $\tau_{1/2} = \ln(2)*t_1$.

Stoichiometry

Cells from overnight cultures were used to inoculate 10ml of LM supplemented with 100 mM KCl and adjusted to a pH of 7.3 to an OD_{600} of 0.05. At mid-exponential growth phase (OD_{600} of 0.2 – 0.3), 1 ml of cells was harvested by centrifugation and washed twice in 4M buffer (50 mM HEPES; 200 mM NaCl; 15 mM lactate, pH 7). 5µl of the suspension was spotted on an agarose pad prepared with 4M buffer. Stoichiometry of MotB stator complexes was determined essentially as described previously (Leake *et al.*, 2006, Paulick *et al.*, 2015) with the following modification: Movies of 300 frames were recorded with each frame being exposed for 0.1 s by applying a laser power of 0.1 mW with an excitation wavelength of 550 nm. Stoichiometry of MotB ΔMVE-mCherry stator was calculated by measuring initial fluorescence intensities of 450 stator cluster using ImageJ and relating them to MotB-mCherry. Statistical analyses were done using R version 3.0.1. Prior to analysis, data was log-transformed to satisfy the assumptions of homoscedasticity and normally distributed residuals. Significant differences were calculated using ANOVA ($p < 0.05$).

Oxygen-speed dependency

Measurement of oxygen concentration has been described in detail in (Kurre and Maier, 2012). In short, an oxygen sensor based on the oxygen sensitive dye Pt(II) meso-tetra(pentafluorophenyl)porphine PtTFPP (Frontier Scientific, Logan, Utah, USA) was fabricated to monitor oxygen consumption and bacterial motility simultaneously (Thomas *et al.*, 2009). The stock solution of PtTFPP (20mM in toluene) was stored at RT. PtTFPP is embedded in a Sylgard 184 polydimethylsiloxane network (PDMS, Dow Corning, Midland, Michigan, USA). Therefore, PDMS was mixed with Sylgard 184 curing agent (Ratio 10:1) and 1mM PtTFPP and directly spin-coated on cover slides to result in ~30 µm thin layers. In the end, oxygen sensors were cured at 60°C for at least 3 hours. Calibration and oxygen measurements are described in (Kurre and Maier, 2012). Images for oxygen measurements were taken every 60 s at a distance of 60 µm away from the site where the swimming speed was imaged to avoid photodamage. The swimming speed experiments were performed in a sealed chamber with a volume of 100µl in LM-medium. The density of bacteria was adjusted to OD_{600}

of 0.1. This density supported swimming motility while enabling undisturbed swimming and tracking. Glass slides were sealed with VALAP. The chamber was mounted into an inverted microscope (Nikon TI). A built-in thermobox in the microscope maintained the temperature at 30°C. Swimming speed was measured as described above.

Immunofluorescence analysis

Production and stability of MotB and its fusions were determined by immunoblot analyses. Protein lysates were prepared from exponentially growing cultures. Cell suspensions were uniformly adjusted to an OD_{600} of 10. Protein separation and immunoblot detection were essentially carried out as described earlier (Bubendorfer *et al.*, 2012, Binnenkade *et al.*, 2014) using polyclonal antibodies raised against mCherry (Eurogentec Deutschland GmbH, Köln, Germany) or the periplasmic part of MotB. Signals were detected using the SuperSignal® West Pico Chemiluminescent Substrate (Thermo Scientific, Schwerte, Germany) and documented using a FUSION-SL chemiluminescence imager (Peqlab, Erlangen, Germany).

Acknowledgments

The project was supported by a grants from the Deutsche Forschungsgemeinschaft (DFG) to KMT (TH831/4-1), BM (MA3898) and MT (SFB 987). SB was supported by the International Max Planck Research School. We are grateful to Ulrike Ruppert for technical support and to Kristof Brenzinger for helping with statistical analysis.

Author Contributions

Design of the study: SB, KMT; acquisition, analysis, and interpretation of data: SB, LD, NJD, OL, VB, RMB, MT, BM, JPA, KMT; writing of the manuscript: SB, KMT.

Conflict of interests

The authors declare no conflict of interests.

References

Asai, Y., Yakushi, T., Kawagishi, I., and Homma, M. (2003) Ion-coupling determinants of Na^+-driven and H^+-driven flagellar motors. *J Mol Biol* 327: 453-463.

Berg, H.C. (2003) The rotary motor of bacterial flagella. *Annu Rev Biochem* 72: 19-54.

Binnenkade, L., Teichmann, L., and Thormann, K.M. (2014) Iron triggers lambdaSo prophage induction and release of extracellular DNA in *Shewanella oneidensis* MR-1 biofilms. *Appl Environ Microbiol* 80: 5304-5316.

Boschert, R., Adler, F.R., and Blair, D.F. (2015) Loose coupling in the bacterial flagellar motor. *Proc Natl Acad Sci U S A* 112: 4755-4760.

Braun, T.F., Al-Mawsawi, L.Q., Kojima, S., and Blair, D.F. (2004) Arrangement of core membrane segments in the MotA/MotB proton-channel complex of *Escherichia coli*. *Biochemistry* 43: 35-45.

Bubendorfer, S., Held, S., Windel, N., Paulick, A., Klingl, A., and Thormann, K.M. (2012) Specificity of motor components in the dual flagellar system of *Shewanella putrefaciens* CN-32. *Mol Microbiol* 83: 335-350.

Castillo, C.J., Nakamura, S., Morimoto, Y.V., Che, Y.S., Nobunori, K., Kudo, S.*, et al.* (2013) The C-terminal periplasmic domain of MotB is responsible for load-dependent control of the number of stators of the bacterial flagellar motor. *Biophysics* 9: 173-181.

Choi, K.H., Gaynor, J.B., White, K.G., Lopez, C., Bosio, C.M., Karkhoff-Schweizer, R.R., and Schweizer, H.P. (2005) A Tn*7*-based broad-range bacterial cloning and expression system. *Nat Methods* 2: 443-448.

Dewenter, L., Volkmann, T.E., and Maier, B. (2015) Oxygen governs gonococcal microcolony stability by enhancing the interaction force between type IV pili. *Integr Biol* 7: 1161-1170.

Fukuoka, H., Wada, T., Kojima, S., Ishijima, A., and Homma, M. (2009) Sodium-dependent dynamic assembly of membrane complexes in sodium-driven flagellar motors. *Mol Microbiol* 71: 825-835.

Fung, D.C., and Berg, H.C. (1995) Powering the flagellar motor of *Escherichia coli* with an external voltage source. *Nature* 375: 809-812.

Gautier, R., Douguet, D., Antonny, B., and Drin, G. (2008) HELIQUEST: a web server to screen sequences with specific alpha-helical properties. *Bioinformatics* 24: 2101-2102.

Gibson, D.G., Young, L., Chuang, R.Y., Venter, J.C., Hutchison, C.A., 3rd, and Smith, H.O. (2009) Enzymatic assembly of DNA molecules up to several hundred kilobases. *Nat Methods* 6: 343-345.

Gosink, K.K., and Häse, C.C. (2000) Requirements for conversion of the Na(+)-driven flagellar motor of *Vibrio cholerae* to the H(+)-driven motor of *Escherichia coli*. *J Bacteriol* 182: 4234-4240.

Hizukuri, Y., Kojima, S., and Homma, M. (2010) Disulphide cross-linking between the stator and the bearing components in the bacterial flagellar motor. *J Biochem* 148: 309-318.

Hosking, E.R., Vogt, C., Bakker, E.P., and Manson, M.D. (2006) The *Escherichia coli* MotAB proton channel unplugged. *J Mol Biol* 364: 921-937.

Kashket, E.R. (1981) Effects of aerobiosis and nitrogen source on the proton motive force in growing *Escherichia coli* and *Klebsiella pneumoniae* cells. *J Bacteriol* 146: 377-384.

Koerdt, A., Paulick, A., Mock, M., Jost, K., and Thormann, K.M. (2009) MotX and MotY are required for flagellar rotation in *Shewanella oneidensis* MR-1. *J Bacteriol* 191: 5085-5093.

Kojima, S. (2015) Dynamism and regulation of the stator, the energy conversion complex of the bacterial flagellar motor. *Curr Opin Microbiol* 28: 66-71.

Kojima, S., and Blair, D.F. (2004) Solubilization and purification of the MotA/MotB complex of *Escherichia coli*. *Biochemistry* 43: 26-34.

Kojima, S., Furukawa, Y., Matsunami, H., Minamino, T., and Namba, K. (2008a) Characterization of the periplasmic domain of MotB and implications for its role in the stator assembly of the bacterial flagellar motor. *J Bacteriol* 190: 3314-3322.

Kojima, S., Imada, K., Sakuma, M., Sudo, Y., Kojima, C., Minamino, T.*, et al.* (2009) Stator assembly and activation mechanism of the flagellar motor by the periplasmic region of MotB. *Mol Microbiol*. 73: 710-718.

Kojima, S., Shinohara, A., Terashima, H., Yakushi, T., Sakuma, M., Homma, M.*, et al.*, (2008b) Insights into the stator assembly of the *Vibrio* flagellar motor from the crystal structure of MotY. *Proc Natl Acad Sci U S A* 105: 7696-7701.

Kurre, R., and Maier, B. (2012) Oxygen depletion triggers switching between discrete speed modes of gonococcal type IV pili. *Biophys J* 102: 2556-2563.

Lassak, J., Henche, A.L., Binnenkade, L., and Thormann, K.M. (2010) ArcS, the cognate sensor kinase in an atypical Arc system of *Shewanella oneidensis* MR-1. *Appl Environ Microbiol* 76: 3263-3274.

Leake, M.C., Chandler, J.H., Wadhams, G.H., Bai, F., Berry, R.M., and Armitage, J.P. (2006) Stoichiometry and turnover in single, functioning membrane protein complexes. *Nature* 443: 355-358.

Lele, P.P., Hosu, B.G., and Berg, H.C. (2013) Dynamics of mechanosensing in the bacterial flagellar motor. *Proc Natl Acad Sci U S A* 110: 11839-11844.

Li, N., Kojima, S., and Homma, M. (2011) Characterization of the periplasmic region of PomB, a Na^+-driven flagellar stator protein in *Vibrio alginolyticus*. *J Bacteriol* 193: 3773-3784.

Mandadapu, K.K., Nirody, J.A., Berry, R.M., and Oster, G. (2015) Mechanics of torque generation in the bacterial flagellar motor. *Proc Natl Acad Sci U S A* 112: 4381-4389.

Meijering, E., Dzyubachyk, O., and Smal, I. (2012) Methods for cell and particle tracking. *Methods Enzymol* 504: 183-200.

Minamino, T., Imada, K., and Namba, K. (2008) Molecular motors of the bacterial flagella. *Curr Opin Struct Biol* 18: 693-701.

Molero, R., Wilhelms, M., Infanzon, B., Tomas, J.M., and Merino, S. (2011) *Aeromonas hydrophila motY* is essential for polar flagellum function, requires coordinate expression of *motX* and Pom proteins. *Microbiology* 157: 2772-2784.

Morimoto, Y.V., Che, Y.S., Minamino, T., and Namba, K. (2010a) Proton-conductivity assay of plugged and unplugged MotA/B proton channel by cytoplasmic pHluorin expressed in *Salmonella*. *FEBS Lett* 584: 1268-1272.

Morimoto, Y.V., and Minamino, T. (2014) Structure and function of the bi-directional bacterial flagellar motor. *Biomolecules* 4: 217-234.

Morimoto, Y.V., Nakamura, S., Kami-ike, N., Namba, K., and Minamino, T. (2010b) Charged residues in the cytoplasmic loop of MotA are required for stator assembly into the bacterial flagellar motor. *Mol Microbiol* 78: 1117-1129.

Muramoto, K., and Macnab, R.M. (1998) Deletion analysis of MotA and MotB, components of the force-generating unit in the flagellar motor of *Salmonella*. *Mol Microbiol* 29: 1191-1202.

Nishihara, Y., and Kitao, A. (2015) Gate-controlled proton diffusion and protonation-induced ratchet motion in the stator of the bacterial flagellar motor. *Proc Natl Acad Sci U S A* 112: 7737-7742.

Partridge, J.D., Nieto, V., and Harshey, R.M. (2015) A new player at the flagellar motor: FliL controls both motor output and bias. *MBio* 6: e02367.

Paulick, A., Delalez, N.J., Brenzinger, S., Steel, B.C., Berry, R.M., Armitage, J.P., and Thormann, K.M. (2015) Dual stator dynamics in the *Shewanella oneidensis* MR-1 flagellar motor. *Mol Microbiol* 96: 993-1001.

Paulick, A., Koerdt, A., Lassak, J., Huntley, S., Wilms, I., Narberhaus, F., and Thormann, K.M. (2009) Two different stator systems drive a single polar flagellum in *Shewanella oneidensis* MR-1. *Mol Microbiol* 71: 836-850.

Reid, S.W., Leake, M.C., Chandler, J.H., Lo, C.J., Armitage, J.P., and Berry, R.M. (2006) The maximum number of torque-generating units in the flagellar motor of *Escherichia coli* is at least 11. *Proc Natl Acad Sci U S A* 103: 8066-8071.

Rossmann, F., Brenzinger, S., Knauer, C., Dorrich, A.K., Bubendorfer, S., Ruppert, U*., et al.* (2015) The role of FlhF and HubP as polar landmark proteins in *Shewanella putrefaciens* CN-32. *Mol Microbiol*. 98: 727-742.

Sato, K., and Homma, M. (2000a) Functional reconstitution of the Na(+)-driven polar flagellar motor component of *Vibrio alginolyticus*. *J Biol Chem* 275: 5718-5722.

Sato, K., and Homma, M. (2000b) Multimeric structure of PomA, a component of the Na^+-driven polar flagellar motor of *Vibrio alginolyticus*. *J Biol Chem* 275: 20223-20228.

Schindelin, J., Arganda-Carreras, I., Frise, E., Kaynig, V., Longair, M., Pietzsch, T.*, et al.* (2012) Fiji: an open-source platform for biological-image analysis. *Nat Methods* 9: 676-682.

Setty, O.H., Hendler, R.W., and Shrager, R.I. (1983) Simultaneous measurements of proton motive force, delta pH, membrane potential, and H^+/O ratios in intact Escherichia coli. *Biophys J* 43: 371-381.

Sowa, Y., and Berry, R.M. (2008) Bacterial flagellar motor. *Q Rev Biophys* 41: 103-132.

Sowa, Y., Rowe, A.D., Leake, M.C., Yakushi, T., Homma, M., Ishijima, A., and Berry, R.M. (2005) Direct observation of steps in rotation of the bacterial flagellar motor. *Nature* 437: 916-919.

Stock, D., Namba, K., and Lee, L.K. (2012) Nanorotors and self-assembling macromolecular machines: the torque ring of the bacterial flagellar motor. *Curr Opin Biotechnol* 23: 545-554.

Suaste-Olmos, F., Domenzain, C., Mireles-Rodriguez, J.C., Poggio, S., Osorio, A., Dreyfus, G., and Camarena, L. (2010) The flagellar protein FliL is essential for swimming in *Rhodobacter sphaeroides*. *J Bacteriol* 192: 6230-6239.

Terahara, N., Fujisawa, M., Powers, B., Henkin, T.M., Krulwich, T.A., and Ito, M. (2006) An intergenic stem-loop mutation in the *Bacillus subtilis ccpA-motPS* operon increases *motPS* transcription and the MotPS contribution to motility. *J. Bacteriol.* 188: 2701-2705.

Terashima, H., Fukuoka, H., Yakushi, T., Kojima, S., and Homma, M. (2006) The *Vibrio* motor proteins, MotX and MotY, are associated with the basal body of Na^+-driven flagella and required for stator formation. *Mol Microbiol* 62: 1170-1180.

Terashima, H., Koike, M., Kojima, S., and Homma, M. (2010) The flagellar basal-body associated protein, FlgT, essential for a novel ring structure in sodium-driven Vibrio motor. *J Bacteriol*. 192: 5609-5615.

Thomas, P.C., Halter, M., Tona, A., Raghavan, S.R., Plant, A.L. and Forry, S.P., (2009) A noninvasive thin film sensor for monitoring oxygen tension during in vitro cell culture. *Anal Chem* 81: 9239-9246.

Thormann, K.M. and Paulick, A., (2010) Tuning the flagellar motor. *Microbiology* 156: 1275-1283.

Tipping, M.J., Delalez, N.J., Lim, R., Berry, R.M. and Armitage, J.P., (2013a) Load-dependent assembly of the bacterial flagellar motor. *MBio* 4: e00551-13.

Tipping, M.J., Steel, B.C., Delalez, N.J., Berry, R.M., and Armitage, J.P. (2013b) Quantification of flagellar motor stator dynamics through *in vivo* proton-motive force control. *Mol Microbiol* 87: 338-347.

Zhu, S., Kumar, A., Kojima, S., and Homma, M. (2015) FliL associates with the stator to support torque generation of the sodium-driven polar flagellar motor of *Vibrio*. *Mol Microbiol* 98: 101-110.

Zhu, S., Takao, M., Li, N., Sakuma, M., Nishino, Y., Homma, M.*, et al.* (2014) Conformational change in the periplamic region of the flagellar stator coupled with the assembly around the rotor. *Proc Natl Acad Sci U S A* 111: 13523-13528.

Mechanistic consequences of functional stator mutations in the bacterial flagellar motor

Susanne Brenzinger[1,2], Lena Dewenter[3], Nicolas J Delalez[4], Oliver Leicht[5], Volker Berndt[2], Richard M. Berry[6], Martin Thanbichler[5,7], Judith P Armitage[4], Berenike Maier[3], Kai M Thormann[1,*]

1) Justus-Liebig-Universität Gießen, Department of Microbiology and Molecular Biology at the IFZ, 35392 Gießen, Germany
2) Max-Planck-Institut für terrestrische Mikrobiologie, Department of Ecophysiology, 35043 Marburg, Germany
3) University of Cologne, Department of Physics, 50674 Cologne, Germany
4) University of Oxford, Biochemistry Department, Oxford OX1 3QU, United Kingdom
5) Philipps-Universität Marburg, Faculty of Biology, Karl-von-Frisch-Str. 8, 35043 Marburg, Germany
LOEWE Center for Synthetic Microbiology, 35043 Marburg, Germany
6) University of Oxford, Physics Department, Oxford OX1 3QU, United Kingdom
7) Max Planck Institute for Terrestrial Microbiology & LOEWE Center for Synthetic Microbiology, 35043 Marburg, Germany

*corresponding author

- supplemental material -

Supplemental Tables

Table S1: Bacterial strains used in this study
Table S2: Plasmids used in this study
Table S3: Oligonucleotides used in this study

Figure S1: Loading controls of MotB immunoblots
Figure S2: Transcriptional levels of motB and motB*
Figure S3: Stability, activity and localizationof fluorescent fusion proteins.

Table S1: Bacterial strains that were used in this study

Strain	Genotype	Reference
Escherichia coli		
DH5α λpir	φ80d*lacZ* ΔM15 Δ(*lacZYA-argF*)U169 *recA1 hsdR17 deoR thi-l supE44 gyrA96 relA1*/λpir	Miller VL, Mekalanos JJ (1988)
WM3064	*thrB1004 pro thi rpsL hsdS lacZ* ΔM15 RP4-1360 Δ(*araBAD*) 567Δ*dapA* 1341::[*erm pir*(wt)]	W. Metcalf, University of Illinois, Urbana-Champaign
Shewanella oneidensis		
S79	MR-1, wild type	(Venkateswaran *et al.*, 1999)
S86	Δ*pomAB,* ΔSO_1529-30	(Paulick *et al.*, 2009)
S91	Δ*motAB,* ΔSO_4287-86	(Paulick *et al.*, 2009)
S92	Δ*pomAB* Δ*motAB,* ΔSO_1529-30 ΔSO_4287-86	(Paulick *et al.*, 2009)
S258	Δ*pomAB*Δ*motX*	Koerdt *et al.,* 2009
S255	Δ*pomAB*Δ*motY*	Koerdt *et al.,* 2009
S1153	Δ*pomAB*Δ*motXY*	Koerdt *et al.,* 2009
S2715	Δ*pomAB motB*_L60S (spontaneous mutant)	This study
S2716	Δ*pomAB motB*_ΔMVE (spontaneous mutant)	This study
S2717	Δ*pomAB motB*_S54P (spontaneous mutant)	This study
S2718	Δ*pomAB motB*_S56P (spontaneous mutant)	This study
S2719	Δ*pomAB motB*_S54P (spontaneous mutant)	This study
S2720	Δ*pomAB motB*_L60S (spontaneous mutant)	This study
S2721	Δ*pomAB motB*_S54P (spontaneous mutant)	This study
S2722	Δ*pomAB motB*_S56P (spontaneous mutant)	This study
S2967	Δ*pomAB mcherry_motB*_ΔMVE (spontaneous mutant)	This study
S2970	Δ*pomAB motB*_ΔMVE (knock in) Δ*motY*	This study
S2973	Δ*pomAB mcherry_motB*	This study
S3305	Δ*pomAB motB*_ΔMVE (knock in) Δ*motXY*	This study
S3416	Δ*pomAB motB*_ΔMVE (knock in)	This study
S3642	Δ*pomAB* Δ*motAB* pBBMt *motB*	This study
S3644	Δ*pomAB* Δ*motAB* pBBMt *motB*_L51D	This study
S3645	Δ*pomAB* Δ*motAB* pBBMt *motB*_ΔMVE	This study
S3656	Δ*pomAB* Δ*motAB* pBBMt *motB*_L51K	This study
S3657	Δ*pomAB* Δ*motAB* pBBMt *motB*_L51P	This study
S3658	Δ*pomAB* Δ*motAB* pBBMt *motB*_F46K	This study
S3866	Δ*pomAB* Δ*fliL*	This study
S3867	Δ*motAB* Δ*fliL*	This study
S3954	Δ*pomAB motB*_ΔMVE (knock in) Δ*fliL* Δ*motXY*	This study
S3955	*fliL_mcherry*	This study
S4053	pBBMt (empty vector control)	This study
S4092	Δ*pomAB mcherry_motB*_ΔMVE (knock in)	This study
S4100	Δ*pomAB motB*_ΔMVE (knock in) Δ*fliL*	This study
S4312	Δ*pomAB motB*_ΔMVE (knock in) Δ*motX*	This study
S4313	Δ*pomAB motB*_ΔMVE (knock in) Δ*motXY*	This study

Table S2: Plasmids that were used in this study

Plasmid	Relevant genotype or phenotype	Source or reference
pNPTS138-R6KT	*mob*RP4^{+} *ori*-R6K *sacB*, suicide plasmid for in frame deletions, Km^{r}	Lassak *et al*., 2010
pBBMt	pBBR1-MCS2 backbone (pBBR origin, Km^{r}); TetR, Promoter and multiple cloning site of pASK-IBA3plus and *E.coli rrnB1* T1 and lambda phage T0 terminator	this study
pET24d(+)	T7 promoter, his-tag fusion site, T7 terminator, *lacI*, pBR322 ori, f1 ori, Km^{r}	Novagen
pGAT3	*bla*, *lacI*, T7-lacO promoter, SP6 promoter, T7 terminator, Ap^{r}	Peränen *et al.*, 1996
In-frame deletion vectors (in pNPTS138-R6KT)		
pNPTS138-R6KT-HubP-KO	*hubP* (Sputcn32_2442), in-frame deletion fragment	this study
pNPTS138-R6KT-FlhF-KO	*flhF* (Sputcn32_2561), in-frame deletion fragment	this study
pNPTS138-R6KT-FlhG ΔN20	*flhG* ΔN20 (deletion of first 20 amino acids in Sputcn32_2560), in-frame deletion fragment	this study
In-frame complementation vectors (in pNPTS138-R6KT)		
pNPTS138-R6KT-HubP-KI	*hubP* (Sputcn32_2442), in-frame insertion fragment for complementation of Δ*hubP*	this study
pNPTS138-R6KT-FlhF-KI	*flhF* (Sputcn32_2561), in-frame insertion fragment for complementation of Δ*flhF*	this study
Fluorescent fusion vectors (in pNPTS138-R6KT)		
pNPTS138-R6KT-FlaAB$_2$-Cys	*flaAB$_2$*-Cys (Sputcn32_3455_T156CT159C, Sputcn32_3456_T159CT160C), in-frame substitution fragment	
pNPTS138-R6KT-FliM$_1$-GL-sfGFP-His6	*fliM$_1$*-6xGly-sfGFP-His6 in pNPTS138-R6KT in-frame insertion fragment	Bubendorfer *et al*., 2012
pNPTS138-R6KT-FliM$_1$-GL-mCherrySO-His6	*fliM$_1$*-6xGly-mCherrySO-His6 in pNPTS138-R6KT in-frame insertion fragment	Bubendorfer *et al*., 2012
pNPTS138-R6KT-mCherry-ParB	mCherry-2xGly-Gly-Ser-*parB* (Sputcn32_3964), in-frame insertion fragment	this study
pNPTS138-R6KT-FlaAB$_1$-Cys	*flaAB$_1$*-Cys (Sputcn32_2586_T159C, Sputcn32_2585_T159C), in-frame substitution fragment	this study
pNPTS138-R6KT-sfGfp-3GGS-CheY	sfGFP-His6-3xGly-Gly-Ser-*cheY* (Sputcn32_2558), in-frame insertion fragment	this study
pNPTS138-R6KT-VENUS-GL-CheZ	VENUS-6xGly-*cheZ* (Sputcn32_2557), in-frame insertion fragment	this study
pNPTS138-R6KT-CheA-mCherry	*cheA*-2xGly-Gly-Ser-mCherry (Sputcn32_2556), in-frame deletion fragment	this study
pNPTS138-R6KT-HubP-sfGFP	*hubP*-3xGly-Gly-Ser-sfGFP (Sputcn32_2442), in-frame insertion fragment	this study
pNPTS138-R6KT-HubP-mCherry	*hubP*-3xGly-Gly-Ser-mCherry (Sputcn32_2442), in-frame insertion fragment	this study
pNPTS138-R6KT-FlhF-mCherry	*flhF*-3xGly-Gly-Ser-mCherry (Sputcn32_2561), in-frame insertion fragment	this study
pNPTS138-R6KT-ZapA-sfGFP	*zapA*-2xGly-Gly-Ser-sfGFP (Sputcn32_3215), in-frame insertion fragment	this study
pJP5603_Sputcn32_0796-sfGFP	*MCP_0796*-sfGFP (Sputcn32_0796), for single homologous insertion	this study

pNPTS138-R6KT-FlhG-sfGFP	*flhG*-1xGly-Ser-sfGFP (Sputcn32_2560), in-frame insertion fragment	This study
Overproduction vectors		
pBTOK-HubP-sfGFP	*hubP*-3xGly-Gly-Ser-*sfGFP* (Sputcn32_2442) in pBTOK	this study
pBTOK-LysM-mCherry	*hubP*_AA1-134-2xPro-*mCherry* (Sputcn32_2442_nt1-402) in pBTOK	this study
pBTOK-FlhF-mCherry	*flhF*-1xGly-Ser-*mCherry* (Sputcn32_2561) in pBTOK	This study
pFlhF	*flhF* (Δ-10) in pET24d	this study
pFlhG	*flhG* in pET24d	this study
pN-FlhG	N-terminus of *flhG* (aa 1-20) in pGAT3	this study

Apr, ampicillin resistance; Km^r, kanamycin resistance

References Table S1 and Table S2

Bubendorfer, S., Held, S., Windel, N., Paulick, A., Klingl, A., and Thormann, K.M. (2012) Specificity of motor components in the dual flagellar system of *Shewanella putrefaciens* CN-32. *Mol Microbiol* 83: 335-350.

Fredrickson, J.K., Zachara, J.M., Kennedy, D.V., Dong, H., Onstott, T.C., Hinman, N.W., and Li, S. (1998) Biogenic iron mineralization accompanying the dissimilatory reduction of hydrous ferric oxide by a groundwater bacterium. *Geochim Cosmochim Acta* **62**: 3239-3257.

Koerdt, A, Paulick A, Mock M, Jost K, and Thormann K.M. (2009) MotX and MotY are required for flagellar rotation in *Shewanella oneidensis* MR-1. *J Bacteriol* 191: 5085-93.

Lassak, J., Henche, A.L., Binnenkade, L., and Thormann, K.M. (2010) ArcS, the cognate sensor kinase in an atypical Arc system of *Shewanella oneidensis* MR-1. *Appl Environ Microbiol* **76**: 3263-3274.

Miller, V.L., and Mekalanos, J.J. (1988) A novel suicide vector and its use in construction of insertion mutations: osmoregulation of outer membrane proteins and virulence determinants in *Vibrio cholerae* requires *toxR*. *J Bacteriol* **170**: 2575-2583.

Paulick, A., Koerdt, A., Lassak, J., Huntley, S., Wilms, I., Narberhaus, F., and Thormann, K.M. (2009) Two different stator systems drive a single polar flagellum in *Shewanella oneidensis* MR-1. *Mol Microbiol* **71**: 836–850

Peränen, J., Rikkonen, M., Hyvonen, M., and Kaariainen, L. (1996) T*7* vectors with modified T*7lac* promoter for expression of proteins in *Escherichia coli*. *Anal Biochem* **236**: 371-373.

Schuhmacher, J.S., Rossmann, F., Dempwolff, F., Knauer, C., Altegoer, F., Steinchen, W.*, et al.* (2015) MinD-like ATPase FlhG effects location and number of bacterial flagella during C-ring assembly. *Proc Natl Acad Sci U S A* **112**: 3092-3097.

Venkateswaran, K., Moser, D.P., Dollhopf, M.E., Lies, D.P., Saffarini, D.A., MacGregor, B.J., *et al.* (1999) Polyphasic taxonomy of the genus Shewanella and description of *Shewanella oneidensis* sp. nov. *Int J Syst Bacteriol* **49**: 705–724.

Table S3: Oligonucleotides used in this study

Identifier of oligonucleotides	Sequence 5'-3'	Purpose
B207 SacI-araBAD-pARA-fwd	C GAG CTC TTA TGA CAA CTT GAC GGC TAC ATC A	Construction of pBBMt
SH144 pBBMt MCS rev	TTC TAG AGC TAG CGT TAG CCC AAA AAA CGG GTA TGG	
B205 PspOMI-terminator-fwd	TCC GGG CCC ATT AGC TGA GCT TGG ACT CCT G	
B206 KpnI-terminator-rev	GG GGT ACC GCA AGC TCC TAG CGG CGG	
SH304 SO MotB C-tag up fw	ACA CTT GGG CCC ATC CGC TGT AGA TGC AGA GC	MotB_mCherry fusion, upstream fragment
SH320 SO MotB C-tag pVENC OL rv	GCA ATT GGA CGT CTC GCG ACT CAG GAA TGG GAA TAT GGC TTT C	
SH302 SO mCherry linker fw	TTC AGA TCT ATG GTT TCC AAA GGG GAA GAG G	MotB_mCherry fusion, mCherry insertion into pVENC-1
SH303 SO mCherry linker rv	AGG AAT TCT TAT TTG TAT AAC TCA TCC ATA CCA CC	
SH311 SO MotB mC C-tag OL rv	CTA AGA AGG AGT ATT TCT AGA CTT TAT TTG TAT AAC TCA TCC ATA CCA CC	MotB_mCherry fusion, addition of homology to mCherry fragment
SH306 SO MotB C-tag dwn OL fw	AGT CTA GAA ATA CTC CTT CTT AGA TG	MotB_mCherry fusion, downstream fragment
SH307 SO MotB C-tag dwn rv	AGC TAG CGT AGT GAC ATA GGG GGA GAT AAA G	
SH325 SO MotB 3aa del ins up fw	ACA CTT GGG CCC AGG CGA TGT GAG AAA AGG TGG	Insertion of three amino acid deletion
SH326 SO MotB 3aa del ins dwn rv	GGC TAG CGA ATG GGA ATA TGG CTT TCA ACG	
SH604 MR1 FliL up fw	GCG AAT TCG TGG ATC CAG AT TCC GAA TGC TAG TGA CGA TAA CC	Deletion of FliL
SH605 MR1 FliL up OL rev	TTA TTG CAT CAC TTC CTT GGC CAT GTT CTG TAC TC	
SH606 MR1 FliL dwn OL fw	ATG GCC AAG GAA GTG ATG CAA TAA CCT TTA TCT TCA GC	
SH607 MR1 FliL dwn rev	GCC AAG CTT CTC TGC AGG AT TCT TGT TTA TCG CTC TGG ACA CC	
SH536 mC fw	TGGCTCTGGTGGCAGCATGGTTTCCAAAGGGGAAGAGG	FliL_mCherry fusion
SH623 FliL mCherry KI up fw	GCG AAT TCG TGG ATC CAG AT TTG CGG ACA GCC ATG TCT CC	
SH624 FliL mCherry KI up rev	GCT GCC ACC AGA GCC ACC GCT ACC GCC TTG CAT CAC AAA ACC GGT AAA GAG	
SH625 FliL mCherry KI rev fw	CTA TTT GTA TAA CTC ATC CAT ACC ACC	
SH626 FliL mCherry KI up fw	GGT ATG GAT GAG TTA TAC AAA TAG CCT TTA TCT TCA GCA CCT TAA AGA G	
SH82 MotB SO AB XhoI Strep-tag rv	G ctc gag TTA TTA TTT TTC GAA CTG CGG GTG GCT CCA AGC GCT CTC AGG AAT GGG AAT ATG GCT TTC AAC	Overexpression of *motAB* carrying point mutations
VB15 NheI_OE_motAB_fwd	ACT ACC GCT AGC AGG AGG ATA GCT AAT GAG TTT TAT AGG TGT AAT TGT TGC G	
SH449 SO MotB F46K up rev	CTT CAA CCA TCT TTT TAG CTT CAT TTT TAT C	
SH450 SO MotB F46K dwn fw	gatAAA AAT GAA GCT AAA AAG ATG GTT GAA GG	
SH451 SO MotB L51P up rev	AGA CAA CGA ATC TAT AGG ACC TTC AAC C	
SH452 SO MotB L51P dwn fw	GGT TGA AGG TCC TAT AGA TTC GTT GTC	
SH453 SO MotB L51K up rev	AGA CAA CGA ATC TAT CTT ACC TTC AAC C	
SH454 SO MotB L51K dwn fw	GGT TGA AGG TAA GAT AGA TTC GTT GTC	
SH455 SO MotB L51D up rev	AGA CAA CGA ATC TAT GTC ACC TTC AAC C	
SH456 SO MotB L51D dwn fw	GGT TGA AGG TGA CAT AGA TTC GTT GTC	

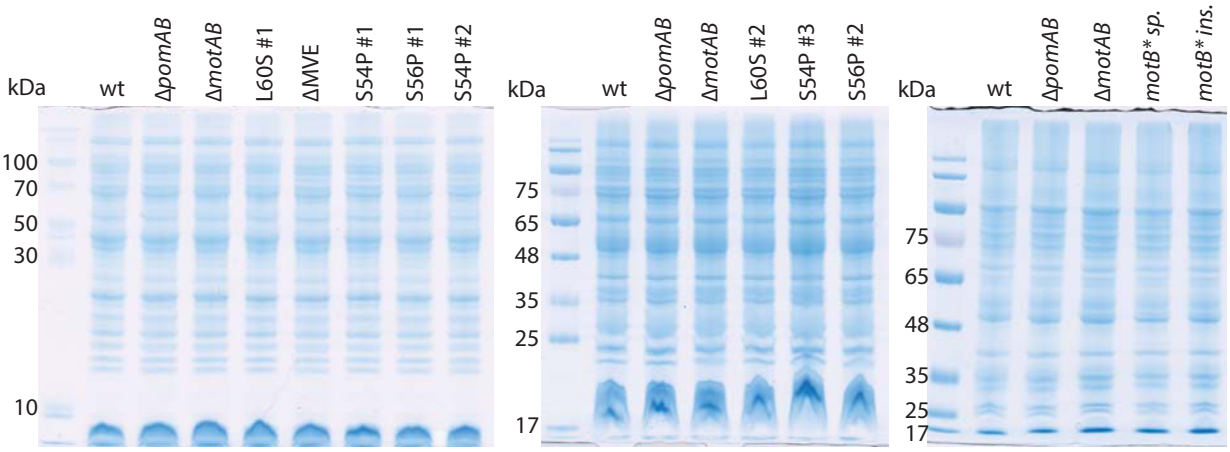

Figure S1: Loading controls of MotB immunoblots.
Coomassie-stained PAGE gels with protein samples of amounts equal to immunoblots against MotB from Fig. 1. The left and middle panels show samples of the spontaneous up-motile mutants from Fig. 1B, right panel displays the samples from Fig. 1C. Each gel contains a wild-type sample (wt) for reference.

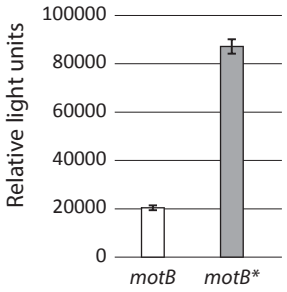

Figure S2: Transcriptional levels of *motB* and *motB.**
Luminescence (as relative light units) of exponentially growing LM100 cultures of MR-1 Δ*pomAB* with wild type *motB* (white bar) or spontaneously mutated *motB** (grey bar) harboring the *luxCDABE* operon integrated into *motB* on the chromosome was determined. Values correspond to the average of 6 independent measurements. Error bars represent the standard deviation.

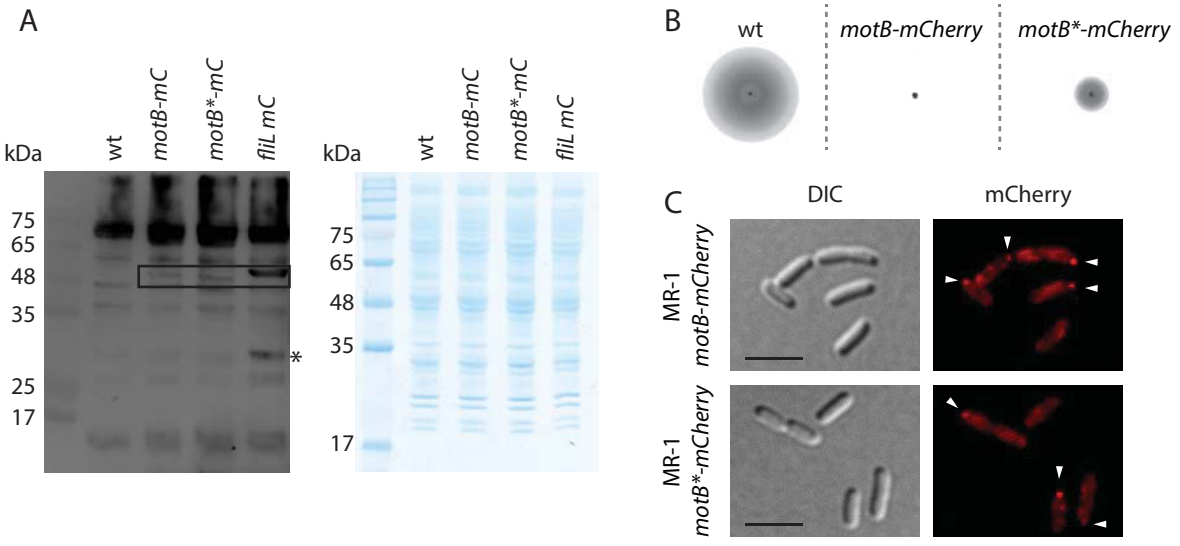

Figure S3: Stability, activity and localizationof fluorescent fusion proteins.
A) Stability of MotB, MotB* and FliL fused to mCherry was determined via immunoblotting using antibodies raised against mCherry (left panel). A Protein sample from wild-type was used as a negative control and shows formation of several signals due to unspecific binding. Signals of fusion proteins were detected at positions corresponding to their estimated size (MotB-mCherry 59.1kDa, FliL-mCherry 46.1 kDa). Asterisk indicated position of presumable degradation product of FliL-mCherry. Right panel shows the Coomassie-stained PAGE gel as loading control. **B)** Soft-agar assay of wild-type (wt), MR-1 *motB-mCherry* and MR-1 *motB* -mCherry*. Cells from a plate were placed on soft agar plates containing 0.25% (w/v) agar and incubated for 24h at 30°C prior to analysis of radial extensions. Dashed lines indicate rearrangement of the original positions on the same soft-agar plate to allow a better comparison in the figure. **C)** Localization of MotB and MotB* fused to mCherry. Displayed are DIC and fluorescent micrograph. Arrows point to polar fluorescent clusters. The scale bar represents 5µm.

Chapter 4

Research article (published in *Molecular Microbiology)*

The role of FlhF and HubP as polar landmark proteins in *Shewanella putrefaciens* CN-32

Florian Rossmann[#,1,2], Susanne Brenzinger[#,1,2], Carina Knauer[3], Anja K. Dörrich[1], Sebastian Bubendorfer[1,4], Ulrike Ruppert[1], Gert Bange[3], Kai M. Thormann[1,*]

1) Justus-Liebig Universität, Department of Microbiology and Molecular Biology, 35392 Giessen, Germany
2) Max-Planck-Institut für terrestrische Mikrobiologie, Department of Ecophysiology, 35043 Marburg, Germany
3) LOEWE Center for Synthetic Microbiology (Synmikro) & Department of Chemistry, Philipps University Marburg, 35043 Marburg, Germany
4) current address: Institute for Medical Microbiology and Hospital Epidemiology, Hannover Medical School, 30625 Hannover, Germany
[#] these authors contributed equally to this study

Contributions:

F.R. designed the study, performed laboratory experiments (strain constructions, motility assay on soft agar, flagellar and hook staining, fluorescence microscopy of all *flhf* deletion and fusion strains and partially of fluorescently tagged chemotaxis components, immunoblot analysis), evaluated the data and wrote the manuscript.

S.Br. designed the study, performed laboratory experiments (strain constructions, pBTOK vector construction, motility assay on soft agar, overproduction of *Sp*HubP-sfGFP and LysM-mCherry, flagellar and hook staining, fluorescence microscopy of all *parB* fusion strains and partially of fluorescently tagged chemotaxis components, Fluorescence Recovery After Photobleaching (FRAP), determination of swimming speed, analysis of twitching motility), evaluated the data and wrote the manuscript.

C.K. performed laboratory experiments (protein production and purification, GTPase activity of FlhF), evaluated the data and wrote the manuscript.

A.K.D. designed the study (strain constructions) and evaluated the data.

S.Bu. performed laboratory experiments (strain constructions).

U.R. performed laboratory experiments (strain constructions).

G.B. designed the study and wrote the manuscript.

K.M.T. designed the study and wrote the manuscript.

Molecular Microbiology (2015) 98(4), 727–742 ■
doi:10.1111/mmi.13152
First published online 10 September 2015

The role of FlhF and HubP as polar landmark proteins in *Shewanella putrefaciens* CN-32

Florian Rossmann,[1,2†] Susanne Brenzinger,[1,2†] Carina Knauer,[3] Anja K. Dörrich,[1] Sebastian Bubendorfer,[1‡] Ulrike Ruppert,[1] Gert Bange[3] and Kai M. Thormann[1*]
[1]*Department of Microbiology and Molecular Biology, Justus-Liebig Universität, 35392 Giessen, Germany.*
[2]*Department of Ecophysiology, Max-Planck-Institut für terrestrische Mikrobiologie, 35043 Marburg, Germany.*
[3]*LOEWE Center for Synthetic Microbiology (Synmikro) & Department of Chemistry, Philipps University Marburg, 35043 Marburg, Germany.*

Summary

Spatiotemporal regulation of cell polarity plays a role in many fundamental processes in bacteria and often relies on 'landmark' proteins which recruit the corresponding clients to their designated position. Here, we explored the localization of two multi-protein complexes, the polar flagellar motor and the chemotaxis array, in *Shewanella putrefaciens* CN-32. We demonstrate that polar positioning of the flagellar system, but not of the chemotaxis system, depends on the GTPase FlhF. In contrast, the chemotaxis array is recruited by a transmembrane protein which we identified as the functional ortholog of *Vibrio cholerae* HubP. Mediated by its periplasmic N-terminal LysM domain, *Sp*HubP exhibits an FlhF-independent localization pattern during cell cycle similar to its *Vibrio* counterpart and also has a role in proper chromosome segregation. In addition, while not affecting flagellar positioning, *Sp*HubP is crucial for normal flagellar function and is involved in type IV pili-mediated twitching motility. We hypothesize that a group of HubP/FimV homologs, characterized by a rather conserved N-terminal periplasmic section required for polar targeting and a highly variable acidic cytoplasmic part, primarily mediating recruitment of client proteins, serves as polar markers in various bacterial species with respect to different cellular functions.

Accepted 30 July, 2015. *For correspondence. E-mail kai.thormann@mikro.bio.uni-giessen.de; Tel. +49 (0) 641 9935545; Fax +49 (0)641 9935549. †These authors contributed equally to this study. ‡Present address: Institute for Medical Microbiology and Hospital Epidemiology, Hannover Medical School, Hannover 30625, Germany.

Introduction

During the recent decades, numerous studies have provided evidence that in bacteria, a variety of fundamental cellular functions depend on the proper spatial and temporal organization of proteins and other macromolecules within the cell. A paradigmatic example for spatiotemporal organization in bacteria is cell division where correct positioning of the cell division proteins and distribution of replicated chromosomal DNA are critical for propagation (Thanbichler, 2010; Reyes-Lamothe *et al*., 2012). Unlike the cell division machinery of most bacteria, numerous other complexes are specifically targeted to the cell pole for proper function. Several different systems involved in the regulation of cell polarity have been identified and studied; this topic has been the subject of recent reviews (Laloux and Jacobs-Wagner, 2014; Treuner-Lange and Søgaard-Andersen, 2014).

One major multiprotein complex that needs to be specifically positioned is the flagellar machinery of polarly flagellated bacterial species. The mechanisms by which this localization is achieved are still poorly understood for most bacteria (summarized in Schuhmacher *et al*., 2015a). In those species that have been studied in detail, polar recruitment of the flagellar system appears to rely on landmark proteins to assign the desired position, and the absence of these polar markers commonly leads to misplacement of the flagella. In the alphaproteobacterium *Caulobacter crescentus*, TipN has been identified as such a landmark protein (Huitema *et al*., 2006; Lam *et al*., 2006). TipN localizes to the new pole of both daughter cells after cell division and recruits a second protein, TipF, a positive regulator of flagellar assembly. TipF in turn recruits PflI, a third protein required for proper flagellar placement (Obuchowski and Jacobs-Wagner, 2008; Davis *et al*., 2013). The concerted action of these three proteins is required for formation of a single flagellum at the designated cell pole (Davis *et al*., 2013).

However, homologs of the TipN/F proteins appear to be absent outside the group of alphaproteobacteria. In many other bacterial species, a set of two proteins, FlhF and FlhG, has been implicated in regulating diverse aspects of

flagellar localization, number, and activity (reviewed in Kazmierczak and Hendrixson, 2013; Altegoer *et al*., 2014). Potential orthologs of the two proteins are present in a wide range of bacterial species (Bange *et al*., 2011). FlhG (orthologs also named YlxH, MinD2, FleN or MotR) belongs to the MinD/ParA ATPase family, and the recently solved crystal structure revealed striking structural homologies to the ATPase MinD of *Escherichia coli* (Schuhmacher *et al*., 2015b). Loss of FlhG in polarly flagellated bacterial species commonly results in hyperflagellation and severe perturbation of flagella-mediated motility (Dasgupta *et al*., 2000; Correa *et al*., 2005; Kusumoto *et al*., 2006; 2008; Schuhmacher *et al*., 2015b). The exact mechanism by which FlhG exerts its role is still elusive; however, its mode of action involves binding to major components of the flagellar rotor, FliM and FliN/FliY, putatively to facilitate their incorporation into the nascent basal body structure (Schuhmacher *et al*., 2015b). The second protein of the system, FlhF, belongs to the signal recognition particle SRP-type GTPase subfamily of the SIMIBI class of nucleotide-binding proteins, and the crystal structure of FlhF from *Bacillus subtilis* has been solved (Bange *et al*., 2007; Bange and Sinning, 2013). Loss of the protein has a range of different consequences with respect to flagellar gene expression, assembly and function in various polarly flagellated species, but consistently results in displacement of the flagellum away from the cell pole (Pandza *et al*., 2000; Murray and Kazmierczak, 2006; Kusumoto *et al*., 2008; Balaban *et al*., 2009; Green *et al*., 2009). FlhF was demonstrated to co-localize with the flagellum to the old cell pole (Murray and Kazmierczak, 2006; Kusumoto *et al*., 2008; Ewing *et al*., 2009). Moreover, studies on *Vibrio cholerae* FlhF have provided evidence that the same spatial organization occurs in the absence of any other flagellar components (Green *et al*., 2009) or upon heterologous production of *Vibrio alginolyticus* FlhF in *E. coli* (Kusumoto *et al*., 2008), indicating that polar localization is an intrinsic feature of the protein. The presence of FlhF at the cell pole is required for correct placement of the early flagellar basal body protein FliF. Thus, it has been speculated that FlhF represents the polar landmark protein which recruits early components of the flagellar machinery to the appropriate subcellular location by a mechanism which is yet elusive. In addition, for *Pseudomonas aeruginosa*, it was reported that the chemotaxis protein CheA also localizes away from the cell pole in the absence of FlhF in a pattern resembling that of the flagellar basal body system (Kulasekara *et al*., 2013). This finding strongly indicates that FlhF might also mediate the recruitment of the chemotaxis machinery in *P. aeruginosa* or that the chemotaxis machinery is directly associated with the flagellar system.

Recent studies on *V. cholerae* have identified another major landmark protein which is involved in the polar accumulation of flagella but primarily directs the chemotaxis system and the chromosome segregation machinery to the cell pole. According to its proposed function as a polar hub, the protein was named HubP (Yamaichi *et al*., 2012). HubP is a transmembrane protein with an N-terminal periplasmic peptidoglycan-binding (LysM) domain and a large cytoplasmic section comprising 10 copies of an imperfect 46-amino-acid repeat. Fluorescence microscopy demonstrated that, mediated by the N-terminal LysM domain, HubP localizes to the cell pole and the cellular division plane. Deletion of *hubP* in *V. cholerae* results in delocalization of the chemotaxis machinery, leading to a defect in chemotactic swimming. In addition, the origin of the larger of the two *V. cholerae* chromosomes, *oriCI*, is not fully targeted to the cell pole and a small fraction of cells displays an increased number of flagella. Interaction of these large complexes with HubP is thought to be mediated through a set of different ParA-like ATPases, ParAI for *oriCI*, ParC for the chemotaxis machinery and FlhG for the flagellar machinery. Potential homologs of HubP have been identified in several other species among the gammaproteobacteria; however, it is not clear whether or not these proteins are functional orthologs and which role they might play in these species.

Shewanella putrefaciens CN-32 is a gammaproteobacterium which possesses two complete flagellar systems encoded by two distinct separate gene clusters (Bubendorfer *et al*., 2012). The primary gene cluster, which is present in all *Shewanella* species and encodes orthologs of FlhF and FlhG, leads to formation of a single polar Na^+-driven flagellum. The secondary flagellar system lacks *flhF* and *flhG* and is expressed in a subpopulation of cells when cultivated in complex media. These cells form one or more lateral flagella which are rotated at the expense of the proton gradient and enable a more effective motility of the corresponding subpopulation by increasing the directional persistence of swimming. However, our studies strongly indicated that the single chemotaxis system of *S. putrefaciens* CN-32 predominantly or even exclusively addresses the primary polar system but not the lateral flagellar motors (Bubendorfer *et al*., 2014). To further elucidate the spatial arrangement of the chemotaxis machinery with respect to the two flagellar systems of *S. putrefaciens* CN-32, we performed localization studies by fluorescence microscopy. We identified the functional ortholog of the *V. cholerae* polar landmark protein HubP in *S. putrefaciens* CN-32, and we demonstrate that FlhF and HubP independently localize the primary flagellar system and the chemotaxis and chromosome segregation machinery, respectively. We thus show that general features and mechanisms are conserved between HubP-like proteins of different species and suggest that HubP-dependent polar localization might be more widespread among bacteria.

Results

The chemotaxis machinery of S. putrefaciens *CN-32 localizes to the flagellated cell pole*

To first explore the subcellular position of the chemotaxis system in *S. putrefaciens* CN-32, we performed fluorescence microscopy on cells producing fluorescently labeled components of the chemotaxis machinery. *S. putrefaciens* CN-32 possesses a single chemotaxis system with 37 predicted putative methyl-accepting sensor proteins (MCPs). To determine the localization of the chemotaxis machinery within CN-32 cells, we generated C-terminal fluorescent protein fusions to 16 of the 37 MCPs. Because all fusions yielded very similar results, we will, within this manuscript, only refer to MCP0796-eGFP. MCP0796 is an MCP with a periplasmic helical bimodular (HBM) sensor domain followed by the typical cytoplasmic HAMP and methyl-accepting chemotaxis-like (MA) domain. The function of this MCP is not yet characterized; however, the fluorescent fusion reliably allowed localization of the protein which was therefore chosen as representative. We further generated a C-terminal fluorescent fusion to CheA (CheA-mCherry) as well as N-terminal fluorescent protein fusions to CheY (sfGFP-CheY) and CheZ (Venus-CheZ). The genes encoding these fusions were separately introduced into the CN-32 chromosome where they replaced the corresponding native genes. Immunoblotting and swimming assays demonstrated that the fluorescently labeled proteins were mostly stably produced (Fig. S1) and fully (Venus-CheZ and CheA-mCherry) or partially (sfGFP-CheY) supported movement through soft agar (Fig. S2). To enable localization of the chemotaxis machinery with respect to the position of the primary polar flagellar system, all fusions were introduced into a CN-32 strain in which $FliM_1$ was functionally labeled with sfGFP or mCherry (Bubendorfer *et al*., 2012) as a marker for the primary basal body complex.

Subsequent fluorescence microscopy revealed that MCP0769-eGFP as well as sfGFP-CheY, CheA-mCherry and Venus-CheZ distinctly localized to the cell pole marked by $FliM_1$ in 73% (CheY and CheA) and 89% (CheZ) respectively (Fig. 1). In addition, some cells displayed a bipolar localization pattern of labeled chemotaxis components (CheY, 19%; CheA, 29%; CheZ, 21%). In cells with a $FliM_1$ focus, the signal intensity of co-localizing foci formed by the labeled chemotaxis components was always stronger than that of foci at the opposite cell pole: For sfGFP-CheY, the signal at the opposite cell poles only reached 38% intensity compared to that of the flagellated pole, CheA-mCherry reached 27% and Venus-CheZ 24%. In contrast, co-localization of any of the labeled chemotaxis components with $FliM_2$-mCherry as a marker for the position of the secondary lateral flagellum was not observed, unless $FliM_2$-mCherry was located close to the cell pole (data not shown). Based on these results, we concluded that in *S. putrefaciens* CN-32, the chemotaxis machinery is localized at, or in close proximity to, the cell pole decorated with the primary flagellar complex and is assembled at the old cell pole during cell division.

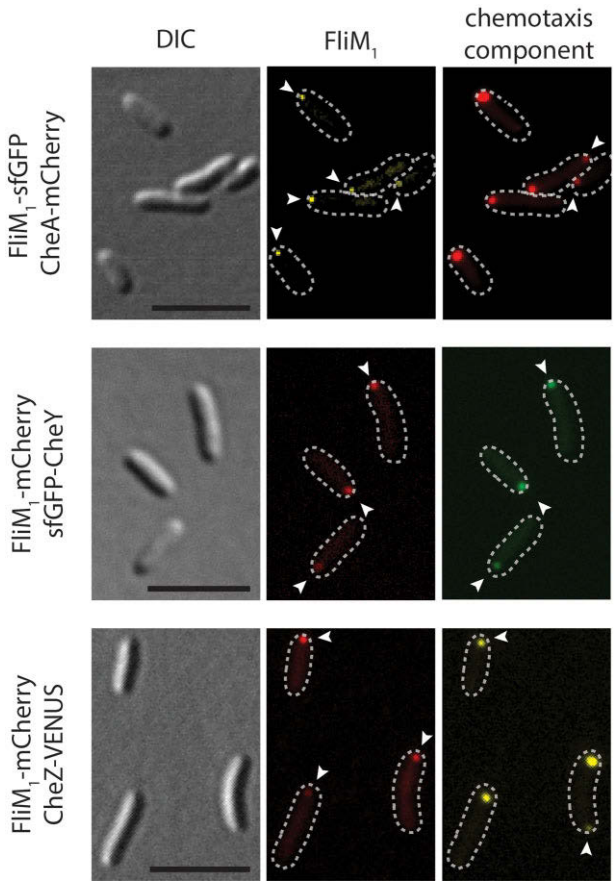

Fig. 1. Localization of the chemotaxis cluster in *S. putrefaciens* CN-32. Displayed are DIC (left panel) and fluorescent micrographs in which $FliM_1$ (middle panels) and CheA, CheY and CheZ (right panel) are fluorescently labeled as indicated. The arrows point out fluorescent foci. The scale bar equals 5 μm.

The SRP-like GTPase FlhF is required for polar localization of the primary flagellar system, but not of the chemotaxis cluster, in CN-32

The SRP-like GTPase FlhF has been demonstrated to be the major determinant for flagellar placement and number in various polarly flagellated gammaproteobacteria. We therefore determined whether this protein has a similar role in *S. putrefaciens* CN-32 and whether *Sp*FlhF also dictates the localization of the chemotaxis system, as has previously been suggested for *P. aeruginosa* (Kulasekara *et al*., 2013). FlhF acts in concert with its antagonist, the MinD-like ATPase FlhG (Kusumoto *et al*., 2008; Ono *et al*., 2015), and in *B. subtilis* it has been shown that the conserved N-terminal region of FlhG stimulates the

GTPase activity of FlhF by approximately three to fivefold (Bange *et al*., 2011). To assess whether FlhF from *S. putrefaciens* CN-32 is an active GTPase whose activity is affected by FlhG, both proteins were purified and the impact of *Sp*FlhG on the GTPase activity of *Sp*FlhF was assessed by high-pressure liquid chromatography (HPLC). While SpFlhF alone showed only minor GTPase activity, an approximately three to fivefold stimulation of SpFlhF was observed in the presence of either full-length FlhG or its N-terminal region. As expected, this stimulation was almost abolished in a GTP hydrolysis-deficient FlhF variant (FlhF-R285A; Fig. 2A). This agrees with observations made for FlhF and FlhG from *B. subtilis*. Correspondingly, an *flhG-ΔN20* mutant in CN-32 displayed a hyperflagellated phenotype (Fig. S3B) which was drastically impaired in flagella-mediated motility similar to a cell completely lacking *flhG* (Fig. S3A). This indicates that FlhG may also stimulate the FlhF GTPase in polarly flagellated gammaproteobacteria such as *S. putrefaciens* CN-32 and that this interaction likely is required for proper flagellation.

To localize *Sp*FlhF within the cells, we created a hybrid gene encoding a C-terminal fusion of FlhF to mCherry (*flhF-mCherry*) which we integrated into the chromosome to replace native *flhF*. FlhF-mCherry was partially stable (Fig. S1) and predominantly localized to the flagellated cell pole in 85% of the population (Fig. 2B). A bipolar localization frequently occurred in cells that evidently were within the process of cell division. To further determine whether FlhF has a function in regulating flagellar placement and number, we studied the localization of $FliM_1$ and the flagellar filament in the absence of *flhF*. To this end, we introduced in-frame deletions of *flhF* into CN-32 wild-type cells and into cells bearing a $FliM_1$-sfGFP fusion. To specifically enable visualization of the primary flagellum, cysteine residues were introduced in both flagellins forming the primary flagellar filament to enable fluorescent labeling ($FlaAB_1$-Cys) in the wild-type and *ΔflhF* background. In mutants lacking FlhF (*ΔflhF*), we observed a significantly lower amount of cells exhibiting $FliM_1$-mCherry foci (wild type, 72%; *ΔflhF*, 27%), and these foci were commonly displaced from the cell pole to lateral positions (Fig. 2D). Fluorescence labeling of the flagellins confirmed that, in the relatively few flagellated *ΔflhF* cells, the filament frequently originated from lateral positions. Significantly fewer cells were observed to be motile, and cells exhibited irregular swimming patterns when observed by light microscopy and decreased lateral extension when moving through soft-agar plates (Fig. 2C). When FlhF or FlhF-mCherry was ectopically overproduced from an inducible promoter in wild-type cells, we observed increased accumulation at the cell pole accompanied by hyperflagellation of the cells which solely occurred at the same cell pole (Fig. S4B). In contrast, deletion of *flhF* had no significant effect on the production or placement of the secondary filaments (Fig. S4C). We then determined the localization of MCP0796, CheY, CheA or CheZ in the absence of FlhF to explore potential effects on the localization of any of the fluorescently labeled components. In contrast to the primary flagellar system, all chemotaxis components retained a polar localization pattern indistinguishable from that observed in the wild-type background (Fig. 2D; Fig. S5).

We thus confirmed that, in *S. putrefaciens* CN-32, FlhF is an active GTPase that shares the common features and properties which have been described for other species of the gammaproteobacteria and serves as a polar landmark protein and regulator for polar flagellar assembly. Furthermore, we showed that FlhF does not direct the chemotaxis system to the flagellated cell pole, which prompted us to screen for other potential landmark proteins that might be required for cell polarity in *Shewanella*.

Shewanella *sp. possess a HubP ortholog*

In *V. cholerae*, polar localization of the chemotaxis machinery was recently demonstrated to be dependent on the transmembrane landmark protein HubP. Genome analysis revealed that HubP showed significant similarities to Sputcn32_2442, a gene of 3294 bp, predicted to encode a protein of 1097 aa. Sputcn32_2442 was preliminary annotated as pilus assembly protein FimV based on its similarity to *P. aeruginosa* FimV, a protein regulating cell polarity during type IV pili-mediated twitching motility (Semmler *et al*., 2000; Wehbi *et al*., 2011). However, at the amino-acid level, significant identity or similarity between Sputcn32_2442, *Vibrio* HubP or *P. aeruginosa* FimV was only observed for the N- and very C-terminal segments of the deduced protein sequence (Fig. S6). Despite the rather low overall similarity and a lower molecular mass (estimated 117 kDa compared with ~ 178 kDa of HubP), the predicted protein exhibited striking similarities to *Vibrio* HubP with respect to domain architecture and some other features (Fig. S7). Both Sputcn32_2442 and *Vibrio* HubP are highly acidic proteins (pI 3.87 and 3.22 respectively). Similar to HubP, Sputcn32_2442 is predicted to possess an N-terminal signal sequence (likely to be cleaved between aa 24 and 25) followed by a putative LysM peptidoglycan-binding domain and a transmembrane domain. Sputcn32_2442 is annotated to directly begin with the signal sequence, while *Vc*HubP features a short cytoplasmic stretch of amino acids prior to the rather hydrophobic residues. Both proteins harbor within their cytoplasmic C-terminal segment a number of copies of an imperfect repeat that is highly enriched in acidic amino acids (10 in *Vc*HubP; 9 in Sputcn32_2442). With a length of 37 aa, these repeats are shorter in Sputcn32_2442 than in *Vc*HubP (46 aa) and are also less well conserved.

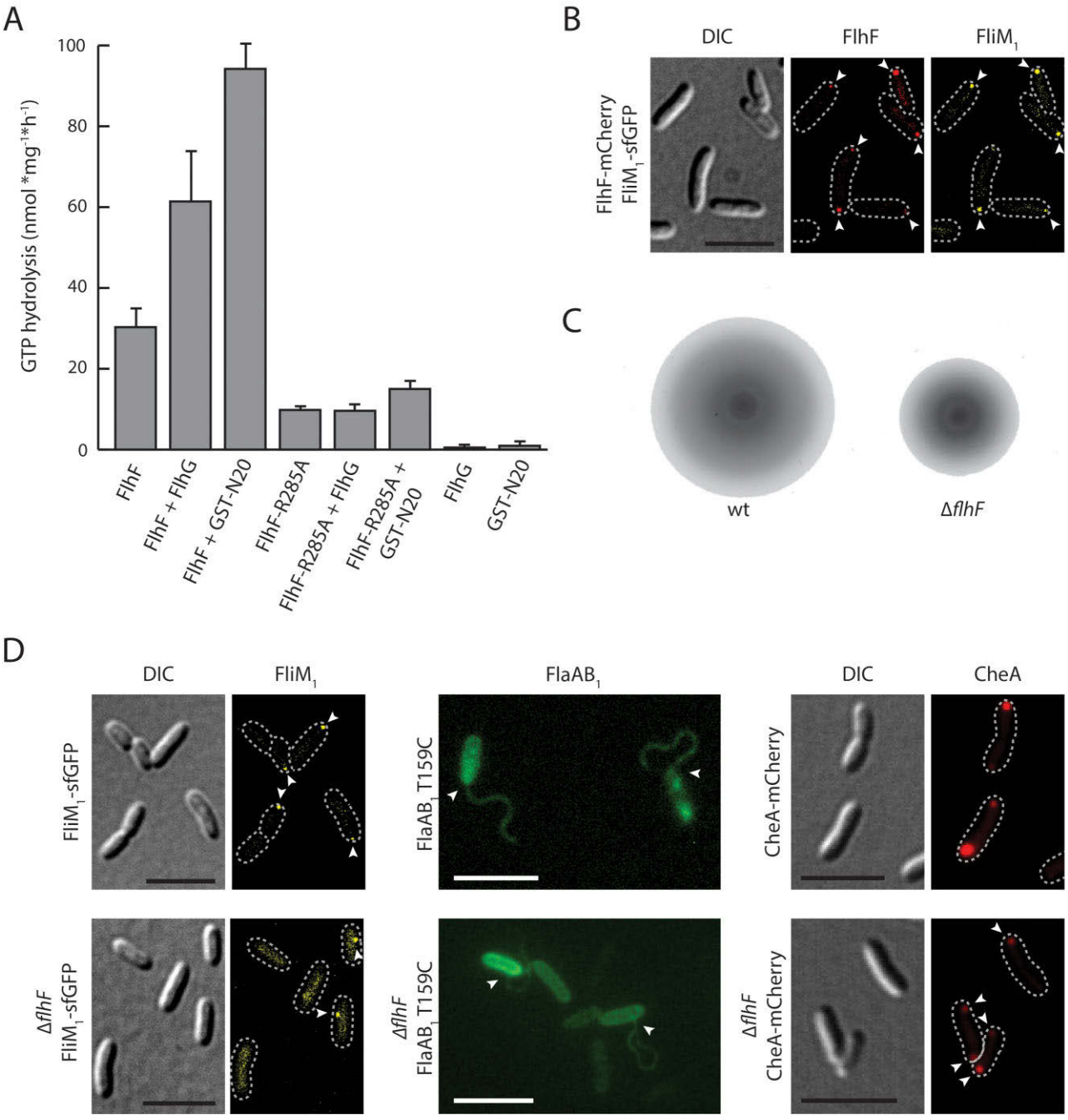

Fig. 2. Activity and role of FlhF in flagellar placement.
A. The GTPase activity of FlhF is stimulated by the N-terminus of FlhG. GTP hydrolysis in nmol per mg FlhF per hour is given as mean value ± standard deviation of three independent measurements.
B. FlhF localizes to the flagellated cell pole. Shown are DIC (left) and corresponding fluorescence micrographs of cells harboring fluorescent fusions to both FlhF and $FliM_1$ as indicated (right).
C. Loss of FlhF results in decreased swimming abilities in soft agar. 3 µl of exponentially growing cultures of the indicated strain were placed on 0.25% soft agar plates and incubated at 30°C for 16 h. Please note that the complete soft agar plate is displayed in Fig. S2.
D. FlhF has a role in localization of flagellar but not of chemotaxis components. In wild-type cells (upper panel), $FliM_1$, the flagellar filaments and CheA occur at the cell pole. In the absence of FlhF (lower panel), both $FliM_1$ and flagellar filaments are shifted to lateral positions. In contrast, chemotaxis components, here CheA, still occur at the cell poles. Displayed are DIC and fluorescent images in which the FlhF, $FliM_1$, CheA or the flagellins are fluorescently labeled (FlhF-mCherry; $FliM_1$-sfGFP, CheA-mCherry, Alexa-Fluor 488). Arrows mark fluorescent clusters and the positions of the flagellar filaments' origins respectively. The scale bar equals 5 µm.

 Molecular Microbiology, **98**, 727–742

With respect to the genetic context, both *hubP* and Sputcn32_2442 are flanked downstream by *truA*, a gene predicted to encode tRNA pseudouridine synthase A. Potential orthologs to Sputcn32_2442 can be readily identified in many other sequenced *Shewanella* species, but these exhibit variations in protein length and similarity particularly within the repeat domain of the protein (Fig. S7). Based on the similarities, and despite the low overall conservation at protein level, we hypothesized that Sputcn32_2442, henceforth *Sp*HubP, represents the functional ortholog of *Vc*HubP.

Sp*HubP localizes the chemotaxis, but not the flagellar system, to the cell pole*

In *V. cholerae*, HubP has been demonstrated to mediate polar localization of the chemotaxis cluster and to be involved in restricting the number of polar flagella to a single filament. To determine whether this similarly applies to *Sp*HubP, corresponding fluorescent protein fusions to $FliM_1$, MCP0976 (Sputcn32_0796-eGFP), CheY (sfGFP-CheY), CheA (CheY-mCherry) and CheZ (Venus-CheZ) were introduced into the CN-32 *ΔhubP* background and their localization was analyzed by fluorescence microscopy (Fig. 3A; Fig. S8A). We observed that, in the absence of *Sp*HubP, $FliM_1$-sfGFP exclusively remained at the pole in all cells. In addition, fluorescence labeling of the flagellar filament in *ΔhubP*-mutants revealed that the cells still displayed a single polar filament undistinguishable from the wild type. However, the number of cells with polar $FliM_1$-sfGFP clusters dropped significantly in the absence of *Sp*HubP (wild type, 72%; *ΔhubP*, 42%), and, accordingly, the number of flagellated cells was correspondingly lower. In contrast to the flagellar system, components of the chemotaxis machinery were no longer restricted to the cell pole but also localized to lateral positions within the cell envelope (Fig. 3A; Fig. S8A).

We also analyzed the major determinants for polar flagellar localization and number, FlhF and FlhG, in the CN-32 *ΔhubP* background (Fig. 3B; Fig. S8B). Polar positioning of FlhF occurred independently of *Sp*HubP as FlhF-mCherry exclusively localized in distinct clusters to the cell poles in both wild-type and the *ΔhubP*-mutant cells. However, as already observed with $FliM_1$-sfGFP, the frequency of cells displaying polar FlhF-mCherry foci dropped significantly in a population of cells lacking *Sp*HubP (wild type, 73%; *ΔhubP*, 46%). As previously observed in *Vibrio* species (Kusumoto *et al*., 2008; Yamaichi *et al*., 2012; Ono *et al*., 2015), stable and fully functional FlhG-sfGFP displayed a cytoplasmic localization but also accumulated at the flagellated pole in a number of cells (51%). These discrete polar foci were virtually absent in a *ΔhubP* mutant (0.25%), strongly suggesting that polar localization of FlhG depends on *Sp*HubP as has previously been observed in *V. cholerae* (Yamaichi *et al*., 2012). Taken together, the results strongly indicate that localization of the chemotaxis cluster is exclusively conferred by *Sp*HubP. Positioning of the polar flagellar system is primarily dictated by FlhF/FlhG; however, *Sp*HubP directly or indirectly affects the amount of polar accumulation of FlhF and FlhG and the size of the cellular subpopulation forming a flagellum.

The absence of Sp*HubP negatively affects motility*

To further determine whether *Sp*HubP might have a direct or indirect effect on the flagellar function, we analyzed the swimming behavior of cells by soft-agar assays and light microscopy (Fig. 4A and B). When placed on soft agar, the *ΔhubP* mutant displayed a significantly lower lateral extension than wild-type cells, indicating a decreased chemotactic drift and/or slower swimming. Analysis of cellular swimming by light microscopy revealed that *ΔhubP* mutant cells, in fact, exhibit a significant decrease in average swimming speed (wild type: 52.7 μm s^{-1}; *ΔhubP*: 29.5 μm s^{-1}). Such a phenotype has not been described for *Vc*HubP before and indicates that *Sp*HubP has further functions in motor performance in addition to ensuring close proximity between the chemotaxis and flagellar motor system.

Because the potential homolog of *Vc*- and *Sp*HubP in *P. aeruginosa*, FimV, is required for normal twitching motility (Semmler *et al*., 2000; Wehbi *et al*., 2011), we also determined type IV pili-mediated twitching motility of *S. putrefaciens* CN-32 wild-type and *ΔhubP* mutant cells. Although this type of movement was not very pronounced under the conditions tested, cells lacking *Sp*HubP showed a significant reduction in the area covered by twitching by a factor of about 4 (Fig. 4C).

Taken together, the results provide evidence that *Sp*HubP has different functions with respect to various aspects of motility in *S. putrefaciens* CN-32.

Sp*HubP has a complex localization pattern in* S. putrefaciens *CN-32*

To determine the localization of *Sp*HubP in *S. putrefaciens* CN-32 cells, we constructed a hybrid gene encoding a C-terminal fusion to sfGFP or mCherry, which we integrated into the chromosome to replace the native *hubP*. Immunoblotting analysis confirmed that *Sp*HubP-sfGFP and *Sp*HubP–mCherry were stably produced, and swimming analysis indicated that the labeled proteins were fully functional (Figs S1 and S2). Fluorescence microscopy revealed that *Sp*HubP-sfGFP mainly co-localizes with $FliM_1$-mCherry to the flagellated cell pole (Fig. 5A). The majority of cells (95%) also displayed minor fluorescence foci at the opposite pole with about half the intensity (47%) of that of the main cluster. In addition, in cells which were in the process of dividing, *Sp*HubP-mCherry was

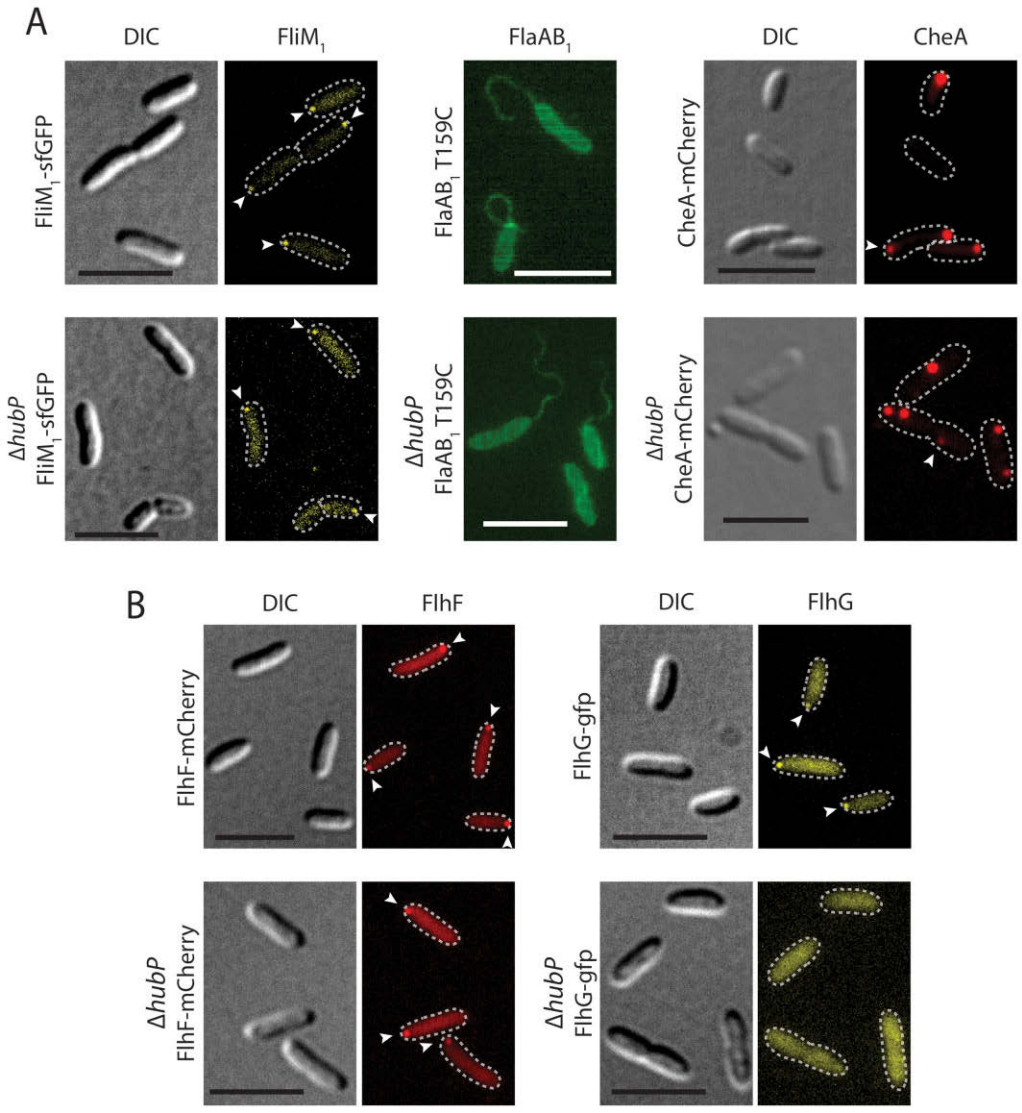

Fig. 3. Localization of flagellar and chemotaxis components in dependence of *Sp*HubP.
A. In the absence of *Sp*HubP, $FliM_1$ and flagellar filaments remain at the cell pole, while chemotaxis components, such as CheA, are delocalized to subpolar positions.
B. In the presence of *Sp*HubP, both FlhF and FlhG occur at the cell pole (upper panels, the corresponding line scan analysis can be found in Fig. S8). In *ΔhubP*-mutant cells (lower panel), FlhF remains at the cell pole while FlhG loses its polar accumulation pattern. Displayed are DIC and fluorescent micrographs in which $FliM_1$, CheA and the flagellar filament are appropriately labeled ($FliM_1$-sfGFP, CheA-mCherry, Alexa-Fluor 488). Arrows mark fluorescent clusters. The scale bar equals 5 μm.

observed to accumulate at the division plane where it co-localized with the fluorescently labeled cell division protein ZapA-sfGFP (Fig. 5B). Time-lapse microscopy and quantification of the fluorescent foci's fluorescence intensity (Fig. 6A and B) strongly suggested that targeting of *Sp*HubP to the cell division plane resulted in formation of the minor *Sp*HubP cluster that is observed at the new, nonflagellated cell poles after completion of cell division and fission. The fluorescent signal at the new cell pole rapidly gained intensity (almost reaching fluorescent intensity observed in the division plane within 10 min; Fig. 6B), strongly indicating an immediate recruitment of further copies of *Sp*HubP to the new cell pole. The signal further increased significantly during cell growth over 40 min (corresponding to one generation time) until reaching the intensity observed at the opposite pole. Both major and minor *Sp*HubP clusters displayed fluorescence recovery after complete bleaching with a half-time of about 3.2 min (major cluster) and 3.7 min (minor cluster). Thus, at least a fraction of *Sp*HubP proteins within the clusters is constantly exchanged, or further copies of the protein are constantly recruited to both clusters (Fig. 5D).

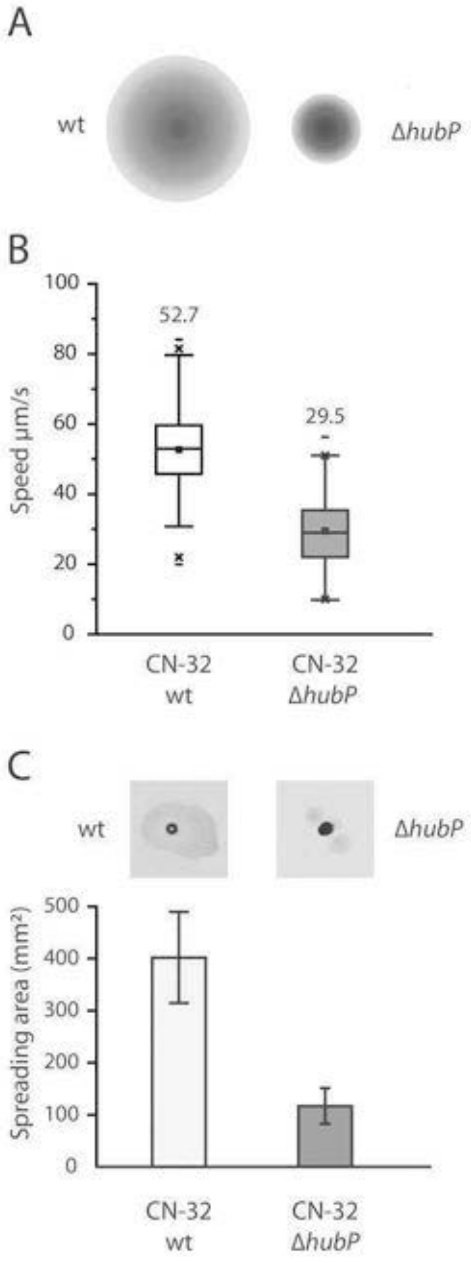

Fig. 4. *Sp*HubP is required for normal motility in *S. putrefaciens* CN-32.
A. Contribution of *Sp*HubP to spreading in soft agar. There was 3 µl of exponentially growing cultures of the corresponding strains placed on an agar plate solidified with 0.25 % agar and incubated for 16 h.
B. Contribution of *Sp*HubP to flagellar performance. Displayed is the swimming speed of wild-type and *ΔhubP* strains. The box represents the interquartile range of the data. The average and the median are shown as '□' and '—', and the whiskers denote the data range of the 5th and 95th percentile. Minimum and maximum are represented by 'x'. Swimming speed was determined for 200 cells each. Performance of the wild-type flagellar motor is significantly different from that of *ΔhubP*-mutant cells (ANOVA, *P* value 0.05).
C. Contribution of *Sp*HubP to twitching motility. The micrographs show images of the radial extension formed by twitching cells, the quantification of which is displayed below. The error bars show the standard deviation of five independent experiments.

The same localization pattern for *Sp*HubP occurred in *S. putrefaciens* cells in which the full gene locus encoding the primary polar flagellar system including *flhF* was deleted (ΔclusterI) (Fig. S9B), confirming that neither FlhF nor any other component of the polar flagellum is directly or indirectly required to target *Sp*HubP to the cell pole or division plane. When expressing a truncated version of *hubP* which only encodes the N-terminal part including the signal sequence and the predicted peptidoglycan-binding LysM domain (aa 1–134), we observed a localization pattern reminiscent to that of full-length *Sp*HubP-sfGFP (Fig. 5C). We thus concluded that the N-terminal LysM-containing domain of *Sp*HubP is sufficient for specific cellular targeting of the protein. When full-length *Sp*HubP-sfGFP or LysM-mCherry was heterologously produced in *E. coli*, both proteins similarly localized to the cell pole regions, the cell envelope, and the division plane (Figs S5 and S9C). Thus, the LysM-targeted localization of *Sp*HubP is not specific for *Shewanella*. Notably, ectopic overproduction of *Sp*HubP-sfGFP in *S. putrefaciens* CN-32 did not result in polar enrichment of the protein, but the excessive amounts were rather targeted to and accumulated at the cell envelope and division plane. These cells exhibited a distinct phenotype during growth in planktonic cultures, i.e. the occurrence of numerous smaller and elongated cells as well as chains of cells that had not separated after completion of cell division. This finding is indicating that an excess of *Sp*HubP interferes with normal cell division (Fig. S9B and D). Because a similar phenotype was observed upon overproduction of LysM-sfGFP, the effect is likely conferred by the N-terminal periplasmic domain of *Sp*HubP.

Sp*HubP, but not FlhF, targets the* oriC *to the cell pole during cell division*

*Vc*HubP has been shown to orchestrate polar localization of the *oriCI* of the larger of the two *V. cholerae* chromosomes. To determine whether or not *Sp*HubP fulfills a similar function in *S. putrefaciens* CN-32, we fused the ParB (Sputcn32_3965) C-terminus to mCherry. The hybrid gene was chromosomally integrated to replace the native *parB*. ParB is an origin-associated centromere-binding protein and thus marks the localization of the chromosomal origin. We observed no phenotype with respect to cell morphology or growth rate in the resulting strain (*mCherry-parB*), indicating that the fusion protein is fully functional.

The mCherry-ParB fusion enabled us to follow chromosome segregation in CN-32 over the cell cycle by fluorescence microscopy (Fig. 6A). Under the growth conditions

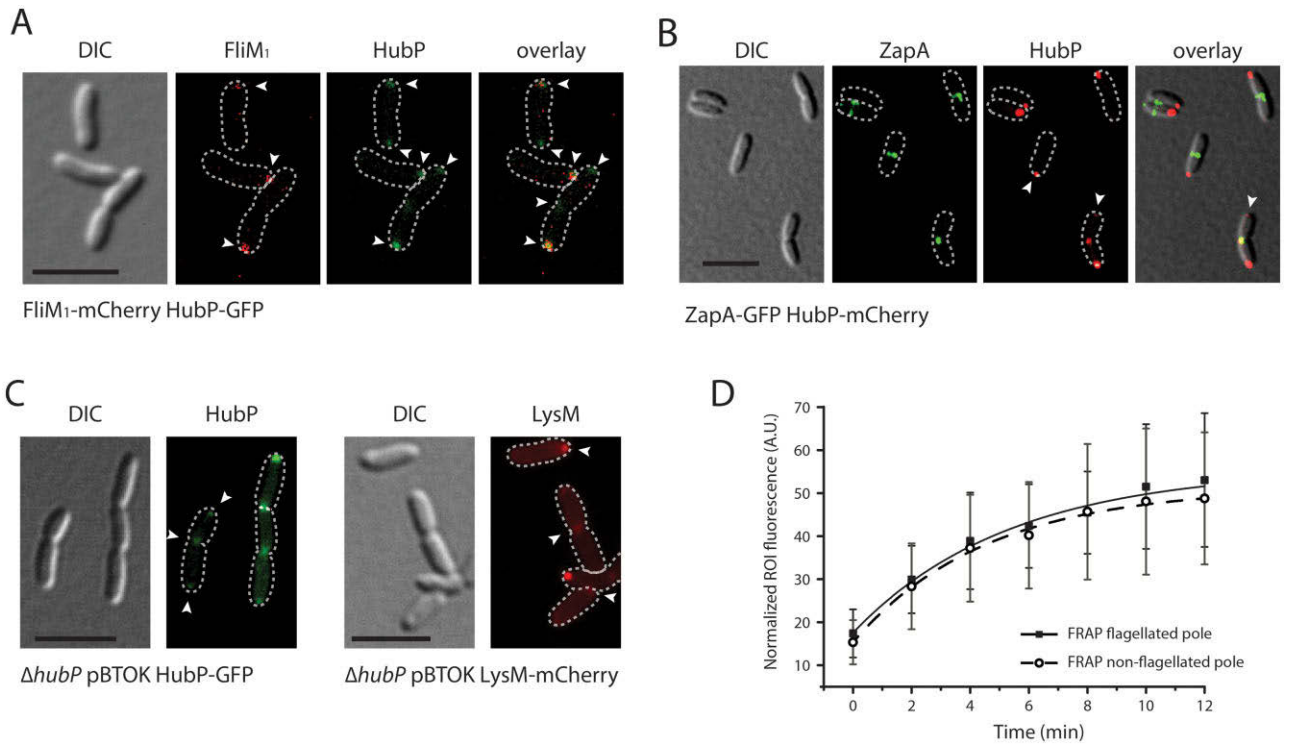

Fig. 5. Localization patterns of *Sp*HubP. Displayed are DIC and fluorescent micrographs of cells harboring fluorescently labeled components as indicated below the corresponding panels. Arrows indicate the position of fluorescent clusters. The scale bar equals 5 μm.
A. *Sp*HubP-sfGFP co-localizes with $FliM_1$ at the corresponding poles but also forms a minor cluster at the opposite cell pole.
B. *Sp*HubP-mCherry also accumulates at the division plane where it co-localizes with ZapA-sfGFP.
C. Localization pattern of *Sp*HubP-sfGFP (left panels) and its periplasmic domain (LysM-mCherry; right panels) upon ectopic production.
D. Rate of *Sp*HubP exchange as determined by FRAP. Displayed is the normalized averaged fluorescence intensity as a function of time for *Sp*HubP-sfGFP at the flagellated (black squares) and the non-flagellated (white circles) pole. Error bars display the standard error. The poles were defined prior to bleaching by co-localization with $FliM_1$-mCherry.

applied, a new replication was already initiated before cell separation, resulting in cells with four mCherry-ParB foci (33% of the population). In wild-type cells, mCherry-ParB fluorescent foci moved towards the opposite cell pole until they co-localized with fluorescently tagged *Sp*HubP directly at the cell pole. In contrast, when *Sp*HubP was absent, the mCherry-ParB foci remained at 1/4 or 3/4 position of the cell and did not resume full localization to the cell pole (Fig. 6C and D, Fig. S10A and B). Based on these observations, we concluded that *Sp*HubP has a function in chromosome segregation and is required for recruitment of *oriC* to the cell pole. Notably, the difference in chromosome segregation between wild-type and *ΔhubP* cells did not result in a significant phenotype with respect to growth or cell morphology. However, we noticed a slight difference in the timing of cell division: Under our experimental conditions, wild-type cells consistently exhibited a visible constriction when cells reached a length of 4.5 μm. In contrast, in *ΔhubP*-mutant cells, formation of the constriction occurred at less-defined cell lengths in a range of 3.6–4.4 μm. In contrast, polar localization of mCherry-ParB-marked *oriC* was unaffected by the presence or absence of FlhF (Fig. S10B).

Taken together, we have shown here that *S. putrefaciens* CN-32 possesses two distinct polar landmark systems, FlhF and *Sp*HubP. Both proteins display distinct localization patterns, and while FlhF regulates the number and polarity of the primary flagellar system, *Sp*HubP is required to target the chromosomal origin region and the chemotaxis system to the designated cell pole and likely performs some additional functions with respect to cellular motility (Fig. S11).

Discussion

For the vast majority of bacterial species, proper spatiotemporal regulation of cell polarity is crucial for a number of important or even essential cellular processes, such as chromosome segregation and cell division, differentiation, and cell motility (Treuner-Lange and Søgaard-Andersen, 2014). The latter is particularly evident for polarly flagellated bacterial species. These bacteria need to synthesize one or more new flagellar machineries at the designated cell pole, and this process often has to be strictly coordinated with the cell cycle to ensure that the daughter cell is immediately motile after separation from the mother cell

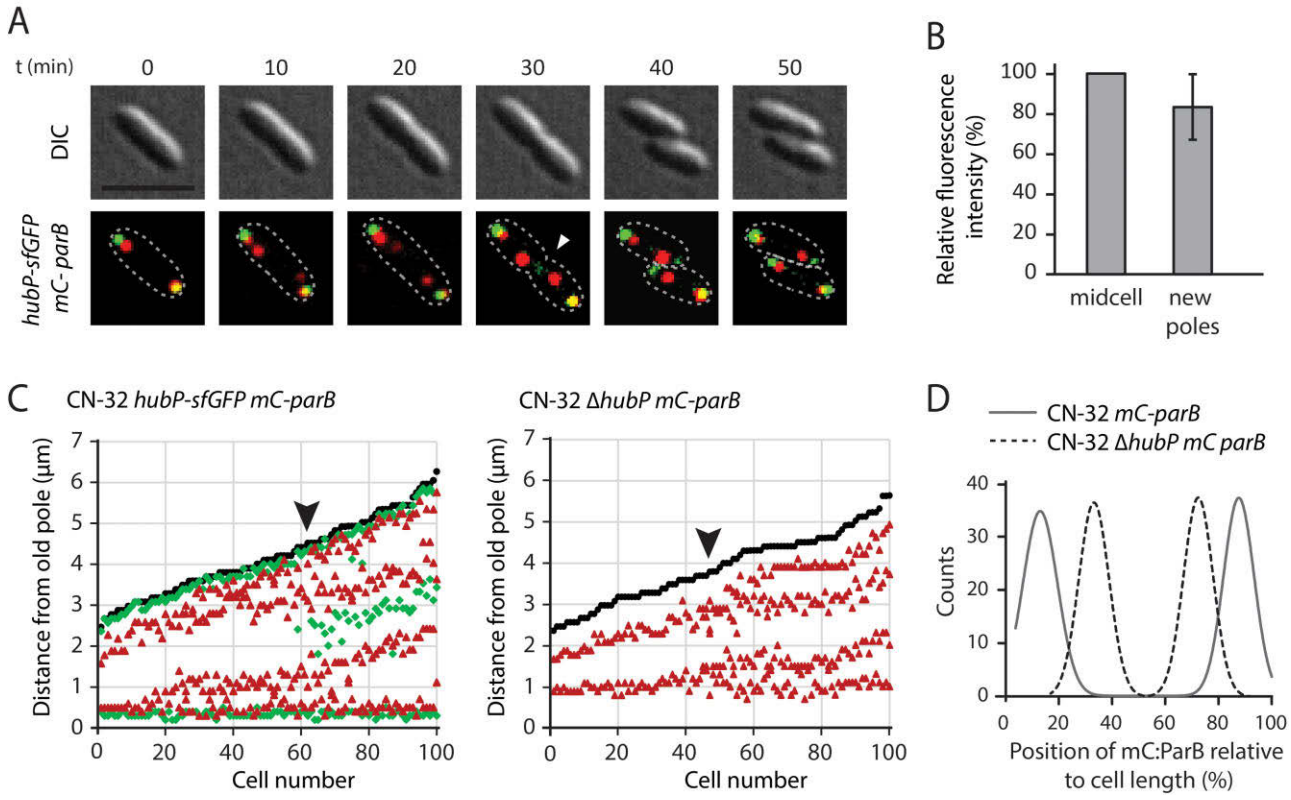

Fig. 6. Localization of *oriC* in dependence of *Sp*HubP.
A. Localization patterns of *Sp*HubP-sfGFP and ParB-mCherry during a full cell cycle. Shown are DIC (upper panel) and corresponding fluorescent micrographs (lower panel) of cells in which ParB as a marker for *oriC* was labeled with mCherry and *Sp*HubP was labeled with sfGFP. Yellow spots mark areas in which ParB and *Sp*HubP co-localize. The scale bar represents 5 µm.
B. HubP-sfGFP fluorescence intensity at midcell prior to cell fission and at each new cell pole 5–10 min after cell fission.
C. Left panel: Positioning of *Sp*HubP-sfGFP (green) and mCherry-ParB (*mC-parB*; red) relative to the cell length (black line). Right panel: Positioning of mCherry-ParB (*mC-parB*; red) relative to the cell length (black line) in the absence of *Sp*HubP. A corresponding image also displaying fluorescence intensity can be found in Fig. S10A.
D. Line scan analysis of the average mCherry-ParB (*mC-parB*) fluorescence intensity relative to the cell length. In wild-type cells (solid line) the *oriC* is localized close to the cell poles while it remains at a 1/3 position in *ΔhubP* cells (dashed line).

(Chilcott and Hughes, 2000; Ryan and Shapiro, 2003). In most bacterial species, motor functions can be modulated by one or more associated chemotaxis systems which allow biased movement towards a source of attractant or away from a repellent (Porter *et al*., 2011; Sourjik and Wingreen, 2012). Components of bacterial chemotaxis systems are commonly arranged in large macromolecular clusters whose size has allowed their visualization and structural characterization by means of electron cryo tomography (Zhang *et al*., 2007; Briegel *et al*., 2009; 2012; Liu *et al*., 2012). In a number of bipolarly or unisemipolarly flagellated bacterial species, such as *Caulobacter crescentus*, *P. aeruginosa* and *V. cholerae*, specific chemotaxis arrays localize in discrete foci at or close to the flagellated cell pole (Alley *et al*., 1992; Wadhams *et al*., 2003; Bardy and Maddock, 2005; Ringgaard *et al*., 2011). This proximity of the chemotaxis system and the receiving flagellar motors has been suggested to facilitate rapid signal exchange via CheY and, hence, chemotactic efficiency (Sourjik and Berg, 2002; Lipkow *et al*., 2005; Ringgaard *et al*., 2014), and to ensure the inheritance of a functional chemotaxis array upon division (Jones and Armitage, 2015). *S. putrefaciens* CN-32 belongs to the bacterial species which are equipped with two complete distinct flagellar systems, a primary polar and a secondary lateral system. Under appropriate conditions, both systems are synchronously assembled (Bubendorfer *et al*., 2012). Our study demonstrates that also in *Shewanella*, the chemotaxis cluster is localized to the flagellated cell pole. We have previously shown that the polar flagellar system primarily mediates cellular propulsion and is directly addressed by CheY. In contrast, the secondary system constantly rotates in a counterclockwise direction and does not respond to the chemotaxis system. This is likely due to the absence of the conserved N-terminal CheY-binding motif in the $FliM_2$ motor protein of the secondary system (Bubendorfer *et al*., 2014). Thus, in *S. putrefaciens* CN-32, the primary flagellar motor and its

corresponding chemotaxis system are localized in close proximity, which likely enables rapid signal exchange via phosphorylated CheY. In contrast, the lateral filaments operate independently to curb the cellular turning angles during chemotaxis to increase spreading efficiency of the population (Bubendorfer *et al*., 2014).

The close proximity of chemotaxis and flagellar systems in various bacterial species might lead to the speculation that polar localization of both molecular machines is mediated by the same polar landmark system. Correspondingly, previous studies on *P. aeruginosa* strongly indicated that both the polar flagellar system as well as at least one of the chemotaxis arrays depend on the polar targeting system FlhF/FlhG (Kulasekara *et al*., 2013). In contrast, in *V. cholerae*, polar localization of the chemotaxis cluster is independent of FlhF (Ringgaard *et al*., 2011) but instead requires the multidomain protein HubP (Yamaichi *et al*., 2012). Our studies demonstrate that in *S. putrefaciens* CN-32, the GTPase FlhF specifically serves as the landmark protein for polar localization of the flagellar system and exhibits the corresponding localization to the old cell pole. In *S. putrefaciens* CN-32, deletion of *flhF* negatively affects production of flagella and results in displacement of the flagellum from the cell pole to more lateral positions. These data are fully consistent with those obtained for other polarly flagellated gammaproteobacteria (summarized in Kazmierczak and Hendrixson, 2013). In contrast to the primary flagellar system, normal polar localization of the chemotaxis system in *S. putrefaciens* CN-32 occurs independently of FlhF and requires the presence of another polar multidomain landmark protein, which we identified as the functional ortholog of *Vc*HubP.

Along most of their length, *Vc*HubP and *Sp*HubP exhibit little similarity at the amino acid level with the exception of the N-terminal and far C-terminal sections (Figs S6, S7, S11). The conserved N-terminal section harbors the periplasmic part of HubP including the LysM domain and the downstream transmembrane domain. In both species, this LysM-containing part of the protein appears to be required for targeting HubP to the designated cellular compartment. The localization pattern of *Sp*HubP is complex: In most cells, the protein forms a distinct cluster at the flagellated cell pole and a smaller cluster at the opposite pole. As indicated by FRAP experiments, *Sp*HubP molecules in both major and minor clusters are constantly exchanged at a similar rate. During cell division, the minor *Sp*HubP cluster appears to increase in size while the chromosomal origin is moved towards that pole. Overproduction of both full-length *Sp*HubP-sfGFP and LysM-sfGFP did not lead to infinite growth of the polar clusters, indicating that only a certain amount of *Sp*HubP may join these clusters. Excess *Sp*HubP occurring in the cell envelope may then be targeted to the cellular division plane. After completion of division, the new poles of both mother and daughter cells bear the minor *Sp*HubP cluster while the major cluster remains at the old pole which is decorated with the primary flagellar and the corresponding chemotaxis system. Thus, similar to what has been shown for TipN in *C. crescentus*, this minor *Sp*HubP cluster might serve as a marker for future polar assembly sites in the progeny cells (Huitema *et al*., 2006; Lam *et al*., 2006). Overproduction of TipN in *C. crescentus* results in the formation of lateral cell poles and leads to cellular branching. In contrast, in *S. putrefaciens* CN-32, *Sp*HubP-sfGFP and LysM-sfGFP do not form subpolar clusters upon overproduction but diffusively accumulate in the cell envelope and at the cell division plane. We thus hypothesize that the observed phenotype with respect to cell size and cell separation in *S. putrefaciens* CN-32 at excessive levels of *Sp*HubP (or its periplasmic part) might rather be due to interference between cell division proteins and the periplasmic domain of *Sp*HubP. The homologous periplasmic region of *P. aeruginosa* FimV has previously been shown to bind peptidoglycan (Wehbi *et al*., 2011) and, upon overproduction, may lead to cell elongation, vaguely reminiscent of the phenotype observed in CN-32 (Semmler *et al*., 2000). It remains to be shown how *Vc*HubP, *Sp*HubP or FimV are targeted to the cell pole and/or the division site. It might be speculated that this targeting is due to specific regions within the peptidoglycan, such as the nascent cell wall formed during cell fission, and that the resulting minor cluster of HubP is then required to recruit further HubP copies to the new cell pole after cell separation. When *Sp*HubP-sfGFP or LysM-sfGFP are ectopically produced in *E. coli*, the protein localizes to the cell poles and cell division plane as observed in *Shewanella*, suggesting that similar structures are recognized by the periplasmic region of *Sp*HubP in both species. However, it should be noted that *Vc*HubP is directed to the cell envelope in *E. coli*, but does not exhibit its normal localization pattern in this species.

In contrast to the periplasmic region, the cytoplasmic parts of *Sp*HubP and *Vc*HubP are far less conserved and, in addition, this section is considerably shorter in *Sp*HubP (Figs S6 and S7). However, both proteins harbor within this domain 9 or 10 copies of an imperfect repeat of an amino acid motif that is highly enriched in aspartate and glutamate residues and thus imparts a highly acidic character on the protein. Studies on *Vc*HubP have provided evidence that the protein exerts its function as a polar hub by directing ParA-like ATPases, which are commonly implicated in spatiotemporal organization processes in bacteria (Lutkenhaus, 2012), to the designated cell pole (Yamaichi *et al*., 2012). ParA1, required for segregation of the larger of the two *V. cholerae* chromosomes, has been shown to directly interact with the repeat region of *Vc*HubP and this might be similarly true for *Sp*ParA and *Sp*HubP, because a deletion in *hubP* results in a very similar phenotype with respect to chromosome segregation in both *V. cholerae*

and *S. putrefaciens*. Direct interaction of *Vc*ParC, which is implicated in positioning of the chemotaxis machinery (Ringgaard *et al*., 2011), and *Vc*HubP could not be demonstrated, strongly indicating that not all *Vc*HubP client proteins have been identified yet (Yamaichi *et al*., 2012). Accordingly, deletion of the obvious *Vc*ParC ortholog in *S. putrefaciens* CN-32 (Sputcn32_2553) did not exhibit a major phenotype with respect to chemotactic swimming (data not shown). The findings strongly suggest that other, yet unidentified, factors are required to mediate polar recruitment of the chemotaxis complex by HubP.

In *S. putrefaciens*, polar targeting of FlhF and *Sp*HubP and localization of flagellar and chemotaxis systems appear to occur independently. However, when *Sp*HubP is absent, FlhF and, accordingly, $FliM_1$ was observed at the cell pole in a significantly smaller cell population, indicating that *Sp*HubP might be involved in regulating the ability of FlhF to accumulate at the cell pole and to recruit basal body proteins. A previous study has provided evidence that a high amount of FlhG negatively affects polar localization of FlhF in *V. alginolyticus* (Kusumoto *et al*., 2008). Recent work on the same species provided further conclusive evidence that polar localization of FlhG strongly depends on the ATPase activity of the protein and has a strong effect on the polar accumulation of FlhF and, hence, the formation of flagella at the cell pole (Ono *et al*., 2015). Notably, HubP was shown to directly interact with FlhF and FlhG in *V. cholerae* (Yamaichi *et al*., 2012), and we have shown here that also in *S. putrefaciens* CN-32, FlhG localizes to the flagellated cell pole in a *Sp*HubP-dependent fashion. This may suggest that while *Sp*HubP might not directly localize FlhF, it might mediate proper FlhF-FlhG interactions at the cell pole to restrict the formation of the number of polar flagella to one in the appropriate number of cells. In addition, we could provide evidence that *Sp*FlhF and *Sp*FlhG interact *in vitro* and that the N-terminal section of *Sp*FlhG stimulates the GTPase activity of *Sp*FlhF. Thus, *Sp*HubP-mediated interaction between FlhF and FlhG and control of the GTPase activity might affect FlhF-related functions such as polar accumulation and recruitment of flagellar components, but also flagellar performance, as has recently been suggested for *P. aeruginosa* (Schniederberend *et al*., 2013). Accordingly, a deletion of *hubP* in both *V. cholerae* and *S. putrefaciens* CN-32 resulted in a significantly decreased ability to navigate through soft agar. In *V. cholerae*, this phenotype has been mainly attributed to a decrease in the chemotactic drift of the population due to the, on average, increased distance between the chemotaxis machinery and the flagellar motor, resulting in a limited ability to induce directional switches appropriately (Ringgaard *et al*., 2011; Yamaichi *et al*., 2012). However, we additionally found that in *S. putrefaciens* CN-32 *ΔhubP* mutants, the average swimming speed in planktonic cultures was significantly reduced which cannot be solely attributed to the loss of chemotaxis (Bubendorfer *et al*., 2014). While this observed decrease in swimming speed might be due to *Sp*HubP-FlhF/FlhG interaction as elaborated above, it might similarly be speculated that *Sp*HubP directly or indirectly recruits other proteins that affect flagellar functions (Boehm *et al*., 2010; Fang and Gomelsky, 2010; Paul *et al*., 2010; Kulasekara *et al*., 2013). We have shown that also type IV pili-mediated twitching motility, which requires polar assembly and disassembly of pili fibers (Burrows, 2012), is affected in *S. putrefaciens ΔhubP*. We thus expect that further interaction partners, or 'client' proteins, of *Sp*HubP remain to be identified which do not belong to the group of ParA-like proteins.

Potential HubP or FimV orthologs can be identified in a number of different bacterial genera (Semmler *et al*., 2000; Yamaichi *et al*., 2012). All of these proteins share an N-terminal periplasmic domain comprising the, putatively peptidoglycan-binding, LysM-domain. This N-terminal domain might also be involved in mediating protein–protein interactions within the periplasm or membrane (Wehbi *et al*., 2011). In addition, all these proteins are characterized by a highly acidic cytoplasmic part which appears to function as the docking region for other appropriate interaction partners. This cytoplasmic region is little conserved at the amino acid level but also with respect to protein length and the presence and organization of repeat units, and even within a group of closely related species, such as in various *Shewanella* sp., the cytoplasmic part of HubP/FimV exhibits a high degree of variation. It might thus be speculated that polar targeting within the cell by the LysM domain is conserved throughout the species. In contrast, the cytoplasmic and also the periplasmic parts may have adapted to the specific requirement of the host species for polar localization of client proteins or protein complexes. These differences might be the reason why the chemotaxis system is localized by HubP in *V. cholerae* and *S. putrefaciens* CN-32, but directly or indirectly depends on FlhF in *P. aeruginosa*. Thus, HubP/FimV proteins might have numerous different functions, including various aspects of motility and chromosome segregation as shown for *P. aeruginosa*, *V. cholerae* and *S. putrefaciens* CN-32 (Semmler *et al*., 2000; Wehbi *et al*., 2011; Yamaichi *et al*., 2012; Fig. S11). We expect that future studies on different species will identify further processes which are spatiotemporally organized by HubP/FimV proteins.

Experimental procedures

Strains, growth conditions and media

All strains used in this study are listed in Table S1. *E. coli* strains were routinely cultured in LB medium at 37°C if not indicated otherwise. *S. putrefaciens* CN-32 strains were cultivated in LB or LM (10 mM HEPES, pH 7.5; 200 mM NaCl;

0.02% yeast extract; 0.01% peptone; 15 mM lactate) media at 30°C. When required, media were supplemented with 50 μg ml^{-1} kanamycin or 10% (w/v) sucrose. Cultures of the *E. coli* conjugation strain were supplemented with 2,6-diamino-pimelic acid (DAP) to a final concentration of 300 μM. Solid media were made by an addition of 1.5% (w/v) agar. Soft agar plates for swimming assays were prepared with LB medium solidified with 0.25% (w/v) agar.

Strain constructions

General DNA manipulations were carried out according to standard protocols (Sambrook *et al*., 1989) using appropriate kits (VWR International GmbH, Darmstadt, Germany) and enzymes (Fermentas, St Leon-Rot, Germany). All vectors/plasmids used in this study are summarized in Table S2. Plasmids were delivered to *S. putrefaciens* CN-32 by conjugation from *E. coli* WM3064. Markerless in-frame deletions were generated by sequential homologous crossover using vector pNTPS-138-R6K essentially as described previously (Lassak *et al*., 2010). Vectors were constructed either by common restriction/ligation approaches using appropriate restriction enzymes, or by enzymatic assembly as previously reported (Gibson *et al*., 2009). The corresponding oligonucleotides used for cloning are listed in Table S3. To complement in-frame deletion mutants, the mutated locus was exchanged with the wild-type gene using the same sequential crossover approach. To generate fluorescent fusions, target proteins were either C- or N-terminally tagged with sfGFP, mCherry, Venus or eCFP using a flexible linker of either 6xGly, 2x(Gly-Gly-Ser), 3x(Gly-Gly-Ser) or (Gly-Ser) (for ectopic overproduction of FlhF-sfGFP and C-terminal tagging of FlhG). The nature of each fluorescent fusion is specified in detail in Table S1. All genetic fusions except those for the MCPs and for ectopic (over-)production were introduced into the chromosome to replace the native copy of the gene essentially as previously described (Bubendorfer *et al*., 2012) by markerless sequential crossover using pNTPS-138-R6K as delivery vector. The fusion to MCP0796 was established by cloning an appropriate PCR-derived DNA fragment of about 500 bp encoding the C-terminal region of the proteins into vector pJP5603-gfp (Koerdt *et al*., 2009) followed by conjugation and single homologous integration, yielding a chromosomal fusion expressed under its native promoter. Correct insertions or deletions were verified by polymerase chain reaction (PCR). Production levels and stability of fusion proteins were checked by immunofluorescence approaches and appropriate phenotypic analysis (Fig. S1). To enable coupling of maleimide-ligated Alexa dyes to the flagellar filaments, a threonine-to-cysteine (T159C) were introduced in both $FlaA_1$ and $FlaB_1$ flagellins by exchange of the appropriate codons within the corresponding genes on the chromosome, resulting in strain $FlaAB_1$-Cys. Accordingly, variants of $FlaA_2$ (T159C; T160C) and $FlaB_2$ (T156C; T159C) were constructed for specific labeling of secondary flagella. For overproduction of FlhF and FlhG and derivatives, the corresponding genes (Sputcn32_2561, *flhF*; Sputcn32_2560, *flhG*) were amplified from *S. putrefaciens* CN-32 genomic DNA by PCR using appropriate primer pairs (Table S3). The forward primer encoded a hexa-histidine tag in frame with the DNA sequence of *flhF* or *flhG*. The resultant PCR fragments were cloned into pET24d(+) (Novagen) or pGAT3 (Peränen *et al*., 1996) vectors via the introduced restriction sites. Due to enhanced purification properties of the produced protein, a truncated version of *flhF* lacking the first 10 codons of the 5′-end was overexpressed.

Overproduction of Sp*HubP-sfGFP and LysM-mCherry*

The vector pBTOK was derived by assembly of the anhydrotetracycline-inducible promoter region of pASK-IBA3plus (IBA GmbH, Göttingen, Germany) followed by the *E. coli rrnB1* T_1 and lambda phage T_0 terminator set into pBBR1-MCS5 (Kovach *et al*., 1995). The vector backbone fragment was amplified with primer pair SH501/SH502 using pBBR1-MCS5 as a template; the promoter region including the MCS of pAS-IBA3plus was derived using SH503/SH504; and the terminator region was produced using SH505/SH506 and pUC18-mini-Tn*7*T-Gm-lux (Choi *et al*., 2005) as a template. Fragment assembly was carried as previously described (Gibson *et al*., 2009). Sequence and vector map are available upon request. The sequence of *hubP-sfgfp*, the LysM domain [*Sp*HubP_AA1-134 (Sputcn32_2442_nt1-402)] and mCherry were amplified with the corresponding primer pairs. The LysM-encoding gene region and *mCherry* were joined by an overlap PCR. The resulting inserts were processed with XbaI and PspOMI and ligated into the vector. The resulting plasmid was transferred into CN-32 *ΔhubP* via conjugation. Prior to overproduction, CN-32 pBTOK-HubP-sfGFP and CN-32 pBTOK-LysM-mCherry were cultured in LB media to an OD_{600} of ~ 0.3 followed by induction with 20 ng·ml^{-1} anhydrotetracycline for 45 min.

Flagellar and hook staining

Fluorescent staining of flagellar filaments (CN-32 $FlaAB_1$-Cys) or hook structures ($FlgE_2$-Cys; Schuhmacher *et al*., 2015b) was essentially carried out on exponentially growing cells as previously described (Guttenplan *et al*., 2013) using Alexa Fluor 488 maleimide (Molecular Probes, Life Technologies) prior to microscopy.

Fluorescence microscopy

Prior to microscopy, strains were cultivated overnight in LM media and subcultured in LM until reaching exponential growth phase (OD_{600} of ~ 0.2). There was 3 μl of culture spotted on an agarose pad (LM media solidified by 1% (w/v) agarose). Fluorescence images were recorded by a Leica DMI 6000 B inverse microscope (Leica, Wetzlar, Germany) equipped with an sCMOS camera and a HCX PL APO 100×/1.4 objective using the VisiView software (Visitron Systems, Puchheim, Germany). Images were further processed using ImageJ and Adobe Illustrator CS6.

Fluorescence recovery after photobleaching (FRAP)

FRAP analyses were carried out with a Axio Imager.M1 microscope (Zeiss), a Zeiss Plan Apochromat 100×/1.40 Oil DIC (Differential Interference Contrast) objective and a

Cascade:1K CCD camera (Photometrics) equipped with a 488 nm-solid state laser and a 2D-VisiFRAP Galvo System multi-point FRAP module (Visitron Systems, Germany). Cells were cultured and immobilized on agarose pads as described above. After acquisition of a pre-bleach image, a single laser pulse of 30 ms was used to bleach individual *Sp*HubP-sfGFP clusters. Fluorescence recovery was subsequently monitored at 2-min intervals for 12 min. The integrated fluorescence intensities of the whole cell, the bleached region and an equally sized unbleached region were measured for each time point using ImageJ. After background correction, the fluorescence intensities of the bleached and unbleached regions were divided by the whole cell intensity to correct for general photobleaching during the imaging process. Average values of 10–13 cells were plotted using OriginPro 9.1. Recovery rates were determined by fitting the data obtained for the bleached region to the single exponential function F(t) = F0*exp(-x/t1) + A, where F(t) is the fluorescence at time t, A the maximum intensity, x the time in min, 1/t1 the rate constant in min^{-1} and F0 the relative fluorescence intensity at t = 0 min. In all cases, fits with $R2 \geq 0.99$ were obtained. Recovery half-times were calculated according to the equation $t_{1/2} = \ln(2)*t1$.

Determination of swimming speed

Cells of *S. putrefaciens* CN-32 and *S. putrefaciens* CN-32 Δ*hubP* from overnight cultures were used to inoculate LM medium to an OD_{600} of 0.02 and cultivated for 3–4 h to an OD_{600} of ~ 0.2. An aliquot of each culture was placed under a coverslip fixed by four droplets of silicone to create a space of 1–2 mm width. Movies of 12 s (157 frames) were taken with an inverse microscope (for specification, see above). Speeds of 200 cells per strain were determined using the MTrackJ plugin of ImageJ. The resulting data were tested for significance by using ANOVA ($P = 0.05$) in R version 3.0.1. Motility was further assessed by placing 3 µl of a planktonic culture of the corresponding strains on soft agar plates containing LB medium with an agar concentration of 0.25% (w/v). Plates were incubated for 12h at 30°C or overnight at room temperature. Strains to be directly compared were always placed on the same plate.

Analysis of twitching motility

Type IV pili-mediated twitching motility was assayed as described previously (Semmler *et al*., 1999) using 1.0 % LB-agar plates at 30°C for up to 48 h.

Protein production and purification

E. coli BL21(DE3) (New England BioLabs, Frankfurt, Germany) cells carrying the appropriate expression plasmid were grown in LB medium supplemented with kanamycin (100 µg ml^{-1}) and D(+)-lactose-monohydrate (12.5 g l^{-1}) for 16 h at 30°C under rigorous shaking (150 r.p.m.). Cells were harvested (3500×*g*, 20 min, 4°C) and resuspended in lysis buffer (20 mM HEPES, pH 8.0; 250 mM NaCl; 40 mM imidazole; 20 mM $MgCl_2$ and 20 mM KCl). Cells were lysed with the M-110L Microfluidizer (Microfluidics). After centrifugation (47 850×*g*, 20 min, 4°C), the clear supernatant was loaded on a 1 ml HisTrap column (GE Healthcare) equilibrated with 10 column volumes (CV) of lysis buffer. After washing with 10 CV lysis buffer, the protein was eluted with 15 ml elution buffer (lysis buffer containing 500 mM imidazole). The protein was concentrated to ≈ 15 mg ml^{-1} using an Amicon Ultracel-10K (Millipore). The concentrated sample was applied to size-exclusion chromatography (HiLoad 26/600 Superdex 200 pg, GE Healthcare) equilibrated with SEC-buffer (20 mM HEPES, pH 7.5, 200 mM NaCl 20 mM MgCl2 and 20 mM KCl). Protein concentration was determined by a spectrophotometer (NanoDrop Lite, Thermo Scientific).

GTPase activity of FlhF

GTPase activity of FlhF was monitored by HPLC. There was 100 µM of each protein (FlhF, FlhG and/or corresponding derivatives as indicated) incubated together with 1 mM GTP in SEC-buffer for 30 min at 37°C. Reactions were stopped by flash-freezing with liquid nitrogen and stored at –20°C until measurement. HPLC measurements were performed with an Agilent 1100 Series HPLC system (Agilent Technologies, Santa Clara) and a C18 column (EC 250/4.6 Nucleodur HTec 3 µm; Macherey-Nagel, Düren, Germany). GDP and GTP were eluted with a buffer containing 50 mM KH_2PO_4, 50 mM K_2HPO_4, 10 mM tetrapentylammonium bromide and 15% (v/v) acetonitrile at 0.8 ml min^{-1} flow rate and detected at a wavelength of 253 nm in agreement with standards. GDP originating from non-enzymatic hydrolysis of GTP was determined by triplicate measurement of 1 mM GTP treated similar as the enzymatic reactions and subtracted from the quantified GDP.

Immunoblot (Western blot) analysis

Production and stability of the fusions were determined by immunoblot analyses. Protein lysates were prepared from exponentially growing cultures. Cell suspensions were uniformly adjusted to an OD_{600} of 10. Protein separation and immunoblot detection were essentially carried out as described earlier (Bubendorfer *et al*., 2012; Binnenkade *et al*., 2014) using polyclonal antibodies raised against mCherry, GFP (Eurogentec Deutschland GmbH, Köln, Germany) or FlhG (Schuhmacher *et al*., 2015b). Signals were detected using the SuperSignal® West Pico Chemiluminescent Substrate (Thermo Scientific, Schwerte, Germany) and documented using a FUSION-SL chemiluminescence imager (Peqlab, Erlangen, Germany).

Acknowledgements

This project was supported by grants from the Deutsche Forschungsgemeinschaft (DFG) to KMT (TH831/5-1) in the framework of the priority program SPP1617. FR and SB were supported by the International Max Planck Research School. The project was further supported by the LOEWE excellence initiative of the state of Hesse (to GB).

We are grateful to Oliver Leicht and Martin Thanbichler at the Philipps-Universität Marburg for help with the FRAP analysis and to Wieland Steinchen of the Bange lab for his assistance during HPLC measurements. We would also like

to thank Martin Thanbichler and Anke Treuner-Lange for critically reading and commenting on the manuscript.

Conflict of interest

The authors declare no conflict of interest.

References

Alley, M.R., Maddock, J.R., and Shapiro, L. (1992) Polar localization of a bacterial chemoreceptor. *Genes Dev* **6:** 825–836.

Altegoer, F., Schuhmacher, J., Pausch, P., and Bange, G. (2014) From molecular evolution to biobricks and synthetic modules: a lesson by the bacterial flagellum. *Biotechnol Genet Eng Rev* **30:** 49–64.

Balaban, M., Joslin, S.N., and Hendrixson, D.R. (2009) FlhF and its GTPase activity are required for distinct processes in flagellar gene regulation and biosynthesis in *Campylobacter jejuni*. *J Bacteriol* **191:** 6602–6611.

Bange, G., and Sinning, I. (2013) SIMIBI twins in protein targeting and localization. *Nat Struct Mol Biol* **20:** 776–780.

Bange, G., Petzold, G., Wild, K., Parlitz, R.O., and Sinning, I. (2007) The crystal structure of the third signal-recognition particle GTPase FlhF reveals a homodimer with bound GTP. *Proc Natl Acad Sci USA* **104:** 13621–13625.

Bange, G., Kümmerer, N., Grudnik, P., Lindner, R., Petzold, G., Kressler, D., *et al*. (2011) Structural basis for the molecular evolution of SRP-GTPase activation by protein. *Nat Struct Mol Biol* **18:** 1376–1380.

Bardy, S.L., and Maddock, J.R. (2005) Polar localization of a soluble methyl-accepting protein of *Pseudomonas aeruginosa*. *J Bacteriol* **187:** 7840–7844.

Binnenkade, L., Teichmann, L., and Thormann, K.M. (2014) Iron triggers lambdaSo prophage induction and release of extracellular DNA in *Shewanella oneidensis* MR-1 biofilms. *Appl Environ Microbiol* **80:** 5304–5316.

Boehm, A., Kaiser, M., Li, H., Spangler, C., Kasper, C.A., Ackermann, M., *et al*. (2010) Second messenger-mediated adjustment of bacterial swimming velocity. *Cell* **141:** 107–116.

Briegel, A., Ortega, D.R., Tocheva, E.I., Wuichet, K., Li, Z., Chen, S., *et al*. (2009) Universal architecture of bacterial chemoreceptor arrays. *Proc Natl Acad Sci USA* **106:** 17181–17186.

Briegel, A., Li, X., Bilwes, A.M., Hughes, K.T., Jensen, G.J., and Crane, B.R. (2012) Bacterial chemoreceptor arrays are hexagonally packed trimers of receptor dimers networked by rings of kinase and coupling proteins. *Proc Natl Acad Sci USA* **109:** 3766–3771.

Bubendorfer, S., Held, S., Windel, N., Paulick, A., Klingl, A., and Thormann, K.M. (2012) Specificity of motor components in the dual flagellar system of *Shewanella putrefaciens* CN-32. *Mol Microbiol* **83:** 335–350.

Bubendorfer, S., Koltai, M., Rossmann, F., Sourjik, V., and Thormann, K.M. (2014) Secondary bacterial flagellar system improves bacterial spreading by increasing the directional persistence of swimming. *Proc Natl Acad Sci USA* **111:** 11485–11490.

Burrows, L.L. (2012) *Pseudomonas aeruginosa* twitching motility: type IV pili in action. *Annu Rev Microbiol* **66:** 493–520.

Chilcott, G.S., and Hughes, K.T. (2000) Coupling of flagellar gene expression to flagellar assembly in *Salmonella enterica* serovar *typhimurium* and *Escherichia coli*. *Microbiol Mol Biol Rev* **64:** 694–708.

Choi, K.H., Gaynor, J.B., White, K.G., Lopez, C., Bosio, C.M., Karkhoff-Schweizer, R.R., and Schweizer, H.P. (2005) A Tn*7*-based broad-range bacterial cloning and expression system. *Nat Methods* **2:** 443–448.

Correa, N.E., Peng, F., and Klose, K.E. (2005) Roles of the regulatory proteins FlhF and FlhG in the *Vibrio cholerae* flagellar transcription hierarchy. *J Bacteriol* **187:** 6324–6332.

Dasgupta, N., Arora, S.K., and Ramphal, R. (2000) fleN, a gene that regulates flagellar number in *Pseudomonas aeruginosa*. *J Bacteriol* **182:** 357–364.

Davis, N.J., Cohen, Y., Sanselicio, S., Fumeaux, C., Ozaki, S., Luciano, J., *et al*. (2013) De- and repolarization mechanism of flagellar morphogenesis during a bacterial cell cycle. *Genes Dev* **27:** 2049–2062.

Ewing, C.P., Andreishcheva, E., and Guerry, P. (2009) Functional characterization of flagellin glycosylation in *Campylobacter jejuni* 81–176. *J Bacteriol* **191:** 7086–7093.

Fang, X., and Gomelsky, M. (2010) A post-translational, c-di-GMP-dependent mechanism regulating flagellar motility. *Mol Microbiol* **76:** 1295–1305.

Gibson, D.G., Young, L., Chuang, R.Y., Venter, J.C., Hutchison, C.A., 3rd, and Smith, H.O. (2009) Enzymatic assembly of DNA molecules up to several hundred kilobases. *Nat Methods* **6:** 343–345.

Green, J.C., Kahramanoglou, C., Rahman, A., Pender, A.M., Charbonnel, N., and Fraser, G.M. (2009) Recruitment of the earliest component of the bacterial flagellum to the old cell division pole by a membrane-associated signal recognition particle family GTP-binding protein. *J Mol Biol* **391:** 679–690.

Guttenplan, S.B., Shaw, S., and Kearns, D.B. (2013) The cell biology of peritrichous flagella in *Bacillus subtilis*. *Mol Microbiol* **87:** 211–229.

Huitema, E., Pritchard, S., Matteson, D., Radhakrishnan, S.K., and Viollier, P.H. (2006) Bacterial birth scar proteins mark future flagellum assembly site. *Cell* **124:** 1025–1037.

Jones, C.W., and Armitage, J.P. (2015) Positioning of bacterial chemoreceptors. *Trends Microbiol* **23:** 247–256.

Kazmierczak, B.I., and Hendrixson, D.R. (2013) Spatial and numerical regulation of flagellar biosynthesis in polarly flagellated bacteria. *Mol Microbiol* **88:** 655–663.

Koerdt, A., Paulick, A., Mock, M., Jost, K., and Thormann, K.M. (2009) MotX and MotY are required for flagellar rotation in *Shewanella oneidensis* MR-1. *J Bacteriol* **191:** 5085–5093.

Kovach, M.E., Elzer, P.H., Hill, D.S., Robertson, G.T., Farris, M.A., Roop, R.M., 2nd, and Peterson, K.M. (1995) Four new derivatives of the broad-host-range cloning vector pBBR1MCS, carrying different antibiotic-resistance cassettes. *Gene* **166:** 175–176.

Kulasekara, B.R., Kamischke, C., Kulasekara, H.D., Christen, M., Wiggins, P.A., and Miller, S.I. (2013) c-di-GMP heterogeneity is generated by the chemotaxis machinery to regulate flagellar motility. *Elife* **2:** e01402.

Kusumoto, A., Kamisaka, K., Yakushi, T., Terashima, H., Shinohara, A., and Homma, M. (2006) Regulation of polar

flagellar number by the *flhF* and *flhG* genes in *Vibrio alginolyticus*. *J Biochem* **139:** 113–121.
Kusumoto, A., Shinohara, A., Terashima, H., Kojima, S., Yakushi, T., and Homma, M. (2008) Collaboration of FlhF and FlhG to regulate polar-flagella number and localization in *Vibrio alginolyticus*. *Microbiology* **154:** 1390–1399.
Laloux, G., and Jacobs-Wagner, C. (2014) How do bacteria localize proteins to the cell pole? *J Cell Sci* **127:** 11–19.
Lam, H., Schofield, W.B., and Jacobs-Wagner, C. (2006) A landmark protein essential for establishing and perpetuating the polarity of a bacterial cell. *Cell* **124:** 1011–1023.
Lassak, J., Henche, A.L., Binnenkade, L., and Thormann, K.M. (2010) ArcS, the cognate sensor kinase in an atypical Arc system of *Shewanella oneidensis* MR-1. *Appl Environ Microbiol* **76:** 3263–3274.
Lipkow, K., Andrews, S.S., and Bray, D. (2005) Simulated diffusion of phosphorylated CheY through the cytoplasm of *Escherichia coli*. *J Bacteriol* **187:** 45–53.
Liu, J., Hu, B., Morado, D.R., Jani, S., Manson, M.D., and Margolin, W. (2012) Molecular architecture of chemoreceptor arrays revealed by cryoelectron tomography of *Escherichia coli* minicells. *Proc Natl Acad Sci USA* **109:** E1481–E1488.
Lutkenhaus, J. (2012) The ParA/MinD family puts things in their place. *Trends Microbiol* **20:** 411–418.
Murray, T.S., and Kazmierczak, B.I. (2006) FlhF is required for swimming and swarming in *Pseudomonas aeruginosa*. *J Bacteriol* **188:** 6995–7004.
Obuchowski, P.L., and Jacobs-Wagner, C. (2008) PfIl, a protein involved in flagellar positioning in *Caulobacter crescentus*. *J Bacteriol* **190:** 1718–1729.
Ono, H., Takashima, A., Hirata, H., Homma, M., and Kojima, S. (2015) The MinD homolog FlhG regulates the synthesis of the single polar flagellum of *Vibrio alginolyticus*. *Mol Microbiol* **98:** 130–141. doi: 10.1111/mmi.13109
Pandza, S., Baetens, M., Park, C.H., Au, T., Keyhan, M., and Matin, A. (2000) The G-protein FlhF has a role in polar flagellar placement and general stress response induction in *Pseudomonas putida*. *Mol Microbiol* **36:** 414–423.
Paul, K., Nieto, V., Carlquist, W.C., Blair, D.F., and Harshey, R.M. (2010) The c-di-GMP binding protein YcgR controls flagellar motor direction and speed to affect chemotaxis by a 'backstop brake' mechanism. *Mol Cell* **38:** 128–139.
Peränen, J., Rikkonen, M., Hyvonen, M., and Kaariainen, L. (1996) T7 vectors with modified T7*lac* promoter for expression of proteins in *Escherichia coli*. *Anal Biochem* **236:** 371–373.
Porter, S.L., Wadhams, G.H., and Armitage, J.P. (2011) Signal processing in complex chemotaxis pathways. *Nat Rev Microbiol* **9:** 153–165.
Reyes-Lamothe, R., Nicolas, E., and Sherratt, D.J. (2012) Chromosome replication and segregation in bacteria. *Annu Rev Genet* **46:** 121–143.
Ringgaard, S., Schirner, K., Davis, B.M., and Waldor, M.K. (2011) A family of ParA-like ATPases promotes cell pole maturation by facilitating polar localization of chemotaxis proteins. *Genes Dev* **25:** 1544–1555.
Ringgaard, S., Zepeda-Rivera, M., Wu, X., Schirner, K., Davis, B.M., and Waldor, M.K. (2014) ParP prevents dissociation of CheA from chemotactic signaling arrays and tethers them to a polar anchor. *Proc Natl Acad Sci USA* **111:** E255–E264.
Ryan, K.R., and Shapiro, L. (2003) Temporal and spatial regulation in prokaryotic cell cycle progression and development. *Annu Rev Biochem* **72:** 367–394.
Sambrook, K., Fritsch, E.F., and Maniatis, T. (1989) *Molecular Cloning: A Laboratory Manual*. Cold Spring Harbor, NY: Cold Spring Harbor Press.
Schniederberend, M., Abdurachim, K., Murray, T.S., and Kazmierczak, B.I. (2013) The GTPase activity of FlhF is dispensable for flagellar localization, but not motility, in *Pseudomonas aeruginosa*. *J Bacteriol* **195:** 1051–1060.
Schuhmacher, J.S., Thormann, K.M., and Bange, G. (2015a) How bacteria maintain location and function of flagella? *FEMS Microbiol Rev* (in press). pii: fuv034.
Schuhmacher, J.S., Rossmann, F., Dempwolff, F., Knauer, C., Altegoer, F., Steinchen, W., *et al*. (2015b) MinD-like ATPase FlhG effects location and number of bacterial flagella during C-ring assembly. *Proc Natl Acad Sci USA* **112:** 3092–3097.
Semmler, A.B., Whitchurch, C.B., and Mattick, J.S. (1999) A re-examination of twitching motility in *Pseudomonas aeruginosa*. *Microbiology* **145** (Part 10): 2863–2873.
Semmler, A.B., Whitchurch, C.B., Leech, A.J., and Mattick, J.S. (2000) Identification of a novel gene, *fimV*, involved in twitching motility in *Pseudomonas aeruginosa*. *Microbiology* **146:** 1321–1332.
Sourjik, V., and Berg, H.C. (2002) Binding of the *Escherichia coli* response regulator CheY to its target measured in vivo by fluorescence resonance energy transfer. *Proc Natl Acad Sci USA* **99:** 12669–12674.
Sourjik, V., and Wingreen, N.S. (2012) Responding to chemical gradients: bacterial chemotaxis. *Curr Opin Cell Biol* **24:** 262–268.
Thanbichler, M. (2010) Synchronization of chromosome dynamics and cell division in bacteria. *Cold Spring Harb Perspect Biol* **2:** a000331.
Treuner-Lange, A., and Søgaard-Andersen, L. (2014) Regulation of cell polarity in bacteria. *J Cell Biol* **206:** 7–17.
Wadhams, G.H., Warren, A.V., Martin, A.C., and Armitage, J.P. (2003) Targeting of two signal transduction pathways to different regions of the bacterial cell. *Mol Microbiol* **50:** 763–770.
Wehbi, H., Portillo, E., Harvey, H., Shimkoff, A.E., Scheurwater, E.M., Howell, P.L., and Burrows, L.L. (2011) The peptidoglycan-binding protein FimV promotes assembly of the *Pseudomonas aeruginosa* type IV pilus secretin. *J Bacteriol* **193:** 540–550.
Yamaichi, Y., Bruckner, R., Ringgaard, S., Möll, A., Cameron, D.E., Briegel, A., *et al*. (2012) A multidomain hub anchors the chromosome segregation and chemotactic machinery to the bacterial pole. *Genes Dev* **26:** 2348–2360.
Zhang, P., Khursigara, C.M., Hartnell, L.M., and Subramaniam, S. (2007) Direct visualization of *Escherichia coli* chemotaxis receptor arrays using cryo-electron microscopy. *Proc Natl Acad Sci USA* **104:** 3777–3781.

Supporting information

Additional supporting information may be found in the online version of this article at the publisher's web-site.

The role of FlhF and HubP as polar landmark proteins in *Shewanella putrefaciens* CN-32

Florian Rossmann[#,1,2], Susanne Brenzinger[#,1,2], Carina Knauer[3], Anja K. Dörrich[1], Sebastian Bubendorfer[1,4], Ulrike Ruppert[1], Gert Bange[3], Kai M. Thormann[1*]

[1] Justus-Liebig Universität, Department of Microbiology and Molecular Biology, 35392 Giessen, Germany
[2] Max-Planck-Institut für terrestrische Mikrobiologie, Department of Ecophysiology, 35043 Marburg, Germany
[3] LOEWE Center for Synthetic Microbiology (Synmikro) & Department of Chemistry, Philipps University Marburg, 35043 Marburg, Germany
[4]current address: Institute for Medical Microbiology and Hospital Epidemiology, Hannover Medical School, 30625 Hannover, Germany

[#] equal contribution

[*] corresponding author

- supplemental material -

Supplemental Tables

Table S1: Bacterial strains used in this study
Table S2: Plasmids used in this study
Table S3: Oligonucleotides used in this study

Supplemental Figures

Figure S1: Protein stability assays for fluorescence tagging
Figure S2: Complementation and motility assays for mutants and fluorescence tagging
Figure S3: FlhG phenotype of a FlhG variant lacking the N-terminal domain (FlhG ΔN20)
Figure S4: Effect of *flhF* deletion or overexpression on the flagellation of CN-32
Figure S5: Effect of flhF deletion on the positioning of chemotaxis components
Figure S6: Amino acid sequence alignment of HubP of *Vibrio cholerae* and *S. putrefaciens* CN-32
Figure S7: HubP/FimV domain organization
Figure S8: *Sp*HubP is required for proper localization of the chemotaxis components
Figure S9: Localization and phenotypic analysis of *Sp*HubP-sfGFP and LysM-sfGFP production
Figure S10: Localization of *oriC* in dependence of *Sp*HubP and FlhF
Figure S11 (graphical abstract): A model summarizing observed and potential functions of HubP/FimV-like proteins

Table S1: Bacterial strains that were used in this study

Strain	Genotype	Reference
Escherichia coli		
DH5α λpir	φ80d*lacZ* ΔM15 Δ*(lacZYA-argF)*U169 *recA1 hsdR17 deoR thi-l supE44 gyrA96 relA1*/λpir	Miller VL, Mekalanos JJ (1988)
WM3064	*thrB1004 pro thi rpsL hsdS lacZ* ΔM15 RP4-1360 Δ(*araBAD*) 567Δ*dapA* 1341::[*erm pir*(wt)]	W. Metcalf, University of IIlinois, Urbana-Champaign
BL21(DE3)	*fhuA2 [lon] ompT gal (λ DE3) [dcm] ΔhsdS λ DE3 = λ sBamHIo ΔEcoRI-B int::(lacI::PlacUV5::T7 gene1) i21 Δnin5*	
E3743	DH5α λpir pBTOK *hubP-sfgfp*, ΔSputcn32_2442 pBTOK- Sputcn32_2442-3xGly-Gly-Ser- sfGFP (N-terminal)	This study
E3744	DH5α λpir pBTOK *lysM-mcherry*, ΔSputcn32_2442 pBTOK-mCherry-2xPro- Sputcn32_2442-AA1-134 tagged with mCherry (N-terminal)	This study
Shewanella putrefaciens		
S271	CN-32, wild type	Fredrickson JK, et al. (1998)
S1995	*Δ$fliF_1$ Δ$fliF_2$*, ΔSputcn32_2576 ΔSputcn32_3476, markerless deletion of *Δ$fliF_1$* and *Δ$fliF_2$*	Bubendorfer et al., (2012)
S2025	*Δcluster I*, ΔSputcn32_2549–ΔSputcn32_2605, markerless deletion of polar flagellar gene cluster	Bubendorfer et al., (2012)
S2240	*$fliM_1$-sfgfp*, Sputcn32_2569-6xGly-sfGFP-His6; markerless chromosomal fusion of *$fliM_1$* to *sfgfp* (C-terminal)	Bubendorfer et al., (2012)
S2241	*$fliM_1$*-mcherry, Sputcn32_2569-6xGly-mcherry-His6; markerless chromosomal fusion of *$fliM_1$* to *mcherry* (C-terminal)	Bubendorfer et al., (2012)
S2866	*sfgfp-cheY*, sfGFP-His6-3xGly-Gly-Ser-Sputcn32_2558; markerless chromosomal fusion of *sfgfp* to *cheY* (N-terminal)	This study
S2875	*sfgfp-cheY $fliM_1$-mcherry*, *sfGFP*-His6-3xGly-Gly-Ser-Sputcn32_2558 Sputcn32_2569-6xGly-mcherry-His6; markerless chromosomal fusion of *sfgfp* to *cheY* (N-terminal) and *$fliM_1$* to *mcherry* (C-terminal)	This study
S3132	*ΔflhF,* ΔSputcn32_2561, markerless deletion of *flhF*	This study
S3133	*ΔflhG*, ΔSputcn32_2560; markerless deletion of *flhG*	Schuhmacher et al., (2015)
S3145	*ΔhubP*, ΔSputcn32_2442, markerless deletion of *hubP*	This study
S3163	*$fliM_1$-mcherry mcp0796-sfgfp*, Sputcn32_2569-6xGly-mCherry Sputcn32_0794-3xGly-Gly-Ser-sfGFP, markerless chromosomal fusion of *mcherry* to *$fliM_1$* (N-terminal) and insertion of pJP5603_Sputcn32_0796-sfGFP chromosomal locus of Sputcn32_0796	This study

S3165	*fliM$_1$-mcherry ΔhubP*, Sputcn32_2569-6xGly-mCherry ΔSputcn32_2442; markerless chromosomal fusion of *mcherry* to *fliM$_1$* (N-terminal) and markerless deletion of *hubP*	This study
S3213	*Δflhf fliM$_1$-sfgfp*, ΔSputcn32_2561 Sputcn32_2569-6xGly-sfGFP-His6, markerless deletion of *flhF* and chromosomal fusion of *fliM$_1$* to *sfgfp* (C-terminal)	This study
S3299	*flaA2-Cys*, Sputcn32_3455_T156CT169C Sputcn32_3456_T159CT160C; markerless exchange of Thr156Cys and Thr159Cys in Sputcn32_3455 and Thr159Cys and Thr160Cys in Sputcn32_3456	This study
S3300	*flaAB1 Cys*, Sputcn32_2585-T159C Sputcn32_2586-T159C, markerless substitution of Threonine 159 with Cysteine in *flaA$_1$* and Threonine 159 with Cysteine in *flaB$_1$*	This study
S3344	*Δflhf fliM2-sfgfps*, ΔSputcn32_2561 Sputcn32_3479-6xGly-sfGFP-His6, markerless deletion of *flhF* and chromosomal fusion of fliM2 to sfgfp (C-terminal)	This study
S3419	*FlgE$_2$-T242C*, Sputcn32_3465_T242C; markerless exchange of Thr242Cys in Sputcn32_3465	Schuhmacher et al., (2015)
S3469	*ΔflhF FlgE$_2$-T242C*, ΔSputcn32_2560 Sputcn32_3465_T242C; markerless deletion of *flhF* and exchange of Thr242Cys in Sputcn32_3465	This study
S3475	*flhF KI*; markerless insertion of *flhF* into *ΔflhF*; complements mutation	This study
S3481	*flhG KI*; markerless insertion of *flhG* into *ΔflhG*; complements mutation	Schuhmacher et al., (2015)
S3555	*mcherry-parB flaAB1 Cys*, mCherry-2xGly-Gly-Ser-Sputcn32_3964 Sputcn32_2586_T159C Sputcn32_2585_S159C, markerless chromosomal fusion of *mcherry* to *parB* (N-terminal) and substitution of Threonine 159 with Cysteine in *flaA$_1$* and Threonine 159 with Cysteine in *flaB$_1$*	This study
S3568	*ΔhubP mcherry-parB flaAB$_1$ Cys*, ΔSputcn32_2442 mCherry-2xGly-Gly-Ser-Sputcn32_3964 Sputcn32_2586_T159C Sputcn32_2585_T159C, markerless deletion of Sputcn32_2442 and chromosomal fusion of mcherry to *parB* (N-terminal) combined with the exchange of Thr159Cys in Sputcn32_2586 and Sputcn32_2585	This study
S3636	*hubP-sfgfp*, Sputcn32_2442-3xGly-Gly-Ser-sfGFP; markerless chromosomal fusion of *hubP* to *sfgfp* (C-terminal)	This study
S3637	*fliM$_1$-mcherry hubP-sfgfp*, Sputcn32_2569-6xGly-mCherry Sputcn32_2442-3xGly-Gly-Ser-sfGFP; markerless chromosomal fusion of *fliM$_1$* to *mcherry* and *hubP* to *sfgfp* (C-terminal)	This study
S3685	*hubP-sfgfp mcherry-parB*, Sputcn32_2442-3xGly-Gly-Ser-sfGFP mCherry-2xGly-Gly-Ser-Sputcn32_3964, markerless chromosomal fusion of *mcherry* to *parB* (N-terminal) and of *hubP* to *sfgfp* (C-terminal)	This study
S3710	*mcherry-parB*, mCherry-2xGly-Gly-Ser-Sputcn32_3964, markerless chromosomal fusion of *mcherry* to *parB* (N-terminal)	This study
S3715	*ΔflhF mcp0796-sfgfp*, ΔSputcn32_2561 Sputcn32 _0794-3xGly-Gly-Ser-sfGFP, markerless deletion of *flhF* and insertion of pJP5603_Sputcn32_0796-sfGFP chromosomal locus of Sputcn32_0796	This study
S3716	*ΔhubP mcp0796-sfgfp*, ΔSputcn32_2442 Sputcn32_0794-3xGly-Gly-Ser-sfGFP, markerless deletion of *hubP* and insertion of pJP5603_Sputcn32_0796-sfGFP chromosomal locus of Sputcn32_0796	This study
S3721	*ΔflhF mcherry-parB*, ΔSputcn32_2561 mCherry-2xGly-Gly-Ser-Sputcn32_3964, markerless deletion of *flhF* and chromosomal fusion of *mcherry* to *parB* (N-terminal)	This study

S3722	*Δcluster I hubP-sfgfp*, ΔSputcn32_2549–ΔSputcn32_2605 Sputcn32_2442-3xGly-Gly-Ser-sfGFP, markerless deletion of polar flagellar cluster and chromosomal fusion of *hubP* to *sfgfp*	This study
S3724	*ΔhubP sfgfp-cheY*, ΔSputcn32_2442 sfGFP-His6-3xGly-Gly-Ser-Sputcn32_2558; markerless deletion of *hubP* and chromosomal fusion of *sfgfp* to *cheY* (N-terminal)	This study
S3725	*ΔflhF sfgfp-cheY*, ΔSputcn32_2561 sfGFP-His6-3xGly-Gly-Ser-Sputcn32_2558; markerless deletion of *flhF* and chromosomal fusion of *sfgfp* to *cheY* (N-terminal)	This study
S3733	*ΔflhG mcp0796-sfgfp*, ΔSputcn32_2560 Sputcn32_0794-3xGly-Gly-Ser-sfGFP, markerless deletion of *flhG* and insertion of pJP5603_Sputcn32_0796-sfGFP chromosomal locus of Sputcn32_0796	This study
S3747	*ΔflhF venus-cheZ*, ΔSputcn32_2561 VENUS-6xGly-Sputcn32_2557, markerless deletion of *flhF* and chromosomal fusion of *venus* to *cheZ* (C-terminal)	This study
S3748	*ΔhubP venus-cheZ*, ΔSputcn32_2442 VENUS-6xGly-Sputcn32_2557, markerless deletion of *hubP* and chromosomal fusion of *venus* to *cheZ* (C-terminal)	This study
S3749	*ΔflhF cheA-mcherry*, ΔSputcn32_2561 Sputcn32_2556-2xGly-Gly-Ser-mCherry, markerless deletion of *flhF* and chromosomal fusion of *mcherry* to *cheA* (C-terminal)	This study
S3750	*cheA-mcherry fliM$_1$-sfgfp*, Sputcn32_2556-2xGly-Gly-Ser-mCherry Sputcn32_2569-6xGly-sfGFP, markerless chromosomal fusion of *mcherry* to *cheA* and *sfgfp* to *fliM$_1$* (N-terminal)	This study
S3751	*ΔhubP cheA-mcherry*, ΔSputcn32_2442 Sputcn32_2556-2xGly-Gly-Ser-mCherry, markerless deletion of *hubP* and chromosomal fusion of *mcherry* to *cheA* (C-terminal)	This study
S3752	*venus-cheZ fliM$_1$-mcherry*, VENUS-6xGly-Sputcn32_2557 Sputcn32_2569-6xGly-mCherry, markerless chromosomal fusion of *venus* to *cheZ* (C-terminal) and *mcherry* to *fliM$_1$* (N-terminal)	This study
S3753	*hubP KI*; markerless insertion of *hubP* into *ΔhubP*; complements mutation	This study
S3754	*ΔflhF flaAB$_1$ Cys*, ΔSputcn32_2561 Sputcn32_2585-T159C Sputcn32_2586-S159C, markerless deletion of *flhF* and substitution of Threonine 159 with Cysteine in *flaA$_1$* and Threonine 159 with Cysteine in *flaB$_1$*	This study
S3755	*ΔhubP flaAB$_1$ Cys*, ΔSputcn32_2442 Sputcn32_2585-T159C Sputcn32_2586-S159C, markerless deletion of *hubP* and substitution of Threonine 159 with Cysteine in *flaA$_1$* and Threonine 159 with Cysteine in *flaB$_1$*	This study
S3761	*ΔhubP* pBTOK hubP-sfgfp, ΔSputcn32_2442 pBTOK- Sputcn32_2442-3xGly-Gly-Ser-sfGFP; markerless deletion of *hubP* and stable integration of overproduction vector pBTOK producing SpHubP tagged with sfGFP (N-terminal)	This study
S3762	Δ*hubP* pBTOK *lysM-mcherry*, ΔSputcn32_2442 pBTOK-mCherry-2xPro- Sputcn32_2442-AA1-134; markerless deletion of *hubP* and stable integration of overproduction vector pBTOK producing the first 134 amino acids of SpHubP tagged with mCherry (N-terminal)	This study
S3771	*flhF-mcherry*, Sputcn32_2561-3xGly-Gly-Ser-mCherry, markerless chromosomal fusion of *mcherry* to *flhF* (C-terminal)	This study
S3772	Δ*hubP flhF-mcherry*, ΔSputcn32_2442 Sputcn32_2561-3xGly-Gly-Ser-mCherry, markerless deletion of *hubP* and chromosomal fusion of *mcherry* to *flhF* (C-terminal)	This study
S3778	*hubP-mcherry*, Sputcn32_2442-3xGly-Gly-Ser-mCherry; markerless chromosomal fusion of *hubP* to *mcherry* (C-terminal)	This study

S3779	*hubP-mcherry zapA-sfgfp*, Sputcn32_2442-3xGly-Gly-Ser-mCherry Sputcn32_3215-2xGly-Gly-Ser-sfGFP; markerless chromosomal fusion of *hubP* to *mcherry* (C-terminal) and of *zapA* to *sfgfp* (C-terminal)	This study
S3783	pBTOK, stable integration of overproduction vector pBTOK as empty vector control	This study
S3859	pBTOK *flhF*, pBTOK-Sputcn32_2561; stable integration of overproduction vector pBTOK producing the full length protein SpFlhF	This study
S4028	*flhG-sfgfp*, Sputcn32_2560-1xGly-Ser-sfGFP, markerless chromosomal fusion of sfgfp to *flhG* (C-terminal)	This study
S4029	Δ*hubP flhG-sfgfp*, ΔSputcn32_2442 Sputcn32_2560-1xGly-Ser-sfGFP, markerless chromosomal fusion of sfgfp to *flhG* (C-terminal)	This study
S4033	*flaAB$_1$ Cys* pBTOK *flhF-mcherry*, Sputcn32_2586_T159C Sputcn32_2585_T159C pBTOK-Sputcn32_2561-1xGly-Ser-mCherry; markerless exchange of Thr159Cys in Sputcn32_2586 and Sputcn32_2585 and stable integration of overproduction vector pBTOK producing SpFlhF tagged with mCherry (C-terminal)	This study
S4034	*fliM$_1$ -sfgfp* pBTOK *flhF*, Sputcn32_2569-6xGly-sfGFP-His6 pBTOK-Sputcn32_2561; markerless chromosomal fusion of *fliM$_1$* to *sfgfp* (C-terminal) combined with stable integration of overproduction vector pBTOK producing the full length protein SpFlhF	This study
S4035	*flaAB$_1$ Cys* pBTOK, Sputcn32_2586_T159C Sputcn32_2585_T159C pBTOK; markerless exchange of Thr159Cys in Sputcn32_2586 and Sputcn32_2585 and stable integration of overproduction vector pBTOK as empty vector control	This study
S4036	*ΔflhF flaA$_2$-Cys flaB$_2$-Cys*, ΔSputcn32_2560 Sputcn32_3455_T156CT159C Sputcn32_3456_T159CT160C; markerless deletion of *flhF* and exchange of Thr156Cys and Thr159Cys in Sputcn32_3455 and Thr159Cys and Thr160Cys in Sputcn32_3456	This study
S4037	*fliM$_1$* -sfgfp pBTOK, Sputcn32_2569-6xGly-sfGFP-His6 pBTOK; markerless chromosomal fusion of *fliM$_1$* to sfgfp (C-terminal) combined with stable integration of overproduction vector pBTOK as empty vector control	This study
S4040	*flhG* ΔN20, Sputcn32_2560 ΔN20; markerless deletion of the first 20 amino acid residues (1-20) in *flhG*	This study
S4041	*flhG* ΔN20 *flaAB$_1$ Cys*, Sputcn32_2560 ΔN20 Sputcn32_2586_T159C Sputcn32_2585_T159C, markerless deletion of the first 20 amino acid residues (1-20) in *flhG* combined with the exchange of Thr159Cys in Sputcn32_2586 and Sputcn32_2585	This study

Table S2: Plasmids that were used in this study

Plasmid	Relevant genotype or phenotype	Source or reference
pNPTS138-R6KT	*mob*RP4$^+$ *ori*-R6K *sacB*, suicide plasmid for in frame deletions, Km^r	Lassak *et al*., 2010
pBTOK	pBBR1-MCS2 backbone (pBBR origin, Km^r); TetR, Promoter and multiple cloning site of pASK-IBA3plus and *E.coli* rrnB1 T1 and lambda phage T0 terminator	this study
pET24d(+)	T7 promoter, his-tag fusion site, T7 terminator, *lacI*, pBR322 ori, f1 ori, Km^r	Novagen
pGAT3	Bla, lacI, T7-lacO promoter, SP6 promoter, T7 terminator, Ap^r	Peränen et al., 1996
In-frame deletion vectors (in pNPTS138-R6KT)		
pNPTS138-R6KT-HubP-KO	*hubP* (Sputcn32_2442), in-frame deletion fragment	this study
pNPTS138-R6KT-FlhF-KO	*flhF* (Sputcn32_2561), in-frame deletion fragment	this study
pNPTS138-R6KT-FlhG ΔN20	*flhG* ΔN20 (deletion of first 20 amino acids in Sputcn32_2560), in-frame deletion fragment	this study
In-frame complementation vectors (in pNPTS138-R6KT)		
pNPTS138-R6KT-HubP-KI	*hubP* (Sputcn32_2442), in-frame insertion fragment for complementation of Δ*hubP*	this study
pNPTS138-R6KT-FlhF-KI	*flhF* (Sputcn32_2561), in-frame insertion fragment for complementation of Δ*flhF*	this study
Fluorescent fusion vectors (in pNPTS138-R6KT)		
pNPTS138-R6KT-FlaAB$_2$-Cys	*flaAB$_2$*-Cys (Sputcn32_3455_T156CT159C, Sputcn32_3456_T159CT160C), in-frame substitution fragment	
pNPTS138-R6KT-FliM$_1$-GL-sfGFP-His6	*fliM$_1$*-6xGly-sfGFP-His6 in pNPTS138-R6KT in-frame insertion fragment	Bubendorfer *et al*., 2012
pNPTS138-R6KT-FliM$_1$-GL-mCherrySO-His6	*fliM$_1$*-6xGly-mCherrySO-His6 in pNPTS138-R6KT in-frame insertion fragment	Bubendorfer *et al*., 2012
pNPTS138-R6KT-mCherry-ParB	mCherry-2xGly-Gly-Ser-*parB* (Sputcn32_3964), in-frame insertion fragment	this study
pNPTS138-R6KT-FlaAB$_1$-Cys	*flaAB$_1$*-Cys (Sputcn32_2586_T159C, Sputcn32_2585_T159C), in-frame substitution fragment	this study
pNPTS138-R6KT-sfGfp-3GGS-CheY	sfGFP-His6-3xGly-Gly-Ser-*cheY* (Sputcn32_2558), in-frame insertion fragment	this study
pNPTS138-R6KT-VENUS-GL-CheZ	VENUS-6xGly-*cheZ* (Sputcn32_2557), in-frame insertion fragment	this study
pNPTS138-R6KT-CheA-mCherry	*cheA*-2xGly-Gly-Ser-mCherry (Sputcn32_2556), in-frame deletion fragment	this study
pNPTS138-R6KT-HubP-sfGFP	*hubP*-3xGly-Gly-Ser-sfGFP (Sputcn32_2442), in-frame insertion fragment	this study
pNPTS138-R6KT-HubP-mCherry	*hubP*-3xGly-Gly-Ser-mCherry (Sputcn32_2442), in-frame insertion fragment	this study
pNPTS138-R6KT-FlhF-mCherry	*flhF*-3xGly-Gly-Ser-mCherry (Sputcn32_2561), in-frame insertion fragment	this study
pNPTS138-R6KT-ZapA-sfGFP	*zapA*-2xGly-Gly-Ser-sfGFP (Sputcn32_3215), in-frame insertion fragment	this study
pJP5603_Sputcn32_0796-sfGFP	*MCP_0796*-sfGFP (Sputcn32_0796), for single homologous insertion	this study
pNPTS138-R6KT-FlhG-sfGFP	*flhG*-1xGly-Ser-sfGFP (Sputcn32_2560), in-frame insertion fragment	This study

Overproduction vectors

pBTOK-HubP-sfGFP	*hubP*-3xGly-Gly-Ser-*sfGFP* (Sputcn32_2442) in pBTOK	this study
pBTOK-LysM-mCherry	*hubP*_AA1-134-2xPro-*mCherry* (Sputcn32_2442_nt1-402) in pBTOK	this study
pBTOK-FlhF-mCherry	*flhF*-1xGly-Ser-*mCherry* (Sputcn32_2561) in pBTOK	This study
pFlhF	*flhF* (Δ-10) in pET24d	this study
pFlhG	*flhG* in pET24d	this study
pN-FlhG	N-terminus of *flhG* (aa 1-20) in pGAT3	this study

References Table S1 and Table S2

Bubendorfer, S., Held, S., Windel, N., Paulick, A., Klingl, A., and Thormann, K.M. (2012) Specificity of motor components in the dual flagellar system of *Shewanella putrefaciens* CN-32. *Mol Microbiol* 83: 335-350.

Fredrickson, J.K., Zachara, J.M., Kennedy, D.V., Dong, H., Onstott, T.C., Hinman, N.W., and Li, S. (1998) Biogenic iron mineralization accompanying the dissimilatory reduction of hydrous ferric oxide by a groundwater bacterium. *Geochim Cosmochim Acta* **62**: 3239-3257.

Lassak, J., Henche, A.L., Binnenkade, L., and Thormann, K.M. (2010) ArcS, the cognate sensor kinase in an atypical Arc system of *Shewanella oneidensis* MR-1. *Appl Environ Microbiol* **76**: 3263-3274.

Miller, V.L., and Mekalanos, J.J. (1988) A novel suicide vector and its use in construction of insertion mutations: osmoregulation of outer membrane proteins and virulence determinants in *Vibrio cholerae* requires *toxR*. *J Bacteriol* **170**: 2575-2583.

Peränen, J., Rikkonen, M., Hyvonen, M., and Kaariainen, L. (1996) T7 vectors with modified T7*lac* promoter for expression of proteins in *Escherichia coli*. *Anal Biochem* **236**: 371-373.

Schuhmacher, J.S., Rossmann, F., Dempwolff, F., Knauer, C., Altegoer, F., Steinchen, W.*, et al.* (2015) MinD-like ATPase FlhG effects location and number of bacterial flagella during C-ring assembly. *Proc Natl Acad Sci U S A* **112**: 3092-3097.

Table S3: Oligonucleotides that were used in this study

Identifier of oligonucleotides	Sequence 5'-3'	Purpose
AD39 ZapA-Cterm-fw	GCGAATTCGTGGATCCAGATGTAACGAAGGAGGGGTAGC	fusion of sfGFP to ZapA
AD40 ZapA-Cterm-3xGGS-OL-RV	GCTGCCGCCGCTGCCGCCGCTGCCGCCTTTAGTTGAACGCTCAACT AAG	
AD41 3xGGS-sfGFP-OL-FW	GGCGGCAGCGGCGGCAGCGGCGGCAGCATGAGCAAAGGAGAAG AACTTTTCAC	
AD42 sfGFP-Strep-OL-RV	TTATTTTTCGAACTGCGGGTGGCTCCAGGATCCTTTGTAGAGCTCA TCC	
AD43 ZapA-DS-Strep-OL-FW	TGGAGCCACCCGCAGTTCGAAAAATAAATTTAAACTGTGCAACTT GGTTATTTAG	
AD44 ZapA-DS-RV	CCAAGCTTCTCTGCAGGATTTCGCCATCGTGAGTTAAATAC	
B232 EcoRI-pJP-cn32_0796-gfp-fwd	A GAA TTC ACG ATA ATG CGC AGA GTG GTC	fusion of MCP_0796 to sfGFP
B233 BamHI-pJP-cn32_0796-gfp-rev	C GGA TCC GAT TTT AAA ATT GCT TAC TGC GCG	
B286 EcoRI-up-cheY1-fwd	A GAA TTC CGA GGT GAT TGG GTT CCA CG	fusion of sfGFP to CheY
B289 OL-GL-VENUS-rev	GCC GCC GCC GCC GCC CTT GTA CAG CTC GTC CAT GC	fusion of VENUS to CheZ
B300 EcoRI-up-cheZ1-fwd	A GAA TTC CGA ATC GCG AGT TAG CCA GAT	
B301 OL-up-cheZ1-rev	CTT GCT CAC CAT AGC TCA TCC CTG CCT AAG CG	
B302 OL-CheZ1-up-VENUS-fwd	CAG GGA TGA GCT ATG GTG AGC AAG GGC GAG G	
B303 OL-GL-cheZ1-Nterm-fwd	GGC GGC GGC GGC GGC ATG AAG TCA CAT ACA TCA GGG CT	
B304 PspOMI-cheZ1-Nterm-rev	CTC GGG CCC TGA GAT CTT GAA AAT CCT GCG C	
B361 3x-GGS-OL-CheY-fwd	GGC GGC AGC GGC GGC AGC GGC GGC AGC TTG GAC AAG AAT ATG AAG ATT CTC ATT	fusion of sfGFP to CheY
B413 OL-up-cheY1-sfGfp-rev	TCC TTT GCT CAT GGT TTC CTC CGG TGA GCT GA	
B415 OL-CheY1-up-sfGfp-fwd	CCG GAG GAA ACC ATG AGC AAA GGA GAA GAA CTT TTC AC	
B417 3x-GGS-OL-sfGFP-rev	GCT GCC GCC GCT GCC GCC GCT GCC GCC GTG GTG GTG GTG GTG GTG	
B31 BamHI-flagL-fwd	A GGA TCC TGA CAC TGT ATT TAT GGC GCA GG	substitution of T156C and T159C in $FlaA_2$ and T159C T160C in $FlaB_2$
B34 PspOMI-flagL-rev	T GTC GGG CCC GTC GCC GTC GCA TTT TCG C	
B480 flaA2-Cys-rev	TCA TCG ATA GCT GTA CAG CAA ACG GCC AAT G	
B481 flaA2-Cys-fwd	ATT GGC CGT TTG CTG TAC AGC TAT CGA TGA CG	
B482 flaB2-Cys-rev	TCA CAT CCA GAC ATT CTG CGC ATC CAG CTC CA	
B483 flaB2-Cys-fwd	GAG CTG GAT GCG CAG AAT GTC TGG ATG TGA AG	
B45 EcoRI-flagP-fwd	A GAA TTC GAA GTT AAA GTG TCT GGG AAA CCC	substitution of T159C in $FlaA_1$ and T159C in $FlaB_1$
B48 PspOMI-flagP-rev	T CTA GGG CCC TAA GCC TCT GTT TTC ATC AAA AGC C	
B476 flaA1-T159CS161C-rev	TAC CAA CGC AAA TAC AGA TAT CTT CAC C	
B477 flaA1-T159CS161C-fwd	TGA AGA TAT CTG TAT TTG CGT TGG TAC C	
B478 flaB1-T159CS161C-rev	TTT TTG ACA CAC AAA TGC AAA TAT CTT CAC C	
B479 flaB1-T159CS161C-fwd	TGA AGA TAT TTG CAT TTG TGT GTC AAA AAC C	
FR48 NheI_Sputcn32_2442_KO_fw	GTA GCT AGC AGT GAA TGC GAC AGC TGT ACG	in-frame deletion of HubP
FR49 OL_Sputcn32_2442_rv	A ACT AAT CTC CAT CAA TCC TTC CCT TTG AAG C	
FR50 OL_Sputcn32_2442_fw	A GGA TTG ATG GAG ATT AGT TAA TCT CGA TTA ACC GA	
FR51 PspOMI_Sputcn32_2442_KO_rv	TCC GGG CCC ATT ACC GTG ATA ATG GCT TAC ACC	
FR99 PspOMI_flhG_rv	TCC GGG CCC GAG CAA TTA GCG ACC TAT GGC	fusion of sfGFP to HubP
FR158 OL_3xGGS_sfGFP_rv	GGC GGC AGC GGC GGC AGC GGC GGC AGC ATG AGC AAA GGA GAA GAA CTT TTC AC	
FR100 NheI_flhF_fw	GTA GCT AGC GTA GGC TCG TCA CAT ACA ACG	
FR101 OL_flhF_KO_rv	GAT TAA ACG ATG TGC ATT TGA GTA GAG TTA TGA CC	in-frame deletion of FlhF
FR102 OL_flhF_KO_fw	CAA ATG CAC ATC GTT TAA TCT TCA CTT ATG CGT CC	

FR103 PspOMI_flhF_rv	TCC GGG CCC TTC CTG ATG TGA TGC CAC TGG	
FR156 OL_strep_flhF_rv	TGG AGC CAC CCG CAG TTC GAA AAA TAG AGT TAT GAC CCT GGA TCA AG	fusion of FlhF to mCherry
FR159 OL_flhF_3xGGS_fw	GCT GCC GCC GCT GCC GCC GCT GCC GCC CTC AAA TGC ACA GGC CAT ATT ATC	
FR262 EcoRI_HubP-Cterm_fw	GTA GAA TTC GAT GAT GAT CTC GAT TTA AGC ACA G	fusion of sfGFP to HubP
FR263 OL_hubP_3xGGS_rv	GCT GCC GCC GCT GCC GCC GCT GCC GCC ACT AAT CTC TTT TAG TAA ACG TCC GG	
FR264 OL_sfGFP_HubP-down_rv	TAG ATT GAA ACT CGG TTA ATC GAG ATT AGG ATC CTT TGT AGA GCT CAT CCA T	fusion of sfGFP to HubP
FR265 OL_HubP-down_fw	TAA TCT CGA TTA ACC GAG TTT CAA TCT A	
FR266 PstI_HubP-Cterm_rv	GTA CTG CAG GCC GCT TGG TGC ATT TTG TCG	
FR279 OL_mCherry_fw	ATG GTT TCC AAA GGG GAA GAG G	overexpression of FlhF-mCherry
FR330 XbaI_FlhF_OE_fw	CGC TCT AGA AGG AGG GCA AAT ATG AAG ATT AAA CGA TTT TTT GCC AAA GAC ATG	
FR332 EcoRV_HubP_komplement_fw	CAA GCT TCT CTG CAG GAT AGT GAA TGC GAC AGC TGT ACG	reconstitution of HubP
FR333 EcoRV_HubP_komplement_rv	GAA TTC GTG GAT CCA GAT ATT ACC GTG ATA ATG GCT TAC ACC	
FR385 OL_FlhF_GS_mCherry_rv	CCT CTT CCC CTT TGG AAA CCA TGC TGC CCT CAA ATG CAC AGG CCA TAT T	overexpression of FlhF-mCherry
FR386 PspOMI_mCherry_rv	TCC GGG CCC TTA TTT GTA TAA CTC ATC CAT ACC ACC A	
FR392 OL_FlhG_-m_gfp_rv	GAA AAG TTC TTC TCC TTT GCT GCT GCC TTC ACT CGT TTT TTC TTC TTG AAA ATC	fusion of FlhG to sfGFP
FR393 OL_-m_gfp_fw	AGC AAA GGA GAA GAA CTT TTC	
FR398 EcoRV_FlhG_fw	CAA GCT TCT CTG CAG GAT ATC CGT GCT TTC AGT GAG ATG C	
FR399 OL_gfp_RBS-fliA_rv	GCT TTA TTC ACT CGT TTT TTC CTC TTT TAG GAT CCT TTG TAG AGC TCA TCC	
FR400 OL_RBS-fliA_fw	AAG AGG AAA AAA CGA GTG AAT AAA GC	
FR401 EcoRV_FlhG_rv	GAA TTC GTG GAT CCA GAT TCT CAG CGA GAG CTT CAA ACG A	
FR402 EcoRV_FlhG_N20_fw	CAA GCT TCT CTG CAG GAT TGA GCA ATT AGC GAC CTA TGG C	deletion of the first 20 amino acids in FlhG
FR403 OL_FlhG_N20_rv	TTA CTT TCA CCA TAA CTC TAC TCA AAT GCA CAG G	
FR404 OL_FlhG_N20_fw	TAG AGT TAT GGT GAA AGT AAT CGC TGT CAC AGG	
FR405 EcoRV_FlhG_N20_rv	GAA TTC GTG GAT CCA GAT CGT AAA CTA CGC ACC ATA TTG GC	
SH501 pBTOK pBBR fw	TTG CGG TAC CAG CTC CAA TTC GCC CTA TAG TG	assembly of pBTOK
SH502 pBTOK pBBR rev	cATT AAT TCC TTC AGA AGA ACT CGT CAA GAA GGC G	
SH503 pBTOK pASK fw	GTT CTT CTG AAG GAA TTA ATG ATG TCT CGT TTA GAT A	
SH504 pBTOK pASK rev	TAA TGG GCC CAA GCT TAT TAT TTT TCG AAC TGC GG	
SH505 pBTOK pBBMt fw	TAA TAA GCT TGG GCC CAT TAG CTG AGC TTG	
SH506 pBTOK pBBMt rev	AAT TGG AGC TGG TAC CGC AAG CTC CTA GC	
SH534 CheA mC up fw	GCG AAT TCG TGG ATC CAG ATT GCC AGC CAA GAA GGT GAC C	fusion of CheA to mCherry
SH535 CheA mC up rev	CCA CCA GAG CCA CCA GTG CCA CTT TTA TTC TTT GCA TAA TGC TTT AAT AG	
SH536 CheA mC fw	AAG TGG CAC TGG TGG CTC TGG TGG CAG CAT GGT TTC CAA AGG GGA AGA GG	
SH537 CheA mC rev	CTT AGC TTG GAA ACT ATT TGT ATA ACT CAT CCA TAC CAC C	
SH538 CheA mC dwn fw	CAA ATA GTT TCC AAG CTA AGG AAT GGA ATG G	
SH539 CheA mC dwn rev	GCC AAG CTT CTC TGC AGG ATT ACA TAA CCC ATT TAG ACG ATT CGC	
SH558 HubP LysM OE fw	GGT CTA GAA GGA GGA CTG ACA TGA AAT TTC GCA CTT CGT ATC TTG	overproduction of LysM domain of HubP tagged with mCherry
SH559 HubP LysM OE OL rev	CCA TAG GAG GTA ACT TAT CAT CAC GTT CAG CAC G	
SH560 HubP LysM mC OE OL fw	GAT GAT AAG TTA CCT CCT ATG GTT TCC AAA GGG GAA GAG G	

SH561 HubP LysM mC OE rev	gcg GGG CCC TTA TTT GTA TAA CTC ATC CAT ACC ACC	
SH562 HubP sfGFP OE rev	gcg GGG CCC TTA GGA TCC TTT GTA GAG CTC ATC C	overproduction of HubP tagged with sfGFP
SH566 FlhF tag up fw	AAT ACG ACT CAC TAG TGG GGC CCG AGC AAT TAG CGA CCT ATG GC	fusion of FlhF to mCherry
SH572 FlhF tag GGS mC rev	CGA ACT GCG GGT GGC TCC ATT TGT ATA ACT CAT CCA TAC CAC CAG	
SH573 FlhF tag 3xGGS mC rev	GGC GGC AGC GGC GGC AGC GGC GGC AGC ATG GTT TCC AAA GGG GAA GAG G	
SpFlhF-BamHI-R	TTAAGGATCCTTACTCAAATGCACAG	overproduction FlhF
SpFlhFdN10-PciI-R	TTAAACATGTTGCACCATCACCATCACCATATGCGTGCCGCTCTGG CC	
SpFlhF-R285A-F	GATCATTATGCCATTGGCGCC	overproduction FlhF R285A
SpFlhF-R285A-R	GGCGCCAATGGCATAATGATC	
SpFlhG N20-XhoI-R	TTAACTCGAGTTACACTTTTTCGTTATA	overproduction FlhG N20
SpFlhG-NcoI-6H-F	TTAACCATGGGCCACCATCACCATCACCATACCCTGGATCAAGCAA G	overproduction FlhG
SpFlhG-XhoI-R	TTAACTCGAGTTATTCACTCGTTTTTTCCTCTT	

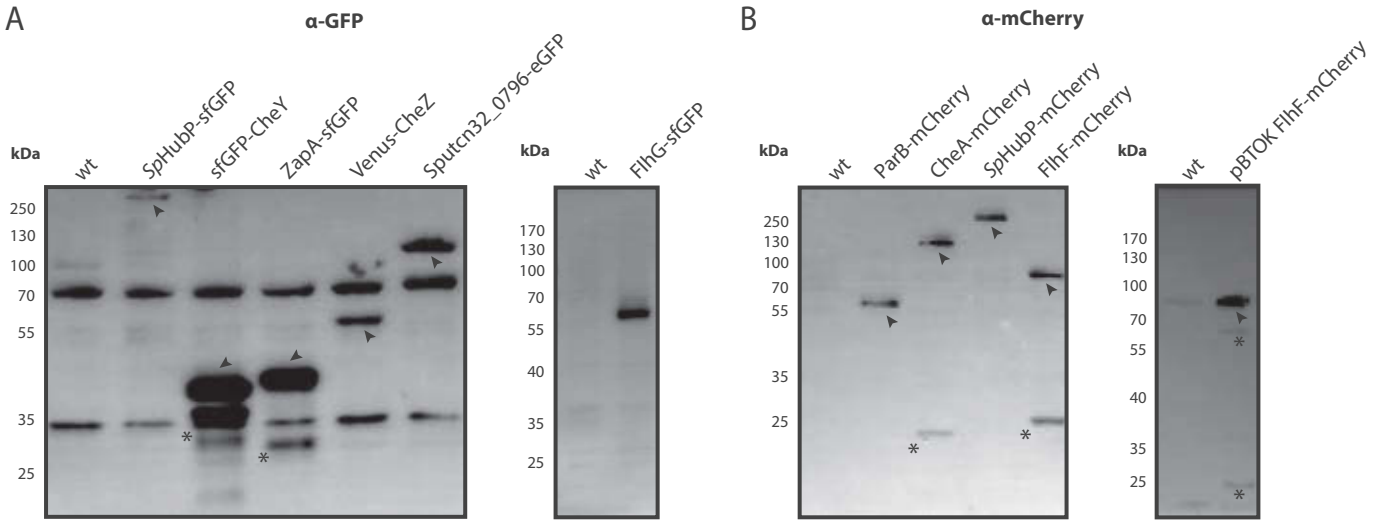

Figure S1: Protein stability assays for fluorescence tagging.
Depicted is the detection of proteins by immunoblotting using an antibody raised against GFP (A) or mCherry (B). The strains producing the corresponding proteins are indicated in each lane. Wild-type protein samples were used as negative control and revealed that the GFP antibody used leads to formation of two distinct signals due to unspecific binding, however, these were not interfering with the positions of the proteins to be detected. All proteins were produced yielding signals at position corresponding to the estimated molecular mass (sfGFP-CheY, 41.1 kDa; ZapA-sfGFP, 38.1 kDa; Venus-CheZ, 54.7 kDa; MCP0796-eGFP, 95.4 kDa; FlhG-sfGFP 59.6 kDa, ParB-mCherry, 59.3 kDa; CheA-mCherry, 105.9 kDa; FlhF-mCherry, 76.7 kDa). *Sp*HubP-sfGFP and –mCherry (145.4 kDa) exhibited mobility smaller than estimated, likely caused by its low overall pI. Arrows mark the positions of the fluorescently tagged proteins, asterisks mark signals likely caused by protein degradation.

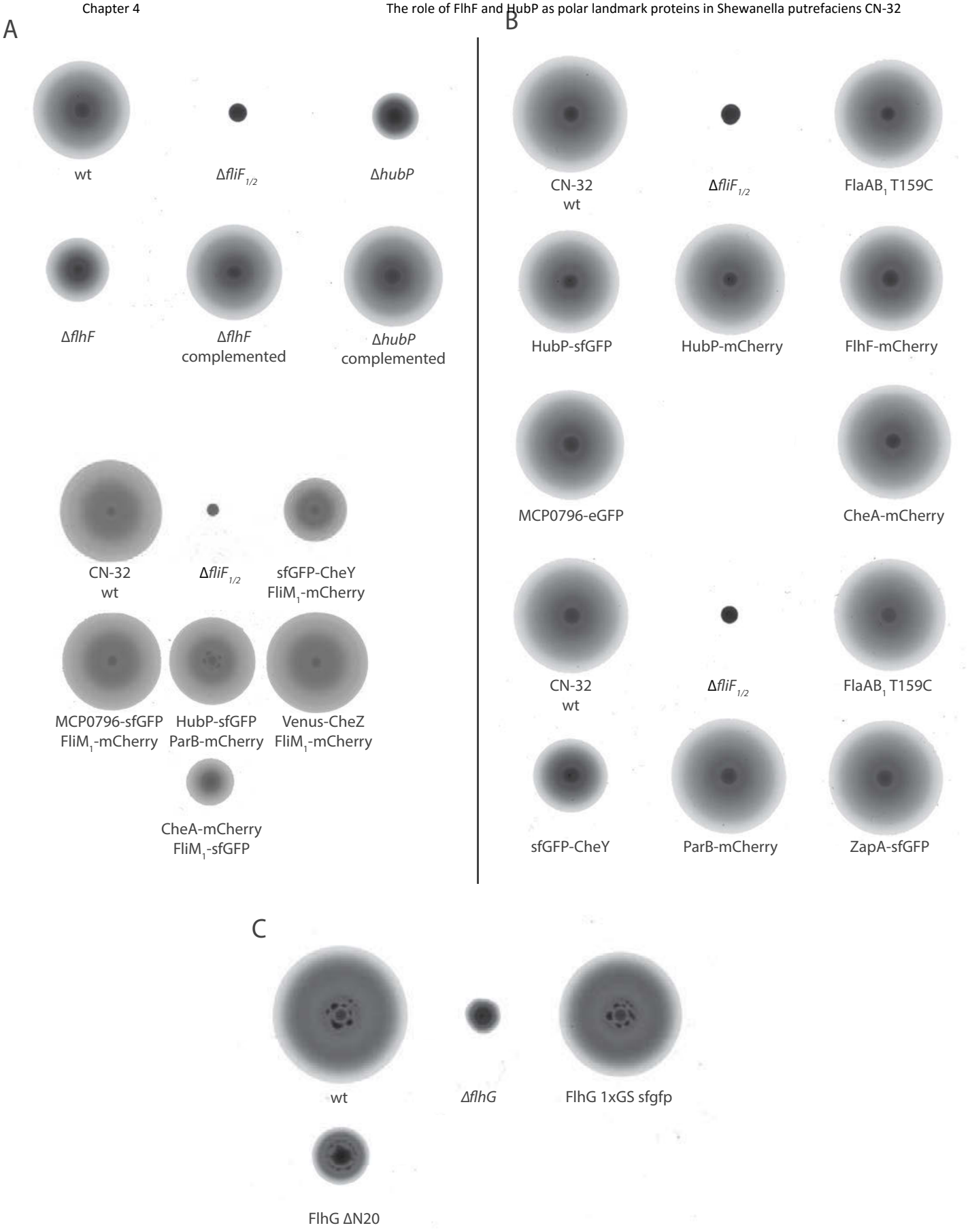

Figure S2: Complementation and motility assays for mutants and fluorescence tagging.
Soft agar assays of wild-type and mutant strains with the corresponding genotype as indicated below. 3 µl of exponentially growing cultures were spotted on 0.25% soft-agar plates and were incubated at 30 °C for 16 h prior documentation of the lateral extension zones. Please note that each experiment (**A**, **B**, **C**) is depicted at an individual scale. Therefore, every experiment has its own wild-type control.

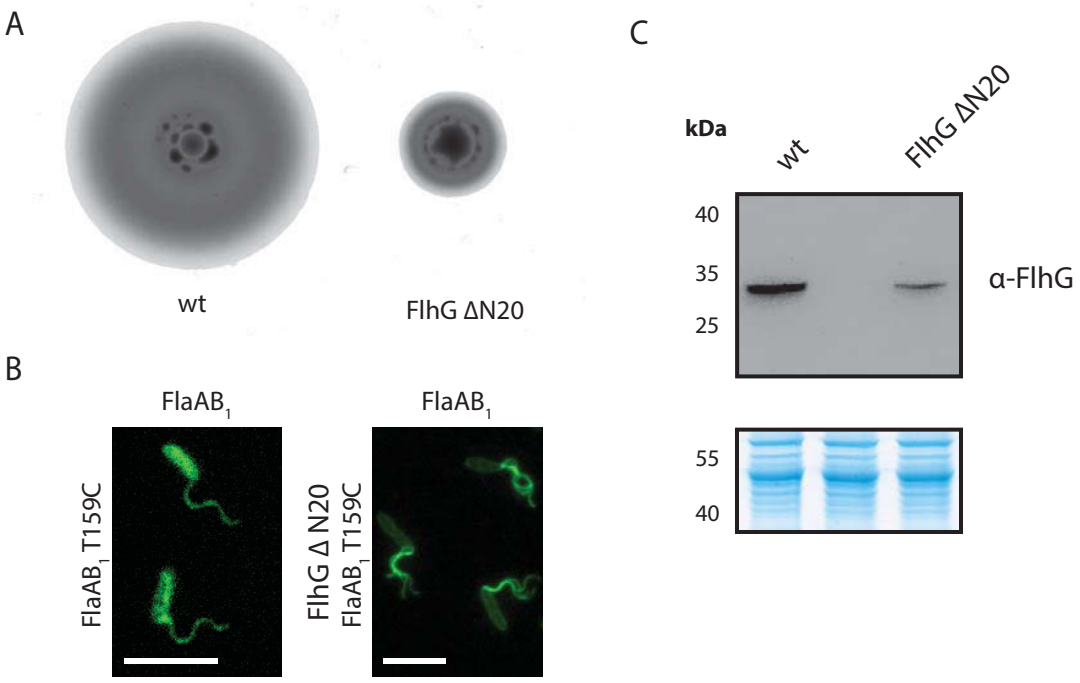

Figure S3: Phenotype of a FlhG variant lacking the N-terminal domain (FlhG ΔN20).
A) Soft-agar assays of wild-type and mutant strain with the corresponding genotype indicated below. 3 µl of exponentially growing cultures were spotted on 0.25% soft-agar plates and were incubated at 30 °C for 16 h prior documentation of the lateral extension zones. **B)** Flagellation phenotype of wild-type and FlhG ΔN20-mutant cells. Shown are micrographs of cells after flagellar staining using maleimide. The scale bar equals 5 µm. **C)** Immunoblot analysis of FlhG ΔN20 production. The corresponding Coomassie-stained gel is depicted below.

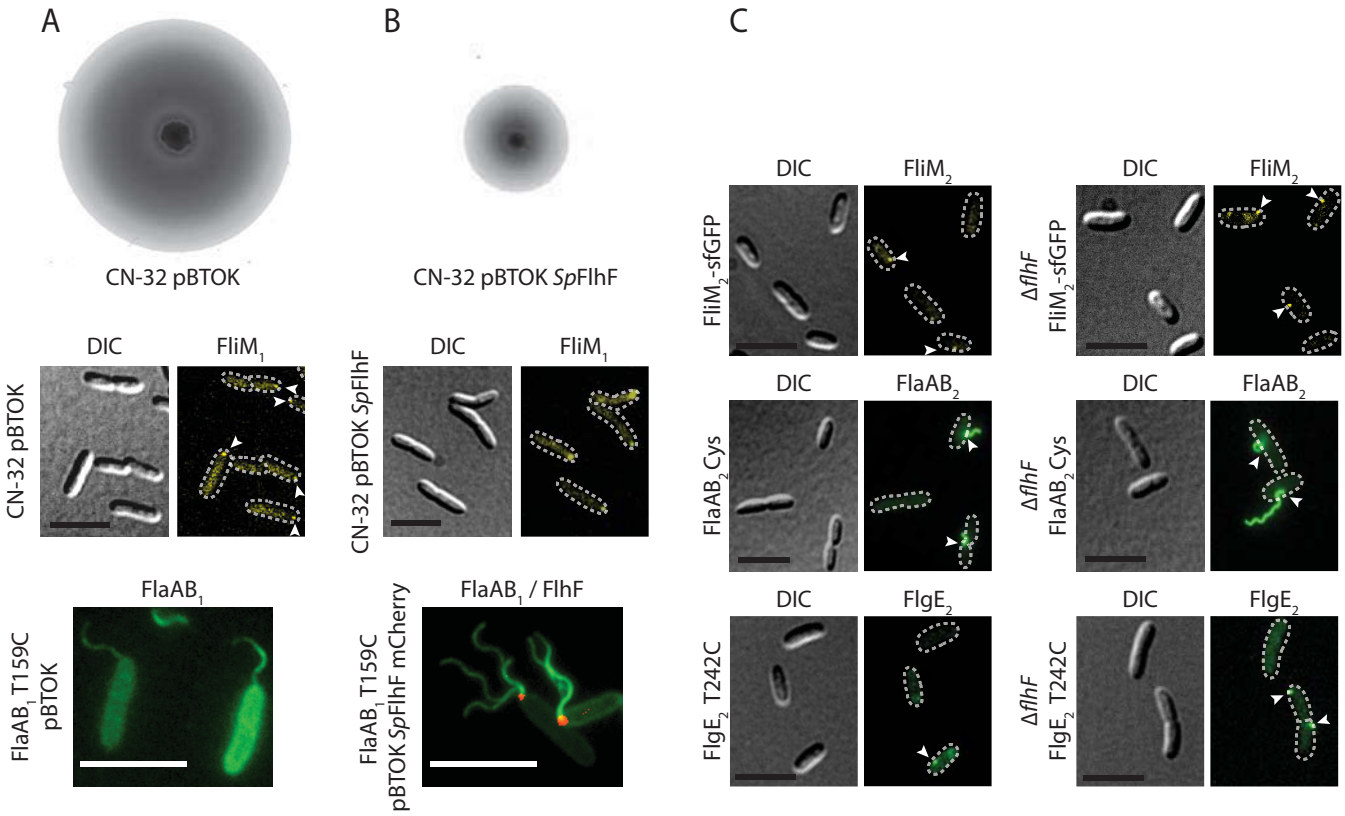

Figure S4: Effect of *flhF* deletion or overexpression on the flagellation of CN-32.
A/B) Effect of *flhF* overexpression on motility (upper panels), localization of $FliM_1$ ($FliM_1$-sfGFP; middle panels), and flagellation state (lower panels). The upper panels display soft-agar swimming assays of the empty-vector control **(A)** and overexpression strain **(B)** with the corresponding genotype indicated below. The middle panels show micrographs of $FliM_1$ localization (using $FliM_1$-sfGFP) in the wild-type control **(A)** and upon FlhF overproduction **(B)**. The lower panel shows the flagellation state in the empty-vector control **(A)** and upon FlhF-mCherry overproduction **(B)** along with localization of FlhF-mCherry. The flagellar filaments were fluorescently labeled by maleimide prior to imaging. **C)** Effect of *flhF* deletion on the production and position of the secondary flagellar system in CN32. Displayes are DIC and corresponding fluorescent micrographs of wild-type and *ΔflhF*-mutant cells bearing a *fliM*$_2$*-sfgfp* fusion (upper panel), or after maleimide labeling of the secondary flagellar filament (middle panels) or secondary hook structures (lower panels). No significant difference was noticed. In all micrographs, the scale bar equals 5 µm and the arrow mark fluorescent foci or flagellar filaments, respectively.

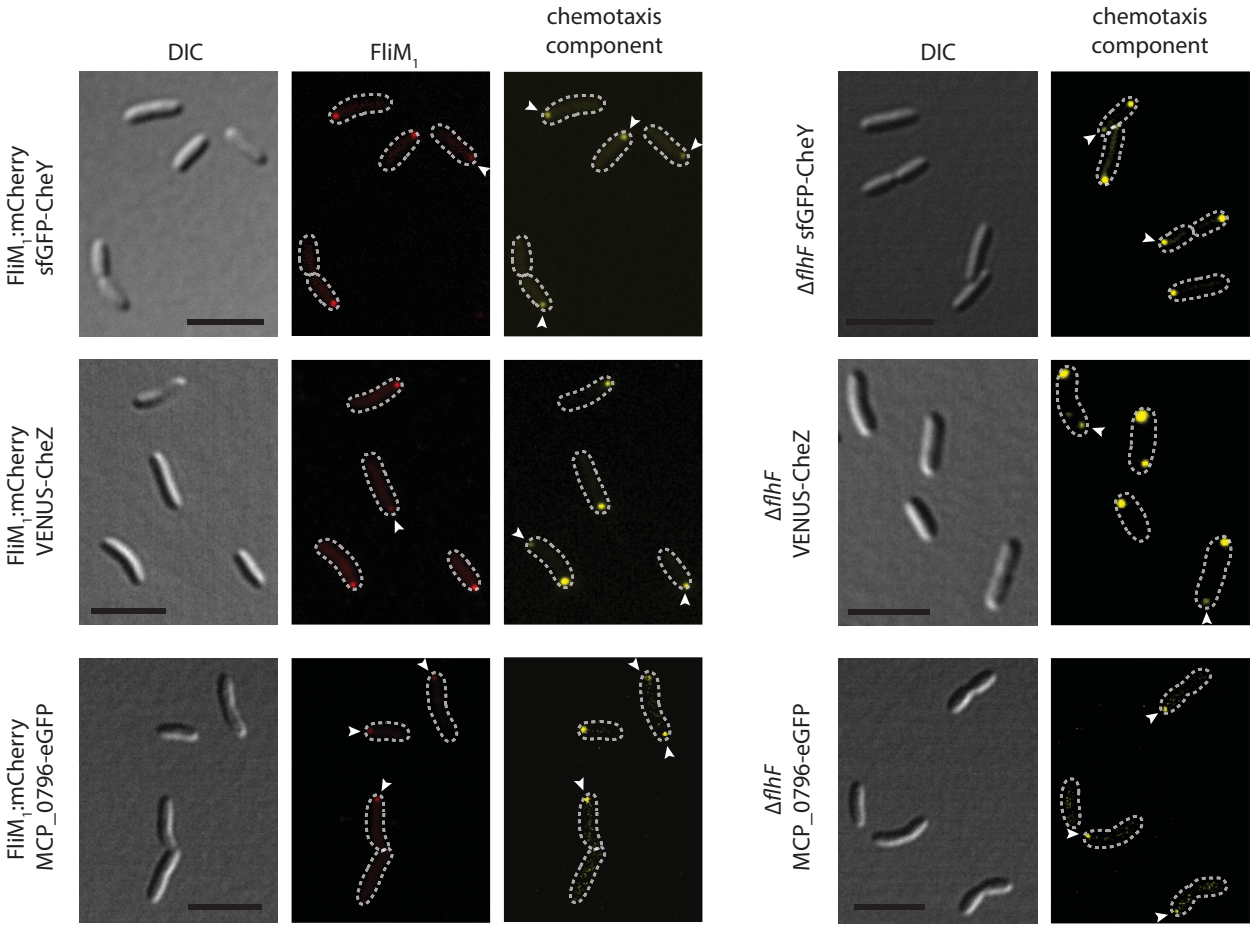

Figure S5: Effects of *flhF deletion* on the positioning of chemotaxis components. Shown are DIC and corresponding fluorescence micrographs of sfGFP-CheY, Venus-CheZ, and MCP_0796-eGFP in relation to the position of $FliM_1$-mCherry in the wild-type (left) and the *ΔflhF* background (right). In the absence of *flhF*, all chemotaxis components tested remained at a polar position. Arrows mark the position of minor fluorescence clusters. The scale bar equals 5 µm.

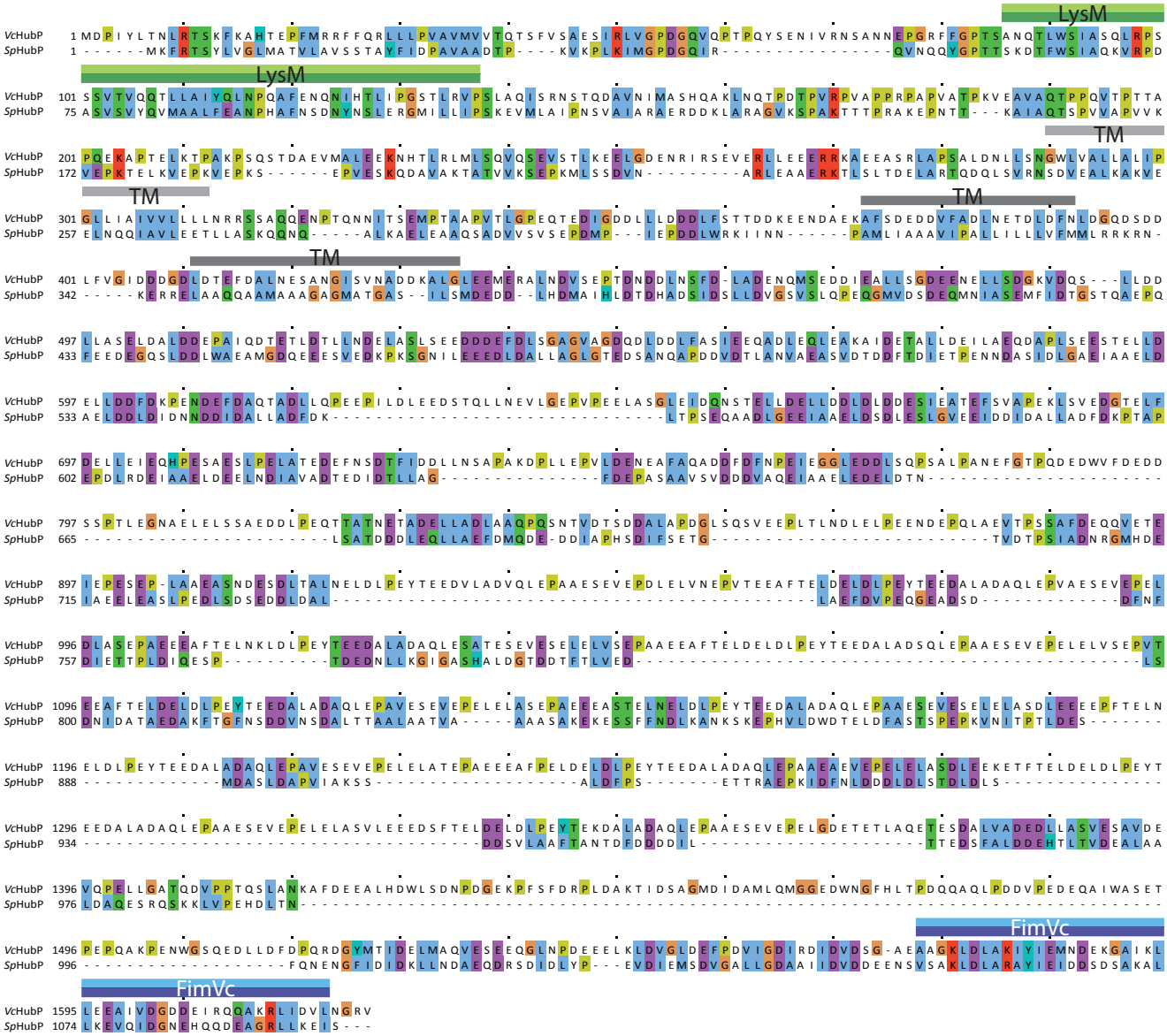

Figure S6: Amino acid sequence alignment of HubP of *Vibrio cholerae* (*Vc*HubP) and *S. putrefaciens* CN-32 (*Sp*HubP). The positions of the predicted LysM and C-terminal FimVc domains are highlighted in green and blue, respectively; the predicted transmembrane regions are marked in grey. Color code of the amino acid residues: A, I, L, M, F, W, V, blue; N, Q, S, T, green; E, D, magenta; G, orange, H, Y, cyan; P, yellow.

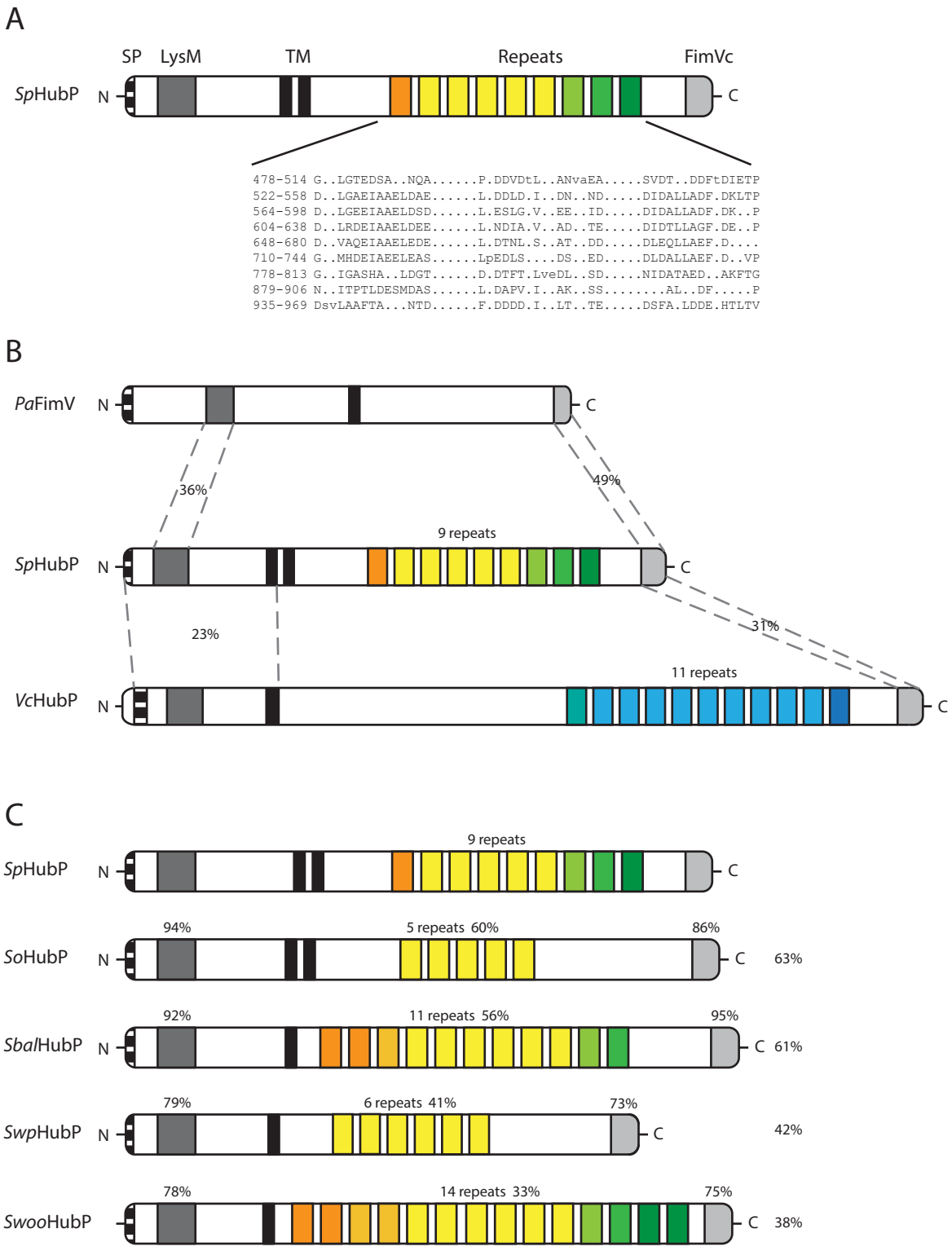

Figure S7: HubP/FimV domain organization. A) Domains of *S. putrefaciens* CN-32 HubP (*Sp*HubP). Indicated are the N-terminal signal domain (SP), the LysM domain, the transmembrane domain (TM), the C-terminal FimV domain (FimVc) and the number and position of repeated amino acid sequences. The sequence of these repeats is specified below. **B) Domain organization comparison of *P. aeruginosa* FimV (*Pa*FimV), *Sp*HubP and *V. cholerae* HubP (*Vc*HubP) drawn to scale.** The domains are indicated similarly as in A). The regions showing the indicated highest identity levels to SpHubP at the sequence level are marked by bracketed lines. It should be noted that, although the repeat structure in *Pa*FimV is little pronounced, the corresponding region is similarly enriched in acidic amino acids. **C) Comparison of putative HubP orthologs in various *Shewanella* sp.** The proteins show high conservation in the N- and C-terminal regions but little conservation with respect to the cytoplasmic repeat region as correspondingly indicated as percentage of identity at the amino acid level for each major region (LysM domain, repeat region, FimV C-terminal domain, overall). *So*HubP, *S. oneidensis* MR-1 SO_3069; *Sb*HubP, *S. baltica* Sbal_2743; *Swp*HubP, *S. piezotolerans* Swp_3117; *Swoo*HubP, *S. woodyi* Swoo_2985. Please note that these are only a few representatives of likely HubP orthologs in *Shewanella* to illustrate the difference in HubP domain organization in closely related species.

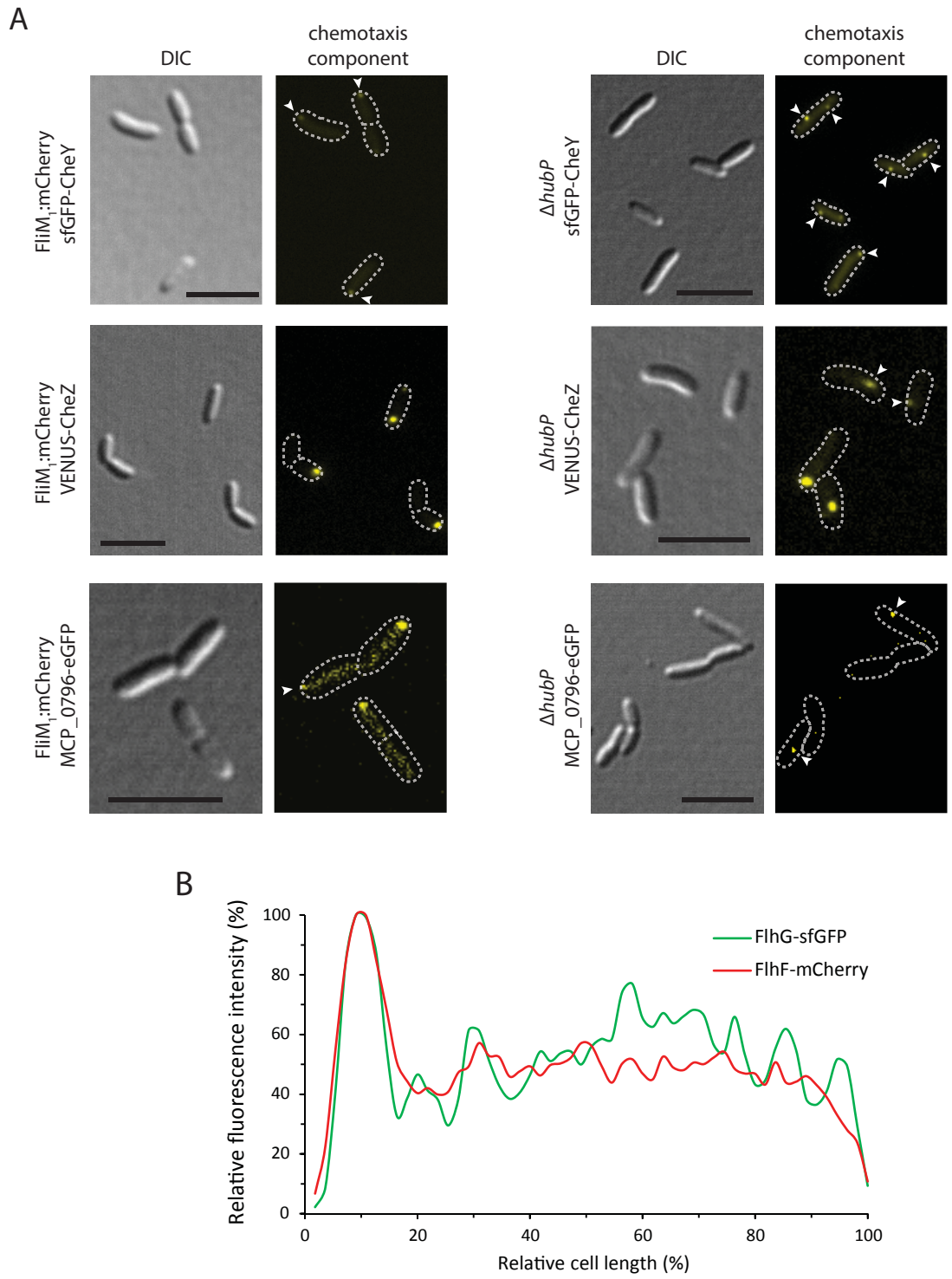

Figure S8: *Sp*HubP is required for proper localization of the chemotaxis components . A) Localization of components of the chemotaxis signaling array in the presence (left) and absence (right) of *Sp*HubP. Displayed are DIC and corresponding fluorescence micrographs of cells bearing sfGFP-CheY, Venus-CheZ, or MCP_0967-eGFP fusions. Loss of *hubP* results in displacement from the cell pole to more lateral position. Arrows indicate the position of fluorescence clusters, and the scale bar equals 5 µm. **B) Both FlhF and FlhG localize to the cell pole.** Displayed are line scans of the relative fluorescence intensity of cells producing FlhG-sfGFP (green line) or FlhF-mCherry (red line). Corresponding fluorescence micrographs are displayed in Fig. 3.

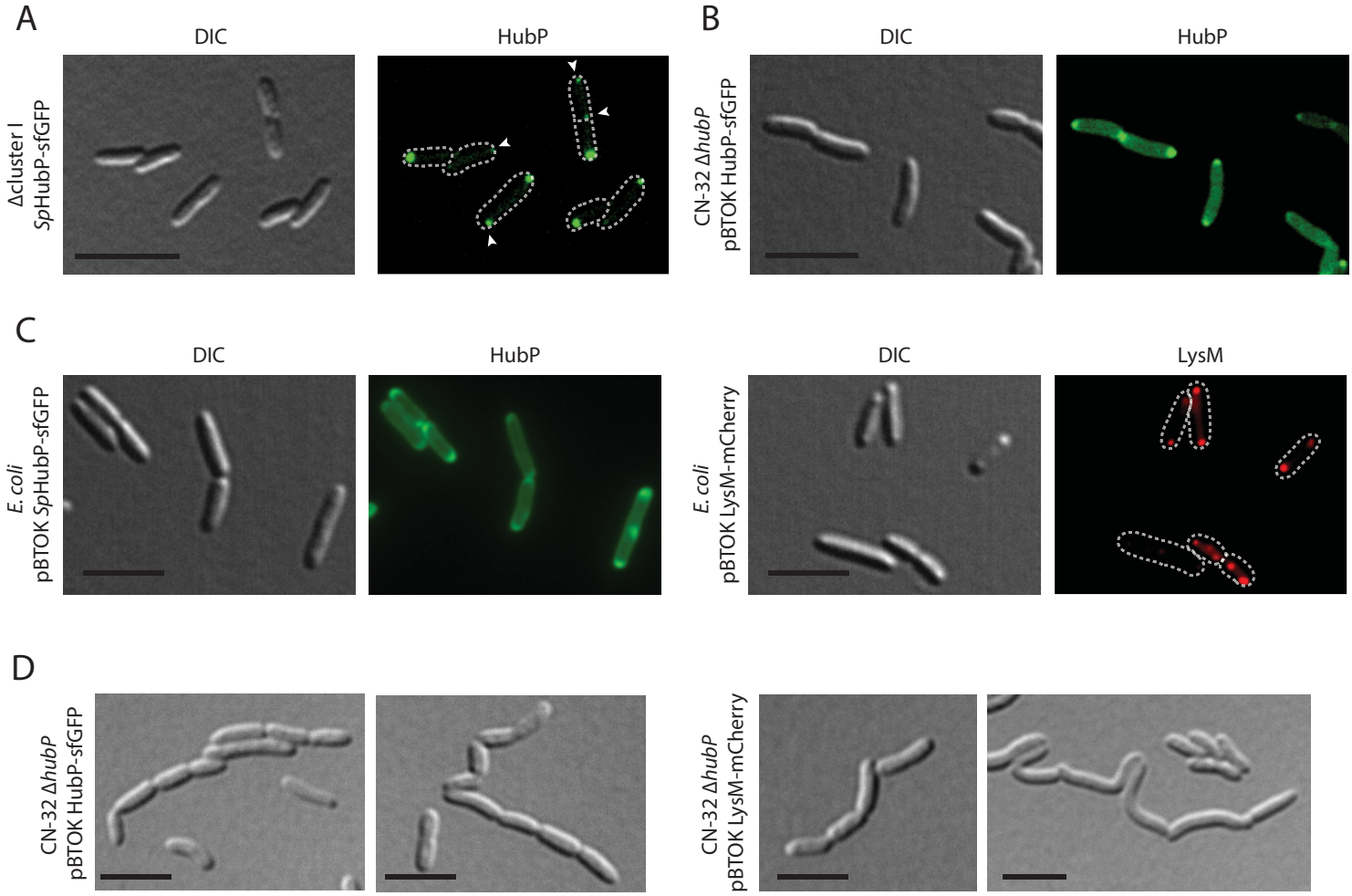

Figure S9: Localization and phenotypic analysis of *Sp*HubP-sfGFP and LysM-sfGFP production. A) *Sp*HubP localizes independently of flagellar components including FlhF. Displayed are a DIC and corresponding fluorescence micrograph of cells in which the complete primary flagellar cluster was deleted and which produce a HubP-sfGFP fusion. **B) Low amounts of *Sp*HubP-sfGFP show normal localization patterns.** Displayed are DIC and corresponding fluorescence micrographs of ΔhubP-mutants cells harboring pBTOK-HubP-sfGFP without induction. The arrow marks the localization of HubP-sfGFP at a newborn cell pole. **C) *Sp*SpHubP-sfGFP and LysM-sfGFP heterologously produced in *E. coli* localizes in similar patterns as in** *S. putrefaciens*. Displayed are DIC and corresponding fluorescence micrographs of *E. coli* cells harboring pBTOK-HubP-sfGFP (left) or pBTOK-LysM-sfGFP (right) at low induction. **D) Overproduction of full-length *Sp*HubP-sfGFP or LysM-sfGFP results in aberrant cell morphologies in *S. putrefaciens* CN-32.** Displayed are DIC micrographs of cells after gene induction for 45 min from pTBOK-HubP-sfGFP or pTBOK-LysM-sfGFP. The cells tend to form chains or elongated cell shapes. For all images: The scale bar equals 5 µm, arrows mark fluorescent foci.

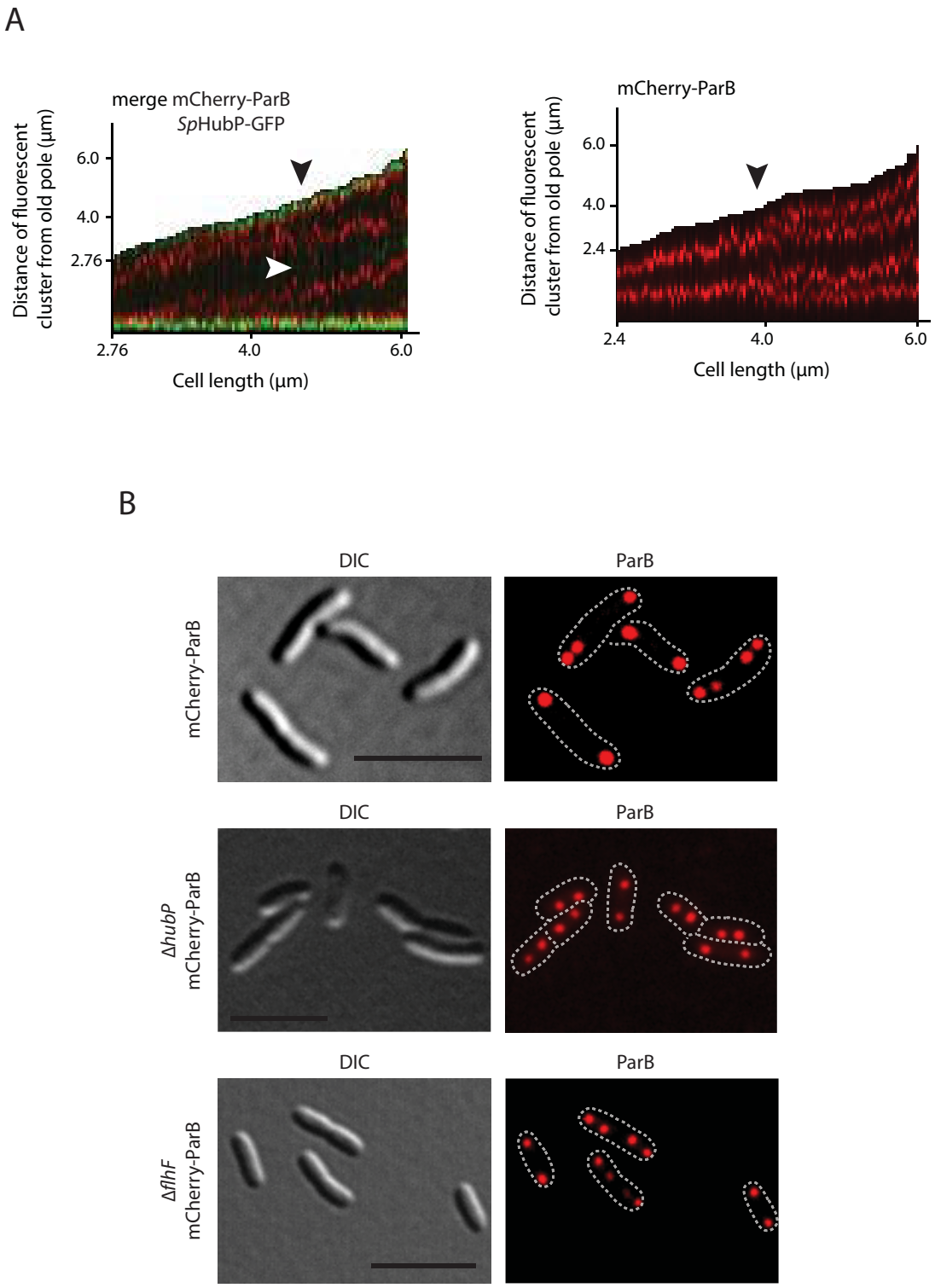

Figure S10: Localization of *oriC* in dependence of *Sp*HubP and FlhF. A) Position and fluorescent intensity of mCherry-ParB (red) and *Sp*HubP-sfGFP (green) as the distance from the old cell pole relative to the cell length over the cell cycle. The cell length is marked by the black area. The black arrows marks the earliest time point of visible cell constriction. The white arrow marks the appearance of *Sp*HubP-sfGFP at the division plane and at the newborn cell poles. In *ΔhubP* cells, the *oriC* marked by mCherry-ParB is never observed at the cell poles but remains at a certain distance to the pole. Also see the corresponding figure displaying the position without fluorescent intensities (Fig. 6). **B) FlhF does not localize the *oriC* to the cell pole.** Shown are DIC and corresponding fluorescence micrographs of wild-type (upper two panels) and *ΔflhF*-mutant (lower two panels) cells in which ParB was fluorescently tagged to mark the position of *oriC* within the cells. In the absence of FlhF, the fluorescent foci still move towards and localize at the cell pole as opposed to cells in which *hubP* was deleted (middle panels). The scale bar equals 5 µm.

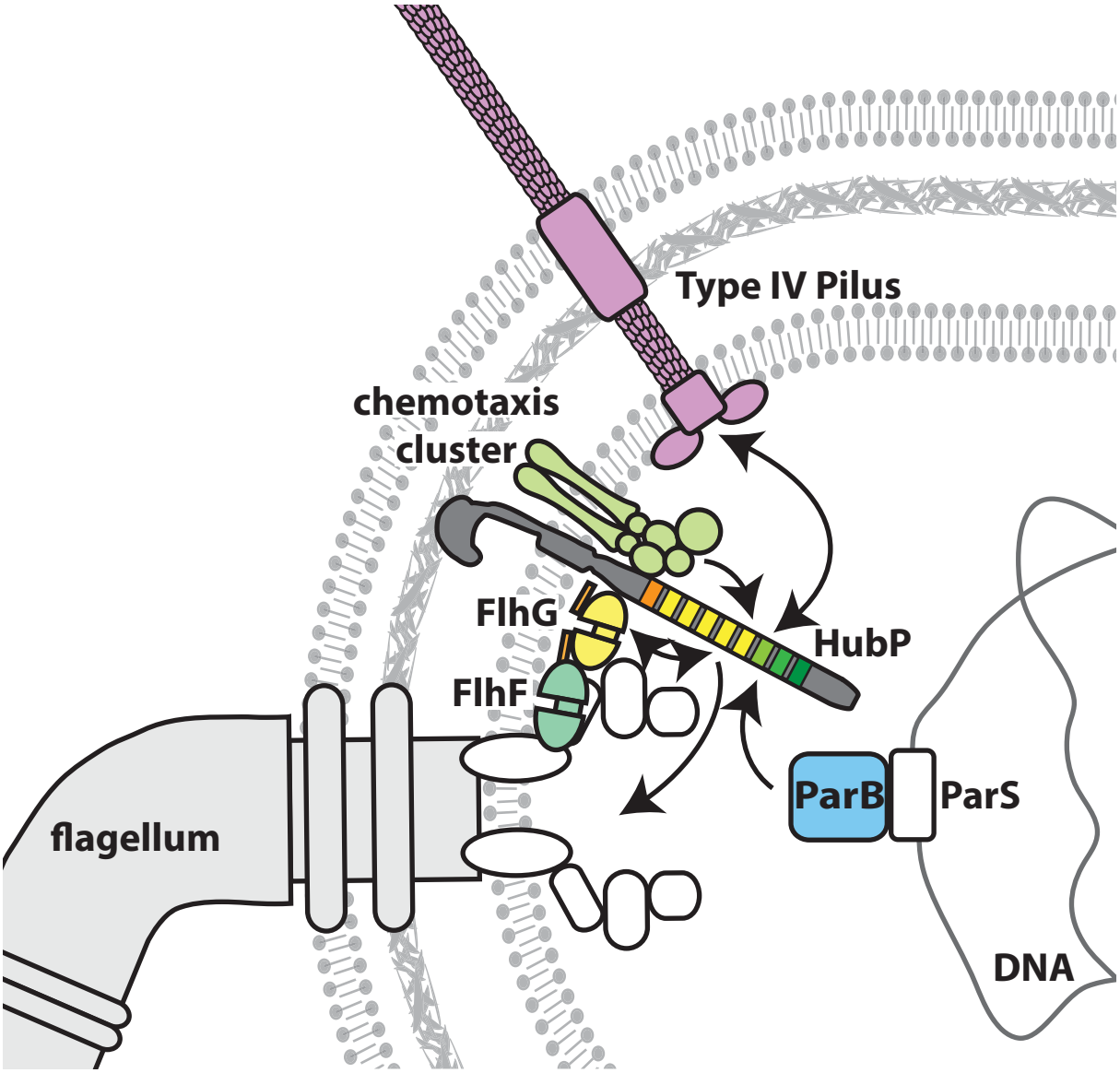

Figure S11: A model summarizing observed and potential functions of HubP/FimV-like proteins. HubP serves as a polar marker protein for recruitment of *oriC* and the chemotaxis array to the flagellated cell pole. In addition, HubP might directly or indirectly affect flagellar biosynthesis (maybe through interaction with the FlhF/G system which targets the flagellum to the cell pole) and affect flagellar performance and/or type IV pili-mediated twitching motility.

Chapter 5:

Discussion

Initial remarks

In order to grow and proliferate environmental bacteria in soil and water bodies have to cope with changing conditions including stress factors such as changing pH, temperature, osmolarity, oxygen availability and accumulation of toxic compounds. In natural habitats these factors can be present in varying steep or shallow gradients. Soil is a highly structured heterogeneous habitat with pores and aggregates that organize a given space into multiple different niches. Marine and fresh water bodies on the other hand can furthermore be structured by a gradient of light. In both habitats, temporal and spatial availability and composition of nutrients fluctuate significantly and can, especially in the open ocean, be overall scarce (Alexandre et al. 2004). All these factors have to be sensed and integrated into a response that allows the individual cells to efficiently maintain an adequate energy level. One strategy against the dissipation of resources is a tight regulation of the production of all cellular components that are energy consuming. However, mRNA and protein synthesis are relatively slow processes, therefore, transcriptional and post-transcriptional regulation mostly do not allow an instant response of single cells to sudden changes in the environment (Booth 2002; Thattai and Van Oudenaarden 2004). Directed movement towards the most favorable location by means of flagellar motility and chemotaxis is a very fast reaction to a given stimulus and essential as an immediate survival strategy (Stocker et al. 2008; Stocker and Seymour 2012). To ensure an efficient motility, the flagellar motor itself can be adapted by the integration of the appropriate stator type and number to meet prevailing conditions such as viscosity, salt concentration or pH (see reviews by Thormann and Paulick 2010; Kojima 2015). *S. oneidensis* MR-1 encodes the Na^+-dependent PomAB (SO_1529 and SO_1530) and H^+-dependent MotAB (SO_4287 and SO_4286) stator but only a single polar flagellum and is, thus, an excellent organism to study the adaptation of flagellar motor function by an additional stator set (Paulick et al. 2009, **Chapter 2**). Wild-type *S. oneidensis* MR-1 cells swim faster at low Na^+ concentrations than cells lacking *motAB* (**Chapter 2**). Therefore, it is conceivable that this stator may be a significant advantage for *S. oneidensis* MR-1 to cope with changing salt concentrations. However, the function of MotAB is limited when the viscosity of the environment is increased or oxygen is depleted (**Chapter 3**). Spontaneous mutations in the plug domain of the B-subunit were found to render this stator functional under these conditions but also decrease the maximum rotational speed. Hence, the dual stator/single flagellum configuration of *S. oneidensis* MR-1 is a perfect system to study several aspects of the functional evolution of a molecular machine as this bacterium clearly benefits from an additional stator set which is either the result of a gene duplication or horizontal gene transfer. To this end, the potential origin of MotAB in *S. oneidensis* MR-1 is discussed below. The frequent occurrence of point mutations that alter stator properties illustrates how quickly flagellar motors may diversify. Therefore, the following discussion will also focus on how such mutations may influence the stator properties.

Modulation of flagellar motility through a dynamic stator exchange can be considered as a quick response to changing conditions, but it does not promote a directed movement towards a more favorable environment. A tactic response to extracellular factors via a biased random walk, the so-called chemotaxis, is a mechanism employed by most flagellated cells (see reviews by Wadhams and Armitage 2004; Sourjik and Wingreen 2012). Complementary to chemotaxis, many bacteria were found to monitor their cellular energy status by receptors that detect changes in the electron transport system and navigate towards locations that provide optimal energy levels (Alexandre et al. 2004). Components of the chemotaxis system were frequently found to localize at the flagellated pole of the cell, but the mechanism that ensures localization of both to the same pole has not been studied in many bacteria yet. Recently, it was established that the landmark protein HubP controls localization of many polar proteins, including the chemotaxis system, in a number of γ-proteobacteria (Yamaichi et al. 2012). In *S. putrefaciens* CN-32 the chemotaxis components and the chromosome division machinery were displaced and spreading on soft agar plates as well as the overall flagellar speed and twitching motility were decreased when *hubP* is deleted (**Chapter 4**). Placement of the polar flagellum, however, is not dependent on HubP but on the GTPase FlhF.

The second part of the discussion will initially focus on the apparent requirement of establishing the polar localization of the chemotaxis system. Finally, a potential mechanism that ensures polarity of the landmark protein HubP will be discussed. As stated in the aims section, the last article (**Chapter 4**) was published in co-first authorship with Florian Rossmann. The results contributed by him are not discussed in detail.

Two for one: Two stator complexes power flagellar rotation of *S. oneidensis* MR-1

The origin of the two stators of S. oneidensis MR-1

Orthologues of *pomAB* are present in all *Shewanella* species. Some *Shewanella* species possess an additional lateral flagellar system along with *motAB*. In all these cases this stator is, however, not homologous to *motAB* of *S. oneidensis* MR-1. Predictions using the online tool EnsemblBacteria (Vilella et al. 2009) suggest that *motB* is a duplication of *pomB* (50% confidence) which occurred in a common ancestor of *Aeromonas* and *Shewanella* and was lost from most other genera of the order of the Alteromonadales. This is supported by alignments of the UCSD genome browser (Kent et al. 2002) which predicts *pomB* of *S. oneidensis* MR-1 (SO_1530), *Shewanella* sp. ANA-3 (Shewana3_2897), *Shewanella* sp. MR-4 (Shewmr4_2727) and *Shewanella* sp. MR-7 (Shewmr7_2800) to be among the closest homologs of *motB*. Notably, this is not entirely true for *motA*, which shows highest similarity to

two *motA* sequences of *Aeromonas hydrophila* ATCC 7966. The genome of this strain encodes two predicted *motAB* and one *pomAB* sequences, the functionality and ion specificity of these stators has not yet been experimentally verified. It is also noteworthy that the GC-content of *S. oneidensis* MR-1 *motAB* is 38% which differs from the rest of the genome including *pomAB*: Here, the average GC-content is 46%. Furthermore, *motAB* of *S. oneidensis* MR-1 is encoded in a stretch of ~47kbp which is overall poorly conserved among other *Shewanella*. These differences could be explained by *motAB* being acquired by lateral gene transfer rather than being duplicated (Paulick et al. 2009). The closest orthologue is found in *Aeromonas* species (A- and B-subunits share 76% and 48% identity, respectively). Despite the low shared homology between the native stator PomAB and the putatively acquired stator MotAB (A- and B-subunits share 27% and 32% identity, respectively), MotAB can be assembled to the motor and power rotation. Accordingly, the mechanism of recruitment and activation as well as the alignment of the interface between stator and rotor appear to be compatible to some extent. This is not self-evident as not all stators can readily interact with a given motor. *S. putrefaciens* CN-32 for example harbors two flagellar systems along with PomAB and MotAB. These stators were found to exclusively interact and localize to their corresponding flagellar system even if both were present in the same cell. Here, PomAB only powers rotation of the polar and MotAB of the lateral flagellum (Bubendorfer et al. 2012). It is unclear which region of MotAB and PomAB or the corresponding rotor components in *S. putrefaciens* CN-32 determines this specificity and, in contrast, which exact properties allow the appropriate interaction of MotAB with the rotor in *S. oneidensis* MR-1.

According to prevailing models of torque generation and activation, stators have to meet several criteria to form functional motors: I) Each stator unit has to be positioned correctly in relation to FliG in order to permit the electrostatic interaction. II) Since stators are present in the membrane as inactive precomplexes prior to incorporation, they have to sense the “docking” to open the channel at the right time. III) The opening process presumably includes a drastic conformational change in the periplasmic domain that allows the B-subunit to span the distance between cytoplasmic membrane and peptidoglycan (PG) and bind to the latter. IV) Once the channel is open, the coupling ion has to bind to the ion-binding site, induce a conformational change and leave the stator followed by restoration of the original conformation of the stator (mechanochemical cycle). V) If the basal body comprises additional structures in the periplasm or cytoplasmic membrane such as the T-ring or FliL, acquired stators have to be capable of interacting with them or function independently of their presence. If *motAB* was acquired, it is interesting to consider the question whether MotAB was readily expressed and functional upon acquisition by the ancestor of *S. oneidensis* MR-1 or attained the capability to drive rotation of the polar flagellum after a process of adaptation. It has been shown in several studies that chimeric stator complexes compiled from stators of different species assembled

into functional motors and powered rotation (Gosink and Häse 2000; Asai et al. 2003; Yakushi et al. 2006). It is therefore conceivable that an acquired stator can be of immediate benefit for a cell. This question could potentially be solved by reconstructing the ancestral gene sequence and testing the performance of its product. A similar approach has been used to study the ancestral version of fluorescent proteins of the coral *Montastraea cavernosa* (Matz et al. 2002; Ugalde et al. 2004). Here, the ancestral genes were predicted, synthesized and the fluorescence spectrum analyzed. The authors could thus determine the most likely color of the common ancestor of all fluorescent proteins from this coral as well as of three nodes of diversification. In case of the stator such a form of "experimental phylogeny" would be more complicated as not only the evolution of the two stator proteins but also of the rotor would have to be considered. Careful analysis of the evolution of *motAB* could also determine whether it is a paralog to *pomAB* or has a different origin. It is likely that such calculations would require more sequence information of closer homologs of MotAB which are not available yet.

The changed properties of MotAB and their implication for* S. oneidensis *MR-1*

Independent of its origin, MotAB is a stator that is beneficial to *S. oneidensis* MR-1 under low sodium concentrations as the mean speed of wild-type cells is higher than the speed of *S. oneidensis* MR-1 Δ*motAB* (**Chapter 2**). However, at low oxygen concentrations or increased viscosity, cells that only contain *motAB* quickly cease to swim. These factors seem not to limit the stator functionality if MotB carries a small mutation in, or close to, its plug domain. Several of these mutations were found in *S. oneidensis* MR-1 Δ*pomAB* cells exhibiting enhanced swimming phenotypes on soft agar plates after prolonged incubation. The plug domain is the region containing a short alpha-helix following the transmembrane domain (TM) of the B-subunit. A deletion of this region has been shown to cause a premature ion-flow through stators that are not incorporated into the motor (Kojima et al. 2009; Li et al. 2011). As the plug alpha-helix has an amphipathic character, it was suggested that the hydrophobic face interacts with the cytoplasmic membrane and thereby keeps the stator in its closed conformation. Following this hypothesis, the activation of the stator would entail a rearrangement that removes the plug domain from the membrane and thus opens the channel (Hosking et al. 2006). Recently, this hypothesis has been challenged by estimating the distance between TM and plug domain to be too short to reach the cytoplasmic membrane (Nishihara and Kitao 2015).

Of the eight sequenced mutated stators, the *motB*ΔMVE mutation (the resulting protein is henceforth denoted as MotB* and the corresponding stator complex as MotAB*) was further characterized (**Chapter 3**). Two aspects that are of high interest in this regard are: How does the cell or flagellar motor sense and integrate cues like increased viscous drag or low oxygen and what is the underlying mechanism that allows the MotAB* stator to provide enough torque under these conditions? A

conclusive explanation for the torque-speed relationship of the *motB*ΔMVE mutant is an alteration of the stator channel properties resulting from a conformational change. The plug domain is mainly thought to prevent premature ion leakage by keeping the channel in a closed conformation. It could, however, also play a role in the suggested conformational change that is required for its opening and potentially for its conformation and performance in the open state.

At high viscosity (= high load on the flagellum) of the environment, many MotAB*-driven cells were still motile while cells producing MotAB were not (**Chapter 3**)**.** Therefore, the torque provided by MotAB* may be higher than of MotAB. The simple equation M = r * F *n calculates the torque (M) of a flagellar motor as the product of the length of the lever (r), the applied force (F) and the number of force generating units (n). Theoretically, any of these factors could be the cause for a larger M. However, the stator number n in motors of *S. oneidensis* MR-1 Δ*pomAB motB-mCherry* and *S. oneidensis* MR-1 Δ*pomAB motB*-mCherry* as well as the turnover were not significantly different (**Chapter 3**), thus, n is likely not different between motors composed of MotAB* and MotAB. The distance (r) of the stators:FliG contact point to the rotational axis has not been determined for *Shewanella* yet. A recent study has demonstrated that some bacteria are capable of producing higher torque by increasing this distance. In *Salmonella*, r is measured to be ~20nm with an observed motor torque of ~ 2,200 pN/nm. The flagellar motor of *Borellia burgendorfi* has a radius of 30.5nm and produces a torque of ~4000 pN/nm while simultaneously incorporating more stator complexes (Beeby et al. 2016). In *E. coli,* the calculated force provided by each stator unit is 7.3 pN (Reid et al. 2006; Beeby et al. 2016). Assuming a similar force for the stators in *Shewanella* and a radius of 21.5 nm, as measured in *V. alginolyticus* (Beeby et al. 2016), a motor of *S. oneidensis* MR-1 driven by seven MotAB complexes should provide a torque of ~1100 pN/nm. Species with larger distance between the rotational axis and the lever contact point of FliG and the stator establish the position of the stators by additional periplasmic structures such as the T-ring and disc structures composed of FlgP, PflA or PflB (Beeby et al. 2016). In those species, the C-ring has evolved a larger diameter and thus ensures a correct interface of MotA and FliG. Considering the amount of further components and the apparently synchronized evolution to increase not only the diameter of the stator-ring but also the rotor-ring, it is unlikely that the *motB*ΔMVE mutation alone could position the stator sufficiently further away from the rotational axis and thus increase r to create a significant higher torque while maintaining the MotA:FliG interface. If n and r are not different between MotAB and MotAB*, it is likely that each single MotAB* stator produces a slightly higher force than the native MotAB complexes. Unfortunately, no study focusing on mutations in the periplasmic part of the B-subunit with phenotypes linked to high torque but slower speed at high load has ever provided information on how the properties of the ion channel may have changed. In general, torque produced by a single stator can differ in dependence to external factors such as the ion motive force or internal properties like altered energy-coupling ratio

or efficiency (Inoue et al. 2008). Assuming a similar ion motif force of *S. oneidensis* MR-1 Δ*pomAB* and *S. oneidensis* MR-1 Δ*pomAB motB**, the stators could indeed have different energy-coupling properties. In the loose-coupling model of Boschert and colleagues, the passage of one ion through the stator induces a less forceful but nevertheless powerstroke-inducing conformational change than the simultaneous passage of two protons (Boschert et al. 2015). In this model, the authors also describe a scenario, which predicts a stator to produce more torque if the pK_a of the ion binding site is high while its stepping rate will be lower. This altered torque/speed profile fits to the observations made for *S. oneidensis* MR-1 Δ*pomAB motB**: At high viscosity more MotAB* driven cells where observed to be motile but the average speed of this mutant is slower than of *S. oneidensis* MR-1 Δ*pomAB.* If mutations in the periplasmic domain slightly alter the position of the TM of the B-subunit, the ion binding site Asp21 (MotB) may have a higher pK_a by being shifted into an unfavorable position that allows less interaction with neighboring amino acids. Accordingly, the pK_a of Asp21 in MotAB* may be higher than in MotAB. This may also explain why *S. oneidensis* MR-1 Δ*pomAB motB** are motile at depleted oxygen concentrations, which likely correlates with a decreased pmf, while *S. oneidensis* MR-1 Δ*pomAB* is not. At low pmf a stator with a high pK_a is predicted to produce more torque than a stator with low pK_a (Boschert et al. 2015). It is not unlikely that MotAB* may have a conformational change as mutations in the C-terminus of MotB have been shown to alter the arrangement of the transmembrane domains of A- and B-subunit to each other (Kojima et al. 2009). Some studies suggested that the deprotonation of the aspartic acid is not stepping rate-limiting. Instead, it was proposed that either gating of the channel on the periplasmic side or the formation of a hydrogen bond between the protonated aspartic acid and a neighboring carbonyl residue which induced the conformational change may limit this rate (Yuan and Berg 2010; Nishihara and Kitao 2015). A conformational change of the channel, resulting from the mutation in MotB, could increase the distance of Asp21 to its neighboring carbonyl residues and/or narrow the channel entrance. This would explain the decreased speed of *S. oneidensis* MR-1 Δ*pomAB motB** compared to *S. oneidensis* MR-1 Δ*pomAB* (**Chapter 3**). As mentioned, no sufficient structural information is available on the flagellar stators. Thus, a reliable prediction of the ion channel properties is currently impossible.

Another possibility for an increased torque production by MotAB* would be a more efficient interaction between MotA and FliG. The proposed interface of the cytoplasmic loop between TM2/TM3 of MotA and FliG harbors several charged amino acids that were found to be important for torque generation but also placement of the stator (Zhou et al. 1998; Morimoto et al. 2010; Morimoto et al. 2013; Takekawa et al. 2014). This interface was found to include more charged amino acids in the motor of *V. alginolyticus* driven by PomAB than in the interface between MotAB and FliG of *E. coli* (Takekawa et al. 2014). All amino acids proposed to promote the stator-rotor interaction in *V. alginolyticus* (FliG and PomA) are also conserved in *S. oneidensis* MR-1. Strikingly, a similar pattern

is also easily detectable in MotA: Several positive and negative charges are arranged in positions comparable to PomA. However, MotA presents additional negative charges in the middle segment of the loop, which may weaken the electrostatic interaction between MotA and FliG. If the *motB*ΔMVE mutation causes a conformational change that brings the MotA loop in a more favorable position relative to the rotor, the force applied to it could be greater than in the wild-type motor. As the number of incorporated stators and their rate of mechanochemical cycles limit the speed at low loads, repositioning of the stator would explain the increased torque at high load but not directly the lower speed at intermediate and low loads. However, a motor which senses the torque it produces and adjusts its stator number accordingly could possess more stators at intermediate loads and thus have an increased speed. In *E. coli*, the number of bound stators were shown to increase relative to the applied load. The maximum number of stators was reached at stall and few or only one single stators drove rotation at low loads. Stators that were incapable of producing torque due to a mutated ion binding site (MotB D32A) were not found to be incorporated into the motor. Therefore, the authors speculated that the torque produced by each complex governs its stability in a motor (Tipping, Delalez, et al. 2013; Lele et al. 2013). A curve describing the load-dependent increase of stator number in motors driven by MotAB* may be more shallow than for MotAB. As I have only determined the number of stators incorporated at high load, I cannot exclude that MotAB* containing motors are composed of less stators than MotAB motors at intermediate or low loads. This has been observed for MotAB(Δ72-100) of *Salmonella* (Castillo et al. 2013). If deleted, MotAB(Δ72-100) motors produce higher torque at high load than wild-type motors with each mutated stator producing slightly higher torque than the wild-type version, which is similar to the phenotype of *S. oneidensis* MR-1 Δ*pomAB motB**. At an intermediate load, however, motors of the *motB*(Δ72-100) strain consisted of less stator complexes and produced less torque than motors driven by MotAB. The authors reasoned that this region is involved in mechanosensing and stabilizing the stator during torque generation. A similar mechanism may apply in *S. oneidensis* MR-1 Δ*pomAB motB*.* Several studies have provided evidence that the stators are involved in mechanosensing and thus promote altered motor configuration or functionality of the stator itself under varying loads.

Besides the apparent dependency of the stator number on external load, the integrity and function of the *E. coli* flagellar motor quickly responds to pmf disruption. Using cells that maintained their pmf solely through the light-powered proton pump proteorhodopsin, Tipping et al. demonstrated that pmf disruption results in a reversible loss of stator function and their dissociation from the motor (Tipping, Steel, et al. 2013). Earlier studies have also provided evidence for a dependence of flagellar motor integrity on the imf although stators do not leave the motor upon depletion of the imf in all species (Sowa et al. 2005; Lo et al. 2007; Fukuoka et al. 2009; Morimoto et al. 2010). Whether a lower imf is directly sensed and integrated into a response or indirectly via a decreased torque production of the

stators has not been determined yet. In most of the quoted studies, the imf was suddenly decreased for example by exchanging the medium or collapsing the pmf by the addition of the protonophor carbonylcyanid-*m*-chlorphenylhydrazon (CCCP). A treatment of *S. oneidensis* MR-1 Δ*pomAB motB-mCherry* with CCCP arrests swimming motility but does not lead to a dissipation of the polar stator clusters. Preliminary experiments that aimed to alter the pmf by using proteorhodopsin were not successful. Thus, while the pmf seems to be limiting for motility of MotAB driven cells although the stators are retained at the motor. Accordingly, the pmf may be important for function of the stator of *S. oneidensis* MR-1 but not its stability at the motor.

It should be emphasized that the presented hypotheses on MotAB* properties are not excluding each other. If the *motB*ΔMVE mutation affects the stator conformation, the channel as well as the gating and sensing properties may be altered equally or to varying degrees.

Outlook

In summary, the core structure of the flagellum and the general mechanism of torque generation are highly conserved among flagellated bacteria but motility is the target of adaptation on multiple levels. As demonstrated for *S. oneidensis* MR-1, an additional stator set with different properties can be an asset to instantly respond to environmental changes. Although MotAB contribution to motility under high sodium concentrations is not detectable in wild type cells, it adds significantly to it under low sodium concentrations (**Chapter 2**). Moreover, the stator properties can be readily modified by small mutations as demonstrated in numerous studies. Specific single point mutations have been shown to alter the ion specificity, conductivity, torque generation, speed or gating resulting in a broad range of phenotypes (Jaques et al. 1999; Kojima et al. 1999; Gosink and Häse 2000; Terahara et al. 2008; Che et al. 2008; Terahara et al. 2012; Takekawa et al. 2012). Additionally, flagellated bacteria are found in multiple habitats providing motility over a broad range of environmental conditions. The above list cannot claim to be exhaustive but it allows an understanding of how the variety of stator properties found in bacteria corresponds to their evolution in diverse environments and under different selective pressures. To understand the different properties and validate the assumptions made on the structure of the stators in previous studies, further studies need to provide detailed structural information of the stator. As crystallization of membrane proteins is challenging, alternative approaches such as the *in meso* approach using a bicontinuous lipidic mesophase may be required.

One for many: HubP recruits a diverse set of components to the cell pole

Bacteria have developed several strategies to determine the localization of cellular components such as the chromosomal DNA, plasmids or proteins. So-called landmark protein that act as a platform or hub recruit many different other proteins to a specific site (see reviews by Shapiro et al. 2009; Laloux and Jacobs-Wagner 2014; Treuner-Lange and Søgaard-Andersen 2014). The reason for tight control of placement and protein concentration is obvious for some components that are targeted to a given site, for example the machinery that facilitates cell division. Here, altered localization or functionality often leads to incomplete or incorrect cell division resulting in phenotypes ranging from anucleated minicells to filamentous cells containing numerous chromosomes and, in most cases, a decreased growth rate (Adler 1967; Reeve et al. 1973; Begg et al. 1980; Lutkenhaus 1998). It has been shown before in the case of flagellar placement and number that motility of monotrichously flagellated cells is impaired if flagella are delocalized or overproduced (Pandza et al. 2000; Huitema et al. 2006; Lam et al. 2006; **Chapter 4**). In the α-proteobacterium *Caulobacter crescentus,* a major landmark protein that marks the new pole is TipN. If deleted, the flagellum, which is always produced at the new pole of the cell, is found at aberrant sites (Huitema et al. 2006; Lam et al. 2006). TipN was to date not found outside α-proteobacteria. In many other flagellated bacteria placement and number of flagella is regulated by FlhF and FlhG, two nucleotide-binding proteins of the SIMIBI class (Kazmierczak and Hendrixson 2013; Bange and Sinning 2013; Altegoer et al. 2014).

As mentioned before, HubP was found to ensure correct placement of many polar proteins, including the chemotaxis system and the chromosome division machinery in the γ-proteobacteria *V. cholerae* and *S. putrefaciens* CN-32 (Figure 1) (Yamaichi et al. 2012, **Chapter 4**). HubP is a membrane bound protein of low pI that harbors a periplasmic LysM PG-binding domain, arrays of acidic repeats in the cytoplasmic part and a C-terminus, which is predicted to be in a tetratricopeptide repeat fold (termed $FimV_c$). At sequence level, functional homologs of HubP are poorly conserved among the γ-proteobacteria, in particular in the cytoplasmic part. Here, the acidic repeats for example can differ in length, motive and number. The periplasmic part of HubP of *S. putrefaciens* CN-32, including the LysM domain, exhibits the highest similarity to HubP of *V. cholerae.* This domain has been confirmed to bind to peptidoglycan in *V. cholerae* (Wehbi et al. 2011). Despite the low homology, the overall structure is conserved among HubP homologs. Moreover, the same architecture is also found in FimV proteins that have first been described to be involved in twitching motility of *Pseudomonas aeruginosa.* In addition, the surrounding genomic context of *P. aeruginosa fimV* and *hubP* of *S. putrefaciens* CN-32 are the same (Semmler et al. 2000). More recent studies found that FimV is also essential for type II and type IV secretion system assembly in *P. aeruginosa* (Michel et al. 2011; Wehbi et al. 2011). Homologs identified in other species were found to be involved in proper adhesion of *Neisseria*

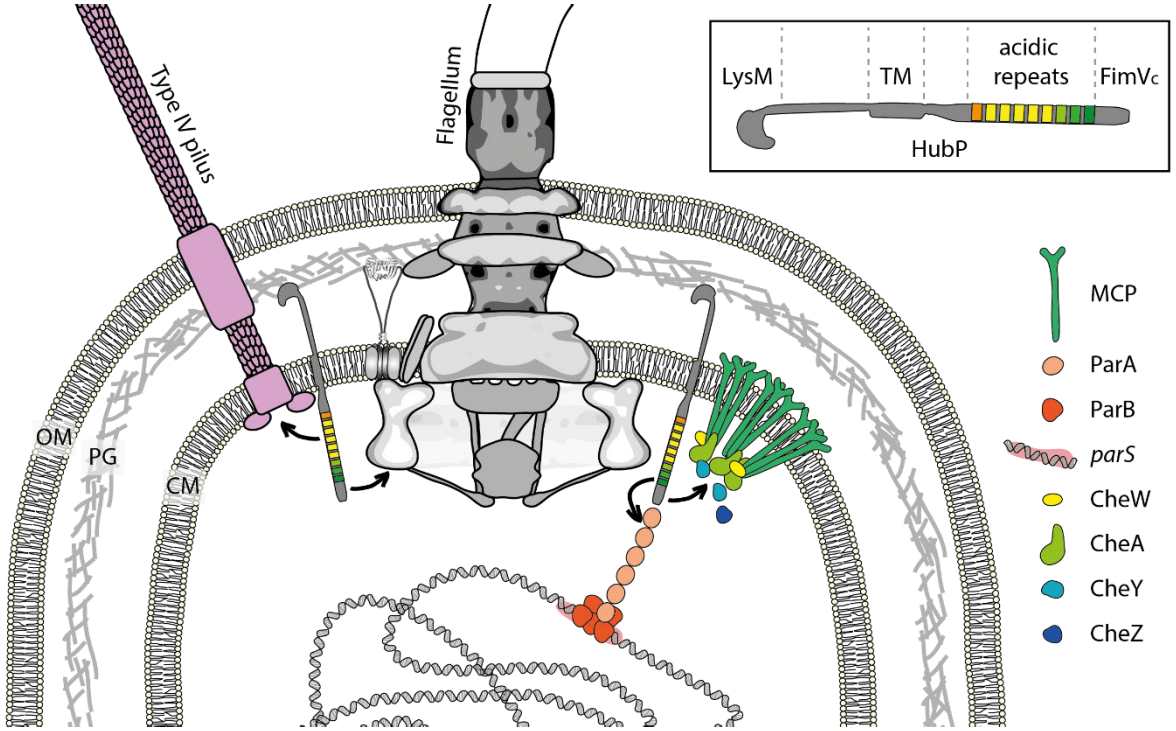

Figure 1: Model of observed and potential functions of HubP. HubP is a polar marker protein consisting of a LysM-type PG binding domain, a TM, several acidic repeats and a so-calles FimVc terminus (see box in the upper right corner). The LysM domain alone localizes to the cell pole and may be responsible for polar localization of HubP. HubP likely recruits the oriC via the ParAB/*parS* system and the chemotaxis array to the flagellated cell pole. In addition, HubP might influence the flagellar performance and type IV pili-mediated twitching motility. OM = outer membrane, PG = peptidoglycan, CM = cytoplasmic membrane.

meningitides to human cells and pigment production and cell shape of *Legionella pneumophila* (Oldfield et al. 2007; Coil and Anné 2010). Due to their structural similarity, and similar genetic context in *P. aeruginosa* and *S. putrefaciens* CN-32, HubP and FimV proteins likely constitute a group of organizational platforms that recruit various different clients to a given site. The set of recruited proteins seems to differ significantly between species, which may be due to the low homology of the cytoplasmic domain.

Loss of polarity of the chemotaxis system is a disadvantage for S. putrefaciens CN-32

The sensors of the chemotaxis system were previously shown to be responsible for the formation of rather stable complexes of the soluble components CheZ and CheY in *E. coli* (Sourjik and Berg 2000). In *S. putrefaciens* CN-32, these clusters localize to the same pole as the flagellum and were found to be frequently delocalized to lateral positions if *hubP* is deleted. The requirement for a precise localization of the chemotaxis system by a landmark protein is, in comparison to the cell division machinery and the flagellum, less apparent. Intuitively, it seems beneficial to localize the input and integration system for a chemotactic stimulus (the chemotaxis system) close to the final receiver of this signal (the switch complex) to allow a quick transmission. The transmitting molecule CheY was

shown to have an average diffusion constant of 4.6 ± 0.8 $\mu m^2 s^{-1}$ when fused to GFP and is estimated to have a diffusion constant of ~10 $\mu m^2 s^{-1}$ without the tag (Cluzel et al. 2000; Lipkow et al. 2005). As a consequence, a single molecule of CheY is estimated to travel through almost the whole cell in just 100 ms. Assuming a polar localization of the kinase CheA and a partially polar localization of phosphatase CheZ, simulations predict a quite shallow gradient of phosphorylated CheY (CheY-P) (Lipkow et al. 2005). It is therefore unlikely that the relative distance of receptor array and motor alone is decisive for efficient chemotactic behavior and overall performance of the cell. The study by Cluzel et al. also demonstrated the bias of rotational direction of the motor to be ultrasensitive to small changes in the overall pool of CheY-P (Cluzel et al. 2000). Thus, the constant maintenance of the optimal operational range of CheY-P concentration seems to be more important. The benefit of polar localization of the chemotaxis system in regard to the maintenance of this optimal CheY-P pool may be based on an efficient regulation of chemotaxis cluster size and distribution during cell division. As described in the introduction, methyl-accepting proteins (MCP) assemble to large arrays at the cell pole in a stochastic fashion, guided by the intrinsic curvature of the arrays (Thiem and Sourjik 2008; Endres 2009). This is likely the reason why many *S. putrefaciens* CN-32 cells exhibit polar cluster of the chemotaxis system, visualized through a fluorescently tagged MCPs, CheA, CheZ and CheY, even when *hubP* is deleted (**Chapter 4**). A possible explanation for the occurrence of lateral cluster of these chemotaxis components in *S. putrefaciens* CN-32 Δ*hubP* is that HubP may act like a nucleation point retaining diffusible MCPs at the new pole. Thereby HubP could ensure polar nucleation of a single chemotaxis array at this pole before it reaches the threshold size that allows localization by the curvature of the polar membrane. Without this mechanism several small cluster could be formed instead of a single large one and these small clusters may be more prone to a lateral localization. By preventing a lateral localization and decreasing the likelihood of the formation of smaller and more mobile arrays, polar localization and retention by a landmark protein in general ensures that both cells contain a certain amount of all components of the chemotaxis system after cell division. The heterogeneous distribution of the chemotaxis cluster in *S. putrefaciens* CN-32 Δ*hubP* correlates with this hypothesis: Many cells exhibited several large chemotaxis cluster while others possessed only very faint accumulations or even none. Especially these more extreme cases were not observed in wild-type cells. Chemotaxis requires cooperative receptor interactions to amplify a given signal (see review: Tu 2013). As stated above, chemotactic cells need to maintain a specific range of CheY-P concentration, determined to center around ~3 µM in *E. coli* (Cluzel et al. 2000). The tendency to form dispersed clusters instead of a single larger one at each pole and the incorrect distribution among daughter cells may result in altered signal amplification and thus diminished capability to maintain the appropriate range of CheY-P concentration in many cells. This would contribute to an altered chemotactic response of the population and in part explain the smaller extension zones of *S. putrefaciens* CN-32 Δ*hubP* cells on soft-

agar plates. Isogenic bacterial populations have previously been shown to exhibit a remarkable heterogeneity of their switching bias which allows them to spread using a bet-hedging strategy (Bai et al. 2013). Following this hypothesis, the distribution of the cellular CheY-P concentrations within a population would broaden if polarity of the chemotaxis clusters is lost. This would decrease the navigation efficiency of a large part of the population, because a significant fraction would be incapable of maintaining the relevant operational range of CheY-P concentration. Thus, the landmark protein HubP could prevent an increased heterogeneity of the cellular CheY-P concentration which otherwise might lead to a subpopulation that is unresponsive to chemotactic signals.

Additionally to the observed differences in placement of chemotaxis components, the loss of *hubP* also results in an altered localization of ParB. This protein is part of the ParAB/*parS* chromosome partitioning system. ParA is an ATPase that interacts with the DNA binding protein ParB. in *V. cholerae*, ParA1 was determined to be a direct interaction partner of HubP (Yamaichi et al. 2012). ParB in turn can bind to *parS*, a conserved DNA sequence that is found in multiple copies close to the chromosomal origin of replication (oriC), and the adjacent DNA regions (Gerdes et al. 2000). Similar to the ParAB/*parS* partitioning system that separates plasmids by pulling them apart, ParA of the chromosomal system pulls ParB bound to the newly replicated chromosome to the new pole (Ghosh et al. 2006; Fogel and Waldor 2006; Ptacin et al. 2010). Therefore, HubP acts as the anchor for ParA that allows it to pull ParB and, consequently, the chromosome to the pole in *Vibrio* (Yamaichi et al. 2012). In *S. putrefaciens* CN-32 Δ*hubP* ParB fused to mCherry does not localize to the extreme poles but at maximum to the 30% and 70% position of the relative cell length (**Chapter 4**). Remarkably, a *hubP* deletion does not result in a growth defect (**Chapter 4**), therefore, the overall chromosome segregation seems to be unaffected. In *C. crescentus* the ParAB/*parS* system is essential while the polar interaction partner of ParA, TipN, is not (Mohl et al. 2001; Lam et al. 2006). This suggests that chromosome segregation of these species relies on additional mechanisms that allow efficient distribution of the chromosomes and, hence, growth under the conditions tested.

Polarity of the landmark protein HubP

How HubP itself is located at the pole and interacts with each client has not been determined experimentally. *In silico* analysis of HubP combined with experimental data from chapter 4 may provide a starting point for future studies. HubP fused to GFP can be found in three distinct positions. A major cluster is formed at the flagellated old pole, a minor at the opposite new pole and a faint accumulation occurred at the site of constriction during cell division. The accumulation at midcell did not disappear after cell division as verified by a time-lapse experiment. It remained at the newly formed pole and therefore may be split into the two minor clusters in the process of constriction. This results in the

formation of the minor cluster opposite to the flagellated pole. As the PG binding LysM domain alone fused to mCherry forms clusters at the same sites in *S. putrefaciens* CN-32 and *E. coli*, it is likely that localization is achieved through this domain. In general, LysM domains can interact with peptidoglycan and could recognize sites of new PG synthesis or remodeling and by this find the pole (Bateman and Bycroft 2000; Buist et al. 2008). A similar localization pattern mediated by a LysM domain has been observed for DipM, a peptidase involved in cell wall remodeling during constriction in *C. crescentus*. DipM was found to interact with FtsZ and FtsN during cell division. This interaction as well as at least one of its four LysM domains are required for proper localization to midcell (Möll et al. 2010). It is possible that HubP is guided to the division plane by a component of the divisome. The Fluorescence Recovery After Photobleaching (FRAP) analysis performed on HubP tagged with GFP suggests that at least a certain part of HubP clusters are constantly exchanged (**Chapter 4**). However, since the recovery of fluorescence does not exceed ~50% of its initial value, it is likely that a fraction of HubP is permanently attached to the pole while the rest remains mobile. Therefore, one can speculate that a small amount of HubP is initially localized to the site of constriction by components of the divisome and stably attached to the PG layer via the LysM domain. Further HubP molecules could be recruited to this site by protein-protein interactions, mediated for example via the predicted tetratricopeptide repeat in the $FimV_c$ domain. Tetratricopeptide repeats have been shown to facilitate protein-protein interactions in numerous eukaryotic and prokaryotic cells (Das et al. 1998; Blatch and Lässle 1999; Cerveny et al. 2013). These can either mediate formation of homo-oligomeres or heterocomplexes (D'Andrea and Regan 2003; Kim et al. 2006). Thus, this site is also a potential binding region that may promote the interaction of HubP with some of its other clients. Preliminary experiments showed an unusual localization pattern of CheA if the $FimV_c$ domain was deleted (data not shown).

Finally, the study presented in chapter 4 also determined the involvement of HubP in flagellar and twitching motility. The localization of the flagellum is not affected by the deletion of *hubP*, the protein is therefore not involved in control of its placement. However, fewer *S. putrefaciens* CN-32 Δ*hubP* cells were found to be flagellated and average swimming speed of these cells in planktonic culture is decreased. As HubP recruits proteins of various functions to the pole, it may also be responsible of retaining a component at the pole that influences motor speed or functionality of the flagellar motor. Unfortunately, a comprehensive pull-down assay of purified HubP with *S. putrefaciens* CN-32 lysate to determine further interaction partners has been unsuccessful and is also lacking for other HubP homologs. Twitching motility of *S. putrefaciens* CN-32 Δ*hubP* was also decreased significantly. In *P. aeruginosa* FimV is essential for twitching motility as it is required for wild-type levels of the pili components PilM, PilN, PilO and PilQ. The stability and multimerization of the secretin PilQ in the outer membrane is likely dependent on the periplasmic LysM motif of FimV (Wehbi et al. 2011). As this

domain exhibits the highest homology between HubP and FimV, the twitching motility defect of *S. putrefaciens* CN-32 may be based on the same mechanism.

Outlook

As HubP is a landmark protein important for multiple processes, future studies should focus on identifying its direct interaction partners and the underlying mechanism of these interactions. To this end, it could be worthwhile to determine the interaction face of HubP and ParA1, an identified binding partner of HubP in *V. cholerae*, to understand the heterocomplex formation. Furthermore, future research should aim to elucidate how HubP finds the pole of the cell as this may be conferred by a rather general mechanism that could mediate polar localization even beyond HubP homologs of the γ-proteobacteria. Finally, the alterations of the chemotaxis system in *S. putrefaciens* CN-32 Δ*hubP* may help to understand why polar localization of these components is required for proper cellular behavior.

Final remarks

Flagellar motility of the bacteria *S. oneidensis* MR-1 and *S. putrefaciens* CN-32 relies on various dynamic systems to efficiently swim and navigate through a given environment. Both systems, the adaptation of motor function by stator swapping and targeting of components to the cell pole, are connected by the notion that flagellar motility and navigation can tolerate a certain amount of alterations without becoming completely non-functional. However, both systems have evolved to be fine-tuned to function in an optimal range. In order to achieve this optimum, flagella and chemotaxis components are tightly controlled on multiple levels such as their placement, stoichiometry, turnover and expression. As flagellar motility is important for survival in changing habitats, all these regulatory aspects are target of constant adaptation to meet the prevailing environmental conditions. The principles addressed here in *Shewanella* likely apply to other γ-proteobacteria and, in case of chapter 2 and 3, even to more distant lineages.

Throughout the three studies presented in this dissertation it is obvious that our current knowledge is limited by technical difficulties concerning the purification and structural and biochemical analysis of the stators and the landmark protein HubP. These obstacles need to be addressed first to close the gaps of knowledge.

Sources

Adler, H.I., Fisher, W.D., Cohen, A. & Hardigree A.A., 1967. Miniature Escherichia coli cells deficient in DNA. *Proceedings of the National Academy of Sciences of the United States of America*, 57(2), p.321.

Alexandre, G., Greer-Phillips, S. & Zhulin, I.B., 2004. Ecological role of energy taxis in microorganisms. *FEMS Microbiology Reviews*, 28(1), pp.113–126.

Altegoer, F. et al., 2014. From molecular evolution to biobricks and synthetic modules: a lesson by the bacterial flagellum. *Biotechnology & genetic engineering reviews*, 30(1-2), pp.49–64.

Asai, Y. et al., 2003. Ion-coupling determinants of Na+-driven and H+-driven flagellar motors. *J Mol Biol*, 327(2), pp.453–463.

Bai, F. et al., 2013. Populational heterogeneity vs. temporal fluctuation in escherichia coli flagellar motor switching. *Biophysical Journal*, 105(9), pp.2123–2129.

Bange, G. & Sinning, I., 2013. SIMIBI twins in protein targeting and localization. *Nature structural & molecular biology*, 20(7), pp.776–80.

Bateman, a & Bycroft, M., 2000. The structure of a LysM domain from E. coli membrane-bound lytic murein transglycosylase D (MltD). *Journal of molecular biology*, 299(4), pp.1113–1119.

Beeby, M. et al., 2016. Diverse high-torque bacterial flagellar motors assemble wider stator rings using a conserved protein scaffold. , pp.1–10.

Begg, K.J., Hatfull, G.F. & Donachie, W.D., 1980. Identification of new genes in a cell envelope-cell division gene cluster of Escherichia coli: Cell division gene ftsQ. *Journal of Bacteriology*, 144(1), pp.435–437.

Blatch, G.L. & Lässle, M., 1999. The tetratricopeptide repeat: A structural motif mediating protein-protein interactions. *BioEssays*, 21(11), pp.932–939.

Booth, I.R., 2002. Stress and the single cell: Intrapopulation diversity is a mechanism to ensure survival upon exposure to stress. *International Journal of Food Microbiology*, 78(1-2), pp.19–30.

Boschert, R., Adler, F.R. & Blair, D.F., 2015. Loose coupling in the bacterial flagellar motor. *Proceedings of the National Academy of Sciences of the United States of America*, 112(15), pp.4755–60.

Bubendorfer, S. et al., 2012. Specificity of motor components in the dual flagellar system of Shewanella putrefaciens CN-32. *Mol Microbiol*, 83(2), pp.335–350.

Buist, G. et al., 2008. LysM, a widely distributed protein motif for binding to (peptido)glycans. *Molecular Microbiology*, 68(4), pp.838–847.

Castillo, D.J. et al., 2013. The C-terminal periplasmic domain of MotB is responsible for load-dependent control of the number of stators of the bacterial flagellar motor. *Biophysics*, 9, pp.173–181.

Cerveny, L. et al., 2013. Tetratricopeptide repeat motifs in the world of bacterial pathogens: Role in virulence mechanisms. *Infection and Immunity*, 81(3), pp.629–635.

Che, Y.S. et al., 2008. Suppressor analysis of the MotB(D33E) mutation to probe bacterial flagellar motor dynamics coupled with proton translocation. *Journal of Bacteriology*, 190(20), pp.6660–6667.

Cluzel, P., Surette, M. & Leibler, S., 2000. An ultrasensitive bacterial motor revealed by monitoring

signaling proteins in single cells. *Science*, 287(5458), pp.1652–1655.

Coil, D. a. & Anné, J., 2010. The role of fimV and the importance of its tandem repeat copy number in twitching motility, pigment production, and morphology in Legionella pneumophila. *Archives of Microbiology*, 192, pp.625–631.

D'Andrea, L.D. & Regan, L., 2003. TPR proteins: The versatile helix. *Trends in Biochemical Sciences*, 28(12), pp.655–662.

Das, A.K., Cohen, P.T.W. & Barford, D., 1998. The structure of the tetratricopeptide repeats of protein phosphatase 5: Implications for TPR-mediated protein-protein interactions. *EMBO Journal*, 17(5), pp.1192–1199.

Endres, R.G., 2009. Polar chemoreceptor clustering by coupled trimers of dimers. *Biophysical Journal*, 96(2), pp.453–463.

Fogel, M.A. & Waldor, M.K., 2006. A dynamic, mitotic-like mechanism for bacterial chromosome segregation. *Genes and Development*, 20(23), pp.3269–3282.

Fukuoka, H. et al., 2009. Sodium-dependent dynamic assembly of membrane complexes in sodium-driven flagellar motors. *Molecular Microbiology*, 71(4), pp.825–835.

Gerdes, K., Moller-Jensen, J. & Jensen, R.B., 2000. Plasmid and chromosome partitioning: Surprises from phylogeny. *Molecular Microbiology*, 37(3), pp.455–466.

Ghosh, S.K., Hajra, S., Paek, A., and Jayaram, M., 2006. Mechanisms for chromosome and plasmid segregation. *Annual review of biochemistry*, 75, pp.211–241.

Gosink, K.K. & Häse, C.C., 2000. Requirements for conversion of the Na+-driven flagellar motor of Vibrio cholerae to the H+-driven motor of Escherichia coli. *Journal of Bacteriology*, 182(15), pp.4234–4240.

Hosking, E.R. et al., 2006. The Escherichia coli MotAB proton channel unplugged. *J Mol Biol*, 364(5), pp.921–937.

Huitema, E. et al., 2006. Bacterial birth scar proteins mark future flagellum assembly site. *Cell*, 124(5), pp.1025–1037.

Inoue, Y. et al., 2008. Torque-Speed Relationships of Na+-driven Chimeric Flagellar Motors in Escherichia coli. *Journal of Molecular Biology*, 376(5), pp.1251–1259.

Jaques, S., Kim, Y.K. & McCarter, L.L., 1999. Mutations conferring resistance to phenamil and amiloride, inhibitors of sodium-driven motility of Vibrio parahaemolyticus. *Proceedings of the National Academy of Sciences of the United States of America*, 96(10), pp.5740–5745.

Kazmierczak, B.I. & Hendrixson, D.R., 2013. Spatial and numerical regulation of flagellar biosynthesis in polarly flagellated bacteria. *Molecular Microbiology*, 88(4), pp.655–663.

Kent, W. et al., 2002. The human genome browser at UCSC. *Genome Research*, 12(6), pp.996–1006.

Kim, K. et al., 2006. Crystal structure of PilF: Functional implication in the type 4 pilus biogenesis in Pseudomonas aeruginosa. *Biochemical and Biophysical Research Communications*, 340(4), pp.1028–1038.

Kojima, S., 2015. Dynamism and regulation of the stator, the energy conversion complex of the bacterial flagellar motor. *Current Opinion in Microbiology*, 28, pp.66–71.

Kojima, S. et al., 1999. Na+-driven flagellar motor resistant to phenamil, an amiloride analog, caused by mutations in putative channel components. *Journal of molecular biology*, 285(4), pp.1537–47.

Kojima, S. et al., 2009. Stator assembly and activation mechanism of the flagellar motor by the periplasms region of MotB. *Molecular Microbiology*, 73(4), pp.710–718.

Laloux, G. & Jacobs-Wagner, C., 2014. How do bacteria localize proteins to the cell pole? *Journal of cell science*, 127(Pt 1), pp.11–9.

Lam, H., Schofield, W.B. & Jacobs-Wagner, C., 2006. A landmark protein essential for establishing and perpetuating the polarity of a bacterial cell. *Cell*, 124(5), pp.1011–1023.

Lele, P.P., Hosu, B.G. & Berg, H.C., 2013. Dynamics of mechanosensing in the bacterial flagellar motor. *Proceedings of the National Academy of Sciences of the United States of America*, 110(29), pp.11839–44.

Li, N., Kojima, S. & Homma, M., 2011. Characterization of the periplasmic region of PomB, a Na +-driven flagellar stator protein in Vibrio alginolyticus. *Journal of Bacteriology*, 193(15), pp.3773–3784.

Lipkow, K., Andrews, S.S. & Bray, D., 2005. Simulated diffusion of phosphorylated CheY through the cytoplasm of Escherichia coli. In *Journal of Bacteriology*. pp. 45–53.

Lo, C.-J. et al., 2007. Nonequivalence of membrane voltage and ion-gradient as driving forces for the bacterial flagellar motor at low load. *Biophysical journal*, 93(1), pp.294–302.

Lutkenhaus, J., 1998. The regulation of bacterial cell division: a time and place for it. *Current opinion in microbiology*, 1(2), pp.210–215.

Matz, M. V., Lukyanov, K.A. & Lukyanov, S.A., 2002. Family of the green fluorescent protein: Journey to the end of the rainbow. *BioEssays*, 24(10), pp.953–959.

Michel, G.P.F. et al., 2011. Role of fimV in type II secretion system-dependent protein secretion of Pseudomonas aeruginosa on solid medium. *Microbiology (Reading, England)*, 157(Pt 7), pp.1945–54.

Mohl, D.A., Easter, J. & Gober, J.W., 2001. The chromosome partitioning protein, ParB, is required for cytokinesis in Caulobacter crescentus. *Molecular Microbiology*, 42(3), pp.741–755.

Möll, A. et al., 2010. DipM, a new factor required for peptidoglycan remodelling during cell division in Caulobacter crescentus. *Molecular Microbiology*, 77(1), pp.90–107.

Morimoto, Y. V. et al., 2010. Charged residues in the cytoplasmic loop of MotA are required for stator assembly into the bacterial flagellar motor. *Molecular Microbiology*, 78(5), pp.1117–1129.

Morimoto, Y. V. et al., 2013. Distinct roles of highly conserved charged residues at the MotA-FliG interface in bacterial flagellar motor rotation. *Journal of Bacteriology*, 195(3), pp.474–481.

Nishihara, Y. & Kitao, A., 2015. Gate-controlled proton diffusion and protonation-induced ratchet motion in the stator of the bacterial flagellar motor. *Proceedings of the National Academy of Sciences*, p.201502991.

Oldfield, N.J. et al., 2007. T-cell stimulating protein A (TspA) of Neisseria meningitidis is required for optimal adhesion to human cells. *Cellular Microbiology*, 9(2), pp.463–478.

Pandza, S. et al., 2000. The G-protein FlhF has a role in polar flagellar placement and general stress response induction in Pseudomonas putida. *Molecular microbiology*, 36(2), pp.414–423.

Paulick, A. et al., 2009. Two different stator systems drive a single polar flagellum in Shewanella oneidensis MR-1. *Molecular Microbiology*, 71(4), pp.836–850.

Ptacin, J.L., Lee, S.F., Garner, E.C., Toro, E., Eckart, M., Comolli, L.R., Moerner, W.E., Shapiro, L., 2010. A spindle-like apparatus guides bacterial chromosome segregation. *Nature cell biology*, 12(8), pp.791–8.

Reeve, J.N. et al., 1973. Minicells of Bacillus subtilis. *Journal of Bacteriology*, 114(2), pp.860–873.

Reid, S.W. et al., 2006. The maximum number of torque-generating units in the flagellar motor of Escherichia coli is at least 11. *Proceedings of the National Academy of Sciences of the United States of America*, 103(21), pp.8066–8071.

Semmler, a. B.T. et al., 2000. Identification of a novel gene, fimV, involved in twitching motility in Pseudomonas aeruginosa. *Microbiology*, 146(6), pp.1321–1332.

Shapiro, L., McAdams, H.H. & Losick, R., 2009. Why and how bacteria localize proteins. *Science (New York, NY)*, 326(5957), pp.1225–1228.

Sourjik, V. & Berg, H.C., 2000. Localization of components of the chemotaxis machinery of Escherichia coli using fluorescent protein fusions. *Molecular Microbiology*, 37(4), pp.740–751.

Sourjik, V. & Wingreen, N.S., 2012. Responding to chemical gradients: bacterial chemotaxis. *Current Opinion in Cell Biology*, 24(2), pp.262–268.

Sowa, Y. et al., 2005. Direct observation of steps in rotation of the bacterial flagellar motor. *Nature*, 437(7060), pp.916–919.

Stocker, R. et al., 2008. Rapid chemotactic response enables marine bacteria to exploit ephemeral microscale nutrient patches. *Proceedings of the National Academy of Sciences of the United States of America*, 105(11), pp.4209–4214.

Stocker, R. & Seymour, J.R., 2012. Ecology and physics of bacterial chemotaxis in the ocean. *Microbiology and molecular biology reviews : MMBR*, 76(4), pp.792–812.

Takekawa, N. et al., 2012. Characterization of PomA mutants defective in the functional assembly of the Na+-driven flagellar motor in Vibrio alginolyticus. *Journal of Bacteriology*, 194(8), pp.1934–1939.

Takekawa, N., Kojima, S. & Homma, M., 2014. Contribution of many charged residues at the stator-rotor interface of the Na+-driven flagellar motor to torque generation in Vibrio alginolyticus. *Journal of Bacteriology*, 196(7), pp.1377–1385.

Terahara, N., Krulwich, T. a & Ito, M., 2008. Mutations alter the sodium versus proton use of a Bacillus clausii flagellar motor and confer dual ion use on Bacillus subtilis motors. *Proceedings of the National Academy of Sciences of the United States of America*, 105(38), pp.14359–64.

Terahara, N., Sano, M. & Ito, M., 2012. A Bacillus Flagellar Motor That Can Use Both Na+ and K+ as a Coupling Ion Is Converted by a Single Mutation to Use Only Na+. *PLoS ONE*, 7(9).

Thattai, M. & Van Oudenaarden, A., 2004. Stochastic gene expression in fluctuating environments. *Genetics*, 167(1), pp.523–530.

Thiem, S. & Sourjik, V., 2008. Stochastic assembly of chemoreceptor clusters in Escherichia coli. *Molecular Microbiology*, 68(5), pp.1228–1236.

Thormann, K.M. & Paulick, A., 2010. Tuning the flagellar motor. *Microbiology*, 156(5), pp.1275–1283.

Tipping, M.J., Delalez, N.J., et al., 2013. Load-dependent assembly of the bacterial flagellar motor. *mBio*, 4(4).

Tipping, M.J., Steel, B.C., et al., 2013. Quantification of flagellar motor stator dynamics through in vivo proton-motive force control. *Molecular Microbiology*, 87(2), pp.338–347.

Treuner-Lange, A. & Søgaard-Andersen, L., 2014. Regulation of cell polarity in bacteria. *The Journal of Cell Biology*, 206(1), pp.7–17.

Tu, Y., 2013. Quantitative modeling of bacterial chemotaxis: signal amplification and accurate adaptation. *Annual review of biophysics*, 42, pp.337–59.

Ugalde, J. a, Chang, B.S.W. & Matz, M. V, 2004. Evolution of coral pigments recreated. *Science (New York, N.Y.)*, 305(5689), p.1433.

Vilella, A.J. et al., 2009. EnsemblCompara GeneTrees: Complete, duplication-aware phylogenetic trees in vertebrates. *Genome Research*, 19(2), pp.327–335.

Wadhams, G.H. & Armitage, J.P., 2004. Making sense of it all: bacterial chemotaxis. *Nat Rev Mol Cell Biol*, 5(12), pp.1024–1037.

Wehbi, H. et al., 2011. The peptidoglycan-binding protein fimv promotes assembly of the pseudomonas aeruginosa type IV pilus secretin. *Journal of Bacteriology*, 193(2), pp.540–550.

Yakushi, T. et al., 2006. Roles of charged residues of rotor and stator in flagellar rotation: Comparative study using H+-driven and Na+-driven motors in Escherichia coli. *Journal of Bacteriology*, 188(4), pp.1466–1472.

Yamaichi, Y. et al., 2012. A multidomain hub anchors the chromosome segregation and chemotactic machinery to the bacterial pole. *Genes and Development*, 26(20), pp.2348–2360.

Yuan, J. & Berg, H.C., 2010. Following the Behavior of the Flagellar Rotary Motor Near Zero Load. *Experimental Mechanics*, 50(9), pp.1263–1265.

Zhou, J., Lloyd, S.A. & Blair, D.F., 1998. Electrostatic interactions between rotor and stator in the bacterial flagellar motor. *Proceedings of the National Academy of Sciences*, 95(11), pp.6436–6441.

Abbreviation

CCCP	=	Carbonylcyanid-*m*-chlorphenylhydrazon
CCW	=	Counter-wlockwise
CM	=	Cytoplasmic membrane
CW	=	Clockwise
DNA	=	Deoxyribonucleic acid
F	=	Force
FRAP	=	Fluorescence recovery after photobleaching
GFP	=	Green fluorescent protein
imf	=	Ion-motive force
M	=	Torque
MCP	=	Methyl-accepting proteins
mRNA	=	Messenger ribonucleic acid
n	=	Number of units
OM	=	Outer membrane
PG	=	Peptidoglycan
pI	=	Isoelectric point
pmf	=	Proton motive force
r	=	Distance of the stators:FliG contact point to the rotational axis
TM	=	Transmembrane domain

Acknowledgements

Curriculum vitae